Late Transition Metal Pre-Catalysts for the Hydrogenation of Carbonyl-Containing Substrates

Zuzana Culakova

A dissertation

submitted in partial fulfillment of the

requirements for the degree of

Doctor of Philosophy

University of Washington

2018

Reading Committee:

Karen I. Goldberg, Chair

D. Michael Heinekey

Julia A. Kovacs

Program Authorized to Offer Degree:

Department of Chemistry

University of Washington

Abstract

Late Transition Metal Pre-Catalysts for the Hydrogenation of Carbonyl-Containing Substrates

Zuzana Culakova

Chair of the Supervisory Committee:
Professor Karen I. Goldberg
Department of Chemistry

This thesis describes efforts to develop new pre-catalysts for the hydrogenation of challenging carbonyl substrates, including esters and amides. We seek to understand the mechanisms by which these catalysts operate, and to use this understanding to rationally design new pre-catalysts, as well as to identify complexes that can operate in a multi-catalyst cascade for the stepwise hydrogenation of CO_2 to methanol. Chapter One outlines the motivations for this

work. The history and development of ester and amide hydrogenation pre-catalysts is discussed, as well as the rationale and precedent for using catalytic cascades to synthesize methanol from CO_2. Chapter Two explores the hydrogenation of lactone substrates by a bipyridine-supported half-sandwich iridium complex. This is a rare example of an ester hydrogenation pre-catalyst that is tolerant to the addition of acid. Chapter Three describes computational studies into the mechanism of ester and amide hydrogenation by aliphatic pincer-supported complexes of iron and ruthenium. Subtle disparities in the hydrogenation mechanism between ester and acid model substrates highlight the influence of substrate identity on reactivity. We find that, surprisingly, the highest calculated barrier in amide hydrogenation involves the rupture of the hemiaminal intermediate, rather than initial hydrogenation of the carbonyl group. Chapter Four describes the hydrogenation of simple formate substrates by PCP- and POCOP-supported complexes of iridium. The crucial roles of acid additives in pre-catalyst activation and catalyst deactivation pathways are explored. These efforts showcase the limitations of ionic ester hydrogenations and illustrate how understanding the reactivity of metal complexes enables rational pre-catalyst selection and design. Finally, in Chapter Five, these iridium pre-catalysts are successfully incorporated into cascade systems for the conversion of CO_2 to methanol.

TABLE OF CONTENTS

LIST OF FIGURES

LIST OF SCHEMES

LIST OF TABLES

ACKNOWLEDGEMENTS

My time at the University of Washington has been quite an adventure, one which would not have been possible without the help of many people.

Firstly, I thank Professor Karen Goldberg for support and mentoring throughout graduate school. Working in your group has been a pleasure. You have an incredible passion for research, integrity, motivation to tackle challenging problems, and ability to make connections between people to solve these problems. These are the skills that I aspire to bring to my future career. Thank you also for being supportive of my personal goals, especially for allowing me to pursue opportunities beyond UW.

Professor Nilay Hazari, thank you for setting an excellent foundation in organometallics during my undergraduate career and supporting me no matter what I am choosing to do. Thank you too, for suggesting UW as a place that may suit me; I've really enjoyed my time in Seattle.

Professors Odile Eisenstein and Eric Clot, I very much enjoyed my stay in Montpellier. Thank you for introducing me to a whole new area of chemistry. You were lovely hosts, and I was privileged to learn from you. To my fellow lab mates Emmeline and Ben, thanks so much for the language lessons and great conversations. Thank you also to my committee members, Professors Mike Heinekey, Julie Kovacs, and Forrest Michael, for being a source of excellent suggestions (and questions) throughout the years.

I owe much gratitude to the members of the Goldberg group throughout the years, as well as students and post docs throughout the inorganic division. The sense of fun and strong camaraderie in the group and in the division went a long way to make graduate school just a bit more bearable. An extra special thanks to Louise and Kelly, the last of Goldberg/Heinekey Group UW, for continuous moral support, bubbly water, patience, scientific advice and draft edits. I would not have made it through the last quarter without you.

I am grateful for the support of my family through my time in Seattle. Though I chose to move across the country, you have remained close-by through many late phone calls and by enduring long flights. Hopefully, I've convinced you that you want to move out west!

Finally, thank you to my broader group of friends in Seattle. You have accompanied me on adventures that I had never imagined, and provided incredible support through my journeys. A special thanks to Chris, for his consistent presence during my PhD and Stephen for teaching me to sail, and always pushing boundaries. Board game nights, tromping through the mountains, lifting fun time, and sailing in weather fair and foul. I've learned an incredible amount from you all and can't wait to see where our next adventures take us.

Chapter One. A review of technologies for homogeneous hydrogenation of esters and amides

1.1 Catalytic carbonyl hydrogenation: history and background

The hydrogenation of the carbonyl functional group, which contains a nucleophilic oxygen and an electrophilic carbon, requires the delivery of two hydrogen atoms, often as a proton and hydride (Figure 1.1), to generate an alcohol. The reduction of carbonyl-containing substrates is a vital transformation in synthetic chemistry, with widespread applications in the production of both commodity and fine chemicals.[1]

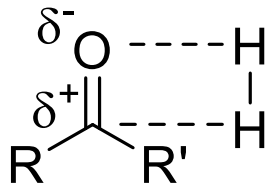

Figure 1.1. Schematic for hydrogenation of carbonyl substrates

Two Nobel Prizes have been awarded for developments in catalytic hydrogenation. Paul Sabatier was given the Nobel Prize in Chemistry in 1912 for his work on the hydrogenation of unsaturated organic compounds using heterogeneous materials, particularly nickel catalysts.[2] Sabatier and coworkers had developed systems using molecular H_2 to directly hydrogenate substrates including alkenes, nitriles, benzene, aldehydes, and ketones.[3,4] This work provided the foundation for modern hydrogenation chemistries, some of which are still in use today.[5] In 2001, William Knowles and Ryoji Noyori shared half of the Nobel Prize in Chemistry with Barry Sharpless for their work on transition metal catalysts for asymmetric hydrogenation of ketones and aldehydes.[6]

Today, ketones and aldehydes are reduced by H_2 using homogeneous catalysts, under mild conditions and with excellent control over stereochemistry.[6,7] In both industrial and laboratory

settings, catalytic homogeneous hydrogenation presents several general advantages over other hydrogenation technologies, such as the use of metal hydride reagents. Dihydrogen is an abundant, inexpensive, and atom-economical reagent for these reactions. Well-tuned homogeneous catalysts perform reactions selectively, eliminating side reactions and enabling sensitive functional groups, such as carbon-carbon double bonds, to remain intact under the reaction conditions.[1]

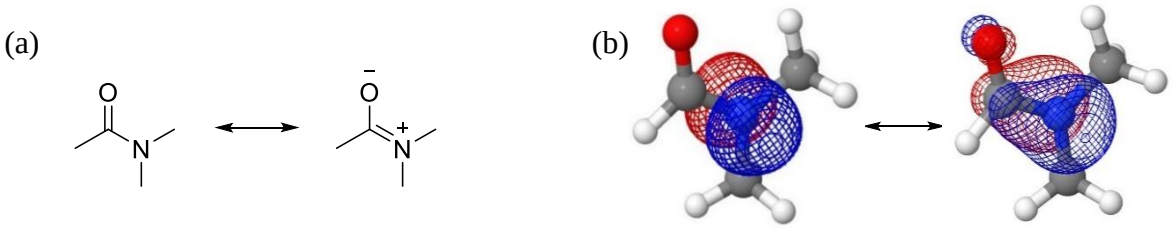

Figure 1.2. Resonance in carbonyl substrates (a) Resonance structures for dimethylformamide. (b) p electrons (left, Natural Bonding Orbital) and delocalization through the carbonyl π system (right, Natural Localized Molecular Orbital) Gaussian 09, PBE0-D, Def2TZVP.Molecular Orbital) Gaussian 09, PBE0-D, Def2TZVP

However, carbonyl substrates with a heteroatom (N or O) α to the carbonyl present a greater challenge than the hydrogenation of ketones and aldehydes,[8,9] and industrially relevant homogeneous hydrogenation catalysts are less prevalent for these substrates. In these molecules, electron density from the heteroatom p orbital is delocalized into the carbon p orbital and carbonyl π* bond. This is formally represented as a combination of two resonance structures (Figure 1.2a), and the delocalization can be easily visualized in calculated PNBO/NBO images (Figure 1.2b). The increased electron density reduces the electrophilicity of the carbonyl carbon, hindering hydride transfer to the substrate. Owing to the challenge presented by the unfavorable electronic structures of esters, amides, carboxylic acids, and other deactivated carbonyls, there are fewer known efficient homogeneous catalysts for these transformations.[1] As such, the development of new homogeneous hydrogenation pre-catalysts, and relevant applications, is the focus of this thesis.

1.2 Ester hydrogenation

In a typical ester hydrogenation, reduction of the carbonyl group is accompanied by cleavage of the bond between the carbonyl carbon and the alkoxy oxygen, ultimately resulting in alcohol products (Scheme 1.1). Historically, the hydrogenation of such materials generally employed an indirect hydrogen source and reductant, for example, elemental sodium as a reductant and an alcohol as a proton source, as in the Boulveault-Blanc reduction of carboxylic acids to primary alcohols, developed in 1903 (Scheme 1.2).[5,8,10]

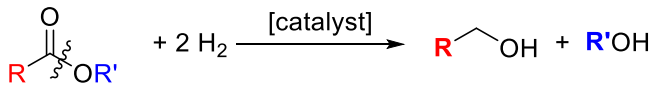

Scheme 1.1. General scheme for hydrogenation of esters

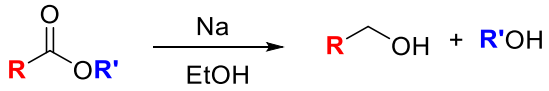

Scheme 1.2. Boulveault-Blanc reduction of carboxylate substrates

More commonly today, metal hydride or borohydride reductants are used to carry out preparative reductions of esters. The most frequently reported reductant for ester hydrogenations in pharmaceutical synthesis is $LiAlH_4$ (LAH), though other reagents used include $NaBH_4$, Di-isobutyl aluminum hydride (DIBAL), and BH_3SMe_2.[7] These reagents are highly reactive and air-sensitive, and therefore require special handling and transportation methods. Some of these reagents lack functional group compatibility; LAH, for example, also reduces carboxylic acids, amides and acyl halides. Additionally, these metal hydride reagents are typically used in excess and must be quenched prior to reaction workup, generating stoichiometric metal waste which must be separated from the desired products.[5]

Heterogeneous hydrogenation catalysts, many similar to those studied by Sabatier, circumvent some of the issues associated with metal hydride regents, namely poor atom economy. Copper chromite catalysts are a common choice for large-scale reductions, with reactions

proceeding at high temperatures (200-300 °C) and pressures (100-300 bar H_2). This method is used industrially to convert lipids and fatty oils, such as coconut oil and tallow, to fatty alcohols, for use as detergents and surfactants.[11] However, these catalysts are sensitive to sulfur and halogen poisons that may be present in substrates in trace quantities. Additionally, they are often not selective for C-O bond hydrogenation, and also reduce other unsaturated functionalities, such as alkenes.[5] Compared to heterogeneous catalysts, the metal hydride reactions described previously operate under milder conditions and can show improved selectivity, for example preserving double bonds and generating fewer side products. Despite their disadvantages, metal hydride reagents continue to be commonly used in the synthesis of pharmaceuticals and other fine chemicals.

Homogeneously catalyzed ester hydrogenation is a rapidly growing area of research in the search for alternative strategies that operate under milder conditions and require a less laborious work-up. After a few early reports using ruthenium-based pre-catalysts, the field has expanded tremendously, with many important developments disclosed in the last two decades. The first example of homogeneous hydrogenation of unactivated esters was reported by Grey and coworkers in 1980. In this work, $[(Ph_3P)(Ph_2P)RuH_2\text{-}K^+\bullet\text{diglyme}]_2$ was used to catalytically reduce methyl acetate and ethyl acetate, albeit with low conversion (22% and 8% respectively).[12,13] In 1998, Teunissen and Elsevier employed a Ru-triphos (triphos = 1,1,1-tris(diphenylphosphinomethyl)ethane) pre-catalyst to hydrogenate unactivated esters with an unprecedentedly high turnover number (TON) (>2000 for benzyl benzoate).[14,15] This system was later re-investigated by Leitner and coworkers for reduction of bio-derived carboxylic acids[16,17] and various carbonyl containing substrates, including esters,[18,19] as well as for the direct conversion of CO_2 to methanol.[20] This versatile system will be discussed in more detail in Chapter Two.

In 2006, Milstein and coworkers first reported a bi-functional ruthenium pre-catalyst for ester hydrogenation. They demonstrated 86% conversion of ethyl acetate to ethanol under moderate conditions (0.2 mol% [Ru], 115 °C, 12 hours, 5.4 bar H_2).[21] First, activation of the pre-catalyst occurs by dehydrohalogenation using base (KO^tBu), resulting in loss of a proton from the ligand methylene arm and dearomatization of the pyridine ring. Based on experimental[21] and computational evidence,[22] hydrogenation is thought to proceed by hydrogen cleavage across the meter center and basic site on the pincer arm, accompanied by rearomatization of the pyridine ring. An outer-sphere transfer subsequently moves the proton and hydride to the substrate (Scheme 1.3).

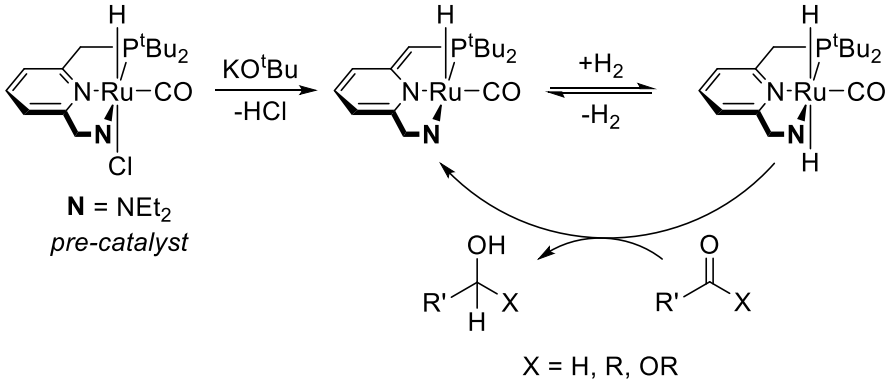

Scheme 1.3. Generalized mechanism for hydrogenation of a carbonyl substrate by Milstein's PNN catalyst[21]

The discovery of a range of effective pre-catalysts for ester hydrogenation, bearing pincer ligands with phosphorous and nitrogen substituents, followed the initial 2006 report by Milstein and coworkers.[1,8,11,23] These systems exhibited faster rates of hydrogenation and/or operated under milder conditions. Most of these complexes require activation by base to access the catalytically active species. Like the complexes in Scheme 1.3**,** these pre-catalysts have in common their reliance on the presence of a basic site on the ligand, which is thought to facilitate heterolytic hydrogen cleavage by storing a proton equivalent. In contrast, ruthenium/triphos, along with a related colbalt/triphos combination,[24] and a half-sandwich iridium complex studied by our group

(see Chapter Two for more details)[25] remain the only systems studied for ester hydrogenation that can operate under acidic conditions.

Notable among this generation of ester hydrogenation pre-catalysts are those with aliphatic PNP ligands (PNP = bis[(2-dialkylphosphino]ethyl)amine). The PNP scaffold allows tuning of both sterics and electronics of the compounds by modifications of the alkyl groups on the phosphorous arms. The resulting complexes are highly efficient for hydrogenation of carbonyl groups, among other reactions. The first of these complexes, $Ru(H)(Cl)(CO)(HN(CH_2CH_2PPh_2)_2$, was reported by researchers from the Takasago International Corporation in 2011. This complex was shown, with addition of a base activator, to be a highly active pre-catalyst for a variety of ester substrates, including methyl benzoate. Since then, a large number of reports have been published exploring variations of this complex, facilitating diverse hydrogenations,[26] and dehydrogenations,[27] among other reactions[28] (see Chapter Three for a more detailed discussion).

Recently, competent ester hydrogenation pre-catalysts based on iron,[29–31] iridium,[25,32] cobalt,[24,33,34] manganese,[35–39] and osmium,[40,41] with sulfur,[42] or N-heterocyclic carbene[43–45] based ligands have been reported. A selection of these pre-catalysts is shown in Figure 1.3. Despite the efficacy of these complexes for hydrogenation reactions, many are sensitive to air and other small molecules, limiting their widespread utility. As such, there is still a need to develop active ester hydrogenation systems that are robust under diverse conditions.

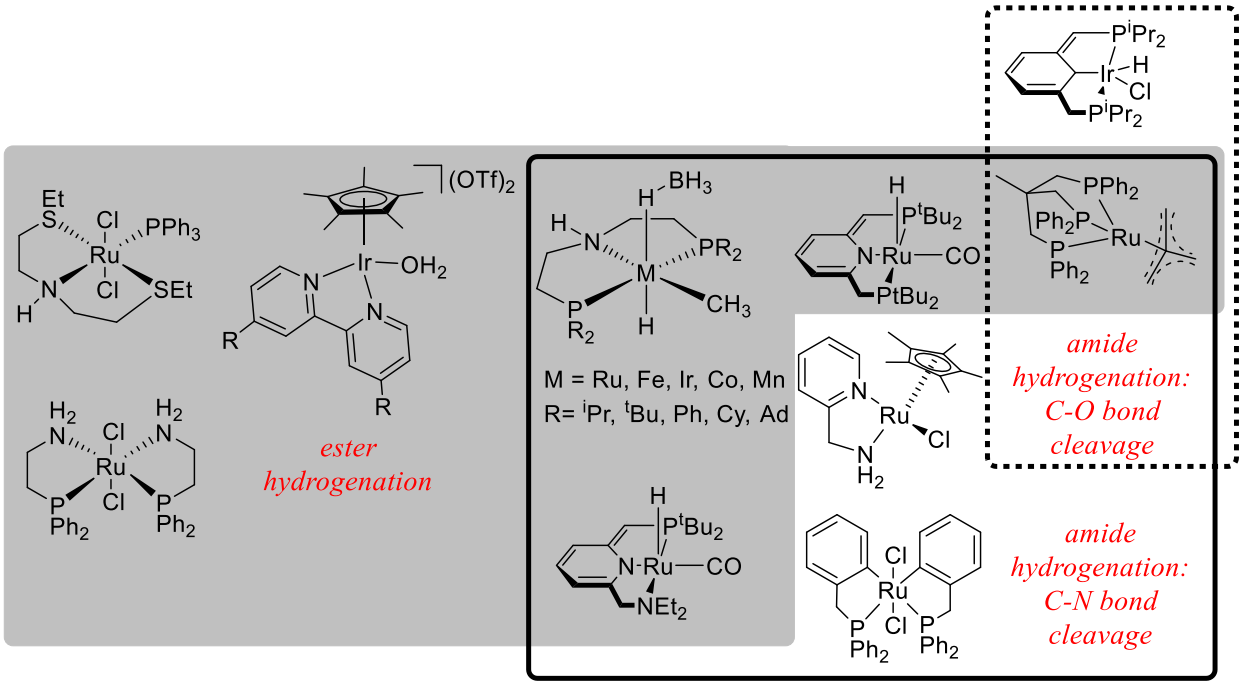

Figure 1.3. Selected pre-catalysts for the hydrogenation of carboxylic acid derivatives

1.3 Amide hydrogenation

Amide hydrogenation reactions usually proceed to give one of two possible sets of products: either an amine and alcohol, resulting from cleavage of the C-N bond, or water and an amine, from C-O bond cleavage (Figure 1.4).[46] Catalysts selective for C-O bond cleavage, such as metal hydride reagents, were developed earlier, and are more widely used in industry.

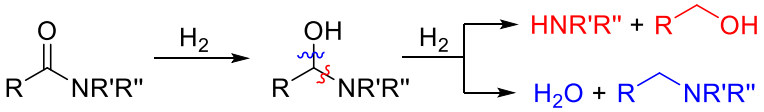

Figure 1.4. Two pathways for amide hydrogenation: C-O bond cleavage vs. C-N bond cleavage

The hydrogenation of amides is conceptualized as mechanistically similar to that of esters, but these reactions generally require more forcing conditions and there are fewer reports of this transformation. The first catalytic hydrogenation of amides was reported in 1934 by Adkins and Wojcik, decades after the first communication of catalytic ester hydrogenation. Copper chromite catalysts under forcing conditions (>140 bar H_2, 250 °C) were used in this study.[47] More recently,

highly efficient bimetallic heterogeneous catalysts that operate under more moderate conditions (typically 160-180 °C and 100 bar H_2) have been developed. However, these catalysts often exhibit low selectivity due to further reactions of the products (e.g. reduction of phenyl to cyclohexyl, conversion of primary amines to secondary amines).[48,49] A heterogeneous Rh/Mo catalyst synthesized from $Mo(CO)_6$ and $RhCl_3{\cdot}3H_2O$ was one of the first efficient bimetallic hydrogenation pre-catalysts for deoxygenative hydrogenation of primary carboxamides that avoids secondary amide formation. It operates at 130-160 °C, and 50-100 bar H_2, though the major drawbacks are its susceptibility to poisoning by the trace CO produced during the reaction, and poor functional group tolerance.[50] These flaws continue to limit the application of these pre-catalysts in pharmaceutical and fine chemical synthesis.[48]

As with esters, stoichiometric metal hydrides, often LAH or $NaBH_4$, are frequently used to reduce amides in the synthesis of phramaceuticals.[7,46] As previously discussed, side reactions are common, especially in the presence of water, and these reagents will also reduce aldehydes, ketones, nitriles, acyl halides and other functional groups. A notable alternative, stoichiometric borane reagents, such as B_2H_6/THF, are also selective for C-O bond cleavage and are tolerant to other carbonyl functional groups, such as ketones and esters.[46] Alternatively, electrochemical techniques for amide hydrogenation have been developed.[46] However, these transformations require the formation of radical intermediates and are limited to amides with stable radical anions, for example substrates with aryl rings. Reduction of amides to amines without use of a hydride reagent is an active research area for pharmaceutical developments,[51] as the shortcomings of existing heterogeneous catalysts and metal hydride reductants continue to motivate a search for improved, selective hydrogenation pre-catalysts that operate under milder conditions. Chapter Three will discuss in more detail a number of highly active homogeneous pre-catalysts that were

recently reported for amide hydrogenation. There is a significant overlap between these catalysts and those that are active for ester hydrogenation. In contrast to heterogeneous catalysts, which are usually selective for deoxygenative hydrogenation, many homogeneous catalysts facilitate C-N bond cleavage to give alcohol and amine products.[1] The mechanistic origin of this difference in selectivity is not fully understood and is investigated in Chapter Three. The development of this previously unrealized transformation creates opportunities for new synthetic pathways.

1.3.1 C-O Bond cleavage

Few homogeneous amide hydrogenation catalysts are selective for C-O bond cleavage. Literature examples are limited to Ru/triphos, especially in the presence of an acid additive,[18] and a PCP pincer-supported iridium complex combined with tetrakis[3,5-bis(trifluoromethyl)-phenyl]borate ($NaBAr_F$) and boron-based Lewis acids, such as $B(C_6F_5)_3$, reported by Zhou and coworkers.[52] Neither of these systems contain an available basic site on the ligand.

1.3.2 C-N Bond cleavage

Catalysts based on aliphatic PNP scaffolds[53,45] or Milstein's catalysts[54] and related scaffolds have been found to be highly active for amide hydrogenation, and are selective for C-N bond cleavage. Figure 1.3 shows a selection of these catalysts. In some cases, both ruthenium and iron-based versions exhibit similar activities, a surprising result since first-row metal catalysts are often less active than their second- or third-row counterparts.[53] These catalysts, and their mechanisms of activity will be discussed in Chapter Three.

1.4 Cascade catalysis

The development of efficient ester and amide hydrogenation catalysts has allowed for new applications, such as cascade catalysis for the conversion of CO_2 to methanol, and other small

molecules. Methanol is an essential chemical feedstock and fuel.[55] Currently, methanol is made by reaction of synthesis gas, or syn-gas, a mix of H_2, CO and CO_2, over a heterogeneous catalyst such as $CuO/ZnO/Al_2O_3$ at 250-300 °C and 50-100 bar,[56] according to the equations in Scheme 1.4.[55] Syn-gas is generated by the partial oxidation of carbon-containing feedstocks, such as coal, natural gas or petroleum, at elevated temperatures and pressures. However, syn-gas obtained from steam reforming of methane (performed at 800-1000 °C, 20-30 bar, over a nickel catalyst) is generally preferred, as it is low in catalyst-poisoning impurities, such as H_2S, COS and mercaptans.[55] Overall, this process is energy intensive and relies on carbon feedstocks.

$$CO + 2H_2 \rightleftharpoons CH_3OH \qquad \Delta H_{298K} = -21.7 \text{ kcal mol}^{-1}$$
$$CO_2 + 3H_2 \rightleftharpoons CH_3OH + H_2O \qquad \Delta H_{298K} = -11.9 \text{ kcal mol}^{-1}$$
$$CO_2 + H_2 \rightleftharpoons CO + H_2O \qquad \Delta H_{298K} = 9.8 \text{ kcal mol}^{-1}$$

Scheme 1.4. Equations governing methanol sysnthesis from syn-gas[55]

Due to the large number of bonds broken and formed, methanol synthesis from CO_2 and H_2 is a challenging transformation for any single catalyst. In using a cascade, the hydrogenation can be separated into simpler steps, and catalysts can be optimized for each transformation, leading to systems that are highly active under more moderate conditions. Overall, this should allow for more sustainable methanol production.

In 2011, Sanford and coworkers reported a single-reactor cascade for the homogeneous hydrogenation of CO_2 to methanol. In their system, CO_2 is hydrogenated to formic acid by cat. A, $((PMe_3)_4Ru(Cl)(OAc))$. Next, the formic acid undergoes transesterification with alcohol solvent assisted by scandium triflate ($Sc(OTf)_3$) (cat. B) to produce a formate ester. The ester is then hydrogenated to generate two equivalents of alcohol using Ru(PNN)(H)(CO) cat. C, (Scheme 1.5). Logistically, the process was limited by incompatibility between catalysts and reaction components. For example, cat. C is incompatible with cat. B. It is likely that $Sc(OTf)_3$ decomposes

under reaction conditions to give triflic acid (HOTf), as the degradation of metal triflates to yield HOTf is well precedented.[57] HOTf then deactivates cat. C, presumably by protonation of the basic site. In the initial publication, this problem was resolved by physically separating cat. A/B from cat. C inside the reactor vessel and relying on distillation to transport methyl formate for further participation in the cascade. However, the activity of this system was limited, producing 21 turnovers of methanol under the optimized conditions, far less than the TON of each of the individual steps with their respective catalysts. A related Ru(PNN) ester hydrogenation pre-catalyst reported by Milstein[21] (Scheme 1.3) was also investigated by Sanford as a potential cat. C. Methyl formate hydrogenation by the complex was severely inhibited in a H_2/CO_2 mixture, as compared to pure H_2.[58] Later studies showed that this complex reacts with CO_2 to make formate adducts.[59] The sequestration of catalyst in these inactive forms is likely responsible for hindering hydrogenation activity in the presence of CO_2.

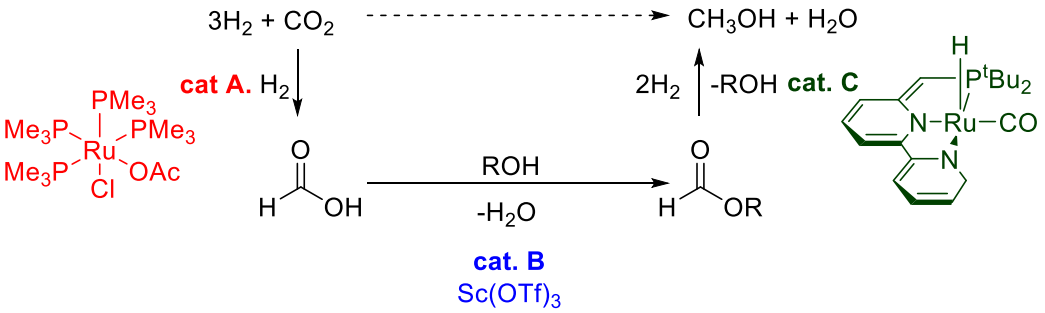

Scheme 1.5. Schematic for cascade hydrogenation of CO_2 to methanol via an ester intermediate. Adapted from Sanford[58]

A number of other cascade systems have been reported since the initial report by Sanford and coworkers. Organic carbamates and carbonates, including propylene carbonate or dimethyl carbonate have been proposed as alternate intermediates for tandem cascades (Figure 1.5).[60–62] The most successful systems reported to date proceed through amide intermediates. Following reports of amide hydrogenation by aliphatic PNP-based catalysts, Sanford and coworkers disclosed a related cascade that operates with dimethylformamide as the intermediate, taking advantage of the

reaction of dialkylamines with CO_2 to assist with carbon capture.[63] Using a PNP ruthenium pre-catalyst and a dimethylamine co-catalyst, they achieved near-complete (95%) conversion of CO_2 to a mixture of methanol, dimethylammonium formate and dimethylformamide, generating up to 550 TON of methanol (Figure 1.6). The entropically disfavored initial carboxylation required lower temperatures than the hydrogenation step, necessitating a temperature ramp over the course of the reaction. The authors found that the rate of dimethylammonium dimethylcarbamate hydrogenation is competitive with catalyst decomposition; compatibility issues continue to limit the performance of cascade systems. In their conclusion, Sanford and coworkers highlight the need for development of improved hydrogenation catalysts.[63]

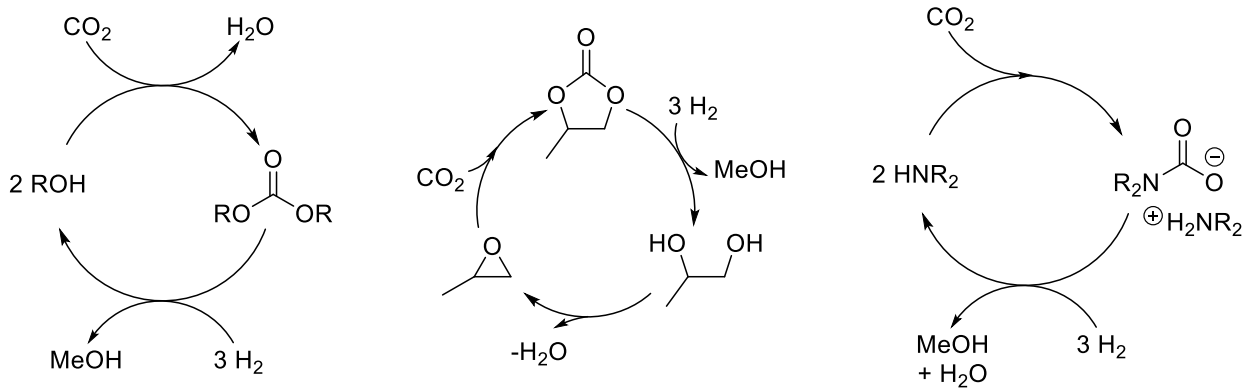

Figure 1.5. Proposed cascades for conversion of CO_2 to methanol[60–62]

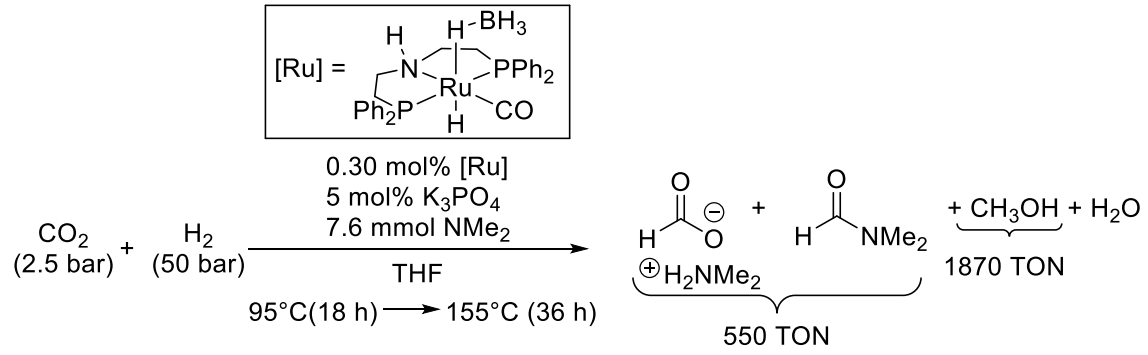

Figure 1.6. Cascade catalysts for production of methanol from CO_2 via carbamate intermediates[63]

Olah and coworkers demonstrated a similar scheme instead using pentaethylenehexamine (PEHA) in tandem with ruthenium pre-catalysts based on the same aliphatic PNP scaffold. After optimization, they were able to produce > 2000 turnovers (79% yield) of methanol relative to initial CO_2, and demonstrate the recyclability of their system with modest loss of activity after 5 recycles.[64] While these early successes are promising, we anticipate that a better understanding of the mechanism by which these catalysts operate and are deactivated will facilitate the rational design of more robust and active systems.

1.5 Dissertation Summary

This work describes efforts to identify and investigate new catalysts for hydrogenation of challenging carbonyl substrates. Chapter Two describes the investigation of the hydrogenation of lactone substrates by a rare example of an acid-tolerant ester hydrogenation catalyst, a half-sandwich iridium complex. Chapter Three explores the mechanism of ester and amide hydrogenation by aliphatic pincer-supported complexes of iron and ruthenium using computational methods. Subtle disparities in the mechanism of hydrogenation between methyl formate and formamide substrates are discussed, highlighting the significant influence of substrate identity on reactivity. Chapter Four describes the development of PCP- and POCOP-supported complexes of iridium as catalysts for the hydrogenation of simple ester substrates. Chapter Five builds upon the understanding of catalysts activation by acids and deactivation pathways built in Chapter Four as these catalysts are effectively applied in cascade systems for the conversion of CO_2 to methanol. Together, Chapters Four and Five show how understanding the reactivity of metal complexes can lead to the rational development of new catalysts systems for specific applications.

1.6 References

(1) Dub, P. A.; Ikariya, T. Catalytic Reductive Transformations of Carboxylic and Carbonic Acid Derivatives Using Molecular Hydrogen. *ACS Catal.* **2012**, *2* (8), 1718–1741.

(2) 2014, N. M. A. Paul Sabatier-biographical https://www.nobelprize.org/nobel_prizes/chemistry/laureates/1912/sabatier-bio.html (accessed Jun 25, 2017).

(3) Sabatier, P.; Senderens, J. B. Transformation Des Aldéhydes et Des Cétones En Alcools Par Hydrogénation Catalytique. *C. R. Hebd. Seances Acad. Sci.* **1903**, *137*, 301–303.

(4) Che, M. Nobel Prize in Chemistry 1912 to Sabatier: Organic Chemistry or Catalysis? *Catal. Today* **2013**, *218–219*, 162–171.

(5) Riemenschneider, W.; Bolt, H. M. Esters, Organic. *Ullmann's Encycl. Ind. Chem.* **2005**, 8676–8694.

(6) Per Ahlberg. Advanced Information on the Nobel Prize in Chemistry 2001: Catalytic Asymmetric Synthesis. 2001, pp 1–12.

(7) Magano, J.; Dunetz, J. R. Large-Scale Carbonyl Reductions in the Pharmaceutical Industry. *Org. Process Res. Dev.* **2012**, *16* (6), 1156–1184.

(8) Pritchard, J.; Filonenko, G. A.; Van Putten, R.; Hensen, E. J. M.; Pidko, E. A. Heterogeneous and Homogeneous Catalysis for the Hydrogenation of Carboxylic Acid Derivatives: History, Advances and Future Directions. *Chem. Soc. Rev.* **2015**, *44* (11), 3808–3833.

(9) McAlees, A. J.; McCrindle, R. Catalytic Hydrogenations of Cyclic Imides and Ayhydrides. *J. Chem. Soc. C* **1969**, 2425.

(10) Bouveault, L. .; Blanc, G. Préparation Des Alcools Primaires Au Moyen Des Acides Correspondants. *C. R. Hebd. Seances Acad. Sci.* **1903**, 1676–1678.

(11) Saudan, L. A. Hydrogenation of Esters. In *Sustainable Catalysis*; Dunn, P. J., Hii, K. K. (Mimi), Kirsche, Michael, J., Williams, M. T., Eds.; John Wiley & Sons, Inc.: Hoboken, New Jersey, 2013; pp 37–61.

(12) Grey, R. A.; Pez, G. P.; Wallo, A. Anionic Metal Hydride Catalysts. 2. Application to the Hydrogenation of Ketones, Aldehydes, Carboxylic Acid Esters and Nitriles. *J. Am. Chem. Soc.* **1981**, *103* (25), 7536–7542.

(13) Grey, R. A.; Pez, G. P.; Wallo, A.; Corsi, J. Homogeneous Catalytic Hydrogenation of Carboxylic Acid Esters to Alcohols. *J. Chem. Soc., Chem. Commun.* **1980**, 783–784.

(14) Teunissen, H. T.; Elsevier, C. J. Ruthenium Catalysed Hydrogenation of Dimethyl Oxalate to Ethylene Glycol. *Chem. Commun.* **1997**, 667–668.

(15) Teunissen, H. T.; Elsevier, C. J. Homogeneous Ruthenium Catalyzed Hydrogenation of Esters to Alcohols. *Chem. Commun.* **1998**, *3* (13), 1367–1368.

(16) Geilen, F. M. A.; Engendahl, B.; Harwardt, A.; Marquardt, W.; Klankermayer, J.; Leitner, W. Selective and Flexible Transformation of Biomass-Derived Platform Chemicals by a Multifunctional Catalytic System. *Angew. Chem. Int. Ed.* **2010**, *49* (32), 5510–5514.

(17) Geilen, F. M. a; Engendahl, B.; Hölscher, M.; Klankermayer, J.; Leitner, W. Selective Homogeneous Hydrogenation of Biogenic Carboxylic Acids with [Ru(TriPhos)H]+: A Mechanistic Study. *J. Am. Chem. Soc.* **2011**, *133* (36), 14349–14358.

(18) vom Stein, T.; Meuresch, M.; Limper, D.; Schmitz, M.; Hölscher, M.; Coetzee, J.; Cole-Hamilton, D. J.; Klankermayer, J.; Leitner, W. Highly Versatile Catalytic Hydrogenation of Carboxylic and Carbonic Acid Derivatives Using a Ru-Triphos Complex: Molecular Control over Selectivity and Substrate Scope. *J. Am. Chem. Soc.* **2014**, *136* (38), 13217–13225.

(19) Meuresch, M.; Westhues, S.; Leitner, W.; Klankermayer, J. Tailor-Made Ruthenium-Triphos Catalysts for the Selective Homogeneous Hydrogenation of Lactams. *Angew. Chem. Int. Ed.* **2016**, *55* (4), 1392–1395.

(20) Wesselbaum, S.; Moha, V.; Meuresch, M.; Brosinski, S.; Thenert, K. M.; Kothe, J.; vom Stein, T.; Englert, U.; Hölscher, M.; Klankermayer, J.; et al. Hydrogenation of Carbon Dioxide to Methanol Using a Homogeneous Ruthenium–Triphos Catalyst: From Mechanistic Investigations to Multiphase Catalysis. *Chem. Sci.* **2015**, *6* (1), 693–704.

(21) Zhang, J.; Leitus, G.; Ben-David, Y.; Milstein, D. Efficient Homogeneous Catalytic Hydrogenation of Esters to Alcohols. *Angew. Chem. Int. Ed.* **2006**, *45* (7), 1113–1115.

(22) Li, H.; Wang, X.; Huang, F.; Lu, G.; Jiang, J.; Wang, Z. X. Computational Study on the Catalytic Role of Pincer Ruthenium(II)-PNN Complex in Directly Synthesizing Amide from Alcohol and Amine: The Origin of Selectivity of Amide over Ester and Imine. *Organometallics* **2011**, *30* (19), 5233–5247.

(23) Clarke, M. L. Recent Developments in the Homogeneous Hydrogenation of Carboxylic Acid Esters. *Catal. Sci. Technol.* **2012**, *2* (12), 2418.

(24) Korstanje, T. J.; Ivar van der Vlugt, J.; Elsevier, C. J.; de Bruin, B. Hydrogenation of Carboxylic Acids with a Homogeneous Cobalt Catalyst. *Science* **2015**, *350* (6258), 298–302.

(25) Brewster, T. P.; Rezayee, N. M.; Culakova, Z.; Sanford, M. S.; Goldberg, K. I. Base-Free Iridium-Catalyzed Hydrogenation of Esters and Lactones. *ACS Catal.* **2016**, *6* (5), 3113–3117.

(26) Smith, N. E.; Bernskoetter, W. H.; Hazari, N.; Mercado, B. Q. Synthesis and Catalytic Activity of PNP-Supported Iron Complexes with Ancillary Isonitrile Ligands. *Organometallics* **2017**, *36* (20), 3995–4004.

(27) Alberico, E.; Lennox, A. J. J.; Vogt, L. K.; Jiao, H.; Baumann, W.; Drexler, H.-J.; Nielsen, M.; Spannenberg, A.; Checinski, M. P.; Junge, H.; et al. Unravelling the Mechanism of Basic Aqueous Methanol Dehydrogenation Catalyzed by Ru–PNP Pincer Complexes. *J. Am. Chem. Soc.* **2016**, *138* (45), 14890–14904.

(28) Zhang, Y.; MacIntosh, A. D.; Wong, J. L.; Bielinski, E. A.; Williard, P. G.; Mercado, B. Q.; Hazari, N.; Bernskoetter, W. H. Iron Catalyzed CO_2 Hydrogenation to Formate Enhanced by Lewis Acid Co-Catalysts. *Chem. Sci.* **2015**, *6* (7), 4291–4299.

(29) Chakraborty, S.; Dai, H.; Bhattacharya, P.; Fairweather, N. T.; Gibson, M. S.; Krause, J. A.; Guan, H. Iron-Based Catalysts for the Hydrogenation of Esters to Alcohols. *J. Am. Chem. Soc.* **2014**, *136* (22), 7869–7872.

(30) Werkmeister, S.; Junge, K.; Wendt, B.; Alberico, E.; Jiao, H.; Baumann, W.; Junge, H.; Gallou, F.; Beller, M. Hydrogenation of Esters to Alcohols with a Well-Defined Iron Complex. *Angew. Chem. Int. Ed.* **2014**, *53* (33), 8722–8726.

(31) Zell, T.; Ben-David, Y.; Milstein, D. Unprecedented Iron-Catalyzed Ester Hydrogenation. Mild, Selective, and Efficient Hydrogenation of Trifluoroacetic Esters to Alcohols Catalyzed by an Iron Pincer Complex. *Angew. Chem. Int. Ed.* **2014**, *53* (18), 4685–4689.

(32) Junge, K.; Wendt, B.; Jiao, H.; Beller, M. Iridium-Catalyzed Hydrogenation of Carboxylic Acid Esters. *ChemCatChem* **2014**, *6* (10), 2810–2814.

(33) Yuwen, J.; Chakraborty, S.; Brennessel, W. W.; Jones, W. D. Additive-Free Cobalt-Catalyzed Hydrogenation of Esters to Alcohols. *ACS Catal.* **2017**, *7* (5), 3735–3740.

(34) Srimani, D.; Mukherjee, A.; Goldberg, A. F. G.; Leitus, G.; Diskin-Posner, Y.; Shimon, L. J. W.; Ben David, Y.; Milstein, D. Cobalt-Catalyzed Hydrogenation of Esters to Alcohols: Unexpected Reactivity Trend Indicates Ester Enolate Intermediacy. *Angew. Chem. Int. Ed.* **2015**, *54* (42), 12357–12360.

(35) Papa, V.; Cabrero-Antonino, J. R.; Alberico, E.; Spanneberg, A.; Junge, K.; Junge, H.; Beller, M. Efficient and Selective Hydrogenation of Amides to Alcohols and Amines Using a Well-Defined Manganese–PNN Pincer Complex. *Chem. Sci.* **2017**, *8* (5), 3576–3585.

(36) Espinosa-Jalapa, N. A.; Nerush, A.; Shimon, L. J. W.; Leitus, G.; Avram, L.; Ben-David, Y.; Milstein, D. Manganese-Catalyzed Hydrogenation of Esters to Alcohols. *Chem. Eur. J.* **2017**, *23* (25), 5934–5938.

(37) Elangovan, S.; Garbe, M.; Jiao, H.; Spannenberg, A.; Junge, K.; Beller, M. Hydrogenation of Esters to Alcohols Catalyzed by Defined Manganese Pincer Complexes. *Angew. Chem. Int. Ed.* **2016**, *55* (49), 15364–15368.

(38) van Putten, R.; Uslamin, E. A.; Garbe, M.; Liu, C.; Gonzalez-de-Castro, A.; Lutz, M.; Junge, K.; Hensen, E. J. M.; Beller, M.; Lefort, L.; et al. Non-Pincer-Type Manganese Complexes as Efficient Catalysts for the Hydrogenation of Esters. *Angew. Chem. Int. Ed.* **2017**, *56* (26), 7531–7534.

(39) Widegren, M. B.; Harkness, G. J.; Slawin, A. M. Z.; Cordes, D. B.; Clarke, M. L. A Highly Active Manganese Catalyst for Enantioselective Ketone and Ester Hydrogenation. *Angew. Chem. Int. Ed.* **2017**, *56* (32), 5825–5828.

(40) Spasyuk, D.; Smith, S.; Gusev, D. G. From Esters to Alcohols and Back with Ruthenium and Osmium Catalysts. *Angew. Chem. Int. Ed.* **2012**, *51* (11), 2772–2775.

(41) Acosta-Ramirez, A.; Bertoli, M.; Gusev, D. G.; Schlaf, M. Homogeneous Catalytic Hydrogenation of Long-Chain Esters by an Osmium Pincer Complex and Its Potential Application in the Direct Conversion of Triglycerides into Fatty Alcohols. *Green Chem.* **2012**, *14* (4), 1178–1188.

(42) Spasyuk, D.; Smith, S.; Gusev, D. G. Replacing Phosphorus with Sulfur for the Efficient Hydrogenation of Esters. *Angew. Chem. Int. Ed.* **2013**, *52* (9), 2538–2542.

(43) Filonenko, G. A.; Aguila, M. J. B.; Schulpen, E. N.; Van Putten, R.; Wiecko, J.; Müller, C.; Lefort, L.; Hensen, E. J. M.; Pidko, E. A. Bis-N-Heterocyclic Carbene Aminopincer Ligands Enable High Activity in Ru-Catalyzed Ester Hydrogenation. *J. Am. Chem. Soc.* **2015**, *137* (24), 7620–7623.

(44) Wylie, W. N. O.; Morris, R. H. Ester Hydrogenation Catalyzed by a Ruthenium(II) Complex Bearing an N-Heterocyclic Carbene Tethered with an "NH_2" Group and a DFT Study of the Proposed Bifunctional Mechanism. *ACS Catal.* **2013**, *3* (1), 32–40.

(45) Ogata, O.; Nakayama, Y.; Nara, H.; Fujiwhara, M.; Kayaki, Y. Atmospheric Hydrogenation of Esters Catalyzed by PNP-Ruthenium Complexes with an N-Heterocyclic Carbene Ligand. *Org. Lett.* **2016**, *18* (15), 3894–3897.

(46) Smith, A. M.; Whyman, R. Review of Methods for the Catalytic Hydrogenation of Carboxamides. *Chem. Rev.* **2014**, *114* (10), 5477–5510.

(47) Adkins, H.; Wojcik, B.; Adkins, H. Hydrogenation of Amides to Amines. *J. Am. Chem. Soc.* **1934**, *56* (1), 247.

(48) Dodds, D. L.; Cole-Hamilton, D. J. Catalytic Reduction of Amides Avoiding $LiAlH_4$ Or B_2H_6. In *Sustainable Catalysis*; Peter J. Dunn, K. K. (Mimi) Hii, Michael J. Krische, and M. T. W., Ed.; John Wiley & Sons, Inc.: Hoboken, New Jersey, 2013; pp 1–36.

(49) Hirosawa, C.; Wakasa, N.; Fuchikami, T. Hydrogenation of Amides by the Use of Bimetallic Catalysts Consisting of Group 8 to 10, and Group 6 or 7 Metals. *Tetrahedron Lett.* **1996**, *37* (37), 6749–6752.

(50) Beamson, G.; Papworth, A. J.; Philipps, C.; Smith, A. M.; Whyman, R. Selective Hydrogenation of Amides Using Rh/Mo Catalysts. *J. Catal.* **2010**, *269* (1), 93–102.

(51) Constable, D. J. C.; Dunn, P. J.; Hayler, J. D.; Humphrey, G. R.; Leazer, Jr., J. L.; Linderman, R. J.; Lorenz, K.; Manley, J.; Pearlman, B. A.; Wells, A.; et al. Key Green Chemistry Research Areas - a Perspective from Pharmaceutical Manufacturers. *Green Chem.* **2007**, *9* (5), 411–420.

(52) Yuan, M.-L.; Xie, J.-H.; Zhu, S.-F.; Zhou, Q.-L. Deoxygenative Hydrogenation of Amides Catalyzed by a Well-Defined Iridium Pincer Complex. *ACS Catal.* **2016**, *6*, 3665–3669.

(53) Rezayee, N. M.; Samblanet, D. C.; Sanford, M. S. Iron-Catalyzed Hydrogenation of Amides to Alcohols and Amines. *ACS Catal.* **2016**, *6* (10), 6377–6383.

(54) Balaraman, E.; Gnanaprakasam, B.; Shimon, L. J. W.; Milstein, D. Direct Hydrogenation of Amides to Alcohols and Amines under Mild Conditions. *J. Am. Chem. Soc.* **2010**, *132* (47), 16756–16758.

(55) Olah, G. A.; Goeppert, A.; Prakash, G. K. S. *Beyond Oil and Gas: The Methanol Economy*, 2nd ed.; Wiley-VCH Verlag GmbH & Co. KGaA: Weinheim, Germany, 2009.

(56) Jadhav, S. G.; Vaidya, P. D.; Bhanage, B. M.; Joshi, J. B. Catalytic Carbon Dioxide Hydrogenation to Methanol: A Review of Recent Studies. *Chem. Eng. Res. Des.* **2014**, *92* (11), 2557–2567.

(57) Dang, T. T.; Boeck, F.; Hintermann, L. Hidden Brønsted Acid Catalysis: Pathways of Accidental or Deliberate Generation of Triflic Acid from Metal Triflates. *J. Org. Chem.* **2011**, *76* (22), 9353–9361.

(58) Huff, C. A.; Sanford, M. S. Cascade Catalysis for the Homogeneous Hydrogenation of CO_2 to Methanol. *J. Am. Chem. Soc.* **2011**, *133* (45), 18122–18125.

(59) Huff, C. A.; Kampf, J. W.; Sanford, M. S. Role of a Noninnocent Pincer Ligand in the Activation of CO_2 at (PNN)Ru(H)(CO). *Organometallics* **2012**, *31* (13), 4643–4645.

(60) Balaraman, E.; Gunanathan, C.; Zhang, J.; Shimon, L. J. W.; Milstein, D. Efficient Hydrogenation of Organic Carbonates, Carbamates and Formates Indicates Alternative Routes to Methanol Based on CO_2 and CO. *Nature. Chem.* **2011**, *3* (8), 609–614.

(61) Han, Z.; Rong, L.; Wu, J.; Zhang, L.; Wang, Z.; Ding, K. Catalytic Hydrogenation of Cyclic Carbonates: A Practical Approach from CO_2 and Epoxides to Methanol and Diols. *Angew. Chem. Int. Ed.* **2012**, *51* (52), 13041–13045.

(62) Li, Y.-N.; Ma, R.; He, L.-N.; Diao, Z.-F. Homogeneous Hydrogenation of Carbon Dioxide to Methanol. *Catal. Sci. Technol.* **2014**, *4* (6), 1498–1512.

(63) Rezayee, N. M.; Huff, C. A.; Sanford, M. S. Tandem Amine and Ruthenium-Catalyzed Hydrogenation of CO_2 to Methanol. *J. Am. Chem. Soc.* **2015**, *137* (3), 1028–1031.

(64) Kothandaraman, J.; Goeppert, A.; Czaun, M.; Olah, G. A.; Prakash, G. K. S. Conversion of CO_2 from Air into Methanol Using a Polyamine and a Homogeneous Ruthenium Catalyst. *J. Am. Chem. Soc.* **2016**, *138* (3), 778–781.

Chapter Two. Iridium catalyzed base-free hydrogenation of lactones[*1]

2.1 Introduction

With characteristic fruity or musky odors, lactones are cyclic esters often used as components in flavors and fragrances.[2] Lactones, which can be obtained from cellulosic biomass by a combination of catalytic transformations and biochemical routes, such as fermentation, are anticipated to be important intermediates in the production of commodity chemicals from bio-derived feedstocks. The development of efficient technologies to transform lactones into commercially valuable products is of great interest.

Depolymerization of cellulosic biomass generates D-glucose, which can be subject to acid-catalyzed dehydration (Scheme 2.1).[3] The resulting hydroxymethylfurfural (HMF) can be converted to levulinic acid, while a final hydrogenation and dehydration affords γ-valerolactone (GVL). Similarly, succinic, fumaric, and malic acids can be produced by fermentation of cellulosic feedstocks[4] and converted to the respective lactones. The diol products from lactone hydrogenation can be used as chemical intermediates, plasticizers, and in lubricants.[5] GVL hydrogenation produces 1,4 pentanediol which, under acidic conditions, is dehydrated to 2-methyl tetrahydrofuran (2-MeTHF) as shown in Scheme 2.1.[6] 2-MeTHF is a (US-approved) drop-in fuel additive for gasoline.[6] It is also often marketed as a "greener" alternative to THF, benefiting from a higher boiling point, and lower propensity for peroxide formation.[7] More broadly, cyclic ethers are valuable as perfumery molecules, solvents in the polymer and pharmaceutical industries, fuels, and precursors for polymers; for example, THF is used to produce LYCRA.[8]

[*]The work in this chapter was previously published in, and is adapted with permission from Brewster, T. P.; Rezayee, N. M.; Culakova, Z.; Sanford, M. S.; Goldberg, K. I. Base-Free Iridium-Catalyzed Hydrogenation of Esters and Lactones. *ACS Catal.* **2016**, *6* (5), 3113–3117. Copyright 2016 American Chemical Society.

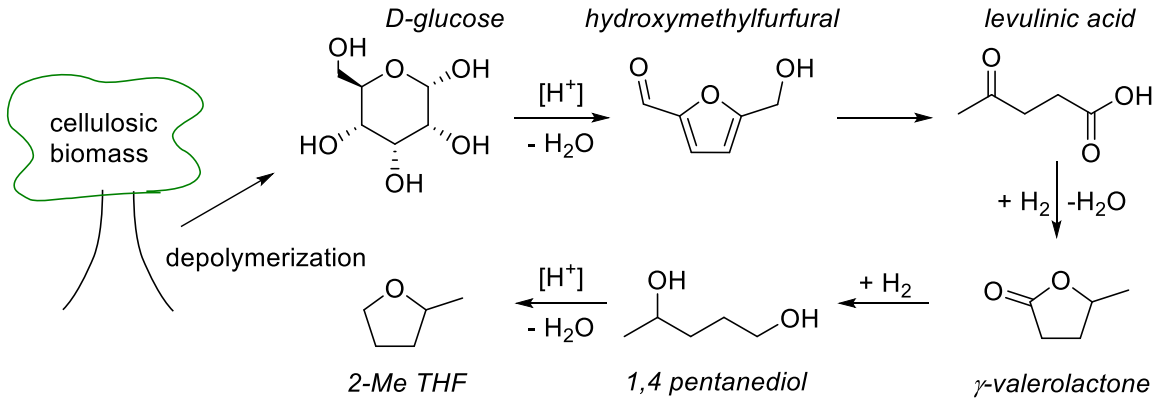

Scheme 2.1. A pathway for transformation of cellulosic biomass to commercial products

Despite recent advances, ester hydrogenation is much less thoroughly studied than other catalytic reactions, such as alkene hydrogenation, and remains a challenge for homogeneous catalysis.[9–11] Reports of homogeneous catalysts for ester hydrogenation that operate under acidic conditions are limited. The development of acid-tolerant ester hydrogenation pre-catalysts would enable their application to a wider variety of situations. For example, a cascade system pioneered by Sanford and coworkers to convert CO_2 to methanol via ester intermediates was ultimately limited by the Lewis acidic transesterification catalyst interacting with, and inhibiting the ester hydrogenation catalyst (See Chapters One, Four and Five for more detail on cascade system).[12]

The most notable reported acid-tolerant ester hydrogenation catalyst is a Ru/triphos (triphos = 1,1,1-tris(diphenylphosphinomethyl)ethane) system originally investigated by Elsevier and coworkers.[13,14] This system was subsequently further explored by Leitner and coworkers[15–17] and other groups,[18] as was a related cobalt/triphos system.[19] Ru/triphos catalyzed reduction of γ-valerolactone is efficient at elevated temperatures (≥140 °C) and pressures (≥50 bar H_2), selectively generating 1,4, propanediol.[17] Acidic additives such as *p*-toluenesulfonic acid catalyze the dehydration of diol to 2-MeTHF.[16] A mechanism for this transformation has been proposed based on experimental investigations and computational modeling, using Density Functional Theory (DFT) (Scheme 2.2). The substrate first coordinates to the Ru center via the carbonyl

oxygen. A hydride transfer from Ru-H to the carbonyl carbon is followed by proton transfer from the dihydrogen ligand to the substrate oxygen. Subsequent metal-free, acid-catalyzed ring opening of the free lactal and substrate re-coordination the metal produces a Ru-hydroxyl aldehyde intermediate. From this intermediate, hydroxyl aldehyde hydrogenation proceeds analogously to the initial lactone hydrogenation to generate the diol product.[15]

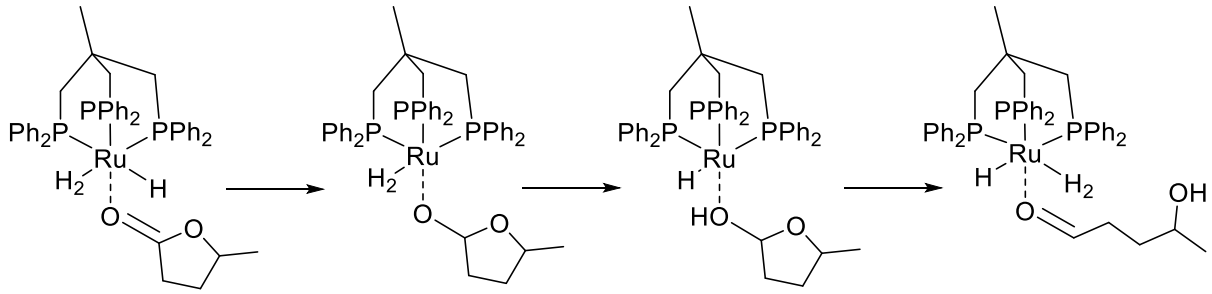

Scheme 2.2. Intermediates in a proposed mechanism for γ-valerolactone hydrogenation by Ru/triphos[15]

2.2 Prior results with Cp*Ir and motivations for studying lactone hydrogenation

Previous work in the Goldberg group identified an iridium half-sandwich complex capable of formic acid disproportionation to methanol, CO_2 and H_2O.[20] This system was then applied to related reactions, including the hydrogenation of carboxylic acid substrates.[21] In addition, several other ruthenium, iridium and rhodium half-sandwich complexes supported by bipyridine ligands were explored for carboxylic acid hydrogenation.[21] Upon optimization, [Cp*Ir(bpyOMe)(H_2O)](OTf)$_2$ (Cp* = pentamethylcyclopentadienyl anion, bpyOMe = 4,4'-dimethoxy-2,2'-bipyridine) complex **1** was identified as the most active pre-catalyst for this reaction.[21] Carboxylic acid hydrogenation using these half-sandwich complexes was proposed to proceed by a mechanism analogous to that shown in Figure 2.1. First, a proton is transferred from the highly acidic iridium dihydrogen complex to the carbonyl group. This is followed by hydride transfer to the carbonyl carbon. The acetal intermediate can further react to form an equivalent each of alcohol and aldehyde, which undergoes a second hydrogenation cycle, producing a second

equivalent of alcohol. The authors found that adding electron donating substituents to the bipyridyl ligand improved catalyst activity, as did the addition of a Lewis acid (LA) additive, scandium triflate ($Sc(OTf)_3$). They postulated that increasing the electron density at the metal leads to a more hydridic hydride that is better able to transfer to substrate, while the LA additive can activate substrate to hydride transfer by interacting with the carbonyl oxygen. In contrast to the mechanism proposed for Ru/triphos, substrate does not coordinate in the inner sphere of the half-sandwich complexes.

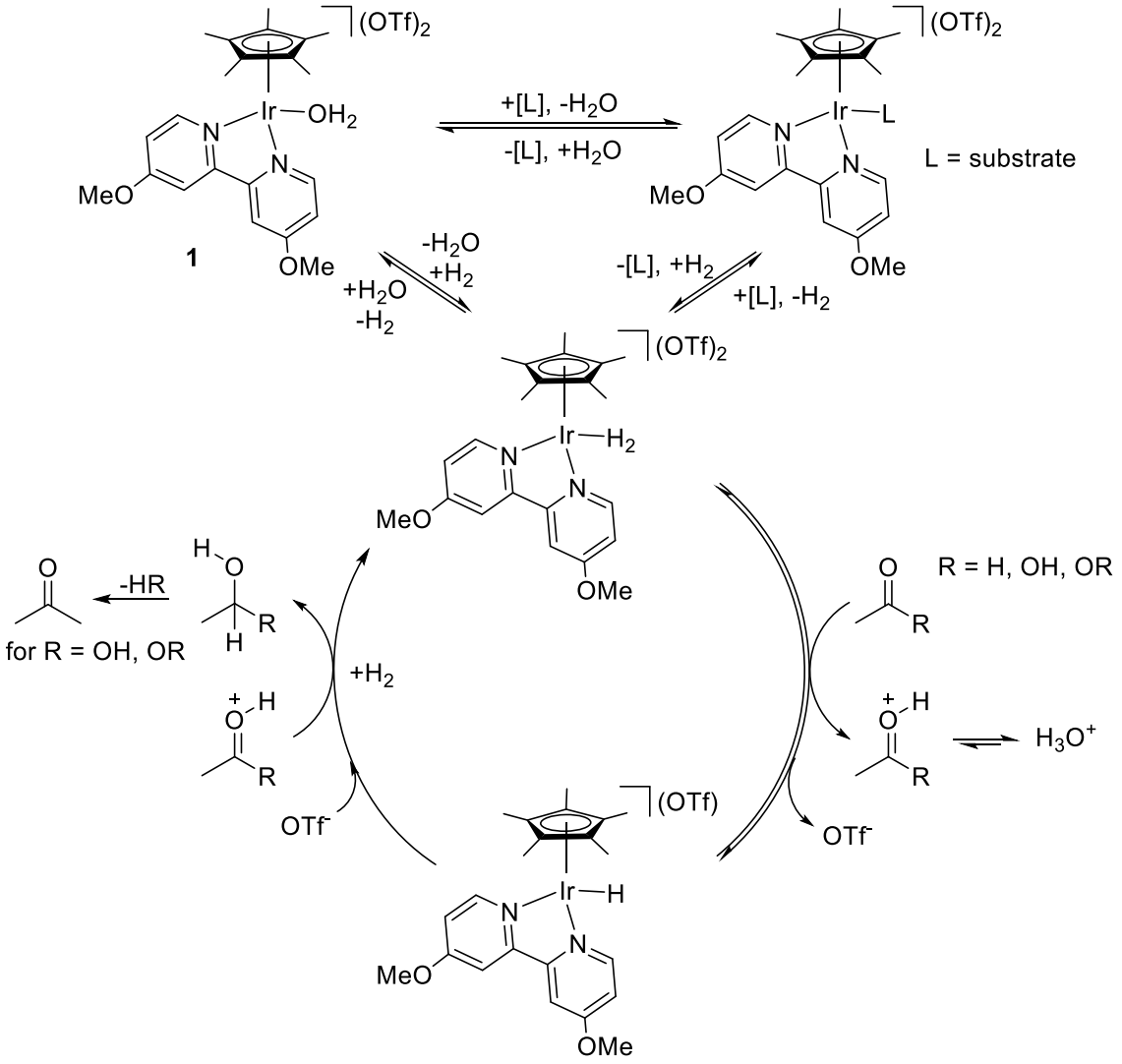

Figure 2.1. General mechanism proposed for ester and carboxylic acid hydrogenation by **1**, adapted from Brewster and coworkers[1]

We sought to generalize this chemistry to hydrogenation of ester substrates. Our group previously reported the hydrogenation of levulinic acid to 90% γ-valerolactone as well as fully reduced 2-MeTHF, indicating some hydrogenation of the cyclic ester.[21] We were interested in further understanding the reactivity of these iridium half sandwich catalysts for the hydrogenation of lactone substrates. The effect of substrate ring size and sterics near the ester on hydrogenation was investigated.

2.3 Hydrogenation of DVL and GVL by iridium pre-catalyst 1

The study of lactone hydrogenation was carried out in conjunction with additional studies of ester hydrogenation by Cp*Ir bipyridine catalysts in our group and the Sanford group.[1] The most active of the catalysts studied for carboxylic acid hydrogenation, **1**, was chosen for our studies.[21] A series of esters and lactones were screened for reactivity under a variety of conditions: neat, in ethereal solvent (1,4-dioxane), and in the presence of the $Sc(OTf)_3$. Lactones with varied ring sizes and with methyl substituents as shown in Figure 2.2 were investigated.

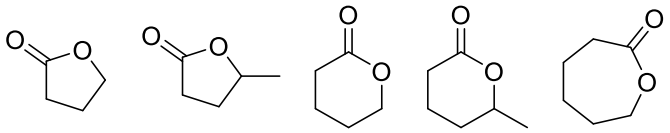

Figure 2.2 Lactone substrates investigated

Hydrogenation of the 5-membered ring γ-butyrolacone (L1) and γ-valerolactone (L2) in the presence of **1** under relatively mild conditions (100 °C, 30 bar H_2) (Table 2.1) afforded trace amounts of the corresponding diol, in addition to cyclic ether formed by acid-catalyzed dehydration (major product). Hydrogenation of L1, bearing a decreased steric profile, was more facile than for L2. This is consistent with the sensitivity to steric bulk observed for other ester substrates. Catalyst turnover number (TON) also decreased when the reaction was carried out in the ethereal solvent, dimethoxyethane (DME) rather than in neat solution. This difference in TON

may be attributed to the lower effective substrate concentration slowing the rate of hydrogenation, leading to less product generated in 16 hours.

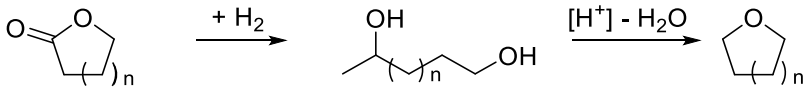

Scheme 2.3. General reaction scheme for lactone hydrogenation

Table 2.1: Hydrogenation of L1 and L2 with **1**

Solvent	Time (h)	Acid additive	L1 TON (st. dev)	L2 TON (st. dev)
Neat	16	--	291 (7)	76 (5)
Neat	16	$Sc(OTf)_3$	410 (53)	200 (19)
Neat	65	--	487 (16)	166 (54)
DME	16	--	33 (4)	27 (5)
DME	16	$Sc(OTf)_3$	23 (6)	19 (3)
DME	65	--	69 (4)	78 (6)

Neat: 2 mL substrate, 2 mM **1**, (20 mM $Sc(OTf)_3$), 30 bar H_2, 100 °C. In solvent: 1 mmol substrate, 0.5 mol% **1**, (0.5 mol% $Sc(OTf)_3$), 1 mL DME, 30 bar H_2, 100 °C. Characterization: GC-FID. TON reported as amount of cyclic ether produced, normalized to substrate quantity.

In contrast to the Ru/triphos catalyst system, **1** directly catalyzes the dehydration of diol to ether. Increased turnover with the increased reaction time (65 h vs 16 h) indicated that the catalyst is still active after 16 hours. However, the increase in TON was not proportional to the increased time, suggesting that some catalyst deactivation occurs over the course of the reaction, perhaps due to product inhibition or catalyst decomposition. In neat substrate, the presence of $Sc(OTf)_3$ increased TON, consistent with previous observations with carboxylic acids. Surprisingly, decreased activity was observed with $Sc(OTf)_3$ additive in reactions with substrates dissolved in DME. We hypothesize that competitive interactions between the LA and solvent may reduce the effectiveness of the acid in activating substrate. However, it is not clear why addition of LA in

solvent would lead to fewer TON of product generated after 16 hours than in the absence of the LA.

2.4 Water sensitivity of lactone hydrogenation

Due to the fact that water is produced in the acid-catalyzed dehydration step, we were curious about the effect of water on the activity of **1**. We found that, when reactions were conducted in THF solvent, the addition of one drop of water (approx. 100 mol%) resulted in a significant decrease in substrate conversion after 16 hours, as determined by ^{1}H NMR spectroscopy (25% conversion for sample without water, 5% conversion for samples with added water, both with and without one eq. $Sc(OTf)_3$). Based on this result, we hypothesize that inhibition by water, which is produced from dehydrative condensation of diols products to cyclic ethers, is contributing to the non-linear increase in TON at longer times.

2.5 Hydrogenation of lactones with ring size ≥ 6 by iridium pre-catalyst 1

For larger-ringed lactone substrates, L3, L4, and L5, we observed relatively rapid conversion of starting material to a mixture of products by NMR spectroscopy (Table 2.2). However, only small amounts of the product mixture could be attributed to diol or cyclic ether, as confirmed by comparison to authentic samples. Electrospray ionization mass spectroscopy revealed product masses corresponding to oligomers with ester subunits. Our evidence suggests that oligomerization outcompetes hydrogenation-dehydration to cylic ethers. For lactones with ring size ≥ 6, the rate of dehydrative polymerization of the ester subunits is competitive with the rate of hydrogenation by catalyst **1**. Conducting the reaction in DME solvent results in a higher proportion of monomeric product but does not entirely suppress oligomer formation. Ring-opening polymerization of lactones is a well-studied reaction, and is known to be catalyzed by both Lewis and Brønsted acids.[22,23] We hypothesize that, in the absence of added acids, cationic Ir-based species may be

filling this role. For example, the electrophilic Ir metal in the coordinatively unsaturated $[Cp^*Ir(bpyOMe)]^+$ complex may act as a LA, or the acidic dihydrogen complex $[Cp^*Ir(bpyOMe)(H_2)]^+$ may be the acid catalyst for diol dehydration.

Table 2.2. Hydrogenation of L3, L4, L5 with **1**

Solvent	Time (h)	Acid additive	L3	L4	L5
			% substrate consumption		
Neat	16	--	97	79	100
DME	16	--	97	100	100

Neat: 2 mL substrate, 2 mM **1**, 30 bar H_2, 100 °C. In solvent: 1 mmol substrate, 0.5 mol% **1**, 1 mL DME, 30 bar H_2, 100 °C. Characterization: ^1H NMR, $CHCl_3$ internal standard.

2.6 Conclusions

In conclusion, we found that **1** was an active catalyst for the hydrogenation of lactones with five membered rings under relatively mild conditions (100 °C, 30 bar H_2). Addition of $Sc(OTf)_3$, enhances TON when added to reactions with neat substrate, though a small decrease in activity is observed upon addition of $Sc(OTf)_3$ in 1,4-dioxane solvent. Pre-catalyst **1** directly catalyzes the dehydration of the diol intermediate to the cyclic ether, regardless of whether or not acid is added. This contrasts with the Ru/triphos system, where, diol products are converted to cyclic ethers only in the presence of added acids. Finally, we found that **1** is not an effective catalyst for hydrogenation of lactones with ring size ≥ 6, as such substrates formed oligomers under hydrogenation conditions.

2.7 Experimental details

General Considerations:

Chemicals were used as received from commercial sources unless otherwise specified. Substrates for hydrogenation were either opened and stored in a nitrogen glovebox or degassed prior to use. THF was dried by passage over activated alumina and molecular sieves. Complex **1**

was synthesized according to literature procedures.[14] Deuterated NMR solvents ($CDCl_3$, CD_2Cl_2, and CD_3CN) were obtained from Cambridge Isotope Laboratories and used as-received. Cyclic ethers tetrahydropyran,[24] 2-methyl tetrahydropyran[25] and oxepane[26] were synthesized independently by dehydration of the corresponding diol over Nafion-H.[27] These samples were used to confirm the identities of hydrogenation products.

NMR analysis: ^{1}H NMR spectra were recorded on 300 MHz or 500 MHz Bruker spectrometers and were referenced to the residual solvent peak. An internal standard was used to determine product yields in aliquots of reaction product mixture. Product identities were confirmed by addition of commercially available pure substances, when available.

GC Analysis: GC-FID analysis was performed on an Agilent Technologies 7890A GC system using an Agilent Technologies DB-FFAP column. Calibration curves were constructed for starting material, diol and cyclic ether products with reference to an internal standard using pure materials obtained from commercial sources. GC was used for substrates where all products were commercially available (γ-valerolactone and γ-butyrolactone).

ESI-MS analysis: Electrospray ionization mass spectrometry was performed by Loren Kruse at the University of Washington. All samples prepared for ESI-MS were obtained with 2 mM catalyst in 2 mL substrate heated at 100 °C for 65 hours.

GC-MS Analysis: GC-MS analysis was performed on an Aligent 5975 GC/MSD instrument. Samples were prepared by dissolving a small amount of reaction product in dichloromethane.

Representative procedures for hydrogenation

High pressure hydrogenation reactions were carried out in 30 mL Parr Instruments 5000 Multiple Reactor system vessels fitted with a PTFE liner at the stated hydrogen pressure.

Neat: In a nitrogen glovebox, 10.3 mg (0.0120 mmol) **1** was massed into a glass vial. 6 mL γ-valerolactone was added to the vial via syringe and the solution was swirled to dissolve. 2 mL aliquots of the resulting yellow solution were dispensed into each of three PTFE-lined Parr reactors with PTFE-covered stir bars. Reactors were closed and removed from the glovebox, pressurized with 30 bar H_2, and purged with a constant flow of H_2 for a minute. Reactors were heated at 100 °C for 16 hours under stirring. After the reactors were allowed to cool, excess pressure was vented. Reactors were shaken and opened in air. Product characterization was conducted as follows:

Sample preparation for NMR spectroscopy: Known volume aliquots (50.0 or 100 μL) of the reaction mixture were dispensed into an NMR tube. Known volumes of chloroform (20.0 or 40.0 μL) or benzene (20.0 μL) internal standard were added directly to the NMR tube, and an appropriate NMR solvent (CD_2Cl_2, $CDCl_3$ or CD_3CN) was added. NMR tubes were capped and shaken prior to spectrum acquisition.

Sample preparation for GC-FID analysis:

Neat: A 50.0 μL aliquot of reaction material and 10.0 μL n-propanol (internal standard) were diluted to 5.00 mL with acetone in a volumetric flask.

In Solvent: 250.0-500.0 μL sample and 10.0 μL n-propanol were diluted to 5.00 mL with acetone in a volumetric flask.

Neat, with acid additive: In a nitrogen glovebox, 19.7 mg (0.040 mmol) $Sc(OTf)_3$ was massed into a PTFE Parr reactor liner. In a glass vial, 10.5 mg (0.0122 mmol) **1** was massed out. 6 mL of γ-valerolactone was added to the vial via syringe and the solution was swirled to dissolve. A PTFE liner and stir bar was inserted into a stainless steel Parr reactor, and 2.0 mL of the catalyst/substrate solution was dispensed into the reactor. Results reported as an average of three trials using the same catalyst/substrate solution.

In solvent with acid: In a nitrogen glovebox, 4.3 mg (0.0050 mmol) pre-catalyst **1** and 2.5 mg (0.0051 mmol) $ScOTf_3$ was weighed into a PTFE Parr reactor liner. The liner with stir bar was inserted into a stainless steel Parr reactor. 1 mL dimethoxyethane and 0.095 mL of γ-valerolactone (0.99 mmol) was dispensed into the reactor via syringe. Reactor was closed, pressurized, heated, cooled and opened as above. Results reported as an average of three trials.

In solvent, no acid: Procedure identical to above, with no acid added.

Water added: A stock solution of L2 (0.25 mL, 2.61 mmol) and catalyst **1** (12.6 mg, 0.0147 mmol) in 3.0 mL THF was prepared, and 1 mL aliquots were dispensed into three PTFE-lined Parr reactors. Nothing additional was added to the first reactor. To the second reactor, one drop of H_2O (approx. 50 μL, 2.8 mmol) was added. To the third reactor, one drop of H_2O and one equivalent of $Sc(OTf)_3$ (2.2 mg, 0.0045 mmol) were added. Reactions were conducted as described above. The reaction solution was analyzed by ^1H NMR, (100 μL solution, 20 μL benzene internal standard in CD_2Cl_2).

2.8 References

(1) Brewster, T. P.; Rezayee, N. M.; Culakova, Z.; Sanford, M. S.; Goldberg, K. I. Base-Free Iridium-Catalyzed Hydrogenation of Esters and Lactones. *ACS Catal.* **2016**, *6* (5), 3113–3117.

(2) Anten, J. O. P.; Surburg, H. Flavors and Fragrances, 2. Aliphatic Compounds. In *Ullmann's Encyclopedia of Industrial Chemistry*; Wiley-VCH Verlag GmbG & Co. KGaA: Weinheim, 2015; pp 1–55.

(3) Matlack, A. S. Green Chemistry, Applications. In *Kirk-Othmer Encyclopedia of Chemical Technology*; American Cancer Society, 1990; pp 1–33.

(4) Werpy, T.; Petersen, G.; Aden, A.; Bozell, J.; Holladay, J.; White, J.; Manheim, A. Top Value Added Chemicals from Biomass Volume I — Results of Screening for Potential Candidates from Sugars and Synthesis Gas. US Department of Energy 2004, pp 1–76.

(5) Werle, P.; Moraweitz, M.; Lundmark, S.; Sörensen Kent; Karvinen, E.; Juha, L. Alcohols, Polyhydric. In *Ullmann's Encyclopedia of Industrial Chemistry*; 2008; Vol. 8, pp 255–271.

(6) Huber, G. W.; Iborra, S.; Corma, A. Synthesis of Transportation Fuels from Biomass: Chemistry, Catalysts, and Engineering. *Chem. Rev.* **2006**, *106* (9), 4044–4098.

(7) Greener Solvent Alternatives. Sigma-Aldrich Co, LLC.: St. Louis, MO 2015, pp 1–4.

(8) Saudan, L. A. Hydrogenation of Esters. In *Sustainable Catalysis*; Dunn, P. J., Hii, K. K. (Mimi), Kirsche, Michael, J., Williams, M. T., Eds.; John Wiley & Sons, Inc.: Hoboken, New Jersey, 2013; pp 37–61.

(9) Dub, P. A.; Ikariya, T. Catalytic Reductive Transformations of Carboxylic and Carbonic Acid Derivatives Using Molecular Hydrogen. *ACS Catal.* **2012**, *2* (8), 1718–1741.

(10) Clarke, M. L. Recent Developments in the Homogeneous Hydrogenation of Carboxylic Acid Esters. *Catal. Sci. Technol.* **2012**, *2* (12), 2418.

(11) Werkmeister, S.; Junge, K.; Beller, M. Catalytic Hydrogenation of Carboxylic Acid Esters, Amides, and Nitriles with Homogeneous Catalysts. *Org. Process Res. Dev.* **2014**, *18*, 289–302.

(12) Huff, C. A.; Sanford, M. S. Cascade Catalysis for the Homogeneous Hydrogenation of CO_2 to Methanol. *J. Am. Chem. Soc.* **2011**, *133* (45), 18122–18125.

(13) Teunissen, H. T.; Elsevier, C. J. Ruthenium Catalysed Hydrogenation of Dimethyl Oxalate to Ethylene Glycol. *Chem. Commun.* **1997**, 667–668.

(14) Teunissen, H. T.; Elsevier, C. J. Homogeneous Ruthenium Catalyzed Hydrogenation of Esters to Alcohols. *Chem. Commun.* **1998**, *3* (13), 1367–1368.

(15) Geilen, F. M. a; Engendahl, B.; Hölscher, M.; Klankermayer, J.; Leitner, W. Selective Homogeneous Hydrogenation of Biogenic Carboxylic Acids with [Ru(TriPhos)H]+: A Mechanistic Study. *J. Am. Chem. Soc.* **2011**, *133* (36), 14349–14358.

(16) Geilen, F. M. A.; Engendahl, B.; Harwardt, A.; Marquardt, W.; Klankermayer, J.; Leitner, W. Selective and Flexible Transformation of Biomass-Derived Platform Chemicals by a Multifunctional Catalytic System. *Angew. Chem. Int. Ed.* **2010**, *49* (32), 5510–5514.

(17) vom Stein, T.; Meuresch, M.; Limper, D.; Schmitz, M.; Hölscher, M.; Coetzee, J.; Cole-Hamilton, D. J.; Klankermayer, J.; Leitner, W. Highly Versatile Catalytic Hydrogenation of Carboxylic and Carbonic Acid Derivatives Using a Ru-Triphos Complex: Molecular Control over Selectivity and Substrate Scope. *J. Am. Chem. Soc.* **2014**, *136* (38), 13217–13225.

(18) Latifi, E.; Marchese, A. D.; Hulls, M. C. W.; Soldatov, D. V.; Schlaf, M. $[Ru(Triphos)(CH_3CN)_3](OTf)_2$ as a Homogeneous Catalyst for the Hydrogenation of Biomass Derived 2,5-Hexanedione and 2,5-Dimethyl-Furan in Aqueous Acidic Medium. *Green Chem.* **2017**, *19*, 4666–4679.

(19) Korstanje, T. J.; Ivar van der Vlugt, J.; Elsevier, C. J.; de Bruin, B. Hydrogenation of Carboxylic Acids with a Homogeneous Cobalt Catalyst. *Science* **2015**, *350* (6258), 298–302.

(20) Miller, A. J. M.; Heinekey, D. M.; Mayer, J. M.; Goldberg, K. I. Catalytic Disproportionation of Formic Acid to Generate Methanol. *Angew. Chem. Int. Ed.* **2013**, *52* (14), 3981–3984.

(21) Brewster, T. P.; Miller, A. J. M.; Heinekey, D. M.; Goldberg, K. I. Hydrogenation of Carboxylic Acids Catalyzed by Half-Sandwich Complexes of Iridium and Rhodium. *J. Am. Chem. Soc.* **2013**, *135* (43), 16022–16025.

(22) Lecomte, P.; Jérôme, C. Recent Developments in Ring-Opening Polymerization of Lactones. *Adv. Polym. Sci.* **2012**, *245*, 173–218.

(23) Sarazin, Y.; Carpentier, J. F. Discrete Cationic Complexes for Ring-Opening Polymerization Catalysis of Cyclic Esters and Epoxides. *Chem. Rev.* **2015**, *115* (9), 3564–3614.

(24) Chu, P.-S.; True, N. S. Pressure-Dependent Gas-Phase NMR Studies of Tetrahydropyran Ring Inversion. *J. Phys. Chem.* **1985**, No. 12, 2625–2630.

(25) Jeong, Y.; Kim, D. Y.; Choi, Y.; Ryu, J. S. Intramolecular Hydroalkoxylation in Brønsted Acidic Ionic Liquids and Its Application to the Synthesis of (±)-Centrolobine. *Org. Biomol. Chem.* **2011**, *9* (2), 374–378.

(26) Spectral Database for Organic Compounds (SDBS); proton NMR spectrum; SDBS No.: 10291; RN 592-90-5 http://riodb01.ibase.aist.go.jp/sdbs/ (accessed Jul 1, 2014).

(27) Olah, G. A.; Fung, A. P.; Malhotra, R. Synthetic Methods and Reactions; 99. Preparation of Cyclic Ethers over Superacidic Perfluorinated Resinsulfonic Acid (Nafion-H) Catalyst. *Synthesis* **1981**, *6*, 474–476.

Chapter Three. A computational investigation of the mechanism of ester and amide hydrogenation by PNP-supported pre-catalysts[†‡]

3.1 Introduction

3.1.1 Motivations for computational studies on PNP-supported ester and amide hydrogenation catalysts

Aliphatic pincer complexes of Fe and Ru are efficient catalysts for ester[2,3] and amide[4–8] hydrogenation. However, hydrogenations with these catalysts require high temperature (≥ 100 °C) and pressures (≥ 30 bar) and are thus carried out in high-pressure reactors. This limits the ability of most laboratories to carry out *in situ* monitoring, conduct kinetic studies, or even observe catalyst speciation under reaction conditions. Owing to the difficulty of conducting mechanistic studies with these complexes, we have turned to computational studies to help elucidate these mechanisms. We hope that developing an understanding of the mechanism for substrate hydrogenation with these pre-catalysts will aid in the rational design of new hydrogenation catalysts that operate under milder conditions, are stable to oxygen and moisture, and are compatible with other pre-catalysts used in CO_2 to methanol cascades, as described in Chapter One. Additionally, we are interested in the mechanistic origin of the reported selectivity for C-N bond cleavage over C-O bond cleavage by these pincer-supported pre-catalysts.

[†] This work was carried out with guidance from Prof. Odile Eisenstein and Prof. Eric Clot at the Chimie Théorique, Méthodologies, Modélisation group at the Université de Montpellier 2, in Montpellier, France. I gratefully acknowledge support from a Chateaubriand STEM Fellowship, administered by the Embassy of France in the United States, which enabled a 6-month stay in France from January to July 2016.

[‡] A portion of the work in this chapter was previously published in, and is adapted with permission from Artús Suàrez, L.; Culakova, Z.; Balcells, D.; Bernskoetter, W. H.; Eisenstein, O.; Goldberg, K. I.; Hazari, N.; Tilset, M.; Nova, A. The Key Role of the Hemiaminal Intermediate in the Iron-Catalyzed Deaminative Hydrogenation of Amides. *ACS Catal.* **2018**, 8751–8762.[1] Copyright 2018 American Chemical Society.

Shvo-and Noyori-type pre-catalysts incorporate bifunctional ligands that have been found to be valuable in catalytic hydrogen transfer reactions. While these catalysts are not active for ester or amide hydrogenation, they are effective catalysts for hydrogenation of ketones and related substrates. Extensive mechanistic studies have been carried with both catalysts, providing insight into the exact role of the bifunctional ligand and a starting point for investigating mechanisms of other hydrogenation catalysts. Differences in these mechanisms will be discussed to give a framework for mechanistic investigations into the hydrogenation by aliphatic PNP-supported catalysts discussed in this chapter.

3.1.2 Shvo's catalyst: evolving mechanistic understanding

The Shvo catalyst was first reported in 1984 by Youval Shvo and colleagues,[9] and has since been found to catalyze a diverse range of oxidative and reductive reactions, including hydrogenation of alkenes, alkynes and carbonyl substrates with H_2, hydroboration of aldehydes, ketones and imines, dehydrogenative coupling of alcohols to esters, and alkylation of amines with alcohols.[10] The pre-catalyst is an air-stable dinuclear species, **A**, shown in Figure 3.1. The cyclopentadienone ligand enables the catalyst to facilitate oxidation and reduction by storing proton equivalents on the ligand; hydride equivalents are stored on the Ru center. Disproportionation of the dimer leads to two species, a reducing 18 electron Ru(II) with cyclopentanol and hydride ligands (**A2**), and an oxidizing 16 electron Ru(0) with cyclopentanone and an open site (**A1**).[11]

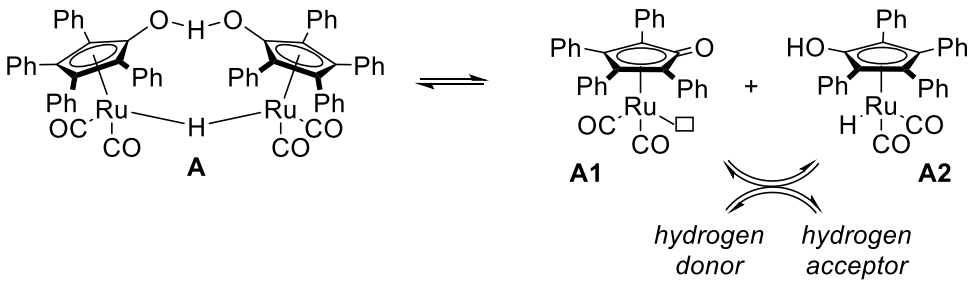

Figure 3.1 Shvo pre-catalyst (**A**) and suggested disproportionation into catalytically relevant species (**A1** and **A2**)

The mechanisms for oxidations and reductions by Shvo's pre-catalyst have been investigated in extensive computational and experimental studies.[11] We will focus here on the mechanism of carbonyl (ketone and aldehyde) reduction and the reverse dehydrogenation reaction, as they are most relevant to the carbonyl substrates presented in this chapter.

The 18-electron species, **A2**, pictured above has been hypothesized to be a crucial intermediate in reactions with Shvo's pre-catalyst, and a number of mechanistic studies have suggested that the hydrogen transfer to carbonyl substrates occurs in a concerted fashion from this complex.[11,12] Two general mechanisms were commonly suggested for hydrogenations/dehydrogenations: an inner-sphere mechanism where the substrate coordinates directly to the metal center, (Shvo[13,14] and Bäckvall[15–17]) or an outer-sphere mechanism, where the substrate does not coordinate to the Ru center, supported by Casey[18] (Figure 3.2). Suggested transition states for each mechanism are shown in Figure 3.2; both mechanisms include **A2**, as well as **A1** (which has never been experimentally observed), as prominent intermediates. Based on these mechanisms, it has been suggested that preventing catalyst dimerization, and thus ensuring a higher effective concentration of **A1**, will result in a more efficient catalyst. Casey and coworkers sought to achieve this by replacing the hydroxy group on the cyclopentadiene ring with a bulkier phenylamine, to make [2,5-dimethyl$_2$-3,4-diphenyl(η^5-C$_4$CNHPh)]Ru(CO)$_2$H.[19] They found that this complex is slow to hydrogenate benzaldehyde, and attribute this drawback to the

reduced acidity of the phenylamine and thus diminished ability to protonate carbonyl groups during reduction. Protonation of the complex with triflic acid resulted in a much more acidic protonated phenylamine and rapid benzaldehyde hydrogenation, but the difficulty of protonating the complex is expected to impede its ability to cleave hydrogen.[19,20]

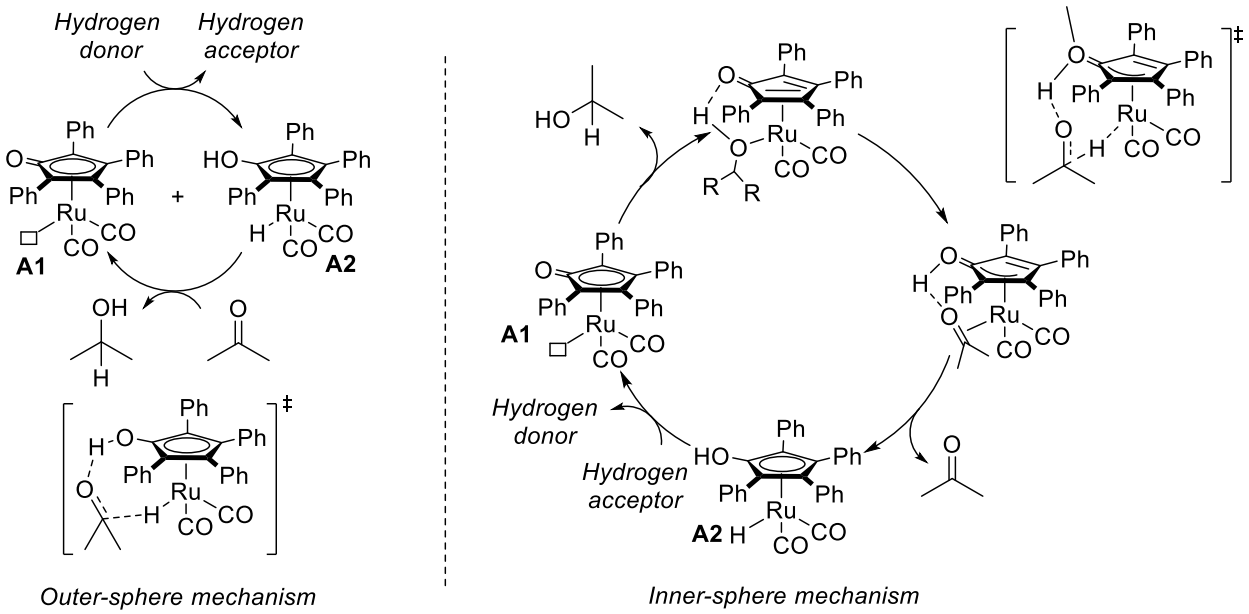

Figure 3.2. Two mechanisms suggested for dehydrogenation (as drawn) and hydrogenation (microscopic reverse) of carbonyl substrates by Shvo's catalyst[11]

Casey and coworkers report experimental evidence against a ring-slip inner sphere mechanism. They found that substituting the cyclopentadienol proton for $SiEt_3$ impedes the H-D exchange between the ruthenium hydride and aldehyde (PhCDO). If a ring-slip mechanism were operative, the $SiEt_3$ complex would still be expected to be susceptible to ring slip and H-D exchange.[18] Recent calculations reveal a low barrier (8 kcal mol^{-1}) for outer sphere hydrogen transfer from 18 electron **A2** to formaldehyde, in contrast to inner-sphere mechanisms involving ring slippage, which were calculated to be at least 34 kcal mol^{-1} higher.[21] An outer-sphere mechanism is also used in the construction of a kinetic model for benzaldehyde and acetophenone hydrogenation by a Shvo catalyst with a [2,5-diphenyl-3,4-ditolyl] cyclopentadienone ligand that accurately reproduced the kinetic behavior of the reactions.[19]

Our understanding of the mechanism has changed over time as new experimental and computational studies have been disclosed. A very recent study of aldehyde disproportionation and related reactions by Gusev and coworkers has suggested a slightly different mechanism. Their calculations support a mechanism that avoids the formation of **A1**. Very slow reactions of **A2** with ethanol suggest that the inner sphere pathway in Figure 3.2 is unlikely; the modern mechanism proposed by Gusev and coworkers for hydrogenation/dehydrogenation reactions by Shvo's catalyst is reproduced in Scheme 3.1.

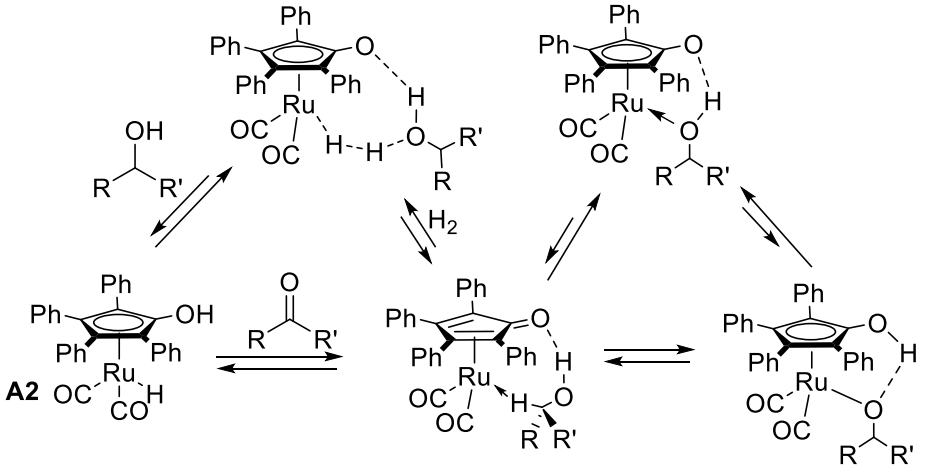

Scheme 3.1. Modern mechanistic proposal for carbonyl hydrogenation/dehydrogenation reactions with Shvo catalyst adapted from Gusev and coworkers[22]

These detailed studies of carbonyl hydrogenation/alcohol dehydrogenation by Shvo's catalyst are notable for a few reasons. Our understanding of this seemingly simple catalyst system has continued to evolve over a 40 year period. There is strong evidence for the formal involvement of the cyclopentadienone oxygen as a basic site that orients substrates and assists hydride transfers. However, while trapping studies were used as evidence for the accessibility of **A1**, Gusev *et al* have demonstrated that, in fact, **A1** is not catalytically relevant.[22] Gusev's study concludes by using the newly developed mechanistic understanding to make recommendations for improving the next generation of Shvo-type catalysts. Specifically, Gusev suggests that energy of reaction of the 18 electron **A2**-like species with an alcohol be within 2 kcal mol^{-1} of the reaction product (the

18 electron Ru-alkoxide and H_2), to ensure the availability of catalytically relevant intermediates. The authors suggest that DFT calculations will be an effective tool for identifying next-generation pre-catalysts with the necessary attributes. We likewise hypothesize that DFT studies will give insight into hydrogenation mechanisms by (PNP)-based pre-catalysts, that allow for the identification of improved systems.

3.1.3 Noyori-type catalysts: evolving mechanistic understanding

Ketones are one of the most commonly hydrogenated substrates, and as pro-chiral molecules, they are a platform for the synthesis of chiral secondary alcohols. However, in the 1990s, Noyori, Ikariya and coworkers developed complexes shown in Figure 3.3 for asymmetric ketone hydrogenation (**B**) and transfer hydrogenation (**C**).[23] Since then, extremely active and selective catalysts that are industrially relevant have been developed based on these systems. In an example published by researchers from Takasago Chemical Corporation, a ruthenium-based pre-catalyst with a xylyl-BINAP ligand (BINAP = 2,2′-bis(diphenylphosphino)-1,1′-binaphthyl), 0.001 mol%) achieved 35,000 TON min^{-1}, with >99% ee for the hydrogenation of acetophenone to 1-phenylethanol at 51 bar H_2 and ambient temperature.[24]

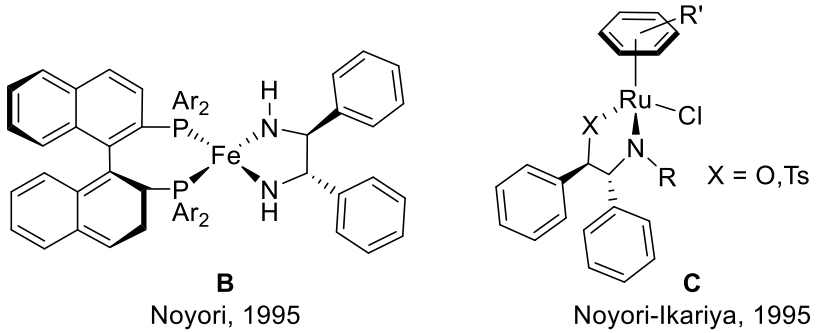

B Noyori, 1995 **C** Noyori-Ikariya, 1995

Figure 3.3. Noyori and Noyori-Ikariya pre-catalysts **B** and **C**[25]

Similar to the Shvo pre-catalyst, the unprecedented activity of these complexes was attributed to the ability of the ligand amine to assist in hydrogen transfer, termed bifunctional metal/ligand

catalysis by Noyori and coworkers.[26] Important transition states implicated in this mechanism are shown in Figure 3.4. Consistent with available experimental and computational studies, hydrogen transfer between catalyst and substrate was thought to occur through one concerted hydrogen transfer transition state. Similarly, hydrogen cleavage is described as a one-step process, assisted by a proton shuttle.[27] These fundamental mechanistic steps have formed the basis for conventional understanding of outer-sphere hydrogenations.[28–31]

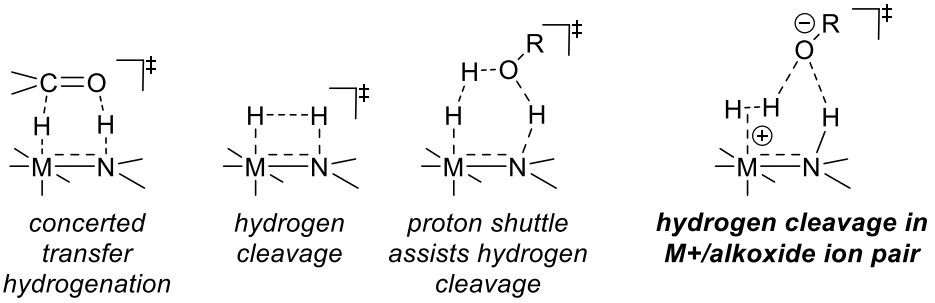

Figure 3.4. Key transition states suggested for transfer hydrogenation and hydrogen cleavage by Noyori-type catalysts[23]

However, recent computational studies suggest a more nuanced situation. With a higher level of theory and the inclusion of explicit solvent molecules, the hydrogen transfer is found to be formally asynchronous. An outer-sphere hydride transfer generates an ion-pair intermediate, while the six membered concerted transfer hydrogenation transition state pictured in Figure 3.4 is only observed in the gas phase.[32–34] This intermediate is a "branching point", and accesses a new pathway for H_2 cleavage that is found to be competitive with proton-shuttle-assisted hydrogen cleavage, where the alkoxide generated serves as a base to deprotonate the metal-bound H_2 (Figure 3.4).[23,34] With this branching point, the lowest energy hydrogenation pathway allows the N-H moiety to be retained, and the ligand is formally a spectator throughout the cycle and thus considered "chemically innocent". However, the N-H does still assist in orientation and stabilization of substrate, allowing it to "dock" at the metal center, facilitating hydrogen transfer.

The amine ligands in Noyori-like catalysts are therefore still considered to have a cooperative effect. Indeed, substitution of N-H for N-Me has been shown to dramatically decrease catalyst activity.[35] This distinction in mechanism has implications for pre-catalyst design; understanding the stabilizing role of the N-H moiety will encourage the development of catalyst variations that can better stabilize and lower the energy of the H-transfer transition states.[23,36]

3.1.4 Ester and amide hydrogenation by aliphatic PNP complexes

As described in Chapter One, homogeneous pre-catalysts with basic nitrogen sites on the ligand have recently been developed for the hydrogenation of carbonyl substrates. Ruthenium and iron-based carbonyl complexes with an aliphatic PNP pincer ligand (PNP = $N(CH_2CH_2PR_2)_2$), (Figure 3.5, (PNP)M(CO))) are selective and efficient catalysts for a wide range of transformations, including ester[2,37–40] and amide hydrogenation[5,6,8] as well as the reverse dehydrogenative reactions.[37,41–45] These catalysts are selective for C-N bond cleavage in the hydrogenation of amides.

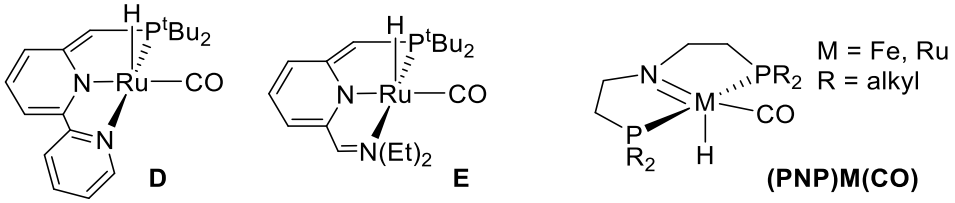

Figure 3.5. Selected ester hydrogenation catalysts[46–48]

A number of groups have performed relevant calculations investigating C-N vs C-O bond cleavage and the formation of esters and amides, respectively, facilitated by Milstein's complexes (Figure 3.5, **D** and **E**) and variants.[46–48] The activity of these pre-catalysts is attributed to the ability to store an H_2 equivalent across the metal and basic site on the ligand arm (see Chapter 1). Analogous computational studies have been carried out on aliphatic (PNP)M(CO) complexes (M = Fe, Ru) and include investigations into methanol dehydrogenation to form CO_2[49,50] and ester

hydrogenation/dehydrogenative coupling of alcohols to form esters.[37,51,52] Most closely related to the studies on ester and amide hydrogenation reported herein is a recent publication by Beller and coworkers, which investigates the hydrogenation of methyl benzoate by (^{iPr}PNP)M(CO), (M = Fe, Ru, and Os).[53] In these studies, the PNP imine group is suggested to be the basic site that assists in hydrogen/dehydrogenation by storing a proton equivalent.

As with the Noyori and Milstein pre-catalysts, the availability of the backbone nitrogen has been implicated as a requirement for efficient hydrogenation. Beller and coworkers found that alkylation of the PNP amine completely inhibited the hydrogenation of methyl benzoate, using two pre-catalysts (^{iPr}PN^{Me}P)Fe(H)$_2$(CO), ^{iPr}PN^{Me}P = bis[2-diisopropylphosphino)ethyl]methyl amine), and (^{iPr}PN^{Me}P)Fe(H)(BH$_4$)(CO). The secondary amine containing (^{iPr}PN^{H}P)Fe(H)(BH$_4$)(CO) was very active for the hydrogenation of methyl benzoate, achieving 97% yield after 6 hours at 100 °C and 30 bar H_2 in THF using 1 mol% Fe. This result shows that accessing a PNP species with protonated nitrogen is essential to catalytic activity and so corroborates an outer-sphere mechanism that includes hydrogenation of the carbonyl substrate by (^{iPr}PN^{H}P)Fe(H)$_2$(CO).[39] Likewise, alkylated (^{iPr}PN^{Me}P)Ru(H)(Cl)(CO) and KOH activator was found to be 2.5 times less active than the equivalent ^{iPr}PNP for the dehydrogenation of MeOH to CO_2.[54] In a related study, Beller and coworkers found that the hydrogenation of 4-phenylbenzonitrile was efficiently catalyzed by pre-catalyst (^{iPr}PN^{H}P)Fe(H)(BH$_4$)(CO), but the methylated pre-catalyst was inactive for nitrile hydrogenation. Once again, the mechanism is proposed to be a concerted outer-sphere hydrogen transfer to substrate.[55] These studies suggest that the backbone nitrogen plays a significant role in ester hydrogenation, and perhaps also amide hydrogenation by aliphatic PNP complexes.

Interestingly, the nitrogen basic site does not fulfill the same role with all substrates and metals. Recent work by Bernskoetter and coworkers investigated the hydrogenation of CO_2 to formate in the presence of base 1,8-diazabicyclo[5.4.0]undec-7-ene (DBU) using (^{iPr}PNP)Co(CO)$_2$(Cl).[56] They found that methylation of the ligand amine improved catalyst activity 50-fold over a protonated ligand backbone. Structural parameters and electrochemical measurements detected no significant electronic differences between the complexes. Similarly, Hazari, Bernskoetter and coworkers demonstrated a similar effect in the iron-catalyzed hydrogenation of CO_2 to formate[57] (Figure 3.6). They found that, for both pre-catalysts, the resting state of the catalyst is the formate-bound complex resulting from CO_2 insertion into the Fe-H bond. Displacement of this formate is likely the rate limiting step in both CO_2 hydrogenation and the reverse formic acid dehydrogenation reaction. The increase in activity with an alkylated nitrogen is attributed to the disruption of a stabilizing N-formate interaction, facilitating formate extrusion from the catalyst.

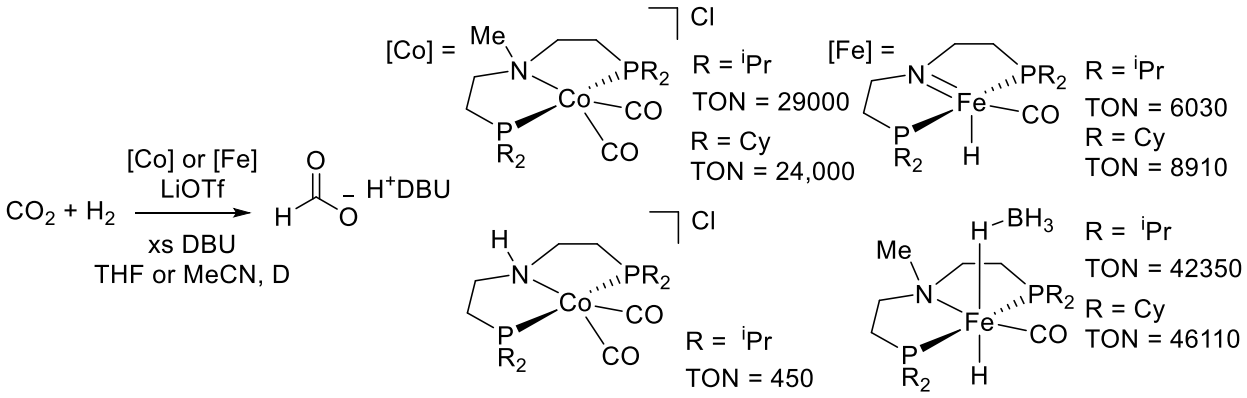

Figure 3.6. CO_2 hydrogenation by methylated and protonated PNP complexes of Co and Fe. Conditions for Co: 3 μmol catalysts, 3.6 g DBU, 500 mg LiOTf, 5 mL MeCN, 34.5 bar CO_2, 34.5 bar H_2, 45 °C, 16 h, average of three runs.[56,58] Conditions for Fe: 70 bar 1:1 H_2/CO_2, 0.3 μmol catalyst, 10 mL THF, 3.6 g DBU, 7.5:1 BDU/LiOTf, 80 °C[57]

3.1.5 Ester and amide hydrogenation by aliphatic PNP complexes

We sought to elucidate the mechanism for hydrogenation of carboxylic acid derivatives (HC(O)ER, where E = NR' or O, R,R' = alkyl) into alcohol and a second equivalent of alcohol (E = O) or amine (E = NR') using aliphatic PNP complexes of Fe and Ru (Scheme 3.2). We aimed to understand similarities and differences between hydrogenation of several reactants, specifically ester, amide, and aldehydes that are produced as a side product and also enter the catalytic cycle (HC(O)X, X = NR_2, OR, H), so that we could design improved cascade systems for CO_2 conversion to MeOH. With this goal in mind, we also investigated CO_2 as another "carbonyl" derivative, with focus on rationalizing the experimentally observed inhibition of hydrogenation activity in the presence of CO_2.

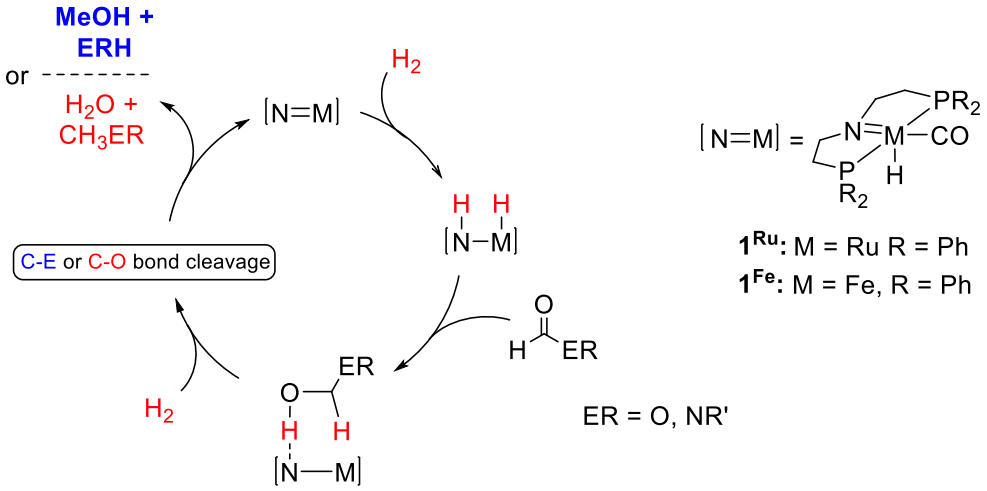

Scheme 3.2. Generalized mechanism for ester/amide hydrogenation by $\mathbf{1^{Ru}}$ and $\mathbf{1^{Fe}}$

A generalized mechanism for ester or amide hydrogenation by PNP-supported complexes of Fe or Ru is shown in Scheme 3.2. The cycle begins with dihydrogen cleavage across the M-N bond. Next, transfer hydrogenation to the substrate results in an intermediate hemiaminal or hemiacetal. This intermediate reacts further to cleave the C-E bond and produce an aldehyde, which is subjected to a second hydrogenation cycle. In the case of ester hydrogenation, the overall

reaction produces two equivalents of alcohol, and for amide hydrogenation, and alcohol and amine are generated. A concern in reactions involving amides is the selectivity of the step proceeding the hydrogenation. The hemiaminal intermediate species that is formed can either undergo cleavage of the C-N bond or the C-O bond. All (^{R}PNP)Ru and Fe complexes studied to date are selective for C-N bond cleavage and the work described in this chapter addresses the origin of this selectivity.

3.2 Results and discussion of computational investigations

3.2.1 Structure of the pre-catalyst

We note that the calculated structure of the (^{iPr}PNP)Fe(CO) is in good agreement with the published solid state structure.[59] In particular, the calculated Fe-N and Fe-CO bond lengths are well reproduced; 1.730 and 1.870 Å respectively (calculated) vs 1.8569(7) and 1.7320(9) Å (experimental). The calculations also reproduce the distorted trigonal bipyramidal structure expected in d^6 ML_5 complexes with π-donating ligands.[60] The calculated geometry of (^{Ph}PNP)Fe(CO), for which an experimental crystal structure is unavailable, is also very similar, with a Fe-C distance of 1.726 Å, and a Fe-N distance of 1.864 Å, suggesting that the changing R = ^{i}Pr to R = Ph does not have a significant effect on the structure. These data suggest that our calculation methodology is appropriate for this system. Crystal structures for the analogous (^{iPr}PNP)Ru(CO) or complexes with R = Ph were not available at the time of this study.

3.2.2 Hydrogen addition and cleavage

Hydrogen coordination and cleavage across the M=N bond (Figure 3.7) is the first step in the catalytic scheme. Even though the hydrogen cleavage mechanism has been established in several previous works,[37,39,51–54] we will discuss it briefly to have a coherent description of the reaction at

the present level of calculations. Coordination of H_2 is endoergic, indicating a weak coordination energy of dihydrogen. The calculated M-H_2 bond dissociation energy, ΔH, is 0.3 and 3.2 kcal mol^{-1} for Fe and Ru respectively. This weak interaction is likely due to the large *trans*-influence of the hydride and limited back-donating power of the metal (that is interacting strongly with CO).[61] As expected, the H_2 ligand is aligned with the P-M-P bond and stabilized by a backbonding interaction between the H_2 σ* and the metal d orbital.[62,63] The orthogonal N-M-CO axis is disfavored as the associated metal d orbital is already engaged in backbonding with the CO ligand.

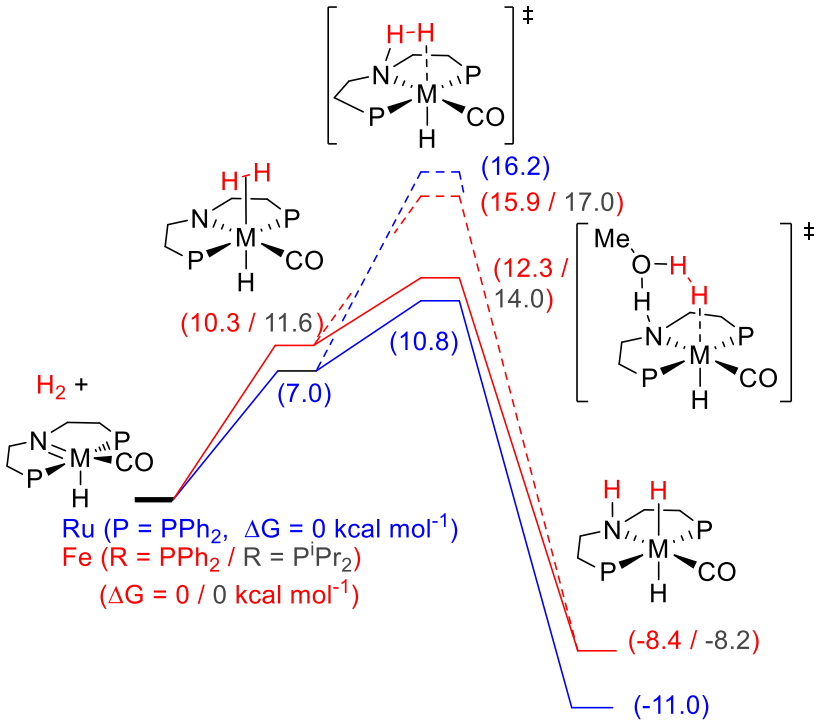

Figure 3.7. Hydrogen cleavage without (solid line) and with (dashed line) an implicit molecule of MeOH

The hydrogenated product is calculated to be exoergic by 8.4/11.0 kcal mol^{-1} (Fe/Ru) relative to separated reactant and H_2. These values agree with those published by the groups of Yang,[51] Guan,[52] and Hazari.[37] Experimentally Schneider, Jones and coworkers,[37] and Beller and coworkers[39] report facile H_2 addition to (^{iPr}PNP)Fe(CO), along with H_2 elimination under vacuum.

We confirmed that for Fe, the substitution of (^{Ph}PNP) by (^{iPr}PNP) does not notably affect these barriers (grey, Figure 3.7).

A computational study by Goldman and coworkers describes thermodynamic corrections for non-standard conditions. They find that the difference between standard conditions and a reduced hydrogen pressure, (p_{H2} = 1.0 x 10^{-7} bar) is approximately 32.0 entropy units, (9.5 kcal mol^{-1} at 298 K) for a state that includes free H_2.[64] When this correction is applied to the energies shown in Figure 3.7, H_2 cleavage and dissociation by (PNP)M(CO) is expected to be nearly thermodynamically neutral, and thus attainable under vacuum. However, our results contradict the recent computational report from Beller and coworkers, who find hydrogen cleavage to be isoergic under standard conditions.[53] Our calculations are consistent with available experimental results and most theoretical studies. Additional calculations suggest that alternative mechanisms for H_2 coordination and cleavage involving CO dissociation (35.9 kcal mol^{-1} for Ru) and phosphorus arm dissociation (24.5 kcal mol^{-1}) are unlikely to contribute to the overall mechanism.

3.2.3 Hydrogenation of esters to alcohols

A number of groups have employed DFT to investigate the mechanism of ester hydrogenation and related reactions by Ru and Fe PNP complexes, particularly focusing on the hydrogen transfer between catalyst and substrate.[37,51–53] To enable direct comparisons, we calculated a pathway for ester hydrogenation with our computational methodology.

The overall Gibbs energy profile for methyl formate hydrogenation is shown in Figure 3.8. The hydrogenation of methyl ester into two methanol molecules is exoergic overall by 14 kcal mol^{-1}. Intermediate **a** shows the substrate coordinating to catalyst via the electrostatic interaction of the carbonyl oxygen to the ligand nitrogen. This positions the carbonyl carbon above the

hydride, and the transition state for transferring the hydride (TS1) is 6.7/6.1 kcal mol^{-1} (Fe/Ru) above the adduct. The product of the hydride transfer, **b**, is a high-lying intermediate. Proton transfer follows with essentially no barrier (TS2) to form **c**, the hemiacetal adduct weakly bound to the metal amido complex. Rotation of the substrate within the metal coordination sphere gives **d**, a more stable intermediate where the methoxy oxygen, rather than the hydride, is coordinated to the metal. This intermediate releases formaldehyde with no detectable activation barrier (TS3 for Ru). No equivalent transition state could be detected for Fe, and a relaxed scan of the relevant C-O bond distance confirms that the potential energy surface is flat. Complex **e** can release methanol with a barrier of 21.0/22.5 kcal mol^{-1} (Fe/Ru) (TS4). The resulting five-coordinate complex (**f**) is re-hydrogenated (**g**) and can further hydrogenate formaldehyde with no detectable barrier, consistent with reported calculations.[37,54] Further hydrogenation regenerates the starting metal complex. We note that calculated energies are very similar for Fe and Ru; there is not a significant difference in the ability of the Fe and Ru complexes to transfer hydrogen to the ester substrate.

Due to the difference in magnitude of the entropic contributions, some intermediates are positioned higher than their respective transition state. In all cases, the endpoint enthalpies are confirmed to be lower than the transition states enthalpies. The overall highest point on this Gibbs free energy surface is 25.9/26.9 kcal mol^{-1} (Fe/Ru) (TS H_2 split), which is consistent with the requirement of heating for the reaction to proceed. This point corresponds to the hydrogen cleavage by the catalyst prior to hydrogen transfer to formaldehyde. A larger network of molecules is expected to assist with hydrogen bonding, likely further lowering the energy of this transition state.[65–67]

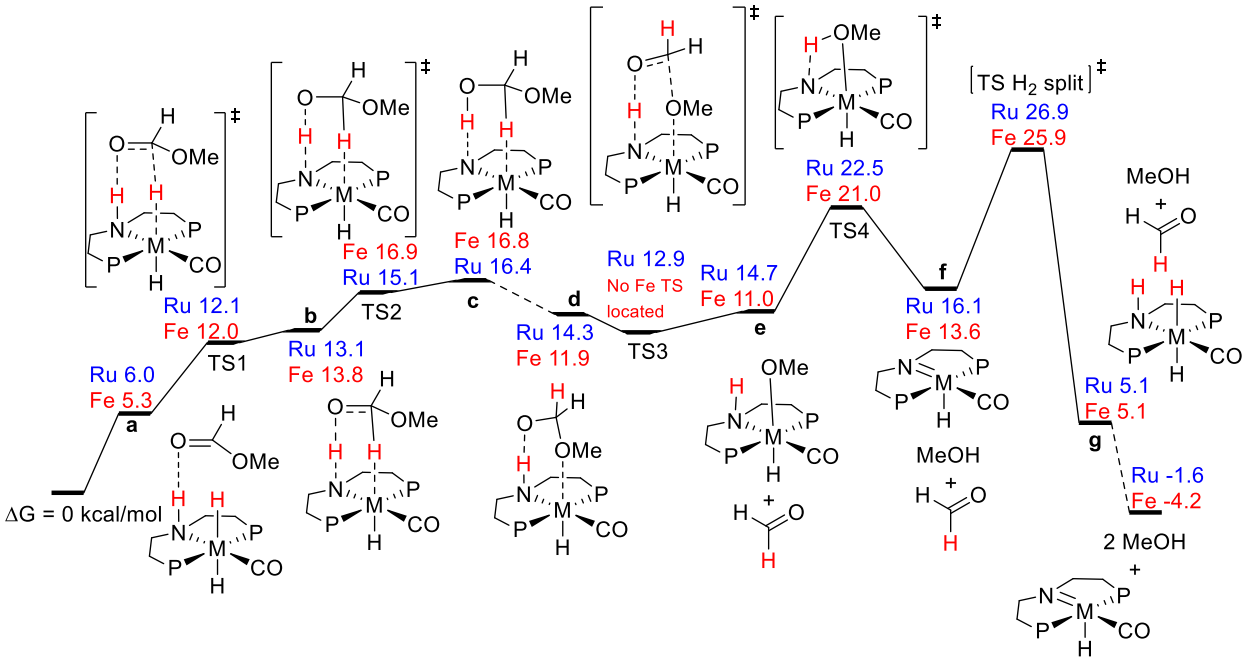

Figure 3.8. Methyl formate hydrogenation free energy profile showing a metal-assisted substrate cleavage via a "slippage" transition state

It is interesting to note that the C-O bond cleavage occurs with no barrier and is exoergic from the hemiacetal adduct, **d**. A related work by Guan and coworkers studied hydrogenation of methyl benzoate by (^{iPr}PNP)Ir(CO). They propose an alternative mechanism that requires re-coordination of substrate prior to C-O bind cleavage rather than release of benzaldehyde analogous to TS3.[52] It is not clear whether this discrepancy arises from calculations or from different choice of substrate and ligand R group. However, computational studies by Hazari and coworkers on methanol dehydrogenation (the reverse of the reaction studied above) using a (^{Me}PNP)Fe(CO) model system also suggest that the reaction proceeds through the equivalent of "slippage" TS3.[37] Our results are also qualitatively similar to those of Beller and coworkers, but provide more detail about how the hemiacetal may evolve into methanol and formaldehyde.[53] Because our calculated energies diverged from those of Beller and coworkers at the hydrogen cleavage step, a direct comparison of energies further along the ester hydrogenation pathway was not made.

3.2.4 Hydrogenation of amide to alcohol and amine

The reaction pathway for amide hydrogenation with Fe and Ru catalysts is shown in Figure 3.9. The transfer of the hydride and proton is concerted but asynchronous and described by only one transition state (TS1), but is otherwise similar to the ester. The main differences between the amide and ester hydrogenation reside in what occurs after the formation of the intermediate hemiacetal/hemiaminal. We could not locate a transition state for the elimination of formaldehyde to form the amido dimethylamine complex. However, the amido complex (**e**) that would result from the C-N cleavage of the hemiaminal with the assistance of the metal has a high energy relative to the starting materials (37.7/35.3 kcal mol^{-1} Ru/Fe) and is an unlikely intermediate. This may be due to the *trans*- influence of the hydride ligand disfavoring the coordination of the amido, which is itself a strong electron-donor relative to a methoxy functional group. Experimental studies of platinum and ruthenium complexes corroborate stronger M-alkoxy vs M-amino bonds.[68] A relaxed scan of the potential energy surface along the C-N bond showed no significant barrier in addition to the unfavorable thermodynamics. A similar result was observed by Hasanayn and Harb in their computational investigation of Milstein's complex **E (**Figure 3.5) for dehydrogenative coupling of alcohols and amines to ester and amides.[48]

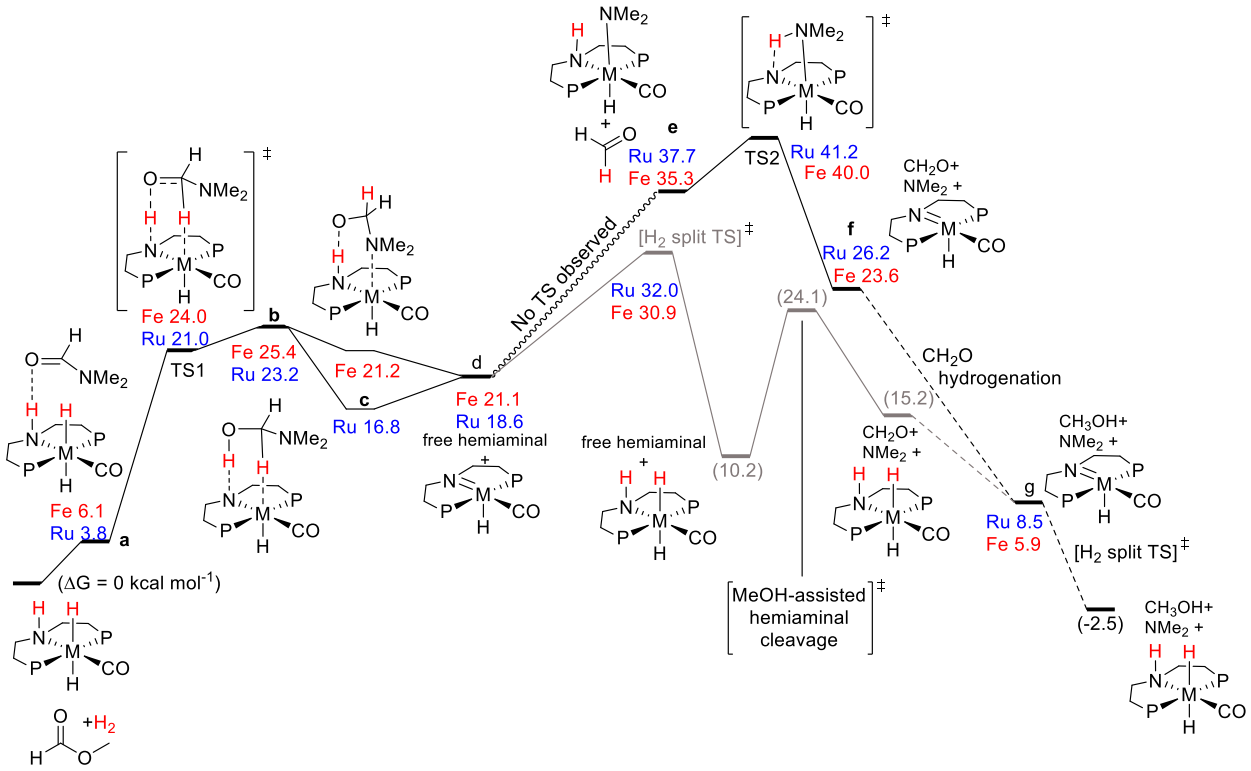

Figure 3.9. Dimethylformamide hydrogenation free energy profile showing metal-assisted substrate cleavage via "slippage". The lower grey pathway corresponds to metal-free hemiaminal decomposition

The high energy of the amido dimethylamine product suggests that the "slippage" transition state to liberate formaldehyde may be much less accessible for amides than it was for esters. We thus investigated alternative pathways to decompose the hemiaminal. Based on work by Guan and coworkers,[46,52] we considered the alternative C-N bond cleavage pathway depicted in Scheme 3.3. This was found to be a lowest-energy pathway for dehydrogenative synthesis for the reverse reaction, amide synthesis by Milstein's PNN catalyst. We found a significant penalty for the formation of C-N bond cleavage species, ($\Delta G^{\ddagger}$ = 42.5/41.9 kcal mol^{-1}, Ru/Fe). Because this product is unlikely to be formed, we chose not to search for the associated transition structures.

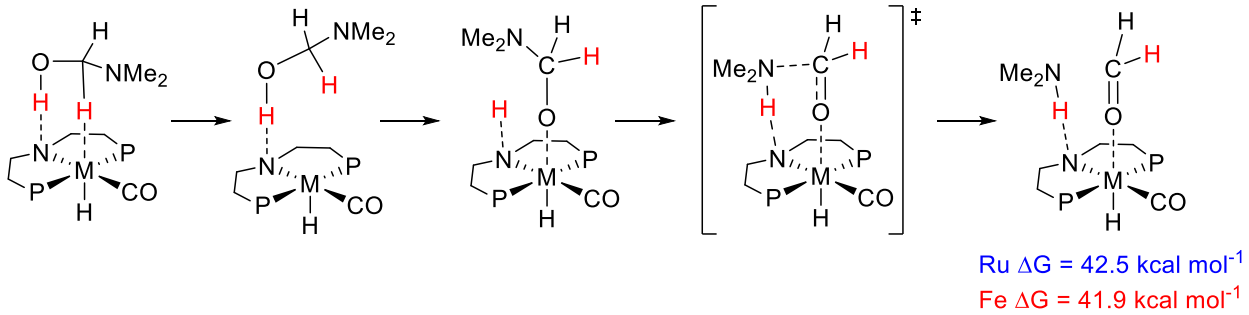

Scheme 3.3 Alternative C-N bond cleavage pathway, analogous to work by Guan and coworkers[46,52]

The lowest pathway we located corresponds to a 24.1 kcal mol^{-1} barrier for decomposition of hemiaminal into amine and formaldehyde with the assistance of a methanol proton relay and no metal (Figure 3.10). The decomposition of the hemiacetal under the same conditions has a higher activation barrier and is not on the calculated lowest energy pathway for methyl formate hydrogenation. Without a proton shuttle, the barrier is significantly higher for the substrates modeled. The key differences between the hydrogenation of ester and amine are not in the initial substrate hydrogenation step, but rather in the C-O vs C-N bond cleavage, and the participation vs absence of the metal catalyst in this process.

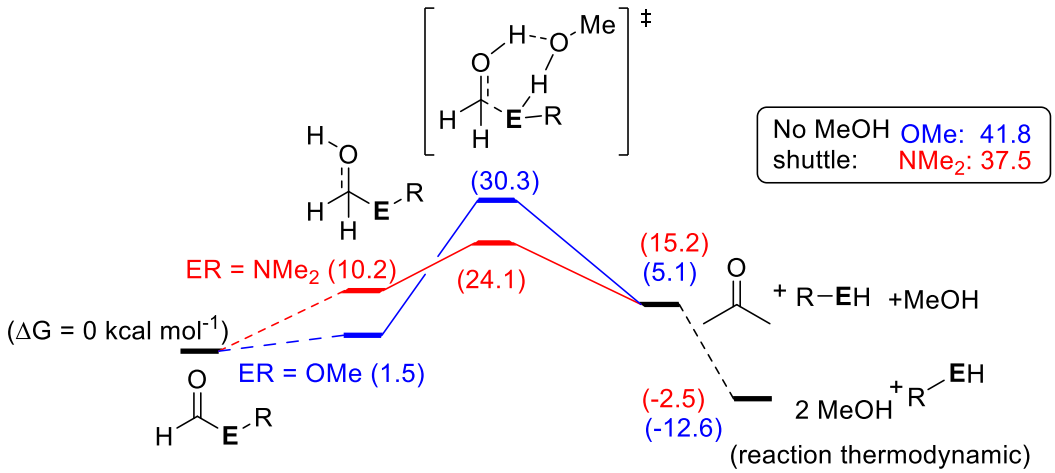

Figure 3.10 Hemiaminal and hemiacetal decomposition outside the metal coordination sphere

Sanford *et al.* have been able to monitor the rate of DMF hydrogenation using (^{Cy}PN^{H}P)Ru(H)(BH$_4$)(CO) and (^{Cy}PN^{H}P)Fe(H)(BH$_4$)(CO) precatalysts by *in situ* Raman

spectroscopy. By comparing the initial rates of hydrogenation, they found that the Ru pre-catalyst was 1.7 times faster than Fe.[8] While we calculated that the highest barrier, H_2 cleavage, was more challenging for Ru, the difference between the mechanisms was overall small, and this discrepancy is within reasonable computational error. We expect that a hydrogen bonding network in solution may further lower the hydrogen cleavage barrier.[65,67] Moreover, calculations provide support for the small difference in Fe vs Ru, though, as Sanford and coworkers noted, large differences in hydride donor ability between 2nd and 3rd row metals are apparent in other systems.[69] Sanford and coworkers also found that the rate of DMF hydrogenation by ($^{Cy}PN^{H}P$)Fe(H)(BH_4)(CO) was slower at 20 bar H_2 than 50 bar H_2, but that there was no further increase in rate at 70 bar H_2. This suggests that at lower H_2 concentrations, the hydrogen cleavage may be rate-limiting, but a different step may be rate-limiting at high pressures.[8] The modest 6 kcal mol^{-1} difference calculated between the highest barriers in Figure 3.9 is consistent with this; higher pressures can be expected to facilitate hydrogen coordination and cleavage.

We were unable to locate energetically accessible transition structures that resulted in deoxygenative carbonyl C-O bond cleavage for either methyl formate or dimethylformamide substrates. This is in agreement with experimental observations of exclusively C-N bond cleavage products and with previous computational works on related systems.[46,47]

3.2.5 CO_2 hydrogenation by $\mathbf{1}^{Fe}$ and $\mathbf{1}^{Ru}$: Inhibition of ester and amide hydrogenation

Similar to observations by Sanford and coworkers for Milstein's complex,[70] (^{iPr}PNP)Fe(CO) is known to react with CO_2 to produce a stable intermediate.[57,59] In our calculations, hydride transfer to the CO_2 occurs in a similar manner as other carbonyl substrates with an achievable barrier (9.2/16.3 kcal mol^{-1}). However, we were unable to isolate a transition state for formal

proton transfer (Figure 3.11). As before, exchanging coordination of the C-H for oxygen results in a more stable adduct.

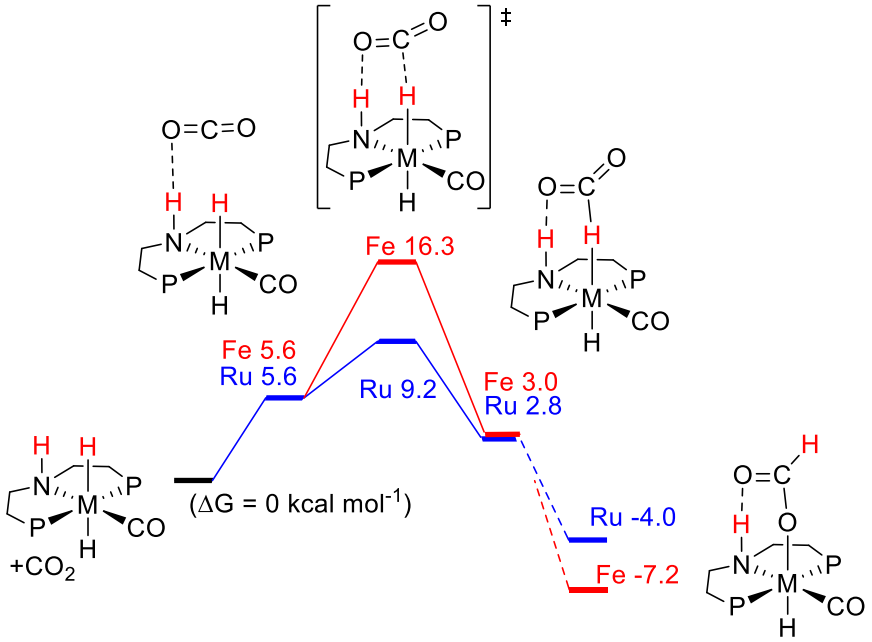

Figure 3.11. CO_2 hydrogenation and formation of a low-lying formate complex

We find that catalyst deactivation in a one-pot CO_2 to MeOH catalytic cascade[7,38] may be attributed to the low barrier to the hydrogenation of CO_2, combined with the low energy of the formate adduct (-7.2/-4.0 kcal mol^{-1} (Fe/Ru)) relative to species calculated on the ester and amide hydrogenation pathways. This mode of deactivation differs from that observed by Sanford for Milstein's complex, where the CO_2 adds across the cooperative ligand arm and ruthenium center but is not hydrogenated.[70] We implicate the relative stability of the formate complex, and observe that, generally, bifunctional basic sites on the ligand make a catalyst vulnerable to deactivation by substrate. Experimentally, in their investigations of CO_2 hydrogenation to formate, Bernskoetter and coworkers have observed similar (^{iPr}PNP)Fe-formate species to be the resting state in their catalytic cycle. They found that addition of a Lewis acid facilitated substrate release by cleaving the N-H bond. Furthermore, they observed much higher CO_2 hydrogenation activity (60000 vs 9000 TON) when using a tertiary amine ligand-based (^{iPr}PNP^{Me})Fe(CO)-based pre-catalysts. They

suggest that hydrogenation proceeds under analogous mechanisms for both systems, but the methyl amine is less strongly associated with the formate, facilitating substrate release.[57]

3.2.6 Insights from recent works

A recent computational/experimental study by Gauvin and coworkers sheds new light onto the mechanism of alcohol dehydrogenative coupling by complexes based on (^{R}PNP)Ru(CO), and thus onto the mechanism of the microscopic reverse reaction, ester hydrogenation, as well.[41] A (^{iPr}PN^{H}P)Ru(H)(OEt)(CO) complex stabilized by a molecule of EtOH, where EtOH has added across the metal and ligand nitrogen, was intercepted and crystallographically characterized (Figure 3.12). NMR spectroscopic studies demonstrated that ethanol facilitates proton/hydride exchange with (^{iPr}PN^{H}P)Ru(H)(CO), and also accelerates the rate of H_2 elimination, consistent with calculations showing a lower barrier for H_2 elimination with a proton shuttle. Gauvin and co-workers confirmed the presence of aldehydes as intermediates in the alcohol dehydrogenative coupling, giving support to a mechanism involving aldehyde intermediates, such as those calculated above. However, they find that, for alcohol dehydrogenative coupling, an alternative Tischenko-like mechanism is also competitive, and that it is likely that changing conditions favor either mechanism and also can change the rate determining step.[41]

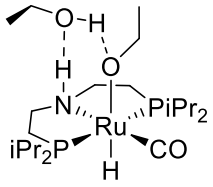

Figure 3.12. (^{iPr}PN^{H}P)Ru(H)(OEt)(CO) complex characterized by Gauvin and coworkers[41]

3.2.7 Initial conclusions

Based on calculated pathways, the rate of hydrogenation of esters by iron and ruthenium alkyl PNP complexes is likely related to the stability of the alcohol adduct formed after the liberation of

formaldehyde. For amide substrates, selectivity for C-N bond cleavage over C-O bond is not determined by the same "slippage" mechanism evident for the ester case. Metal-free hemiaminal decomposition assisted by a proton shuttle is a viable pathway for C-N bond cleavage, and proceeds with a lower barrier than the metal-assisted C-N bond cleavage that were evaluated. Finally, we see that formate adducts are relatively stable compared to ester and amine hydrogenation intermediates, rationalizing CO_2 inhibition of carbonyl hydrogenation, suggesting that these complexes are not a good choice for one-pot tandem CO_2 to methanol cascade systems.

Conventionally, esters, amides and related substrates are considered difficult to hydrogenate due to the difficulty in transferring hydrides to carbonyl carbons of reduced electrophilicity.[71] In this study we note that, for both ester and amide hydrogenation, the transfer hydrogenation of the substrate does not provide the highest energy barrier in the calculated reaction profiles. Improved hydrogenation efficiency will thus not come from increasing the hydricity of the metal hydride, but rather from better facilitating cleavage of the C-N or C-O bond between the carbonyl carbon and amine or alkoxy group, respectively.

More broadly, as with the Shvo and Noyori systems, we again encounter the idea that mechanistic schemes initially proposed are often incorrect – and these inaccuracies can impact experimental design. These works illustrate both the power of calculations as an aid to elucidating mechanism, but also the pitfalls: a mechanism that has not been considered cannot be found. We emphasize the necessity of experimentally verifying calculations as much as possible, the need to computationally explore diverse ideas, and the need to re-visit mechanistic proposals based on new experimental or computational results.

3.3 Further computational investigation of amide hydrogenation by (^{iPr}PNP)Fe(CO)

Further computational studies of amide hydrogenation were conducted in a multi-site collaboration with researchers at Yale University, the University of Missouri, and the University of Oslo.[1] Hydrogenation of a secondary amide, formanilide was investigated. The (^{iPr}PNP)Fe(CO) pre-catalyst was considered in this work, as the goal was to understand the differences in hydrogenation activity between the two substrates. Experimental hydrogenation of formanilide resulted in 99% conversion to methanol and aniline at 100 °C and 30 bar H_2, using (^{iPr}PNP)Fe(H)(CO) catalyst. Under the same conditions, DMF hydrogenation was only achieved upon addition of formanilide as a co-catalyst.[5]

The hydrogen cleavage step was found to proceed as described above. Analogous to methanol (Figure 3.7), the formanilide is also capable of acting as a proton relay, resulting in a 4 kcal mol^{-1} barrier for the addition of H_2 to across the Fe-N bond of (^{iPr}PNP)Fe(H)(CO). The subsequent hydride transfer/proton transfer to substrate proceeds by the same mechanism for both substrates. As expected, the barriers for this transformation are significantly higher for DMF, due to the reduced electrophilicity of the carbonyl carbon, due to more electron donation from the dimethyl than phenyl substituent. This difference is also reflected in the higher energy of the hemiaminal intermediates, Figure 3.13.

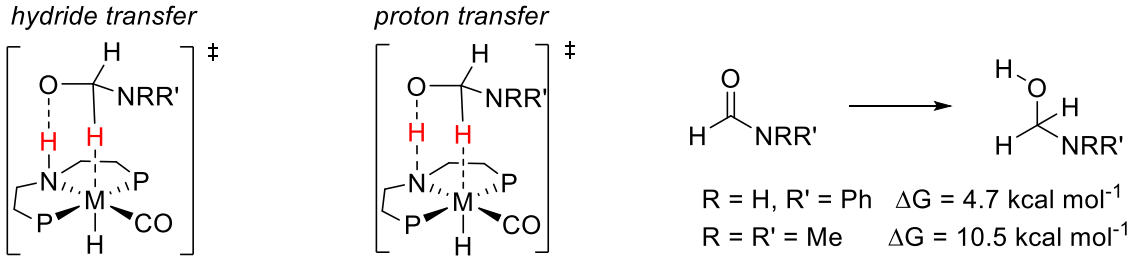

Figure 3.13. Energies of transfer hydrogenation of formanilide and DMF

The biggest differences in the mechanism arose in the C-N bond cleavage step, which is the highest-barrier step in the hydrogenation of both substrates, and likely the rate determining step. For formanilide, the highest-energy barrier is C-N bond cleavage assisted by the catalyst (Figure 3.14 (a)) with an overall highest barrier of 24.9 kcal mol^{-1}. The equivalent C-N bond cleavage in the case of DMF is inaccessible, at 41.0 kcal mol^{-1} (Figure 3.14 (b)). Instead, we found that for DMF, hemiaminal decomposition can be assisted by a proton relay, for example, formanilide (Figure 3.14 (c)). Other proton shuttles, for example MeOH and dimethylamine, gave higher overall barriers for proton-assisted C-N bond cleavage (29.6 kcal mol^{-1} and 33.8 kcal mol^{-1}). We note that the barrier for this transformation is still higher than for the metal-assisted pathway for formanilide, in line with the experimental results of slower DMF hydrogenation relative to formanilide hydrogenation, even in the presence of formanilide co-catalyst.[5]

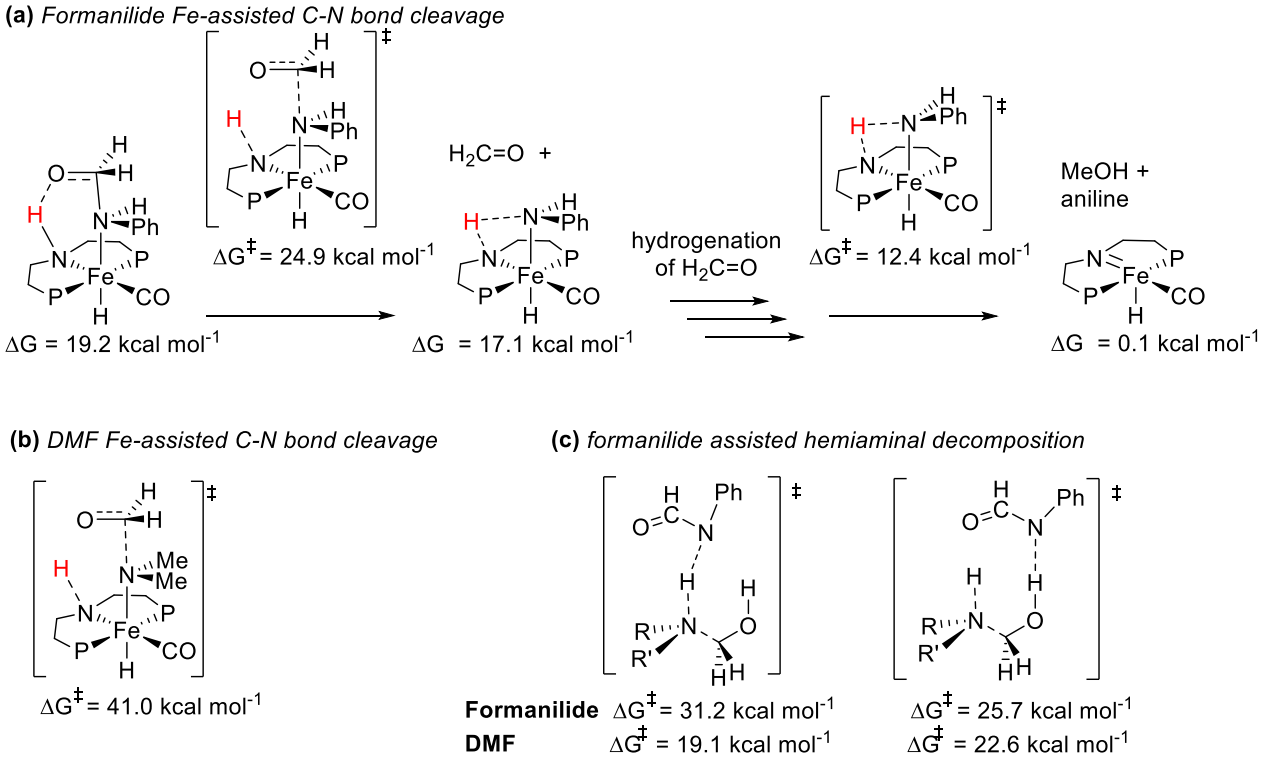

Figure 3.14. Selected pathways for formanilide and DMF hydrogenation by (^{iPr}PNP)Fe(H)(CO): (a) Fe-assisted cleavage of formanilide C-N bond and elimination of phenylamine (b) Fe-assisted cleavage of DMF C-N bond, (c) formanilide-assisted (metal-free) hemiaminal decomposition for hydrogenated DMF and formanilide.

This work re-emphasizes the fact that the traditional wisdom that the hydrogenation of electron-rich carbonyls is limited by the transfer hydrogenation step does not hold for all catalysts. The efficiency of hydrogen transfer is not limiting for either case and so focusing on, for example, increasing catalyst hydricity may not appreciably improve reaction rates. Furthermore, we find the mechanism for hydrogenation may vary even for seemingly similar substrates and, consequentially, different approaches are needed to improve catalytic activity with different substrates. Specifically, formanilide hydrogenation would benefit from a catalyst that better facilitates C-N bond cleavage and is not susceptible to poisoning by intermediates. In the case of DMF, an improved co-catalyst may improve reactivity.

3.4 Computational details

Calculations in Section 3.2 were performed using the Gaussian09 software package.[72] The computations were performed using complexes $\mathbf{1^{Ru}}$ and $\mathbf{1^{Fe}}$ without simplification of the ligand framework. Methyl formate and dimethylformamide were chosen as models of experimentally used substrates. Tetrahydrofuran is commonly used as a solvent in these hydrogenation reactions and was chosen for the self-consistent reaction field (SCRF) solvent correction calculations. Geometry optimizations were performed in the gas phase on the complete molecule using the PBE0 functional and the full DEF2SVP basis set for all atoms, with an effective core potential (ECP) for Ru. Dispersion correction was included using the GD3BJ model. This combination of basis set and functional have been shown to effectively model iridium systems.[73] Minima and transition structures were verified by frequency calculations. Transition structures were perturbed along the reaction coordinate (by IRC calculations, or by manually perturbing in the direction of the imaginary frequency) to verify connecting minima. Single point energies were calculated for optimized structures using the DEF2QZVPP basis set and the SMD solvent model (tetrahydrofuran

solvent). Single point energy calculations were repeated with the optimized geometries and the DEF2QZVPP basis set with a variety of functionals. For proton transfer events with high barriers, an explicit methanol molecule was used to investigate the lowering of barriers via a proton shuttle. For this study we assume that an appropriate model of the catalyst as shown in Figure 3.2, even though in practice, a pre-catalyst such (PN^HP)M(H)(BH_4)(CO) or (PN^HP)M(H)(Cl)(CO) along with stoichiometric alkoxide base are commonly used. Catalyst activation has been previously studied and was not further considered.[52]

The computational methodology in section 3.3 differed from that described above. The GGA MO6 functional was used for all calculations. Structures were optimized using the LANL2DZ basis set on Fe and the 6-31+G** basis set for all other elements. Vibrational frequencies were computed to verify energy minima and transition states. Thermochemistry corrections were obtained for experimentally relevant conditions, p = 30 atm and T = 373 K. Energies were refined with single-point calculations using LANL2TZ for Fe and 6-311+G** on the other atoms. Solvation was incorporated in both optimizations and single point calculations using THF solvent in the SMD model. To increase numerical accuracy and facilitate convergence, the ultrafine grid was used in all calculations.

3.5 References

(1) Artús Suàrez, L.; Culakova, Z.; Balcells, D.; Bernskoetter, W. H.; Eisenstein, O.; Goldberg, K. I.; Hazari, N.; Tilset, M.; Nova, A. The Key Role of the Hemiaminal Intermediate in the Iron-Catalyzed Deaminative Hydrogenation of Amides. *ACS Catal.* **2018**, *8* (9), 8751–8762.

(2) Kuriyama, W.; Matsumoto, T.; Ogata, O.; Ino, Y.; Aoki, K.; Tanaka, S.; Ishida, K.; Kobayashi, T.; Sayo, N.; Saito, T. Catalytic Hydrogenation of Esters. Development of an Efficient Catalyst and Processes for Synthesising (R)-1,2-Propanediol and 2-(*l*-Menthoxy)Ethanol. *Org. Process Res. Dev.* **2012**, *16*, 166–171.

(3) Chakraborty, S.; Dai, H.; Bhattacharya, P.; Fairweather, N. T.; Gibson, M. S.; Krause, J. A.; Guan, H. Iron-Based Catalysts for the Hydrogenation of Esters to Alcohols. *J. Am. Chem. Soc.* **2014**, *136* (22), 7869–7872.

(4) Zhang, L.; Han, Z.; Zhao, X.; Wang, Z.; Ding, K. Highly Efficient Ruthenium-Catalyzed N-Formylation of Amines with H_2 and CO_2. *Angew. Chem. Int. Ed.* **2015**, *54* (21), 6186–6189.

(5) Jayarathne, U.; Zhang, Y.; Hazari, N.; Bernskoetter, W. H. Selective Iron-Catalyzed Deaminative Hydrogenation of Amides. *Organometallics* **2017**, *36* (2), 409–416.

(6) Schneck, F.; Assmann, M.; Balmer, M.; Harms, K.; Langer, R. Selective Hydrogenation of Amides to Amines and Alcohols Catalyzed by Improved Iron Pincer Complexes. *Organometallics* **2016**, *35* (11), 1931–1943.

(7) Rezayee, N. M.; Huff, C. A.; Sanford, M. S. Tandem Amine and Ruthenium-Catalyzed Hydrogenation of CO_2 to Methanol. *J. Am. Chem. Soc.* **2015**, *137* (3), 1028–1031.

(8) Rezayee, N. M.; Samblanet, D. C.; Sanford, M. S. Iron-Catalyzed Hydrogenation of Amides to Alcohols and Amines. *ACS Catal.* **2016**, *6* (10), 6377–6383.

(9) Blum, Y.; Shvo, Y. Catalytic Reactive Ruthenium Intermediates in the Homogeneous Oxidation of Alcohols to Esters. *Isr. J. Chem.* **1984**, *24*, 144–148.

(10) Karvembu, R.; Prabhakaran, R.; Natarajan, K. Shvo's Diruthenium Complex: A Robust Catalyst. *Coord. Chem. Rev.* **2005**, *249*, 911–918.

(11) Conley, B. L.; Pennington-Boggio, M. K.; Boz, E.; Williams, T. J. Discovery, Applications, and Catalytic Mechanisms of Shvo' s Catalyst. *Chem. Rev.* **2010**, *110* (4), 2294–2312.

(12) Johnson, J. B.; Bäckvall, J. E. Mechanism of Ruthenium-Catalyzed Hydrogen Transfer Reactions. Concerted Transfer of OH and CH Hydrogens from an Alcohol to a (Cyclopentadienone)Ruthenium Complex. *J. Org. Chem.* **2003**, *68* (20), 7681–7684.

(13) Menashe, N.; Shvo, Y. Catalytic Disproportionation of Aldehydes with Ruthenium Complexes. *Organometallics* **1991**, *10* (11), 3885–3891.

(14) Menashe, N.; Salant, E.; Shvo, Y. Efficient Catalytic Reduction of Ketones with Formic Acid and Ruthenium Complexes. *J. Organomet. Chem.* **1996**, *514* (1–2), 97–102.

(15) Almeida, M. L. S.; Beller, M.; Wang, G. Z.; Bäckvall, J. E. Ruthenium(II)-Catalyzed Oppenauer-Type Oxidation of Secondary Alcohols. *Chem. Eur. J.* **1996**, *2* (12), 1533–1536.

(16) Laxmi, Y. R. S.; Bäckvall, J.-E. Mechanistic Studies on Ruthenium-Catalyzed Hydrogen Transfer Reactions. *Chem. Commun.* **2000**, 611–612.

(17) Csjernyik, G.; Éll, A. H.; Fadini, L.; Pugin, B.; Bäckvall, J.-E. Efficient Ruthenium-Catalyzed Aerobic Oxidation of Alcohols Using a Biomimetic Coupled Catalytic System. *J. Org. Chem.* **2002**, *67* (5), 1657–1662.

(18) Casey, C. P.; Singer, S. W.; Powell, D. R.; Hayashi, R. K.; Kavana, M. Hydrogen Transfer to Carbonyls and Imines from a Hydroxycyclopentadienyl Ruthenium Hydride: Evidence for Concerted Hydride and Proton Transfer. *J. Am. Chem. Soc.* **2001**, *123* (6), 1090–1100.

(19) Casey, C. P.; Beetner, S. E.; Johnson, J. B. Spectroscopic Determination of Hydrogenation Rates and Intermediates during Carbonyl Hydrogenation Catalyzed by Shvo's Hydroxycyclopentadienyl Diruthenium Hydride Agrees with Kinetic Modeling Based on Independently Measured Rates of Elementary Reactions. *J. Am. Chem. Soc.* **2008**, *130* (7), 2285–2295.

(20) Casey, C. P.; Vos, T. E.; Singer, S. W.; Guzei, I. A. Protonated Aminocyclopentadienyl Ruthenium Hydride Reduction of Benzaldehyde and the Conversion of the Resulting Ruthenium Triflate to a Ruthenium Hydride with H_2 and Base. *Organometallics* **2002**, *21* (23), 5038–5046.

(21) Comas-Vives, A.; Ujaque, G.; Lledós, A. Hydrogen Transfer to Ketones Catalyzed by Shvo's Ruthenium Hydride Complex: A Mechanistic Insight. *Organometallics* **2007**, *26* (17), 4135–4144.

(22) Gusev, D. G.; Spasyuk, D. M. Revised Mechanisms for Aldehyde Disproportionation and the Related Reactions of the Shvo Catalyst. *ACS Catal.* **2018**, *8* (8), 6851–6861.

(23) Dub, P. A.; Gordon, J. C. The Mechanism of Enantioselective Ketone Reduction with Noyori and Noyori-Ikariya Bifunctional Catalysts. *Dalton Trans.* **2016**, *45* (16), 6756–6781.

(24) Matsumura, K.; Arai, N.; Hori, K.; Saito, T.; Sayo, N.; Ohkuma, T. Chiral Ruthenabicyclic Complexes: Precatalysts for Rapid, Enantioselective, and Wide-Scope Hydrogenation of Ketones. *J. Am. Chem. Soc.* **2011**, *133* (28), 10696–10699.

(25) Ohkuma, T.; Ooka, H.; Hashiguchi, S.; Ikariya, T.; Noyori, R. Practical Enantioselective Hydrogenation of Aromatic Ketones. *J. Am. Chem. Soc.* **1995**, *117* (9), 2675–2676.

(26) Haack, K. J.; Hashiguchi, S.; Fujii, A.; Ikariya, T.; Noyori, R. The Catalyst Precursor, Catalyst, and Intermediate in the Ru^{II}-Promoted Asymmetric Hydrogen Transfer between Alcohols and Ketones. *Angew. Chem. Int. Ed.* **1997**, *36* (3), 285–288.

(27) Noyori, R. Asymmetric Catalysis: Science and Opportunities (Nobel Lecture). *Angew. Chem. Int. Ed.* **2002**, *41* (12), 2008–2022.

(28) Eisenstein, O.; Crabtree, R. H. Outer Sphere Hydrogenation Catalysis. *New J. Chem.* **2013**, *37* (1), 21–27.

(29) Morris, R. H. Exploiting Metal-Ligand Bifunctional Reactions in the Design of Iron Asymmetric Hydrogenation Catalysts. *Acc. Chem. Res.* **2015**, *48* (5), 1494–1502.

(30) Khusnutdinova, J. R.; Milstein, D. Metal-Ligand Cooperation. *Angew. Chem. Int. Ed.* **2015**, *54* (42), 12236–12273.

(31) Kitamura, M.; Nakatsuka, H. Mechanistic Insight into NOYORI Asymmetric Hydrogenations. *Chem. Commun.* **2011**, *47* (3), 842–846.

(32) Hasanayn, F.; Morris, R. H. Symmetry Aspects of H2 Splitting by Five-Coordinate D6 Ruthenium Amides, and Calculations on Acetophenone Hydrogenation, Ruthenium Alkoxide Formation, and Subsequent Hydrogenolysis in a Model Trans-Ru(H)2(Diamine)(Diphosphine) System. *Inorg. Chem.* **2012**, *51* (20), 10808–10818.

(33) Pavlova, A.; Meijer, E. J. Understanding the Role of Water in Aqueous Ruthenium-Catalyzed Transfer Hydrogenation of Ketones. *ChemPhysChem* **2012**, *13* (15), 3492–3496.

(34) Dub, P. A.; Henson, N. J.; Martin, R. L.; Gordon, J. C. Unravelling the Mechanism of the Asymmetric Hydrogenation of Acetophenone by [RuX_2(Diphosphine)(1,2-Diamine)] Catalysts. *J. Am. Chem. Soc.* **2014**, *136* (9), 3505–3521.

(35) Noyori, R.; Ohkuma, T. Asymmetric Catalysis by Architectural and Functional Molecular Engineering: Practical Chemo- and Stereoselective Hydrogenation of Ketones. *Angew. Chem. Int. Ed.* **2001**, *40* (1), 40–73.

(36) Dub, P. A.; Gordon, J. C. Metal-Ligand Bifunctional Catalysis: The "Accepted" Mechanism, the Issue of Concertedness, and the Function of the Ligand in Catalytic Cycles Involving Hydrogen Atoms. *ACS Catal.* **2017**, *7* (10), 6635–6655.

(37) Chakraborty, S.; Lagaditis, P. O.; Förster, M.; Bielinski, E. A.; Hazari, N.; Holthausen, M. C.; Jones, W. D.; Schneider, S. Well-Defined Iron Catalysts for the Acceptorless Reversible Dehydrogenation-Hydrogenation of Alcohols and Ketones. *ACS Catal.* **2014**, *4* (11), 3994–4003.

(38) Huff, C. A.; Sanford, M. S. Cascade Catalysis for the Homogeneous Hydrogenation of CO_2 to Methanol. *J. Am. Chem. Soc.* **2011**, *133* (45), 18122–18125.

(39) Werkmeister, S.; Junge, K.; Wendt, B.; Alberico, E.; Jiao, H.; Baumann, W.; Junge, H.; Gallou, F.; Beller, M. Hydrogenation of Esters to Alcohols with a Well-Defined Iron Complex. *Angew. Chem. Int. Ed.* **2014**, *53* (33), 8722–8726.

(40) Zhang, L.; Raffa, G.; Nguyen, D. H.; Swesi, Y.; Corbel-Demailly, L.; Capet, F.; Trivelli, X.; Desset, S.; Paul, S.; Paul, J. F.; et al. Acceptorless Dehydrogenative Coupling of Alcohols Catalysed by Ruthenium PNP Complexes: Influence of Catalyst Structure and of Hydrogen Mass Transfer. *J. Catal.* **2016**, *340*, 331–343.

(41) Nguyen, D. H.; Trivelli, X.; Capet, F.; Swesi, Y.; Favre-Réguillon, A.; Vanoye, L.; Dumeignil, F.; Gauvin, R. M. Deeper Mechanistic Insight into Ru Pincer-Mediated Acceptorless Dehydrogenative Coupling of Alcohols: Exchanges, Intermediates, and Deactivation Species. *ACS Catal.* **2018**, *8* (5), 4719–4734.

(42) Nielsen, M.; Junge, H.; Kammer, A.; Beller, M. Towards a Green Process for Bulk-Scale Synthesis of Ethyl Acetate: Efficient Acceptorless Dehydrogenation of Ethanol. *Angew. Chem. Int. Ed.* **2012**, *51* (23), 5711–5713.

(43) Bertoli, M.; Choualeb, A.; Lough, A. J.; Moore, B.; Spasyuk, D.; Gusev, D. G. Osmium and Ruthenium Catalysts for Dehydrogenation of Alcohols. *Organometallics* **2011**, *30* (13), 3479–3482.

(44) Spasyuk, D.; Vicent, C.; Gusev, D. G. Chemoselective Hydrogenation of Carbonyl Compounds and Acceptorless Dehydrogenative Coupling of Alcohols. *J. Am. Chem. Soc.* **2015**, *137* (11), 3743–3746.

(45) Oldenhuis, N. J.; Dong, V. M.; Guan, Z. Catalytic Acceptorless Dehydrogenations: Ru-Macho Catalyzed Construction of Amides and Imines. *Tetrahedron* **2014**, *70* (27–28), 4213–4218.

(46) Li, H.; Wang, X.; Huang, F.; Lu, G.; Jiang, J.; Wang, Z. X. Computational Study on the Catalytic Role of Pincer Ruthenium(II)-PNN Complex in Directly Synthesizing Amide from Alcohol and Amine: The Origin of Selectivity of Amide over Ester and Imine. *Organometallics* **2011**, *30* (19), 5233–5247.

(47) Cantillo, D. Mechanistic Insights on the Ruthenium-Catalyzed Hydrogenation of Amides - C-N vs. C-O Cleavage. *Eur. J. Inorg. Chem.* **2011**, 3008–3013.

(48) Hasanayn, F.; Harb, H. A Metathesis Model for the Dehydrogenative Coupling of Amines with Alcohols and Esters into Carboxamides by Milstein's [Ru(PNN)(CO)(H)] Catalysts. *Inorg. Chem.* **2014**, *53* (16), 8334–8349.

(49) Lei, M.; Pan, Y.; Ma, X. The Nature of Hydrogen Production from Aqueous-Phase Methanol Dehydrogenation with Ruthenium Pincer Complexes under Mild Conditions. *Eur. J. Inorg. Chem.* **2015**, 794–803.

(50) Yang, X. Mechanistic Insights into Ruthenium-Catalyzed Production of H_2 and CO_2 from Methanol and Water: A DFT Study. *ACS Catal.* **2014**, *4* (4), 1129–1133.

(51) Yang, X. A Self-Promotion Mechanism for Efficient Dehydrogenation of Ethanol Catalyzed by Pincer Ruthenium and Iron Complexes: Aliphatic versus Aromatic Ligands. *ACS Catal.* **2013**, *3* (12), 2684–2688.

(52) Qu, S.; Dai, H.; Dang, Y.; Song, C.; Wang, Z. X.; Guan, H. Computational Mechanistic Study of Fe-Catalyzed Hydrogenation of Esters to Alcohols: Improving Catalysis by Accelerating Precatalyst Activation with a Lewis Base. *ACS Catal.* **2014**, *4* (12), 4377–4388.

(53) Jiao, H.; Junge, K.; Alberico, E.; Beller, M. A Comparative Computationally Study about the Defined M(II) Pincer Hydrogenation Catalysts (M = Fe, Ru, Os). *J. Comput. Chem.* **2016**, *37*, 168–176.

(54) Alberico, E.; Lennox, A. J. J.; Vogt, L. K.; Jiao, H.; Baumann, W.; Drexler, H.-J.; Nielsen, M.; Spannenberg, A.; Checinski, M. P.; Junge, H.; et al. Unravelling the Mechanism of Basic Aqueous Methanol Dehydrogenation Catalyzed by Ru–PNP Pincer Complexes. *J. Am. Chem. Soc.* **2016**, *138* (45), 14890–14904.

(55) Bornschein, C.; Werkmeister, S.; Wendt, B.; Jiao, H.; Alberico, E.; Baumann, W.; Junge, H.; Junge, K.; Beller, M. Mild and Selective Hydrogenation of Aromatic and Aliphatic (Di)Nitriles with a Well-Defined Iron Pincer Complex. *Nat. Commun.* **2014**, *5* (1), 1–11.

(56) Mills, M. R.; Barnes, C. L.; Bernskoetter, W. H. Influences of Bifunctional PNP-Pincer Ligands on Low Valent Cobalt Complexes Relevant to CO_2 Hydrogenation. *Inorg. Chem.* **2018**, *57* (3), 1590–1597.

(57) Zhang, Y.; MacIntosh, A. D.; Wong, J. L.; Bielinski, E. A.; Williard, P. G.; Mercado, B. Q.; Hazari, N.; Bernskoetter, W. H. Iron Catalyzed CO_2 Hydrogenation to Formate Enhanced by Lewis Acid Co-Catalysts. *Chem. Sci.* **2015**, *6* (7), 4291–4299.

(58) Spentzos, A. Z.; Barnes, C. L.; Bernskoetter, W. H. Effective Pincer Cobalt Precatalysts for Lewis Acid Assisted CO_2 Hydrogenation. *Inorg. Chem.* **2016**, *55* (16), 8225–8233.

(59) Bielinski, E. A.; Lagaditis, P. O.; Zhang, Y.; Mercado, B. Q.; Würtele, C.; Bernskoetter, W. H.; Hazari, N.; Schneider, S. Lewis Acid-Assisted Formic Acid Dehydrogenation Using a Pincer-Supported Iron Catalyst. *J. Am. Chem. Soc.* **2014**, *136* (29), 10234–10237.

(60) Riehl, J. F.; Jean, Y.; Eisenstein, O.; Pélissier, M. Theoretical Study of the Structures of Electron-Deficient d^6 ML_5 Complexes. Importance of a π-Donating Ligand. *Organometallics* **1992**, *11* (2), 729–737.

(61) Crabtree, R. H. Dihydrogen Complexation. *Chem. Rev.* **2016**, *116* (15), 8750–8769.

(62) Riehl, J. F.; Pélissier, M.; Eisenstein, O. Influence of a Cis Hydride on a Coordinated H_2 Ligand. Ab Initio Calculations. *Inorg. Chem.* **1992**, *31* (16), 3344–3345.

(63) Kubas, G. J.; Ryan, R. R.; Swanson, B. I.; Vergamini, P. J.; Wasserman, H. J. Characterization of the First Examples of Isolable Molecular Hydrogen Complexes, $M(CO)_3(PR_3)_2(H_2)$ (M = Mo, W; R = Cy, *i*-Pr). Evidence for a Side-on Bonded H_2 Ligand. *J. Am. Chem. Soc.* **1984**, *106* (2), 451–452.

(64) Krogh-Jespersen, K.; Czerw, M.; Summa, N.; Renkema, K. B.; Achord, P. D.; Goldman, A. S. On the Mechanism of (PCP)Ir-Catalyzed Acceptorless Dehydrogenation of Alkanes: A Combined Computational and Experimental Study. *J. Am. Chem. Soc.* **2002**, *124* (38), 11404–11416.

(65) Iron, M. A.; Ben-Ari, E.; Cohen, R.; Milstein, D. Metal–ligand Cooperation in the *Trans* Addition of Dihydrogen to a Pincer Ir(I) Complex: A DFT Study. *Dalton Trans.* **2009**, No. 43, 9433–9439.

(66) Zhang, Q.; Bell, R.; Truong, T. N. Ab Initio and Density Functional Theory Studies of Proton Transfer Reactions in Multiple Hydrogen Bond Systems. *J. Phys. Chem.* **1995**, *99* (2), 592–599.

(67) Chen, T.; Li, H.; Qu, S.; Zheng, B.; He, L.; Lai, Z.; Wang, Z. X.; Huang, K. W. Hydrogenation of Esters Catalyzed by Ruthenium PN^3-Pincer Complexes Containing an Aminophosphine Arm. *Organometallics* **2014**, *33* (15), 4152–4155.

(68) Bryndza, H. E.; Fong, L. K.; Paciello, R. A.; Tam, W.; Bercaw, J. E. Relative Metal-Hydrogen, -Oxygen, -Nitrogen, and -Carbon Bond Strengths for Organoruthenium and Organoplatinum Compounds; Equilibrium Studies of $Cp^*(PMe_3)_2RuX$ and (DPPE)MePtX Systems. *J. Am. Chem. Soc.* **1987**, *109* (5), 1444–1456.

(69) Cheng, T. Y.; Brunschwig, B. S.; Bullock, R. M. Hydride Transfer Reactions of Transition Metal Hydrides: Kinetic Hydricity of Metal Carbonyl Hydrides. *J. Am. Chem. Soc.* **1998**, *120* (50), 13121–13137.

(70) Huff, C. A.; Kampf, J. W.; Sanford, M. S. Role of a Noninnocent Pincer Ligand in the Activation of CO_2 at (PNN)Ru(H)(CO). *Organometallics* **2012**, *31* (13), 4643–4645.

(71) Dub, P. A.; Ikariya, T. Catalytic Reductive Transformations of Carboxylic and Carbonic Acid Derivatives Using Molecular Hydrogen. *ACS Catal.* **2012**, *2* (8), 1718–1741.

(72) Frisch, M. J.; Trucks, G. W.; Schlegel, H. B.; Scuseria, G. E.; Robb, M. A.; Cheeseman, J. R.; Scalmani, G.; Barone, V.; Mennucci, B.; Petersson, G. A.; et al. Gaussian09. *Gaussian 09*. 2009.

(73) Hopmann, K. H. How Accurate Is DFT for Iridium-Mediated Chemistry? *Organometallics* **2016**, *35* (22), 3795–3807.

Chapter Four. Base-free hydrogenation of formate esters by pincer-supported iridium complexes

4.1 Introduction

4.1.1 Motivations: Catalyst incompatibility in tandem cascades

Tandem catalytic cascades present a promising route for the hydrogenation of CO_2 to methanol (MeOH) and other commercially relevant products, as described in Chapter One. The Sanford group pioneered cascade systems for the hydrogenation of CO_2 to MeOH via a process that employed three separate catalysts in one vessel to achieve the overall transformation in a series of three simpler reactions (Scheme 4.1).[1] Thus far, the success of this and similar cascades systems has been limited by incompatibility of hydrogenation catalysts with CO_2 or other system components.[1–3] Many ester hydrogenation catalysts used in these cascade systems have a basic site that is essential for hydrogenation activity (see Chapter Three for further discussion). Catalyst basic sites, such as the nitrogen in the (PNN)Ru catalyst used in Sanford's first-generation cascade (Scheme 4.1, cat. C), are susceptible to interactions with acids that render these complexes inactive for ester hydrogenation and diminish the overall activity of the cascade system. Sanford and coworkers found that the scandium triflate ($Sc(OTf)_3$) co-catalyst in their cascade inhibits the (PNN)Ru ester hydrogenation catalyst. While $Sc(OTf)_3$ is often considered to be water-stable, metal triflates have been demonstrated to undergo decomposition, for example by reaction with benzene or methylene chloride solvent, to generate triflic acid (HOTf).[4] Though Sanford partially solved this issue by physically separating cat. B from cats. A and C, substitution of an acid-tolerant cat. C would circumvent this co-compatibility issue and operationally simplify the system.

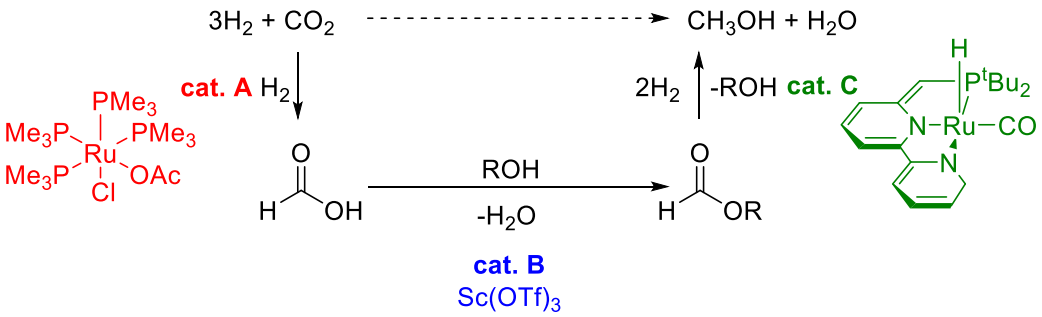

Scheme 4.1. Schematic for cascade hydrogenation of CO_2 to MeOH via an ester intermediate. Adapted from Sanford[1]

To our knowledge, there are three reported homogeneous systems that can hydrogenate ester substrates using molecular H_2 under protic conditions.[5–7] In all of these examples, the ligand is thought to be a spectator. However, these proton-tolerant pre-catalysts typically exhibit lower activity (TON >1000 vs TON >10,000) and require more forcing conditions than catalysts that operate under neutral or basic conditions.[8]

We are therefore interested in developing new pre-catalysts for acid-tolerant ester hydrogenation. Pincer-supported iridium complexes exhibit good thermal stability and have been well-studied as catalysts for transformations such as the hydrogenation of olefins and the reverse reaction, the dehydrogenation of sp^3 carbon-carbon bonds,[9–11] as well as related reactions, such as silane dehydrocoupling,[12] and the borylation of small molecules.[13] Recent work in our group has studied steric and electronic factors affecting the structure and reactivity of (^{R}PCP)Ir(CO) (PCP = κ^3-C_6H_4-2,6-[CH_2PR_2]$_2$, R = ^{i}Pr, ^{t}Bu) and (^{R}POCOP)Ir(CO), (POCOP = κ^3-C_6H_4-2,6-[OPR_2]$_2$), R= ^{i}Pr, ^{t}Bu) complexes, particularly hydrogen addition to these complexes.[14–16] Oxidative addition of hydrogen in a *cis*- fashion was only found to be possible with the smaller alkyl group, R = ^{i}Pr [17]and R = Me.[18] When R= ^{i}Pr, thermally induced isomerization converts the *cis*- dihydride to the *trans*-dihydride while the reduced steric profile allows the interconversion to proceed at room temperature, reaching equilibrium between the *cis*- and *trans*- isomers in a day. A second proton-

catalyzed hydrogen addition pathway that directly generates the *trans*- dihydride was observed for both R = ^{i}Pr and R = ^{t}Bu (Scheme 4.2).

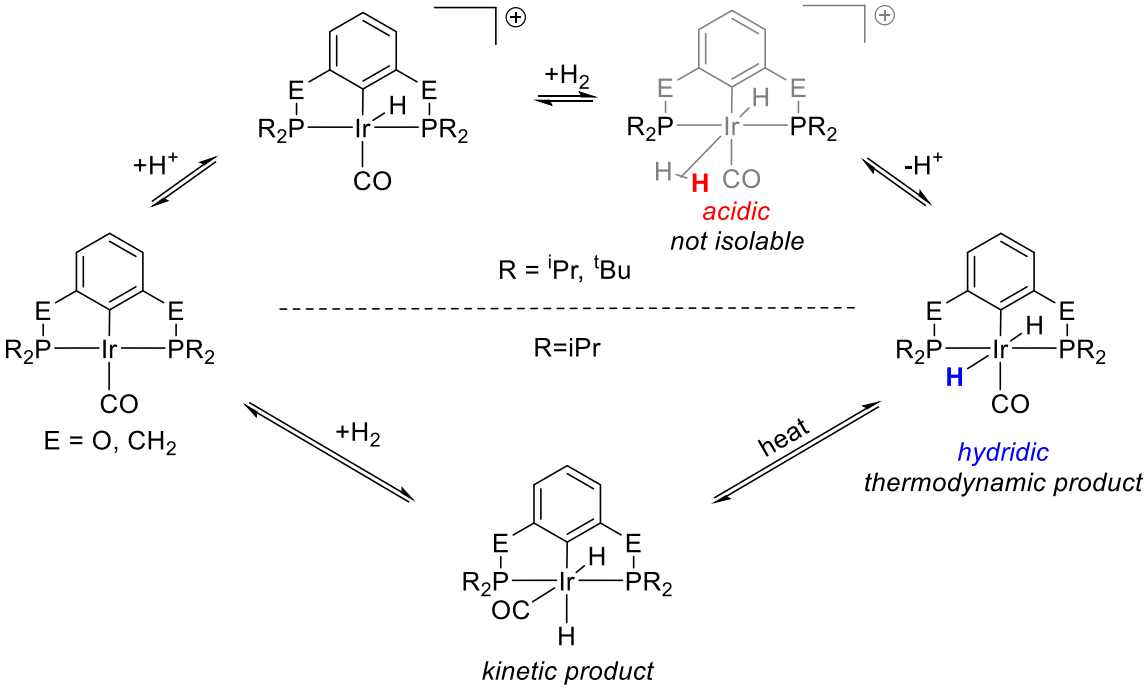

Scheme 4.2. Iridium species accessible by reaction of the (pincer)Ir(CO) scaffold with acid and/or hydrogen, adapted from Goldberg and Heinekey[15]

Recently, Goldberg, Heinekey and coworkers obtained NMR evidence for (^{tBu}POCOP)Ir(H)(H_2) complexes (Figure 4.1)[16] Electron poor (Lewis acidic) metal centers better stabilize coordinated dihydrogen. Hydrides of electron deficient metal centers are less hydridic, and less susceptible to protonation. Indeed, installation of an electron-withdrawing protonated dimethylamino ($NHMe_2^+$) group on the ^{tBu}POCOP backbone results in the generation of dihydrogen complex under milder conditions (40 vs 80 bar H_2) than when ligand is unfunctionalized. The isolation and characterization of dihydrogen complexes is well documented,[16,19–22] and dihydrogen complexes of iridium are known to be strong acids.[23] As such, pincer (^{tBu}POCOP)Ir(CO)-based dihydrogen complexes have been suggested as catalytic intermediates in the deoxygenation of glycerol to 1,3-propanediol and 1-propanol by

(^{tBu}POCOP)Ir(CO).[16,24,25] Iridium dihydrogen complexes are also invoked as intermediates in related transformations, such as H_2 addition to a (^{tBu}POCOP)Ir(CH_3) complex[26]

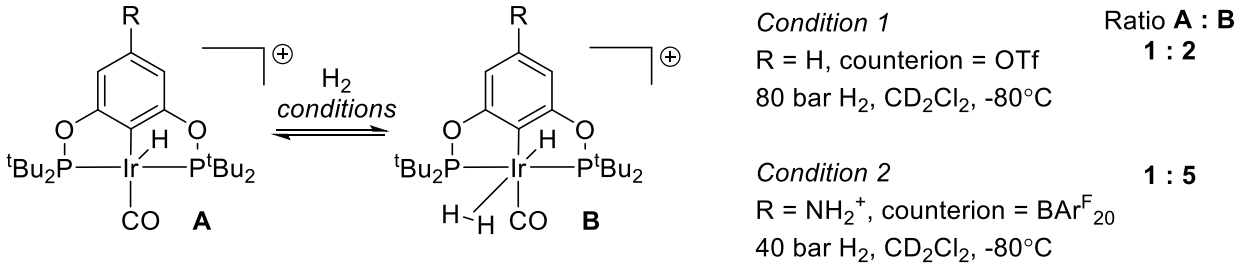

Figure 4.1. $[(POCOP)Ir(H)(H_2)CO]^+$ species observed via NMR spectroscopy[16]

4.1.2 Proposed catalytic cycle for ester hydrogenation

The ability of POCOP-supported complexes to deliver proton and hydride equivalents has been exploited in previous studies of polyol conversion to alcohols.[24,25] We hypothesized that the characteristics that facilitate these reactions would also make these pincer-supported iridium complexes viable ester hydrogenation pre-catalysts.

A proposed mechanism for ester hydrogenation by these complexes is shown in Scheme 4.3. We envision an ionic hydrogenation mechanism, where after coordination of H_2 to an Ir(III) hydride, a strongly acidic dihydrogen ligand can deliver a proton to the substrate. Protonation of the carbonyl oxygen will increase the electrophilicity of the carbonyl carbon. The iridium *trans*-dihydride is expected to an accessible hydride donor, as hydrides typically exhibit a strong *trans*-effect.[27] As proposed in previous studies, the hemiacetal intermediate generated after the first H^+/H^- transfer will decompose in solution to produce an equivalent of alcohol and aldehyde.[6] The aldehyde will then be rapidly hydrogenated by a second iteration of the transfer hydrogenation cycle. Additionally, we hypothesized that the absence of basic functional groups on the ligand scaffold would limit acid sensitivity, and also catalyst deactivation due to CO_2 coordination.

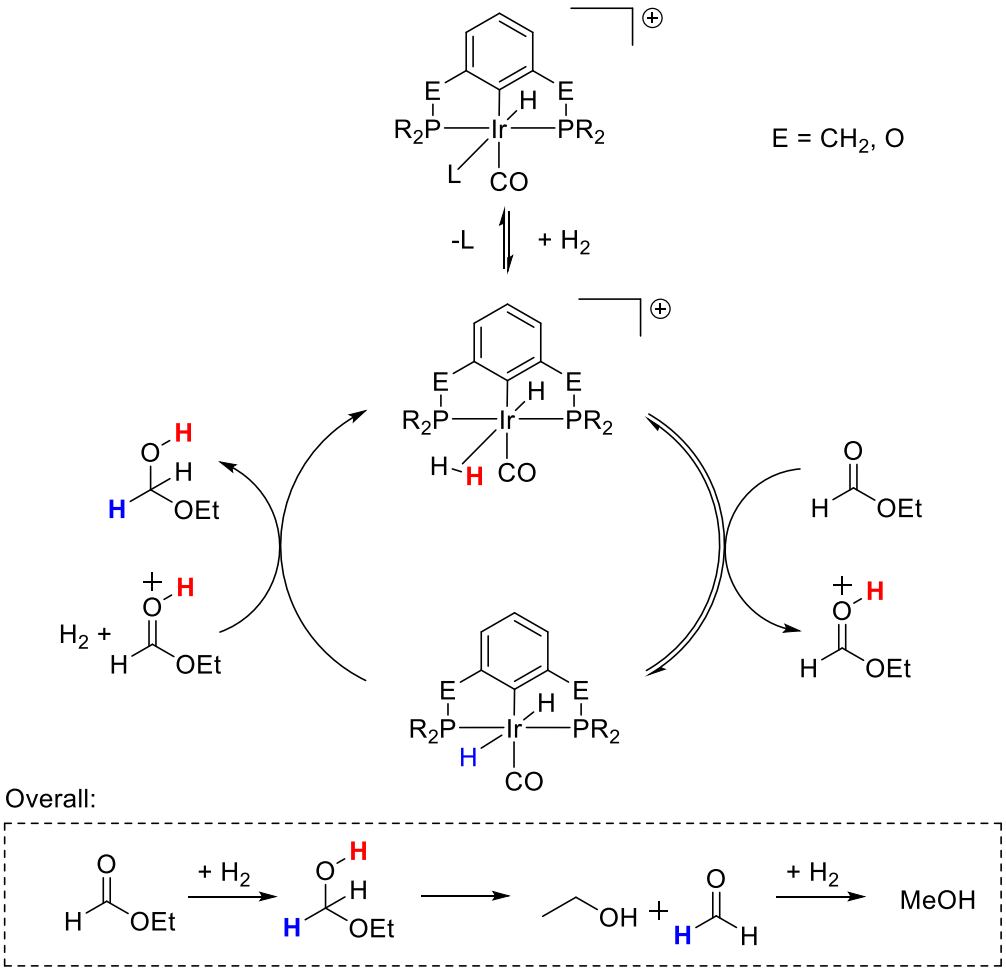

Scheme 4.3. Envisioned ionic ester hydrogenation mechanism using a (pincer)Ir(CO)-based catalyst

Relatedly, Jensen *et al* reported the stoichiometric reaction of (^{tBu}PCP)Ir(H)$_2$ with MeOH to produce (^{tBu}PCP)Ir(CO) at 200 °C in toluene and in the presence of *tert*-butyl ethylene.[28] Heinekey and Goldberg found that polyol deoxygenation reactions using 5-coordinate (pincer)Ir(H)$_2$ complexes generated (pincer)Ir(CO) species, with CO arising from substrate decarbonylation.[24,25] Reactions of alcohol and aldehyde decarbonylation by pincer Ir complexes based on the ^{tBu}POCOP ligand have been studied in more detail by Koridze *et al*.[29] They found that 5-coordinate (^{tBu}POCOP)Ir(H)$_2$ will decarbonylate primary alcohols ethanol (EtOH) and MeOH at room temperature. Additionally, they disclosed decarbonylation of acetaldehyde by (^{tBu}POCOP)Ir(H)$_2$, was well as the formation of a Ir-hydrido acetaldehyde adduct. Further reactions show that the Ir-

acetaldehyde adduct is unlikely to be an intermediate in the decarbonylation of EtOH, and they propose a mechanism for alcohol decarbonylation that proceeds via a hydrido-dihydride intermediate (Figure 4.2). Reactions of MeOH and paraformaldehyde with (^{tBu}POCOP)Ir(H)$_2$ generate a mixture of *trans*-(^{tBu}POCOP)Ir(H)$_2$(CO) and (^{tBu}POCOP)Ir(CO), the latter arising from hydrogen elimination from the dihydride.

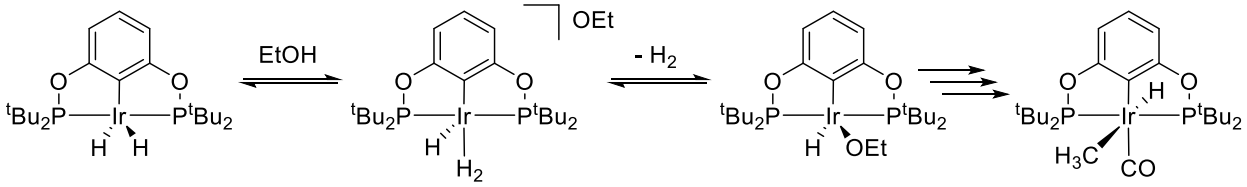

Figure 4.2. Mechanism for EtOH decarbonylation by (tBuPOCOP)Ir(H)$_2$ proposed by Koridze and coworkers[29]

Goldberg, Heinekey and coworkers note that pre-installation of a CO trans- to the pincer aryl carbon suppresses further substrate decarbonylation by the pincer catalyst.[24,25] Given that alcohol products and aldehyde intermediates are expected to be generated over the course of ester hydrogenation reactions, we chose to investigate pre-catalysts containing CO ligands.

After we began our investigations into ester hydrogenation using PCP and POCOP complexes, Zhou and coworkers published the deoxygenative hydrogenation of N-phenylacetamide to water and ethylphenylamine using 2 mol% (^{tBu}POCOP)Ir(H)(Cl) or (^{iPr}POCOP)Ir(H)(Cl) at 50 bar H_2 and 120 °C in toluene.[30] They reported high yields and selectivity only in the presence of stoichiometric boron-based Lewis acids (LAs), notably $B(C_6H_5)_3$, and 2 mol% [Na][B(3,5-$(CF_3)_2C_6H_3)_4$] ($NaBAr^F{}_{24}$). They proposed a mechanism related to that presented in Scheme 4.3. Envisioned ionic ester hydrogenation mechanism using a (pincer)Ir(CO)-based catalyst The catalytic cycle begins with sequential proton transfer from an iridium dihydrogen-hydride complex to the carbonyl oxygen of the amide substrate, followed by hydride transfer to the carbonyl carbon from the resulting iridium dihydride, generating hemiaminal. They

suggest that the LA is necessary to activate the substrate by coordination to the carbonyl oxygen prior to proton transfer. To complete the cycle, the hemiaminal undergoes dehydration to generate an imine, which is then further hydrogenated. Deuterium incorporation studies provided evidence for an imine intermediate.[30]

4.1.3 Sterics and electronics of pincer iridium complexes

We chose to investigate a series of iridium complexes with varied steric and electronic features, based on the Ir(I) complexes showed in Figure 4.3. Larger ^{t}Bu groups on the pincer phosphines are expected to slightly increase the electron density at the metal center versus R = ^{i}Pr, as the more substituted alkyl groups are more electron-rich.[31] An electron-rich metal center would facilitate fundamental reactions such as C-H activation, and, in our proposed hydrogenation scheme, is expected to result in a more hydridic hydride and, by extension, produce a more acidic dihydrogen complex. However, the effect of a decreased steric profile often dominates over electronic differences, and experiments have shown that (^{iPr}PCP)Ir-based pre-catalysts are more efficient at alkane dehydrogenation than (^{tBu}PCP)Ir(CO) based pre-catalysts.[32]

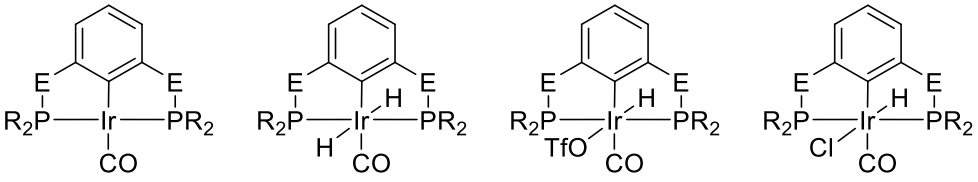

E = O, R = ^{i}Pr (**1**)	**1a**	**1b**	**1c**	**1d**
E = O, R = ^{t}Bu (**2**)	**2a**	**2b**	-	-
E = CH_2, R = ^{i}Pr (**3**)	**3a**	**3b**	**3c**	**3d**
E = CH_2, R = ^{t}Bu (**4**)	**4a**	**4b**	**4c**	**4d**

Figure 4.3. (pincer)Ir complexes screened for ethyl formate hydrogenation

Electronic effects from substitution of the R groups or methylene linker for O are more nuanced. The oxygen present in the POCOP ligand contributes π electron density to the aryl ligand.[33] Additionally, σ-electron donation from the phosphorus to the ligand oxygen creates a net

positive charge on the phosphorous. However, overall charge on the iridium remains nearly unchanged from PCP to POCOP, as the positive phosphorus is balanced by the increased negative charge on the aryl carbon. This results in a difference in charge distribution in the CO ligand, with the POCOP backbone giving a more polarized bond, more triple bond character, and a higher stretching frequency.[33] This effect is observed experimentally in the blue shift (increase) of CO stretching frequencies when O is substituted for CH_2 as the linker in the pincer arm; for example (^{tBu}PCP)Ir(CO)[15] (**4a**) vs (^{tBu}POCOP)Ir(CO)[14] (**2a)** (ν_{CO} (CH_2Cl_2) = 1913 vs 1937 cm^{-1} respectively). Previous work has shown that π rather than σ effects tend to dominate the differences in the CO stretching frequency.[34] Similarly, elongation of the H-D distance (determined by decreased J_{HD}) in (R-^{tBu}POCOP)Ir *cis*-hydride-deuteride complexes provides evidence for increased π- backdonation from iridium to the D-H σ*.when electron-rich R-substituents are installed on the ligand backbone *para*- to the Ir-C bond.[35] In general, we expect more electron-rich metal centers to exhibit more facile oxidative addition of H_2 (or aryl C-H) bonds.[36]

4.2 Catalytic hydrogenation of ethyl formate by pincer iridium pre-catalysts

4.2.1 General considerations

Pincer-supported iridium pre-catalysts (Figure 4.3) were screened for hydrogenation activity of a simple model substrate, ethyl formate (EF). EF is relevant as a proxy for the methyl formate intermediate in the Sanford cascade for MeOH production from CO_2 and H_2.[1] The ethyl group allows us to differentiate alcohol equivalents produced from the carbonyl moiety of the substrate from the ethoxy fragment.

Scheme 4.4 shows the products we observed in ethyl formate hydrogenation reactions. In addition to MeOH and EtOH, the expected hydrogenation products, methyl formate (MF), (from

transesterification), and diethyl ether (from dehydrative coupling of EtOH) were sometimes observed. Dialkoxy methane products, $ROCH_2OR'$, (R, R' = Me or Et) are observed in reactions with neat substrate or alcohol solvent. These may be attributed to the reaction of a hemiacetal intermediate with an equivalent of alcohol.

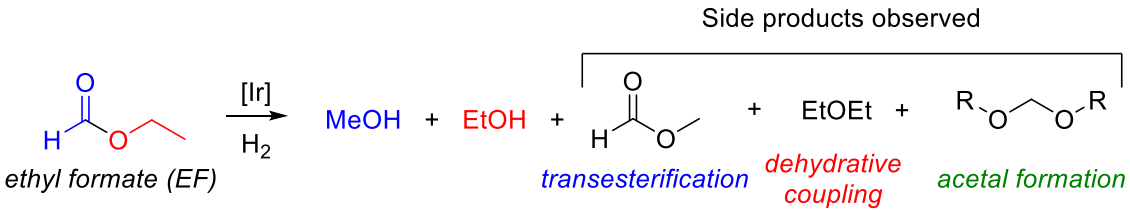

Scheme 4.4. Observed products from ethyl formate hydrogenation reactions

In many reactions, we observe less MeOH, MF and EF (total C_1 equivalents, originating from the formate portion of the EF) than expected based on the amount of substrate added to the reaction. Mass balance for C_1 equivalents is shown in Table 4.1 as the ratio of measured C_1 fragments to C_2 fragments from the ethyl portion of the substrate (MeOH equiv: EtOH equiv, Table 4.1). Though we are not sure of the origin of this disparity, we hypothesize that some C_1 equivalents are lost to the formation of low-boiling products, such as MF (bp 31.8 °C) that are easily liberated during workup. Another explanation is decomposition of intermediates, such as the decomposition of formic acid (produced from transesterification of formate ester and water) to CO_2 and H_2, as well as decomposition of formaldehyde to CO and H_2. Poor mass balance is exacerbated in reactions with added acid and with low TON. We also noted that control reactions with no catalyst or additive returned EF in 95% recovery, as quantified by ^{13}C NMR spectroscopy. This is likely due to physical losses, resulting from the high volatility of EF (boiling point = 54.3 °C) and substrate loss in reactor headspace.

4.2.2 ^{iPr}POCOP pre-catalysts

The Ir(I) species (^{iPr}POCOP)Ir(CO) (**1a**) was found to be a poor pre-catalyst for EF hydrogenation under the chosen conditions, producing 6 TON MeOH after 16 hours (Table 4.1, Entry 1). Analysis of ^{31}P NMR spectra of the reaction mixture post-reaction revealed one resonance at 174.0 ppm, corresponding to dihydride complex *trans*-(^{iPr}POCOP)Ir(H)$_2$(CO), (**1b**). This is consistent with previous observations of hydrogen addition to **1a**,[15] and indicates that the iridium dihydride is accessed under reaction conditions. Independently prepared **1b** gave an identical result when used as a pre-catalyst (entry 9 vs 1).

Table 4.1. EF hydrogenation by (^{R}POCOP)Ir complexes.[a]

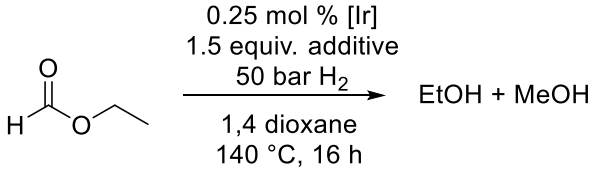

Entry	[Ir] pre-catalyst	Additive	TON MeOH equiv. (st. dev.)	MeOH equiv.: EtOH equiv.
1	**1a**	--	6.4 (6)	31:100
2	**1a**	NaOTf*	58 (8)	44:100
3	**1a**	LiOTf*	4 (6)	20:100
4	**1a**	HBF_4.Et_2O	74 (4)	64:100
5	**1a**	HOTf	158(21)	67:100
6	**1a**	$HNTf_2$	All substrate consumed	
7[#]	**1a**	$HNTf_2$	222(2)	74:100
8	**1c**	H_2O**	111 (1)	42:100
9	**1b**	--	5.2 (2)	33:100
10	**1b**	HOTf	138 (14)	69:100
11	**1c**	--	149 (16)	78:100
12[†]	**1d**	--	0	--
13[†]	**1e**	--	164	74:100
14	**2a**	--	15 (8)	56:100
15	**2a**	HOTf	0 0)	0:100

[a] Conditions: 0.50 mol% [Ir] catalyst, 1.5 equiv additive, 4 mmol EF, 2 mL 1,4-dioxane, 50 atm H_2, 140 °C, 16 hours. MeOH equiv = MeOH + MF, EtOH equiv = EtOH + 2x diethyl ether – MF. *5 equivalents. **20 μL. Entries based on the average of two or more trials. [†]One trial. [#]5 hours. Products in entry 6 not quantified.

Protonation of the substrate at the carbonyl oxygen is expected to activate the carbon, making it more susceptible to hydride transfer by increasing the electrophilicity. We hypothesized that addition of a Brønsted acid would achieve this either by direct protonation of the substrate or by generation of a highly acidic iridium dihydrogen hydride complex. The use of Brønsted acid additives as promoters for ester hydrogenation has been previously reported for other ester hydrogenation catalysts that do not have a basic site on the ligand. As described in Chapter Two, we have found that addition of HOTf promotes the hydrogenation of lactones and other ester substrates by a half-sandwich iridium complex, $[Cp^*Ir(bpyOMe)(H_2O)](OTf)_2$ (Cp^* = pentamethylcyclopentadienyl anion, bpyOMe = 4,4'-dimethoxy-2,2'-bipyridine).[6] Similarly, p-toluenesulfonic acid, bis(trifluoromethanesulfonyl)imide ($HNTf_2$) and other acids have been shown to facilitate the hydrogenation of ester substrates by Ru/triphos (triphos = 1,1,1-tris(diphenylphosphinomethyl)ethane).[5,37–39]

Gratifyingly, addition of 1.5 equiv. of HOTf (relative to **1a**) to the reaction mixture resulted in 158 TON of MeOH produced over 16 hours (entry 5). We observed, within error, the same results with pre-catalyst **1b** and added HOTf (TON = 138, entry 10), confirming that both complexes are catalytically competent. We found that **1a** reacts with HOTf to give (^{iPr}POCOP)Ir(H)(CO)(OTf) (**1c**). This complex can also be prepared by treatment of **1d** with AgOTf. The presence of a triplet at -25.59 ppm in the ^{1}H NMR spectrum suggests triflate is coordinated to the metal in solution. The solid-state structure of **1c** also shows the triflate anion is bound to the iridium center. The use of **1c** as a pre-catalyst resulted in similar activity (148 vs 158 TON MeOH, entry 11 vs entry 5). For experiments with triflate, added either as HOTf or in **1c**, ^{31}P and ^{1}H NMR spectra of the reaction mixture obtained after catalysis revealed a large number (< 7) of Ir species, among which we identified **1b** and **1c**. Consistent with earlier experiments, **1a**

was not present. From these experiments, we conclude that accessing an Ir(III) mono-hydride aids catalyst activation with the ^{iPr}POCOP scaffold. This activation can occur *in situ* via addition of HOTf to a suitable pre-catalyst.

We next sought to investigate the effects of acid strength and counterion identity. The addition of 1.5 equiv. of HBF_4•Et_2O, a weaker acid (pK_a = -10.3 vs -11.4 for HOTf)[40] with a less-coordinating anion, produced less MeOH (74 vs 158 TON, entry 4 vs entry 5) after 16 hours. The post-reaction ^{31}P NMR spectra showed a singlet at 174.2 ppm, suggesting that **1b** remains the predominant complex in solution. We then investigated the addition of superacid $HNTf_2$, a notable alternative to HOTf.[41] $HNTf_2$ is a stronger acid than HOTf (pK_a = -11.9 vs -11.4 in 1,2-dichloroethane),[40] while low nucleophilicity, large steric profile, and delocalization of negative charge over the whole molecule makes the NTf_2^- anion a particularly poor ligand to metal centers.[42] Additionally, as it is a solid, $HNTf_2$ is also easier to handle and purify than HOTf. When $HNTf_2$ was introduced as the acid additive, substrate was entirely consumed after the 16 hour reaction time (entry 6, TON MeOH not determined). Based on the H_2 pressure consumption recorded for the 16 hour experiment, we determined that the reaction was nearly complete at 5 hours; indeed, an experiment with a 5 hour reaction time generated 222 TON MeOH (entry 7). We propose that the increased acidity and diminished propensity for counterion coordination of this additive have contributed to the increased the rate of substrate hydrogenation and increased MeOH production.

To further investigate the effect of anion coordination to the metal center, *trans*-(^{iPr}POCOP)Ir(H)(Cl)(CO), *trans*-**1d** was introduced as a pre-catalyst. Chloride is expected to coordinate much more strongly to the metal center than all counterions studied above. Supporting our previous hypothesis, we found that this complex was inactive for EF hydrogenation (entry 12). ^{1}H and ^{31}P NMR spectroscopy revealed that the chloride remains coordinated *trans*- to the hydride;

trans-**1d** remains the only iridium-containing species detected in solution following reaction. We hypothesize two reasons for the inactivity of **1d**: 1) strong coordination of the chloride blocks the open site necessary for hydrogen coordination, and 2) hydride *trans*- to the chloride is expected to be less hydridic than hydride *trans*- to hydride as in **1b**, making the hydride transfer from **1d** less favorable. The ability of the iridium center to lose an anion is essential to generating an active EF hydrogenation catalyst based on the ^{iPr}POCOP scaffold. Overall, these results suggest the binding of counterions *trans*- to the Ir(III) hydride inhibits hydrogenation activity; less or non-coordinating counterions are essential to effective acid additives for enhancing MeOH generation. The greatest activity for EF hydrogenation by (^{iPr}POCOP)Ir(CO)-based pre-catalysts is observed with a strong acid with a less-coordinating anion, $HNTf_2$ (e.g. entries 6-7).

LAs have been shown to improve catalyst activity for the hydrogenation of esters and amides.[6] It is thought that coordination of electrophilic LAs to the carbonyl oxygen renders the carbonyl carbon more electrophilic. Testing this hypothesis, we found that the addition of 5 equiv. NaOTf to hydrogenation experiments with **1a** resulted in an increase in MeOH produced (58 vs 6, Table 4.1, entry 2 vs entry 1) for **1a** with no additive. This is still notably less than the 158 TON (entry 5) by **1a** and 1.5 equiv. HOTf. However, addition of 5 equiv. LiOTf resulted in 4 equiv. MeOH produced (entry 3), demonstrating no improvement over experiments without added LA. We do not understand the origin of this enhancement or the difference between NaOTf and LiOTf, but we note that metal-triflate LAs studied are less effective additives for assisting EF hydrogenation by ^{iPr}POCOP complexes than the equivalent protic acid, HOTf. This result further emphasizes the observed necessity of catalyst activation by protonation.

The lifetime of **1c** was assessed in a recycling experiment. In this experiment, a reactor was loaded, pressurized and heated as usual. Instead of the usual workup, the reactor was loaded with

additional substrate, and re-pressurized for a second cycle. Comparison of aliquots of reaction mixture before and after the second pressurization showed 134 TON MeOH in the first cycle and 298 TON MeOH in the second cycle (Table 4.2, entries 1a and 1b), representing 164 TON MeOH produced in the second pressurization. The increase in TON during the second cycle may be due to increased total concentration of EF substrate in the reactor. Internal pressure inside the reactor was monitored, and steady rates of pressure decrease measured in the reactor suggest consistent hydrogen consumption throughout both cycles. From these results, we can conclude that the catalytic species is not deteriorating. Furthermore, TON numbers in the screening reactions in Table 4.1 are limited by availability of substrate; this suggests that catalyst activity is robust beyond 160 TON, and that we have not yet reached the upper bound on TON possible. We expect that optimization of reaction conditions could dramatically increase the activity of EF hydrogenation reactions with **1a.**

Table 4.2. Two EF hydrogenation cycles with reactor recharge[a]*

Entry	pre-catalyst	time	TON MeOH equiv.	TON EtOH equiv.	TON formate equiv. remain
1a	**1c**	16 h	134	174	586
1b		recharge + 16 h	298	558	236
2a	**4a**	16 h	93	151	684
2b		recharge + 16 h	241	340	327

[a]Initial conditions: 0.50 mol% [Ir] catalyst, 4 mmol EF, 2 mL 1,4-dioxane, 50 atm H_2, 140 °C, 16 hours. Recharge = addition of 4 mmol EF. *calculations use 2.323 mL total original solution volume. MeOH Equiv = MeOH + MeOF. TON EtOH Equiv. = EtOH + EtOEt. TON formate equiv. represents formate remaining = EtOEt + MeOF.

In an effort to improve TON by increasing substrate concentration, EF hydrogenation was attempted in neat substrate. Using a low catalyst loading (0.0062 mol% **1c**), we were able to observe up to 3175 TON MeOH equivalents in a single trial at 140 °C, and 6840 TON MeOH when the temperature was increased to 160 °C for 18 hours). A screen of the effects of reaction pressure, temperature and catalyst concertation was carried out. Under the conditions investigated,

increasing catalyst loading, increasing reaction pressure and increasing temperature were all found to increase substrate consumption and TON MeOH produced.

In these neat reactions, we also identified the formation of dialkoxy methane products of the form ($ROCH_2OR$, R = Et or Me), in addition to MeOH and EtOH. We hypothesize that this occurs by reaction of the hemiacetal intermediate with alcohol. Notably, we did not observe these side-products under the more dilute reaction conditions. It is likely that dilution in 1,4-dioxane decreases the likelihood that hemiaminal intermediates are intercepted by alcohol equivalents; we do not observe dialkoxy methane products. Because of this formation of side products, and significant loss of C_1 products, we did not conduct further studies in neat substrate.

4.2.3 ^{tBu}POCOP pre-catalysts

We found that the more sterically hindered (^{tBu}POCOP)Ir(CO) (**2a**) was a poor catalyst for EF hydrogenation, both with and without an HOTf additive (0 TON and 15 TON MeOH, Table 4.1, entries 15 and 14 respectively). The addition of hydrogen to **2a** to form dihydride complex (^{tBu}POCOP)Ir(H)$_2$(CO) (**2b**) is not observed in the absence of catalytic acid.[15,24] The difficulty of accessing these Ir(III) species and decreased access to the metal due to steric demands from the ^{t}Bu- groups[14,15,24] may both contribute to the inability **2a** to of serve as an efficient EF hydrogenation pre-catalyst.

4.2.4 ^{iPr}PCP pre-catalysts

We hypothesized that increasing the hydride donor ability of the iridium center while retaining the reduced steric profile of the isopropyl-substituted phosphorous atoms might improve catalyst activity by facilitating hydride transfer. These features are present in (^{iPr}PCP)Ir(CO) (**3a**), which is also reported to react with H_2 in a facile manner to form *trans*-**3b**.[15] The lower carbonyl

stretching frequency ($\nu(CO)_{CH2Cl2}$ = 1920 cm^{-1}) of **3a** suggests a more electron-rich metal center than **1a** ($\nu(CO)_{CH2Cl2}$ = 1944 cm^{-1}).[15,17] By extension, we expect that the corresponding dihydride complexes of the more electron rich ligand scaffold will be more hydridic.

Table 4.3. EF hydrogenation by ^{iPr}PCP complex **3a** and derivatives.[a]

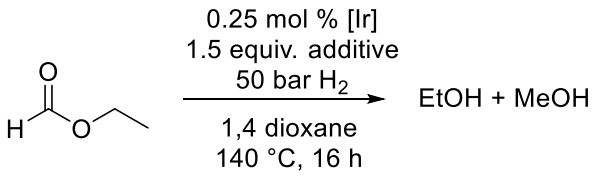

Entry	[Ir] pre-catalyst	Additive	TON MeOH equiv. (st. dev.)	MeOH equiv.: EtOH equiv.
1	3a	--	9.4 (0.4)	48:100
2	**3a**	LiOTf*	23 (8)	53:100
3	**3a**	HBF_4.Et_2O	231 (25)	70:100
4[#†]	**3a**	HBF_4.Et_2O	200	76:100
5	**3a**	HOTf	9.5 (1.4)	46:100
6[†]	**3a**	$HNTf_2$	227	73:100
7[#†]	**3a**	$HNTf_2$	106	51:100
8	**3f**	--	159 (13)	73:100
9	**3e**	--	20 (5)	68:100
10[†]	**3d**	--	0	--

[a] Conditions: 0.50 mol% [Ir] catalyst, 1.5 equiv. additive, 4 mmol EF, 2 mL 1,4-dioxane, 50 atm H_2, 140 °C, 16 hours. MeOH equiv. = MeOH + MF, EtOH equiv. = EtOH + 2x diethyl ether – MF. *5 equivalents. [#]5 hrs. Entries based the average of two or three trials. [†]One trial.

The results of EF hydrogenation screening reactions using ^{iPr}PCP-based pre-catalysts are presented in Table 4.3. Analogous to the results obtained with **1a**, **3a** is a poor pre-catalyst for EF hydrogenation, resulting in 9.4 TON MeOH after 16 hours (Table 4.3, entry 1). ^{31}P NMR spectra of the reaction mixture showed a single signal at 58.8 ppm, corresponding to dihydride complex (^{iPr}PCPIr(H)$_2$(CO) (**3b**), again indicating hydrogen addition to the catalyst under reaction conditions. As with the ^{iPr}POCOP analog, LA additive LiOTf produced only a modest increase activity, with 23 TON MeOH after 16 hours (entry 2). When (^{iPr}PCP)Ir(H)(Cl)(CO) (**3d**) pre-catalyst is introduced as a mixture of *cis*- and *trans*-**3d** (entry 10), we also observe no activity for EF hydrogenation (like **1d**). The only iridium-containing species detected in solution after the

hydrogenation experiment is *trans*-**3d**, consistent with previously observed isomerization to the more thermodynamically stable *trans*- isomer upon heating of *cis*- **3d** in solution.[14]

The behavior of **3a** with protic acid additives differed from **1a**. Use of HBF_4•Et_2O additive resulted in 231 TON MeOH and near-complete substrate consumption after 16 hours (Table entry 3), with 200 TON MeOH after only 5 hours (entry 4), a higher activity than with the POCOP scaffold (74 TON MeOH after 16 hrs). Retention of C_1 equivalents was higher at the shorter time point, suggesting that side reactions with the MeOH product may be contributing to poor mass balance. Curiously, addition of $HNTf_2$ resulted in 227 TON MeOH at 16 hours, but only 106 TON at 5 hours, indicating that for ^{iPr}PCP complexes, $HNTf_2$ is a less effective additive than weaker acid HBF_4•Et_2O.

The addition of HOTf to reactions with **3a** suppressed hydrogenation, leading to only 9.5 TON MeOH after 16 hours. In these reactions, a white precipitate was observed during workup. Analysis by ^{1}H NMR spectroscopy revealed a triplet corresponding to a hydride at -10.24 ppm, characteristic of a strong donor ligand *trans*- to the hydride. This complex was identified to be bis-carbonyl [(^{iPr}PCP)Ir(H)$(CO)_2$][OTf] (**3e**), which can be prepared independently by treatment of **3a** with HOTf in CH_2Cl_2, followed by exposure to an atmosphere of CO. Complex **3e** is not a competent pre-catalyst for EF hydrogenation (entry 9). To further investigate the origin of the higher activity of HBF_4•Et_2O, [(^{iPr}PCP)Ir(H)$(CO)_2$][BF_4] (**3f**) was prepared by addition of HBF_4•Et_2O to **3a**, followed by exposure to CO atmosphere. We noted that **3f** was moderately active for EF hydrogenation (TON = 159, entry 8), but still less so than **3a**/HBF_4•Et_2 (entry 3). Additionally, we did not see evidence for **3a** in NMR spectra of reaction mixtures from experiments with **3a**/HBF_4•Et_2O. Clearly, differences in anion identity and ligand scaffold

determine whether (pincer)Ir(CO)$_2$(H)(X) species are produced, and to what extent these species sequester iridium intermediates off-cycle.

4.2.5 ^{tBu}PCP pre-catalysts

Based on the improved activity of (^{iPr}PCP)Ir-based systems over (^{iPr}POCOP)Ir based pre-catalysts, we investigated the (^{tBu}PCP)Ir(CO) (**4a**) scaffold. Despite the increased steric profile of the ligand, we hypothesized that increased hydricity of the dihydride and better stability of these complexes may result in greater reactivity for EF hydrogenation. Gratifyingly, the EF hydrogenation reaction using **4a** in the absence of acid produced 164 TON MeOH after 16 hours (Table 4.4, entry 1), significantly more than using **3a** (9.4 TON, Table 4.3, entry 1) or **1a** (6.4 TON, Table 4.1, entry 1). The ^{31}P NMR spectra of the reaction mixtures showed two signals, **4a** and *trans*- (^{tBu}PCP)Ir(H)$_2$(CO), **4b**. This suggests that a significant amount of dihydride **4b** is accessed under high H_2 pressures, despite the reported challenge of adding H_2 to **4a** at lower pressures.[15,32] As the EF and high-pressure reactors are not vigorously dried, trace water, as well as alcohols produced during reaction, presumably are available to provide a source of protons to catalyze hydrogen addition to the pre-catalyst.[15] A color change from colorless to yellow is observed in minutes after the reactors are opened. As with the hydrogen addition, acid-catalyzed elimination of H_2 from **4b** (colorless) to make **4a** (yellow) has been reported,[15] and is likely catalyzed by alcohol products or trace water when the H_2 atmosphere is released. We also noted the same (or increased) catalyst activity in a reactor recharge experiment analogous to that carried out with **1c**, with 93 TON MeOH measured after the first cycle and 241 TON after the second (Table 4.2).

Table 4.4. EF hydrogenation by ^{tBu}PCP complex **4a** and derivatives.[a]

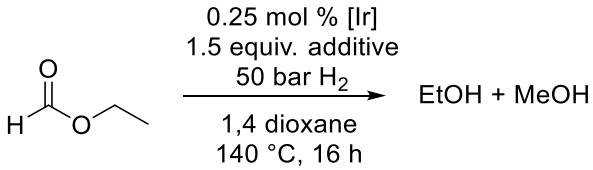

Entry	[Ir] pre-catalyst	Additive	TON MeOH equiv (st dev)	MeOH Equiv: EtOH Equiv
1	**4a**	--	163 (10)	87:100
2	**4a**	LiOTf*	114 (5)	82:100
3	**4a**	HBF_4•Et_2O	158 (2)	69:100
4	**4a**	HOTf	22.4 (20.3)	32:100
5	**4a**	H_2O**	180 (20)	80:100
8[†]	**4d**	--	0	--
9	**4e**	--	20 (6)	58:100
10	**4f**	--	127 (3)	81:100

[a] Conditions: 0.25 mol% [Ir] catalyst, 1.5 equiv. additive, 4 mmol EF, 2 mL 1,4-dioxane, 50 atm H_2, 140 °C, 16 hours. MeOH equiv. = MeOH + MF, EtOH equiv. = EtOH + 2x diethyl ether - MF. *5 equivalents. **20 μL. Entries based on two or three trials. One trial[†]

In contrast to catalyst scaffolds **1a** and **3a**, the addition of Lewis acid and Brønsted acid additives to hydrogenation reactions with **4a** either had no effect (entry 3) or reduced EF hydrogenation activity (entries 2 and 4). When HBF_4•Et_2O was used, the iridium species in solution after reaction were primarily **4a** and **4b**, just as when only **4a** was used as pre-catalyst. However, addition of HOTf decreased MeOH turnover, (22 TON, entry 4). Upon workup, reactions with added HOTf yielded a white precipitate that is partially soluble in reaction solution at room temperature. The ^{1}H NMR spectrum of this product indicated a single species with a hydride shift at -10.20 ppm in the ^{1}H NMR spectrum, indicative of a strong donor ligand *trans*- to the hydride, as well as a single ^{31}P NMR signal at 68.9 ppm (in CD_2Cl_2). The solid state structure showed a second CO molecule bound *trans*- to hydride, [(^{tBu}PCP)Ir(H)$(CO)_2$][OTf] (**4e**). As was the case for analogous complex **3e**, **4e** was not an active EF hydrogenation catalyst, producing 20 TON MeOH after 16 hours (entry 9). However, related complex [(^{tBu}PCP)Ir(H)$(CO)_2$][BF_4] (**4f**) produced 127 TON MeOH (entry 10), a partial restoration of catalytic activity of the **4a**/

HBF_4•Et_2O combination. ^{31}P NMR spectroscopy showed **4b** as the most abundant iridium species in solution after the reaction.

We also investigated the effect of LiOTf, which decreased TON MeOH from 164 to 114 (Table 4.4 entry 2). Finally, we also noted that addition of 20 μL water to the reaction mixture did not impact hydrogenation activity, as we observed the same activity within error with water added as without (180 TON, entry 5 vs 163 TON, entry 1, respectively).

4.2.6 Discussion of catalyst inactivation by CO coordination

Over the course of our studies, we isolated species of the form [(^{R}pincer)Ir(H)$(CO)_2$][X] reaction mixture after EF hydrogenation reactions using **4a**/H^+ and **3a**/H^+. A related complex, [(^{tBu}POCOP)Ir(H)$(CO)_2$][BF_4], obtained by addition of CO to [(^{tBu}POCOP)Ir(H)(CO)][BF_4], has been previously reported by Goldberg and Heinekey.[14] Complexes of the type [(^{R}pincer)Ir(H)$(CO)_2$][X] were readily synthesized by addition of relevant acid to (^{R}pincer)Ir(CO), followed by addition of 1 atm CO in CH_2Cl_2, as shown in Scheme 4.5. Consistent with the result of Goldberg and Heinekey, we found that all of the dicarbonyl complexes synthesized were stable to loss of CO under vacuum.[14] However, we were able to observe partial CO dissociation when a J-Young tube containing solutions of [(^{R}pincer)Ir(H)$(CO)_2$][X] were heated to 80 °C under static vacuum (see section 4.7.4).

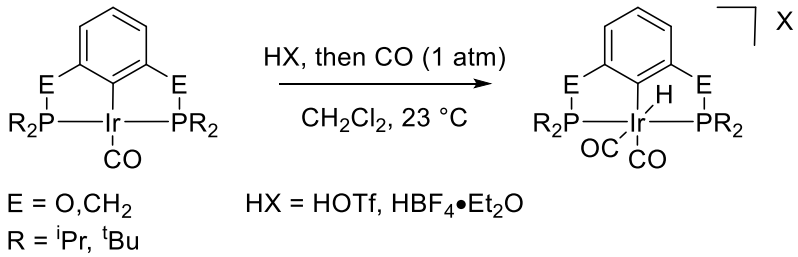

Scheme 4.5. General synthesis of [(^{R}pincer)Ir(H)$(CO)_2$][X] dicarbonyl complexes

We were then curious whether [(^{iPr}POCOP)Ir(H)(CO)$_2$][OTf] (**1e)** complex is formed in EF hydrogenation reactions with **1a**/HOTf, and synthesized **1e** by addition of CO to a solution of **1c**. We confirmed that a small amount of **1e** is present in the reaction mixture after EF hydrogenation using **1c** pre-catalyst. Additionally, **1e** showed similar activity for EF hydrogenation as **1c** (Table 4.1, entries 13 and 11, respectively) indicating that, while the dicarbonyl species may be an off-cycle species, in the case of the ^{iPr}POCOP-based pre-catalysts, the catalytically relevant intermediate may still be accessed from **1e**. ^{31}P NMR spectra of this solution after reaction showed a similar distribution of numerous phosphorous-containing iridium species as when the **1c** pre-catalyst is used.

We were surprised to find that for both ^{iPr}PCP and ^{tBu}PCP-based complexes, [(^{R}pincer)Ir(H)(CO)$_2$][OTf] was a much less effective pre-catalyst than [(^{R}pincer)Ir(H)(CO)$_2$][BF$_4$]. The identity of the counterion has a significant impact on catalyst inhibition; triflate anion is more deleterious to catalyst activity than BF$_4$, both when protic acid is added to the Ir(I) pre-catalyst and when part of a complex of the form [(^{R}pincer)Ir(H)(CO)$_2$][X]. More work would be necessary to elucidate origin of this difference. However, decomposition of BF$_4^-$ anions to BF$_3$ is known, especially at high temperatures.[43] It is possible that decomposition of BF$_4^-$ prevents either CO formation or generation of [(^{R}pincer)Ir(H)(CO)$_2$]$^+$. It would be interesting to investigate the effect of BF$_3$ on hydrogenation activity, as preliminary experiments have suggested that tris(pentafluorophenyl)borane (B(C$_6$F$_5$)$_3$) significantly assists EF hydrogenation by **3a**. Single trials with B(C$_6$F$_5$)$_3$ additive and **1a** resulted in 52 TON MeOH, **3a** = 240 TON MeOH and **4a** = 131 TON MeOH, (4 mmol EF, 0.25 mol% [Ir], 1.25 mol% B(C$_6$F$_5$)$_3$, 50 bar H$_2$, 140 °C, 16 hrs.) Boron LAs including B(C$_6$F$_5$)$_3$ and BF$_3$•OEt$_2$ have been shown by Zhou and coworkers to act as promoters in a related reaction, the deoxygenative hydrogenation of

secondary amides using a Ru(triphos)$(H)_2$CO pre-catalyst.[44] Similarly, they report that $B(C_6F_5)_3$ promotes deoxygenative hydrogenation of amides by (^{R}POCOP)Ir(H)(Cl) (R= ^{i}Pr, ^{t}Bu) pre-catalysts related to those studied in this chapter.[30] Given these promising initial results, and that borane LAs do not have available protons, we believe that borane LAs warrant further study as alternative additives for activating (^{R}pincer)Ir(CO) while avoiding proton-catalyzed side reactions, such as ether formation.

A control experiment was conducted using **1c** and MeOH in place of substrate. Because CO coordinates readily to **1c** to generate **1e**, we expected that if MeOH decomposition was the source of CO, **1e** would be generated and easily identified by diagnostic NMR signatures. There was no evidence of **1e** in both ^{1}H and ^{31}P NMR spectra of the reaction solution. Thus, we hypothesize that CO produced during the reaction must come from other species present in the reaction mixture, such as formate or hemiacetal intermediate.

Together, these experiments suggest that for ^{iPr}POCOP, ^{iPr}PCP and ^{tBu}PCP pre-catalysts, the presence of Brønsted acids facilitates decarbonylation. Excess CO coordinates to protonated Ir(III) species, generating a *cis*-dicarbonyl complex that is not catalytically active. For each pincer scaffold, counterion identity is critical for determining if the dicarbonyl complex can easily access the catalytic cycle. We find that ^{iPr}POCOP-based pre-catalysts are most active with the strongest acid and least coordinating counterion $HNTf_2$, but is still active with added HBF_4•Et_2O and HOTf (increasing activity ordered with acid strength). In contrast, ^{iPr}PCP supported pre-catalyst **3a** is most active with HBF_4•Et_2O additive, followed by $HNTf_2$, but addition of HOTf does not result in an active pre-catalyst/acid combination. Finally, **4a** did not require the addition of acid additives, unlike **1a** and **3a**. Addition of HBF_4•Et_2O did not impact EF hydrogenation, while HOTf was detrimental. Overall, the two most active pre-catalyst/additive combinations were **1a**/$HNTF_2$,

generating 222 TON MeOH after 5 hours, (Table 4.1 entry 7) and **3a**/HBF_4•Et_2O, with 220 TON MeOH after 5 hours, (Table 4.3, entry 4). Careful consideration of additive identity is thus an important factor in the design of improved pre-catalyst/additive combinations.

4.3 Expanded substrate scope

We sought to expand the scope for hydrogenations using (^{R}pincer)Ir(CO) catalysts. We investigated the hydrogenation of ethyl acetate (EA) with **1a** under the conditions in Table 4.1 and did not observe conversion of substrate after 16 hours, as comfirmed by quantitative ^{13}C NMR spectroscopy. Addition of 2 equivalents of HOTf to the reactions did not facilitate catalysis. At 10 equiv. HOTf relative to catalyst, hydrolysis of EA was observed (1%), as evidenced by the observed 1:1 ratio of acetic acid and diethyl ether (presumably from EtOH dehydration) and EtOH. Similarly, use of **3a** and 1.5 equiv. $HNTf_2$ or HBF_4•Et_2O (conditions active for EF hydrogenation) resulted in only the trace formation of EtOH (~2% conversion, 8 TON). The difference in EF and EA hydrogenation may be due to the increased steric bulk at the carbonyl carbon. This decreased activity may also be compounded by the 1,4-dioxane solvent. In the reported hydrogenation of esters by [Cp*Ir(bpy-OMe)OH_2][$OTf]_2$, neat EF is hydrogenated about three times faster than EA (341 TON vs 106 TON). In DME solvent, EF is hydrogenated seven times faster than EA (173 TON vs 24 TON).[6] Further studies would be necessary to determine if the solvent (in this case 1,4-dioxane) is suppressing hydrogenation activity compared to neat substrate by the (pincer)Ir pre-catalysts studied here. It is also possible that (^{R}pincer)Ir(CO)/additive combinations not yet investigated are active for EA hydrogenation

Aiming to compare to our previous results hydrogenating γ-valerolactone (GVL) using a [Cp*Ir(bpy-OMe)OH_2][$OTf]_2$, pre-catalyst in Chapter Two, we investigated the hydrogenation of GVL by the two (pincer)Ir/additive combinations most active for EF hydrogenation. We found

that **4a** was inactive for GVL hydrogenation under the conditions employed for EF hydrogenation above (4 mmol GVL, 0.25 mol% [Ir], 2 mL 1,4-dioxane, 50 atm H_2, 140 °C, 16 hours). The combination of **3a** and 1.5 equiv. HBF_4**.**Et_2O under the same conditions resulted in 12% conversion of substrate (TON = 48) to 2-MeTHF. Published systems for GVL hydrogenation under acidic conditions give similar results.[6,37] We conclude that the (^{R}pincer)Ir(CO) catalysts studied are not highly active for the transformation of GVL.

Attempts to hydrogenate dimethylformamide (DMF) using **1a**, **1c**, or **3a** resulted in no conversion of DMF (Scheme 4.6). This contrasts with results reported by Zhou and coworkers using (^{iPr}POCOP)Ir(H)(Cl) pre-catalysts, despite similar temperatures, pressures and reaction times. However, the experiments of Zhou and coworkers use toluene as the solvent instead of neat substrate, a much higher catalyst loading (1 mol% vs 0.055 mol%) and require stoichiometric LA additive. It is possible that conditions similar to those reported by Zhou would result successful amide hydrogenation by the iridium pre-catalysts studied here.

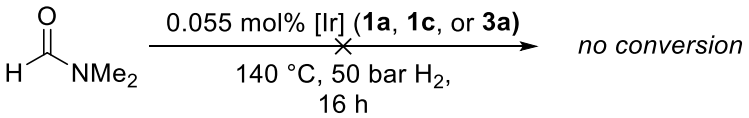

Scheme 4.6. Attempted hydrogenation of DMF using pre-catalysts **1a**, **1c**, or **3a**

We were also interested in the hydrogenation of dimethyl carbonate (DMC), as a potential intermediate in a CO_2 capture cascade (See Chapter One, Figure 1.5). To distinguish MeOH produced hydrogenation of the carbonyl carbon from that originating from the alkoxy fragments, we assessed the hydrogenation of diethyl carbonate (DEC). When DEC (2 mL, 16.50 mmol) was subjected to hydrogenation conditions (0.05 mol% **1c**, 18 h, 140 °C), no discernable MeOH was produced, but consumption of DEC and EtOH was observed by ^{1}H NMR spectroscopy. We hypothesize that acid-catalyzed transesterification of water for the alkoxy fragments will generate carbonic acid, H_2CO_3, which can decompose to CO_2 and H_2O. Control experiments showed that

this decomposition of DEC can also be catalyzed by 1 mol% sulfuric acid under the same conditions.

Overall, we found that any increases in the steric demand of substrates significantly impacted hydrogenation activity. As we are interested in catalysts that operate under mild conditions, we chose not to pursue more forcing conditions (e.g. higher temperatures, pressures or catalyst loadings) in an effort to increase catalyst activity.

4.4 Probing the EF hydrogenation mechanism

Initial screening reactions with **1c** in neat substrate suggest that increasing pressure, temperature, and pre-catalyst loading increases MeOH production from EF hydrogenation. The details of these experiments are given in section 4.8.5. We have observed EF hydrogenation by ^{iPr}PCP and ^{iPr}POCOP-based pre-catalysts and acid, either with acid and iridium pre-catalyst added separately to the reaction vessel, or added together as pre-formed Ir(III)(H)(X)(CO). We hypothesize that for these hydrogenations, substrate protonation (either by an iridium dihydrogen complex or directly by HX) is essential for hydrogenation. However, in the case of ^{tBu}PCP pre-catalysts, this activation is unnecessary. This may be due to the increased hydride donor ability of dihydride complex **4b** eliminating the need for activation by H^+. For PCP-based catalysts, sequestration of [(^{R}pincer)Ir(H)$(CO)_2$][OTf] species impedes hydrogenation activity while catalytically active species may be accessed from the ^{iPr}POCOP pre-catalyst, **1c**. This may be because the ^{iPr}POCOP ligand scaffold contributes less electron density to iridium than the analogous PCP ligand, leading to a CO ligand that is more weakly bound and more easily displaced. We have not identified the source of the additional CO, but hypothesize that CO may be generated by decarbonylation of aldehyde intermediates competitive with aldehyde hydrogenation.[29]

4.5 Structural comparison of (pincer)Ir(CO)-based species

4.5.1 Geometries of (^{R}pincer)Ir(H)(CO)$^{+}$- based complexes

We were able to characterize [(^{R}pincer)Ir(H)(CO)$_2$][OTf] species (^{R}pincer = ^{iPr}PCP, ^{iPr}POCOP ^{tBu}PCP) by X-ray crystallography. Like related six-coordinate pincer Ir complexes, these molecules have pseudo-octahedral geometry, with one CO bound equatorially and one CO bound in the axial position. Crystal structures of related (^{R}pincer)Ir(H)(CO)$^{+}$ species **1c** and **4c** were obtained and show triflate anion binding to the metal center *trans*- to the hydride, via the sulfonate oxygen. Attempts to synthesize (^{iPr}PCP)Ir(H)(CO)(OTf) either by chloride abstraction from **3d** (mixture of *cis*- and *trans*-) or by addition of HOTf to **3a** resulted in mixtures of products. However, we were able structurally characterize [(^{iPr}PCP)Ir(H)(H$_2$O)(CO)][HBF$_4$], from a catalytic reaction mixture from EF hydrogenation by **3a** and HBF$_4$•Et$_2$O (section 4.8, Figure 4.14). In this structure, water is coordinated *trans*- to the hydride, analogous to a structure of closely related [(^{iPr}POCOP)Ir(H)(H$_2$O)(CO)][HBF$_4$] reported by Goldberg and Heinekey as was the related structure of [(^{tBu}POCOP)Ir(H)(CO)][HBF$_4$], without water coordinated.[14] The steric profile of the ^{t}Bu groups is thought to hinder coordination of adventitious water to the metal center. We are not aware of any (^{R}pincer)Ir(H)(CO)$^{+}$ structure with BF$_4^-$ bound at the metal center, consistent with our understanding of BF$_4^-$, as a less coordinating counterion.

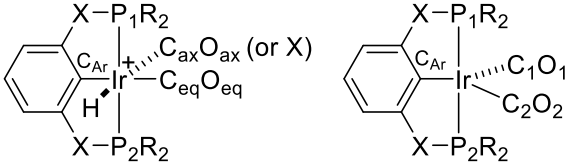

Figure 4.4 (pincer)Ir complexes and labeling scheme.

Along with previously reported (^{R}pincer)Ir(CO)-based complexes, we now have available a set of molecules that allows structural comparisons based on small changes in ligation. A chart of structural parameters for complexes presented in this work as well as selected complexes from the

literature is available in Table 4.5. Figure 4.4 describes the geometry of these complexes and the labeling of substituents used in this section. Overall, we note that complexes with the more electron-rich PCP scaffold show a larger P-Ir-P bite angle, but longer Ir-P and Ir-aryl bonds, compared with POCOP-based complexes (for example, see Table 4.5 entry 1 vs entry 3). However, changes in the Ir-O_{eq} distance are minimal, suggesting that the increased oxygen pi-donation to Ir in the POCOP complexes roughly balances out the increased electron density available on Ir from the PCP ligand. These trends are consistent through the different (^{R}pincer)Ir species studied.

4.5.2 Structural parameters for (^{R}pincer)Ir(H)(CO)(X) complexes

Structures for Ir(I) (^{R}pincer)Ir(CO) complexes analogous to (^{R}pincer)Ir(H)(CO)$^{+}$ species are known and provide a point for comparison. The structural changes resulting from addition of H-X are small. ^{iPr}POCOP complexes may be taken as a representative case study for these differences, as we observe that these trends hold within sets of complexes with each ligand scaffold. The most striking change is an increase in the Ir-O_{eq} distance, (from 3.018(8) to 3.055(1) Å (**1a** vs **1c**, Table 4.5, entry 15a vs 5), suggesting weaker coordination of the CO group, due to less electron density available for backbonding to CO. Small increases are also seen in the aryl C-Ir and P-Ir bond lengths, while the P-Ir-P bond angle decreases slightly. This is consistent with decreased electron density available from Ir in a higher oxidation state and having formed additional Ir-ligand bonds.

There are fewer notable structural differences within (^{R}pincer)Ir(H)(CO)$^{+}$; as expected for complexes with similar electronic structures, there are no significant differences in bond lengths when comparing available structures of (^{R}pincer)Ir(H)(CO)$^{+}$ species. However, the steric demand of the ligand bound *trans*- to hydride can distort the C_{eq}-Ir-X bond angle, as in the case of sterically crowded **4c** (96.47(8)°, entry 9) or when water is bound, as in [(^{iPr}PCP)Ir(H)(H_2O)(CO)][HBF_4] (96.53(9)°, entry 6). Structures of *trans*-(^{R}POCOP)Ir(H)(Cl) show CO-Ir-Cl angles close to 90°

(91.8(2)° for **1d**, entry 12), as expected for bound anion with a smaller steric profile. Analogous structures of *trans*-(^{R}PCP)Ir(H)(Cl) are not available for comparison.

4.5.3 Structural changes from coordinating CO trans to hydride

We observe that the coordination of a second CO ligand *trans* to hydride, causes significant structural changes. The axial CO-Ir-CO_{eq} angle is distorted significantly away from the 90° expected in an octahedral geometry (C_{eq}-Ir-C_{ax} = 98.64(9)° for **1e**) We hypothesize that this is due to the orientation of the axial CO ligand to maximize backbonding interactions. The metal dz^2 orbital best available in the axial position does not have the correct symmetry to donate into the π^* orbital of the axial CO. Examining the Ir-O bond distance can give insight into the character of the Ir-CO interaction without relying on Ir-C bond distances where the location of the carbon is more uncertain due to the high electron density near the Ir. The Ir-O_{eq} distance increases upon binding of the second CO, (O_{eq}-Ir = 3.086(2) Å for **1e** and 3.055(1) Å for **1c**, entries 1 and 5), due to decreased electron density at iridium available for backbonding to CO_{eq} in competition with CO_{ax}. Similarly, Ir-C_{Ar} increases in length upon coordination of axial CO, as does Ir-P, while the P-Ir-P angle decreases (154.01(2)° vs 157.303(14)°for **1e** vs **1c**, entries 1 and 5). The CO in the axial position is located further from the iridium (Ir-O_{ax} = 3.107(2) Å for **1e**, entry 1), consistent with the higher *trans*- influence of hydride relative to C_{Ar}. It is therefore the axial CO that is likely to dissociate from the complex first (see section 4.8.4).

Table 4.5. Selected structural parameters for (pincer)Ir(CO) molecules

	Name	PIrP (°)	$C_{eq}IrC_{ax}$(°)	Ir-P1 (Å)	Ir-P2 (Å)	Ir-C_{Ar} (Å)	Ir-O_{eq}(Å)	Ir-O_{ax} (Å)	Ir-C_{eq} (Å)	Ir-C_{ax} (Å)
1	[(^{iPr}POCOP)Ir(H)$(CO)_2$][OTf]	154.01(2)	98.64(9)	2.3154(6)	2.3276(6)	2.068(2)	3.086(2)	3.107(2)	1.964(2)	1.994(2)
2	[(^{tBu}POCOP)Ir(H)$(CO)_2$][BF_4][14]	152.52(2)	98.76(8)	2.3641(6)	2.3635(6)	2.061(2)	3.062(2)	3.091(1)	1.941(2)	1.974(2)
3	[(^{iPr}PCP)Ir(H)$(CO)_2$][OTf]	154.52(5)	99.8(3)	2.3412(10)		2.114(6)	3.082(5)	3.098(5)	1.960(7)	1.978(7)
4	[(^{tBu}PCPIr)(H)$(CO)_2$][OTf]	156.61(12)	102.8(6)	2.375(3)		2.120(13)	3.049(11)	3.106(10)	1.954(12)	1.949(11)
		PIrP (°)	**C_{eq}IrX**	**Ir-P1 (Å)**	**Ir-P2 (Å)**	**Ir-C_{Ar} (Å)**	**Ir-O_{eq}(Å)**	**Ir-anion**	**Ir-Ceq (Å)**	**Ir-OH_2**
5	(^{iPr}POCOP)Ir(H)(CO)(OTf)	157.303(14)	88.19(6)	2.3088(4)	2.3154(4)	2.0602(15)	**3.055(1)**	**2.267(1)**	**1.9117(16)**	
6	[(^{iPr}POCOP)Ir(H)(H_2O)(CO)][BF_4][14]	157.62(2)	96.53(9)	2.3146(7)	2.3181(7)	2.051(2)	3.058(2)	-	1.925(3)	2.241(1)
7	[(^{tBu}POCOP)Ir(H)(CO)][BF_4][14]	158.29(2)	-	2.3258(5)	2.3225(5)	2.028(2)	3.049(2)	-	1.917(2)	
8	[(^{iPr}PCP)Ir(H)(H_2O)(CO)][BF_4]	163.26(6)	97.4(3)	2.327(2)	2.331(2)	2.090(7)	3.057(5)	-	1.906(6)	2.245(6)
9	(^{tBu}PCP)Ir(H)(CO)(OTf)	159.62(2)	96.47(8)	2.3428(8)	2.3460(7)	2.087(2)	3.051(2)	2.276(1)	1.919(2)	
		PIrP (°)	**C1IrC2 (°)**	**Ir-P1 (Å)**	**Ir-P2 (Å)**	**Ir-C_{Ar} (Å)**	**Ir-O1 (Å)**	**Ir-O2 (Å)**	**Ir-C1 (Å)**	**Ir-C2 (Å)**
10	(^{iPr}POCOP)Ir$(CO)_2$[45]	152.22(7)	113.5(4)	2.306(2)	2.291(2)	2.114(8)	3.053(7)	3.040(6)	1.934(9)	1.876(9)
11	(^{iPr}PCP)Ir$(CO)_2$[45] (^{tBu} versions not stable)[45]	142.86(3)	105.3(1)	2.3117(9)	2.3055(9)	2.119(3)	3.060(3)	3.037(3)	1.920(3)	1.894(3)
		PIrP (°)	**C_{eq}IrCl**	**Ir-P1 (Å)**	**Ir-P2 (Å)**	**Ir-C_{Ar} (Å)**	**Ir-O1(Å)**		**Ir-C1 (Å)**	**Ir-Cl**
12	(^{iPr}POCOP)Ir(H)(Cl)(CO)[14]	157.36(7)	91.8(2)	2.304(1)	2.296(2)	2.051(7)	3.053(5)		1.906(7)	2.483(2)
13	(^{tBu}POCOP)Ir(H)(Cl)(CO)	155.48(4)	91.4(1)	2.335(1)	2.347(1)	2.058(4)	3.046(4)		1.903(4)	2.511(1)
14	*cis*-(^{iPr}PCP)(H)(Cl)(CO)	161.12(4)	91.6(1)	2.319(1)	2.321(1)	2.063(5)	3.078(4)		1.946(4)	2.468(1)
		PIrP (°)		**Ir-P1 (Å)**	**Ir-P2 (Å)**	**Ir-C_{Ar} (Å)**	**Ir-O_{eq}(Å)**		**Ir-C_{eq} (Å)**	
15	(^{iPr}POCOP)Ir(CO) (1)*	157.39(9)		2.260(2)	2.258(3)	2.05(1)	3.02(1)		1.88(1)	
15a	(^{iPr}POCOP)Ir(CO) (2)*	157.95(8)		2.274(2)	2.245(2)	2.027(8)	3.018(8)		1.86(1)	
16	(^{iPr}POCOP)Ir$(H)_2$(CO)[15]	157.13(2)		2.2814(6)	2.2894(6)	2.062(1)	3.039(1)		1.894(2)	
17	(^{tBu}POCOP)Ir(CO)[24]	157.51(4)		2.279(2)	2.285(2)	2.060(4)	3.036(4)		1.884(4)	
18	(^{iPr}PCP)Ir(CO) (1)*	163.70(4)		2.277(1)	2.291(1)	2.096(4)	3.008(4)		1.850(4)	
19a	(^{iPr}PCP)Ir(CO) (2)*	163.53(4)		2.271(1)	2.287(1)	2.087(4)	3.016(4)		1.857(4)	
20	(^{tBu}PCP)Ir(CO)[28]	163.1(1)		2.298(3)	2.305(3)	2.09(1)	2.98(1)		1.85(1)	
20a	(^{tBu}PCP)Ir(CO)[28]	164.6(1)		2.292(3)	2.297(4)	2.100(8)	3.039(6)		1.875(9)	

C_{eq} = carbon of CO ligand in plane with pincer, C_{ax} = carbon of CO ligand bound in the axial position, O_{eq} and O_{ax} are respective oxygen atoms. C_{Ar} is carbon of pincer aryl ring bound to Ir, P1 and P2 are ligand phosphorous atoms. [(^{tBu}PCP)Ir(H)$(CO)_2$][OTf] representative bond lengths and angles shown from major species. [(^{iPr}PCP)Ir(H)$(CO)_2$][OTf] had two unit cells with similar bond lengths; data for one is given as representative.

Related Ir(I) (^{iPr}pincer)Ir(CO)$_2$ complexes have also been reported (entries 10 and 11).[45] As these complexes are 5-coordinate and can take a distorted square planar or trigonal bipyramidal geometry, a wider CO-Ir-CO angle is observed (ex. 113.5(4)° for (^{iPr}POCOP)Ir(CO)$_2$, entry 10) as well as a smaller P-Ir-P angle (152.22(7)° for (^{iPr}POCOP)Ir(CO)$_2$, entry 10). As expected, Ir(I) complexes have shorter Ir-P bonds, longer Ir-C_{Ar} bonds and shorter Ir-CO bonds than the Ir(III) dicarbonyls, due to the increased electron density available (for example, see entry 1 vs 10). Overall, observed trends in structural parameters reflect differences expected from associated steric and electronic contributions.

4.6 Conclusions

Understanding the reactivity of a family of pincer iridium complexes with hydrogen has led to the development of a new system capable of hydrogenating formate esters. In investigating four pincer scaffolds with small differences in steric and electronic characteristics (^{iPr}POCOP, ^{iPr}PCP, ^{tBu}POCOP, and ^{tBu}PCP), we observed a range of catalytic activity. Building on prior reports of ester hydrogenation by catalysts with spectator (chemically innocent)[5,6,37,46] ligands, we expected acid additives to increase hydrogenation activity. ^{tBu}PCP-supported pre-catalyst **4a** was found to be the most active for EF hydrogenation without additives. In fact, we did not identify any acid additives that accelerated EF hydrogenation by **4a**. As this is the most electron-rich scaffold studied, we hypothesize that the dihydride **4b** would have most hydridic hydrides, and the most acidic corresponding dihydrogen hydride complex, enabling the transfer of protons and hydride to substrate without additional activation. In contrast, we found that ^{iPr}POCOP- and ^{iPr}PCP-supported **1a** and **3a,** respectively, were poor pre-catalysts for EF hydrogenation when employed on their own. However, the addition of protic acids served to activate these pre-catalysts. Activity was strongly dependent on the acid strength and counterion identity. For the

^{iPr}POCOP scaffold, $HNTf_2$ additive resulted in the most active pre-catalyst/additive combination, while for ^{iPr}PCP, HBF_4•Et_2O was the most effective additive, followed by $HNTf_2$ and then HOTf.

With added HOTf, we observed deactivation of ^{iPr}PCP **3a** and ^{tBu}PCP **4a** by formation of catalytically inactive dicarbonyl complexes **3e** and **4e.** Interestingly, the formation of ^{iPr}POCOP **1e** is not a deactivation pathway; **1e** is an active pre-catalyst. Additionally, dicarbonyl complexes with BF_4^- counterion instead of OTf^- (**3f** and **4f)** are also active pre-catalysts, indicating a strong anion dependence. We note that metal triflate LAs LiOTf and NaOTf did not lead to significant enhancements in MeOH TON, and when added with ^{tBu}PCP pre-catalyst **4a**, were detrimental to EF hydrogenation. Finally, ^{tBu}POCOP pre-catalyst **2a** was not active, which we attribute to the large steric profile and relatively electron-poor ligand.

While hydrogenations by pre-catalysts reported here are confined to formate esters, they are robust under conditions that impede many reported systems (added water, added LA or protic acid). Though we have not optimized reaction conditions to maximize TON of MeOH produced, single experiments with pre-catalyst **1c** demonstrated over 6000 TON of MeOH produced, though **1c** was not the most active pre-catalyst combination screened. Given this, we are optimistic about the possibility of further increases in TON of MeOH. These qualities may make them viable candidates for cascade systems that convert CO_2 and H_2 into MeOH via formate ester intermediates. The inclusion of these catalysts in cascade systems is the subject of ongoing work in our group, and preliminary investigations are reported in Chapter Five.

4.7 Experimental

4.7.1 General Considerations

Experiments and manipulations were performed using Schlenk technique under N_2 atmosphere or a nitrogen-filled glovebox, unless otherwise specified. All solvents and liquid reagents were degassed with N_2 prior to use. 1,4-dioxane, ethyl acetate and formic acid were stored over 4Å molecular sieves, and EtOH was stored over 3Å molecular sieves under inert atmosphere. $HNTf_2$ was purified by sublimation. All other reagents were used as received. NMR spectra were obtained on a Bruker AV 700, Bruker AV-500, DRX-500 or AV300 NMR instrument. High-pressure experiments were conducted using a Parr Series 5000 Multi Reactor system, equipped with stirring and pressure monitoring. Reactor temperature monitored by thermocouples embedded in the aluminum heating block and regulated by SpecView software. Infrared spectra were recorded on a Bruker Tensor 27 FTIR instrument. X-ray data was collected at -173 °C on a Bruker APEX II single crystal X-ray diffractometer, using Mo-radiation.

Complexes **1d**,[14] **3d**,[15] **4d**,[47] **2b**,[15] **1a**,[15] **2a**,[24] **3a,**[15] and **4a**[15] were synthesized according to literature procedures.

4.7.2 Experimental procedures

Sample procedure for high pressure reactor hydrogenation experiment with HOTf

In a N_2 atmosphere glovebox, 6.1 mg (0.0099 mmol) **4a** was massed into a PTFE Parr reactor liner. Into a glass vial, 5.3 μL (0.060 mmol) HOTf was dispensed via microliter pipette, and 2 mL 1,4-dioxane was added. The HOTF solution was agitated to mix, and 0.5 mL was dispensed into the PTFE liner via syringe. A further 1.5 mL of 1,4-dioxane was added via syringe to bring the total solvent volume to 2.0 mL, and 323 μL (4.0 mmol) EF was added to the reactor via μL

syringe. The reactor was equipped with a stir bar and sealed and removed from the glovebox. The reactor was connected to the Parr gas manifold, and the manifold was purged with H_2. The reactor atmosphere was exchanged for H_2 through 3-4 pressurize-purge cycles, and the reactor was pressurized to 50 bar H_2. The reactor was heated to 140 °C and stirred at 300 rpm. After 16 hours, the reactor was removed from the heat, allowed to cool for twenty minutes and then cooled on ice. The reactor was vented, opened and the contents were analyzed.

Analysis of Parr reactor experiments

The reactor was opened, and 50 μL mesitylene were added to the reactor via μL syringe. The contents of the reactor were agitated to ensure good mixing. For ^{13}C experiments, 4.5-5 mg $Cr(acac)_3$ was weighed into a NMR tube. A 500 μL aliquot of solution was placed into the tube. Quantitative ^{13}C NMR spectra were collected using an inverse-gated pulse sequence. For ^{1}H NMR spectroscopic analysis, a 500 uL aliquot was placed into an NMR tube containing a C_6D_6 glass capillary. ^{31}P NMR spectra were obtained of neat reaction solution and referenced to an external H_3PO_4 standard.

Synthesis of [(^{iPr}POCOP)Ir(H)(CO)][OTf] ***1c***

In an N_2 atmosphere glovebox, 0.3153 g (0.531 mmol) of *trans*-**1d** and 0.135 g (0.525 mmol) AgOTf were loaded into a 50 mL Schlenk flask. 20 mL of N_2 sparged CH_2Cl_2 was added via syringe. The resulting solution was stirred in the dark for two hours, after which time an orange solution with white precipitate was observed. The solution was cannula filtered to a second Schlenk flask, and the solvent was removed under vacuum. In a nitrogen atmosphere box, the resulting solid was dissolved in 2 mL CH_2Cl_2, transferred to a vial, layered with Et_2O and pentane, and left to crystallize at -30 °C. The resulting product was recrystallized three times, and the final product was obtained as colorless to pale pink crystals. Yield: 0.341 g (0.480 mmol), 90%.

NMR: ^{1}H NMR (CD_2Cl_2, 300 MHz): δ 7.03 (t, $^{3}J_{HH}$ = 8.02 Hz, 1H; Ar-*H*), 6.64 (d, $^{3}J_{HH}$ = 8.04, 2H; Ar-*H*), 3.11, (m, 2H, C*H*(CH3)$_2$), 2.58 (m, 2H, C*H*(CH3)$_2$), 1.50-1.35 (m, 12H; ^{i}Pr-*H*), 1.20-1.05 (m, 6 H; ^{i}Pr-*H*), 0.99-0.87 (m, 6H; ^{i}Pr-*H*), -25.19 (t, $^{2}J_{PH}$ = 13.26, Ir-*H*). ^{31}P NMR (CD_2Cl_2, 121 MHz) δ 171.4 (s). ^{13}C{^{1}H} NMR (CD_2Cl_2, 125.7 MHz, 27.65 °C): δ 180.31 (m, Ir-*C*O), 165.82 (m, C_{Ar}), 130.07 (s; C_{Ar}), 128.81 (m; C_{Ar}), 106.27 (m; C_{Ar}), 31.37 (vt, $^{1}J_{PC}$ + $^{3}J_{PC}$ = 15.7 Hz; P*C*H(CH$_3$)$_2$), 28.68 (m, P*C*H(CH$_3$)$_2$), 18.91 (m, PCH(*C*H$_3$)$_2$), 18.63 (m; PCH(*C*H$_3$)$_2$), 18.14 (s; PCH(*C*H$_3$)$_2$), 15.91 (s; PCH(*C*H$_3$)$_2$). IR (solution, CH_2Cl_2, cm^{-1}): ν(CO) = 2048.

Synthesis of [(^{iPr}POCOP)Ir(H)(CO)$_2$][OTf] ***1e***

In a 20 mL Kontes valve flask, 40.7 mg (0.0571 mmol) **1c** was dissolved in 4 mL CH_2Cl_2. The flask was briefly exposed to vacuum and filled with CO gas. The solution was stirred for half an hour remaining colorless. CH_2Cl_2 was removed under vacuum. In a nitrogen atmosphere drybox, the resulting white solid was dissolved in minimal (0.5 mL) CH_2Cl_2, transferred to a vial, layered with 1 mL pentane and 0.5 mL Et_2O, and stored at -30 °C. The mother liquor was decanted, leaving 28.2 mg (0.0381 mmol, 67% yield) of a colorless crystalline product, which was further dried under vacuum. Crystals obtained were suitable for X-ray crystallography.

^{1}H NMR (CD_2Cl_2, 300.10 MHz, 24 °C, δ) 7.10 (tt, $^{3}J_{HH}$ = 8.13 Hz, J_{PH} = 1.06 Hz, 1H; Ar-*H*), 6.74 (d, $^{3}J_{HH}$ = 8.13 Hz, 2H; Ar-*H*), 2.84 (m, 2H; P-C*H*(CH$_3$)$_2$), 2.65 (m, 2H; P-C*H*(CH$_3$)$_2$), 1.46 (m, 12H; P-CH(C*H*$_3$)$_2$), 1.19 (m, 6 H, P- CH(C*H*$_3$)$_2$), 1.07 (m, 6 H, P- CH(C*H*$_3$)$_2$, -10.67 (t, $^{2}J_{PH}$ = 14.43 Hz, Ir-*H*). ^{31}P{^{1}H} NMR (CD_2Cl_2, 121.49 MHz, 24 °C, δ) 160.5 (s). ^{13}C{^{1}H} NMR (CD_2Cl_2, 125.7 MHz, 27.65 °C, δ) 165.15 (m, Ir-*C*O), 163.49 (m, C_{Ar}), 130.68 (s; C_{Ar}), 108.75 (m; C_{Ar}), 108.11 (m, C_{Ar}), 33.83 (vt, $^{1}J_{PC}$ + $^{3}J_{PC}$ = 17.42 Hz; P*C*H(CH$_3$)$_2$), 32.50 (m, P*C*H(CH$_3$)$_2$), 17.85-17.73 (m, PCH(*C*H$_3$)$_2$), 17.31 (s PCH(*C*H$_3$)$_2$. One Ir-*C*O not observed, consistent with reported spectra of (^{iPr}POCOP)Ir carbonyl species.[45]

Synthesis of [(^{tBu}PCP)Ir(H)(CO)$_2$][OTf] ***4e***

In a nitrogen atmosphere drybox, a 50 mL Kontes valve flask was charged with 46.5 mg (0.0758 mmol) **4a** dissolved in 5 mL CH_2Cl_2. To this yellow solution, triflic acid (11.7 μL, 0.0132 mmol) was added. On a vacuum manifold, the flask was subjected to one freeze-pump-thaw cycle, and was backfilled with CO, resulting in a color change to pale yellow. The solution was allowed to stir for half an hour. CH_2Cl_2 was removed under vacuum, producing colorless crystals and a brown residue. In a nitrogen atmosphere drybox, the solids were dissolved in minimal (1 mL) CH_2Cl_2, transferred to a vial, layered with 1 mL pentane and 0.5 mL Et_2O, and stored at -30 °C. The filtrate was decanted, leaving a colorless crystalline product which was further dried under vacuum. Crystals obtained were of sufficient quality for X-ray diffraction.

^{1}H NMR (CD_2Cl_2, 300.10 MHz, 27 °C, δ) 7.18 (d, J_{HH} = 7.5 Hz, 1H; Ar-*H*), 7.09 (t, J_{HH} = 7.5 Hz, 2H; Ar-*H*), 3.75 (dvt, $^2J_{HH}$ = 17.4, $^2J_{PH}$ + $^4J_{PH}$ = 4.4 Hz, 2H; Ar-C*H*$_2$PR), (dvt, $^2J_{HH}$ = 17.4, $^2J_{PH}$ + $^4J_{PH}$ = 4.0 Hz, 2H; Ar-C*H*$_2$PR), 1.5 (vt, $^3J_{PH}$ + $^5J_{PH}$ = 7.8 Hz, 18H; PC(C*H*$_3$)$_3$), 1.31 (vt, $^3J_{PH}$ + $^5J_{PH}$ = 7.7 Hz, 18H; PC(C*H*$_3$)$_3$), -10.20 (t, $^2J_{PH}$ = 12.2 Hz, 1H). ^{31}P{^{1}H} NMR (CD_2Cl_2, 121.49 MHz, 27 °C, δ) 69.7 (s). ^{13}C{^{1}H} NMR (CD_2Cl_2, MHz, 25 °C): δ 170.77 (m, Ir-*C*O), 168.53 (m, Ir-*C*O), 148.52 (m; C_{Ar}), 137.15 (s; C_{Ar}), 128.17 (s; C_{Ar}), 124.08 (m; C_{Ar}), 38.49 (m, *C*H$_2$PR$_2$), 37.55 (m,; Ar*C*H$_2$PR$_2$), 30.19 (s; PC(*C*H$_3$)$_3$), 29.19 (s; PC(*C*H$_3$)$_3$).

Synthesis of [(^{iPr}PCP)Ir(H)(CO)$_2$][BF$_4$] ***3f***

In a nitrogen atmosphere drybox, a 20 mL Kontes valve flask was charged with 42.5 mg (0.076 mmol) **3a** dissolved in 2 mL CH_2Cl_2. To this yellow solution, HBF_4•Et_2O (12 μL, 0.088 mmol) was added, resulting in a pale yellow solution. On a vacuum manifold, the flask was subjected to three freeze-pump-thaw cycles and then was backfilled with CO, resulting in a rapid color change to pale yellow. The solution was allowed to stir overnight. CH_2Cl_2 was removed

under vacuum to yield colorless solid. In a nitrogen atmosphere drybox, the solids were dissolved in minimal (1 mL) CH_2Cl_2, transferred to a vial, layered with 1.5 mL pentane and 0.2 mL Et_2O, and stored at -30 °C. The filtrate was decanted, leaving behind 30 mg (0.044 mmol, 58% yield) of a pale yellow crystalline product.

^{1}H NMR (CD_2Cl_2, 300.10 MHz, 25 °C): δ 7.17 (d, J_{HH} = 7.5 Hz, 1H; Ar-*H*), 7.07 (m, 2H; Ar-*H*), 3.67 (m, 2H; Ar-C*H*$_2$PR), 2.56 (m, 2H; PC*H*$(CH_3)_2$), 2.40 (m, 2H; PC*H*$(CH_3)_2$), 0.91-1.47 (m, 24H; PCH(C*H*$_2)_2$), -10.24 (t, $^2J_{PH}$ = 12.66 Hz, 1H; Ir-*H*). ^{31}P{^{1}H} NMR (CD_2Cl_2, 121.49 MHz, 25 °C): δ 51.8 (s). ^{13}C{^{1}H} NMR (CD_2Cl_2, MHz, 24.7 °C): δ 167.28 (m, Ir-*C*O), 166.25 (t, $^2J_{PC}$ = 5.07 Hz; Ir-*C*O), 147.33 (m; *C*$_{Ar}$), 135.16 (s; *C*$_{Ar}$), 127.76 (m; *C*$_{Ar}$), 124.12 (m; *C*$_{Ar}$), 39.13 (vt, $^1J_{PC}$ + $^3J_{PC}$ = 17.95 Hz; *C*H$_2$PR$_2$), 27.73 (vt, $^1J_{PC}$ + $^3J_{PC}$ = 15.09 Hz; P*C*H$(CH_3)_2$), 26.67 (vt, $^1J_{PC}$ + $^3J_{PC}$ = 17.31 Hz; P*C*H$(CH_3)_2$), 19.61 (s; PCH(*C*H$_3)_2$), 19.57 (s; PCH(*C*H$_3)_2$), 18.74 (s; PCH(*C*H$_3)_2$), 18.23 (s; PCH(*C*H$_3)_2$).

Synthesis of [(^{iPr}PCP)Ir(H)(CO)$_2$][OTf] ***3e***

In a nitrogen atmosphere drybox, a 20 mL Kontes valve flask was charged with 54.3 mg (0.097 mmol) **3a** dissolved in 3 mL CH_2Cl_2. To this yellow solution, 9 μL HOTf (0.102 mmol) was added, resulting in a pale yellow solution. On a vacuum manifold, the flask was subjected to two freeze-pump-thaw cycles and then was backfilled with CO, resulting in a color change to paler yellow. The solution was allowed to stir overnight. CH_2Cl_2 was removed under vacuum, producing pale yellow solid. In a nitrogen atmosphere drybox, the solids were dissolved in minimal (0.5 mL) CH_2Cl_2, transferred to a vial, layered with 2 mL pentane and 0.2 mL Et_2O, and stored at -30 °C. The filtrate was decanted, leaving behind approximately 40 mg (0.054 mmol, 56 % yield) of a pale yellow-green crystals that were X-ray suitable for diffraction. The product was dried under vacuum prior to use in catalytic reactions

^{1}H NMR (CD_2Cl_2, 499.71 MHz**,** 24.3 °C): δ 7.17 (d, J_{HH} = 7.5 Hz, 1H; Ar-*H*), 7.08 (m, 2H; Ar-*H*)**,** 3.68 (m, 4H; Ar-CH_2PR), 2.57 (m, 2H; PC*H*$(CH_3)_2$), 2.41 (m, 2H; PC*H*$(CH_3)_2$), 1.31-1.43 (m, 12H; PCH(CH_2)$_2$), 1.19 (m, 6H; PCH(CH_2)$_2$), 1.00 (m, 6H; PCH(CH_2)$_2$), -10.24 (t, $^{2}J_{PH}$ = 12.66 Hz, 1H; Ir-*H*). ^{31}P{^{1}H} NMR (CD_2Cl_2, 121.49 MHz, 25 °C): δ 51.8 (s). ^{13}C{^{1}H} NMR (CD_2Cl_2, MHz, 24.7 °C): δ 167.31 (t, $^{2}J_{PC}$ = 5.05 Hz; Ir-*C*O), 166.28 (t, $^{2}J_{PC}$ = 5.05 Hz; Ir-*C*O), 147.35 (m; C_{Ar}), 135.13 (s; C_{Ar}), 127.69 (s; C_{Ar}), 124.07 (m; C_{Ar}), 39.09 (vt, $^{1}J_{PC}$ + $^{3}J_{PC}$ = 17.78 Hz; *C*H_2PR_2), 27.68 (vt, $^{1}J_{PC}$ + $^{3}J_{PC}$ = 15.18 Hz; P*C*H$(CH_3)_2$), 26.61 (vt, $^{1}J_{PC}$ + $^{3}J_{PC}$ = 17.29 Hz; P*C*H$(CH_3)_2$), 19.59 (s; PCH(*C*$H_3)_2$), 19.54 (s; PCH(*C*$H_3)_2$), 18.71 (s; PCH(*C*$H_3)_2$), 18.19 (s; PCH(*C*$H_3)_2$).

Synthesis of [(^{tBu}PCP)Ir(H)(CO)$_2$][BF4] ***4f***

In a nitrogen atmosphere drybox, a 20 mL Kontes valve flask was charged with 43.4 mg (0.0707 mmol) **4a** dissolved in 2 mL CH_2Cl_2. To this yellow solution, 10 μL HBF_4•Et_2O (0.0735 mmol) was added, resulting in a green solution. On a vacuum manifold, the flask was subjected to three freeze-pump-thaw cycles and then was backfilled with CO, resulting in a rapid color change to pale peach. The solution was allowed to stir for three days. CH_2Cl_2 was removed under vacuum, producing pale brown solid. In a nitrogen atmosphere drybox, the solids were dissolved in minimal (1 mL) CH_2Cl_2, filtered through a pipette celite filter, transferred to a vial, layered with 2 mL pentane and 0.2 mL Et_2O, and stored at -30 °C. The filtrate was removed, leaving behind 46 mg (0.063 mmol, 89 % yield) of a pale brown crystalline product.

^{1}H NMR (CD_2Cl_2, 300.10 MHz, 25 °C): δ 7.18 (d, J_{HH} = 7.5 Hz, 1H; Ar-*H*), 7.09 (t, $^{2}J_{HH}$ = 7.4 Hz, 2H; Ar-*H*), 3.75 (dvt, $^{2}J_{HH}$ = 17.3, $^{2}J_{PH}$ + $^{4}J_{PH}$ = 4.1 Hz, 2H; Ar-CH_2PR), (dvt, $^{2}J_{HH}$ = 17.4, $^{2}J_{PH}$ + $^{4}J_{PH}$ = 3.7 Hz, 2H; Ar-CH_2PR), 1.51 (vt, $^{3}J_{PH}$ + $^{5}J_{PH}$ = 7.6 Hz, 18*H*; PC(C$H_3)_3$), 1.31 (vt, $^{3}J_{PH}$ + $^{5}J_{PH}$ = 7.7 Hz, 18H; PC(C$H_3)_3$), -10.20 (t, $^{2}J_{PH}$ = 12.2 Hz, 1H; Ir-*H*). ^{31}P{^{1}H} NMR (CD_2Cl_2,

121.49 MHz, 25 °C): δ 68.7 (s). $^{13}C\{^{1}H\}$ NMR (CD_2Cl_2, MHz, 25 °C): δ 170.7 (t, $^{2}J_{PC}$ = 4.6 Hz, Ir-*C*O), 168.3 (t, $^{2}J_{PC}$ = 5.6 Hz; Ir-CO), 148.44 (m; C_{Ar}), 137.05 (s; C_{Ar}), 128.02 (s; C_{Ar}), 123.93 (m; C_{Ar}), 38.33 (vt, $^{1}J_{PC}$ + $^{3}J_{PC}$ = 14.8Hz; *C*H_2PR_2), 37.39 (m,; Ar*C*H_2PR_2), 30.05 (s; PC(*C*H_3)$_3$), 29.03 (s; PC(*C*H_3)$_3$).

Preparation of (^{R}pincer)Ir(H)(Cl)(CO) samples for X-ray diffraction

Crystals of *cis*-**3d** suitable for X-ray diffraction were grown by slow evaporation of **3d** in a ternary mixture of CH_2Cl_2, Et_2O, and pentane under ambient atmosphere. Crystals of **2d** suitable for X-ray diffraction were obtained by addition of excess HCl•Et_2O to a sample of **2a** dissolved in CH_2Cl_2, followed by precipitation from a mixture of CH_2Cl_2, pentane and HCl•Et_2O stored at -30 °C under ambient atmosphere.

*Preparation of (^{tBu}PCP)Ir(H)(CO)(OTf) **4c** sample for X-ray diffraction*

A sample of **4a** (36.2 mg, 0.0593 mmol) was dissolved in pentane in a 20 mL vial, resulting in a yellow solution. In a second vial, 6.5 μL HOTf (0.073 mmol), was diluted in approximately 5 mL of pentane. Acid solution was gradually added to the solution of **4a**, which decolorized as a pale yellow solid precipitated, until no further color change was observed. The vial was stored at -30 °C overnight before solvent was removed, generating pale yellow solid that was ~5% **4a** and 95% (^{tBu}PCP)Ir(H)(CO)(OTf) **4c**, analyzed by ^{1}H and ^{31}P NMR spectroscopy. Crystals of **4c** suitable for X-ray diffraction were obtained by crystallization from a ternary mixture of CH_2Cl_2, Et_2O, and pentane stored at -30 °C.

*4.7.3 Catalyst longevity experiment: **1c** and **4a***

In a nitrogen atmosphere drybox, a stainless steel high-pressure reactor was charged with 6.1 mg (0.025 mmol) **4a,** [or 7.1 mg (0.025 mmol) **1c**], 323 μL (4 mmol) EF and 2 mL dioxane. The reactor was placed onto the high-pressure manifold, purged with H_2 and pressurized to 50 atm.

The reactor was heated for 16 hours, cooled on ice, and the excess H_2 pressure was released. The reactor was brought into the drybox and opened. An additional aliquot of 323 μL (4 mmol) EF was added, the solution was briefly stirred to mix, and a small amount (~500 μl) was removed, and the reactor was closed. This aliquot was used to make a sample for NMR spectroscopy containing 400 μL reaction mixture, 5 mg $Cr(acac)_3$ and 10 μL mesitylene. The reactor was once more placed onto the high-pressure manifold, purged with H_2 and pressurized to 50 bar. The reactor was heated for 16 hours, then cooled on ice. A second sample was made up for ^{13}C NMR spectroscopy as above.

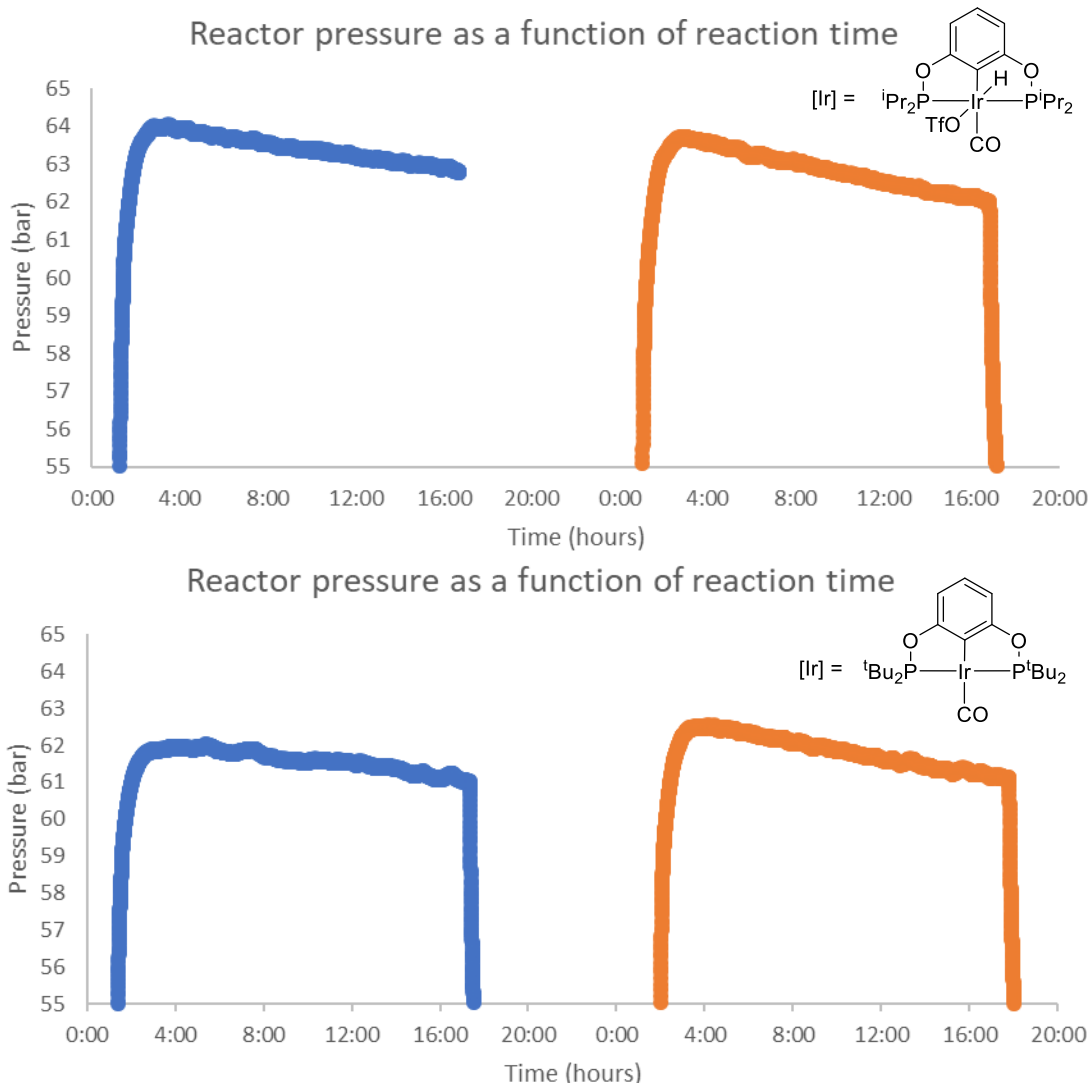

Figure 4.5. Reactor pressure as a function of reaction time during EF hydrogenation and recharge experiments with pre-catalysts **1c** and **4a**

*4.7.4 CO dissociation NMR experiment: Example with **1e***

A J-Young NMR tube was charged with approximately 2 mg (0.0027 mmol) **1e**. Approximately 0.4 mL CD_2Cl_2 was vacuum transferred into the tube. ^{1}H and ^{31}P NMR spectra were recorded. The tube was heated at 80 °C for 30 minutes, without mixing. The tube was removed from heat, and NMR spectra were recorded.

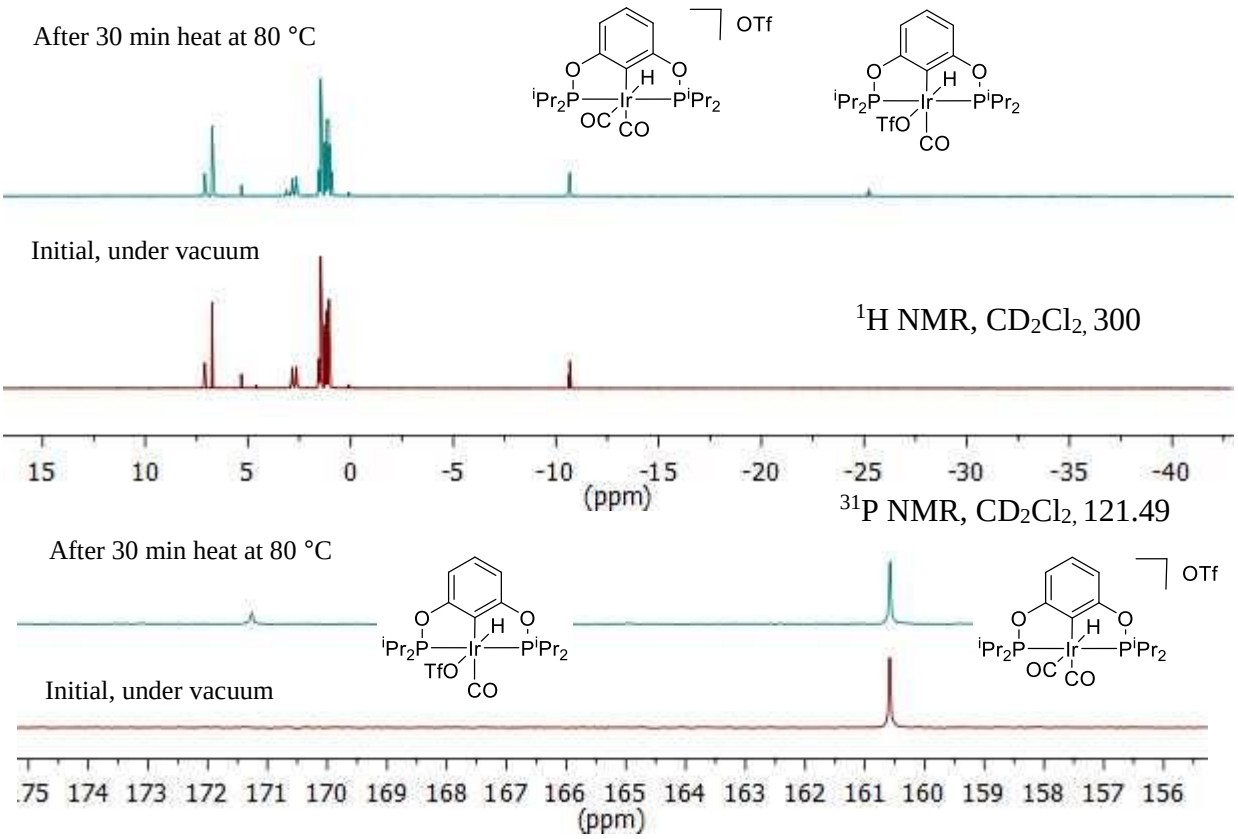

Figure 4.6. ^{1}H and ^{31}P NMR spectra of **1e** in CD_2Cl_2, demonstrating CO dissociation after heating at 80°C under static vacuum

*4.7.5 Pressure/temperature/catalyst concentration screen using **1c***

High-pressure reactors equipped with PTFE liners were loaded on the benchtop with the specified amount of **1c** (between 0.00625 and 0.05 mol%, see Figure 4.7**)** and with 2mL EF. Reactors were sealed, purged with H_2 and pressurized with the specified amount of H_2 (between 10 and 85 bar, see Figure 4.7) and heated for 18 hours under stirring. Reactors were cooled on ice, vented, opened and 200 µL mesitylene was added to each reactor. Reactors were agitated to mix, and a 500 µL aliquot of reaction mixture was analyzed by quantitative ^{13}C NMR spectroscopy.

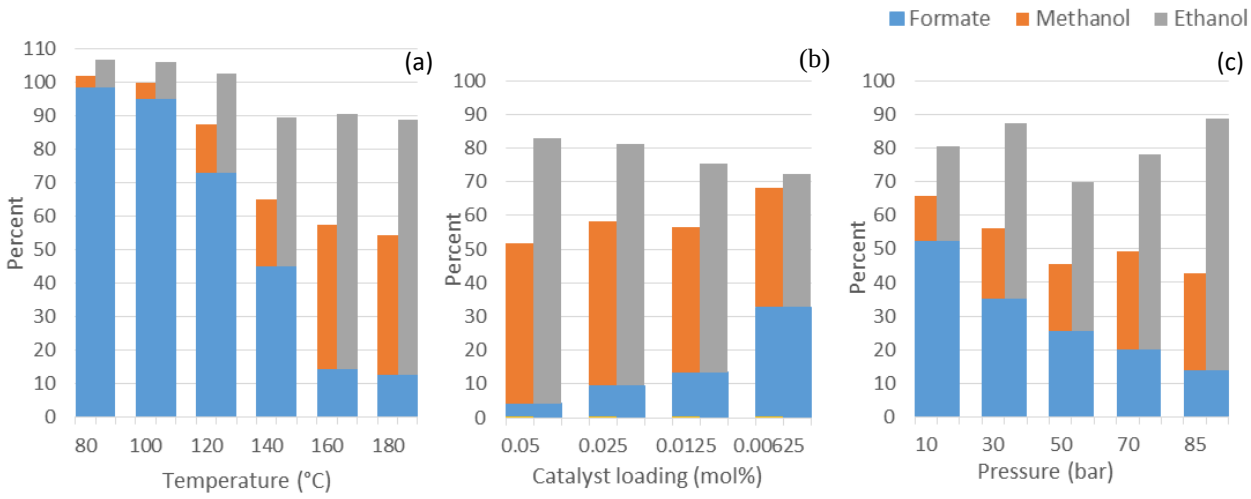

Figure 4.7. EF hydrogenation by **1c** as a function of pressure, temperature and catalyst concentrations. Chart (a) represents varied temperatures at 50 bar H_2, 0.00625% **1c**, (b) increasing pressure at 140 °C, 0.0125% **1c** (c) concentration dependence at 50 bar H_2, 140 °C. Note: [formate = MeOF + EtOF, methanol = MeOH + MeOF + 2MeOMe, ethanol = EtOH - MeOF +2 EtOEt]

4.7.6 NMR spectra

^{1}H NMR spectrum (CD_2Cl_2, 300 MHz) and $^{31}P\{^{1}H\}$ spectrum (CD_2Cl_2, 121 MHz) (inset) of (^{iPr}POCOP)Ir(H)(CO)(OTf), **1c**

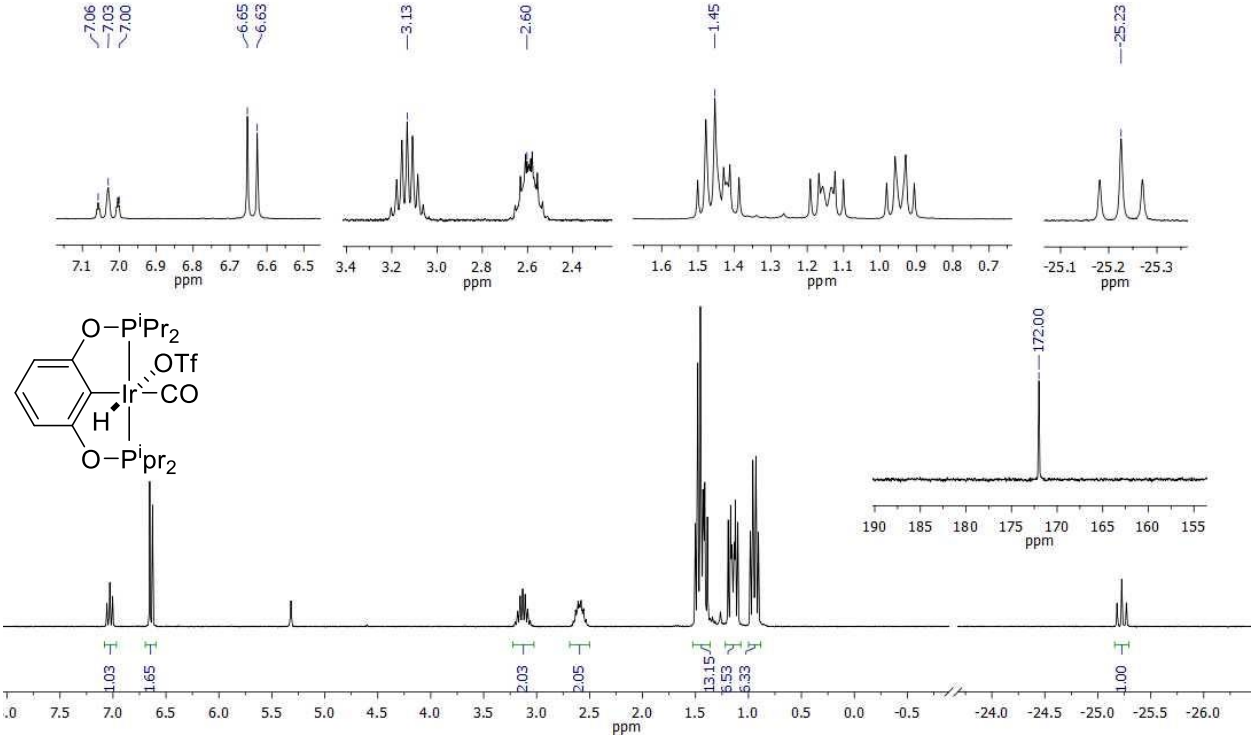

^{13}C NMR spectrum (CD_2Cl_2, 126 MHz), **1c**

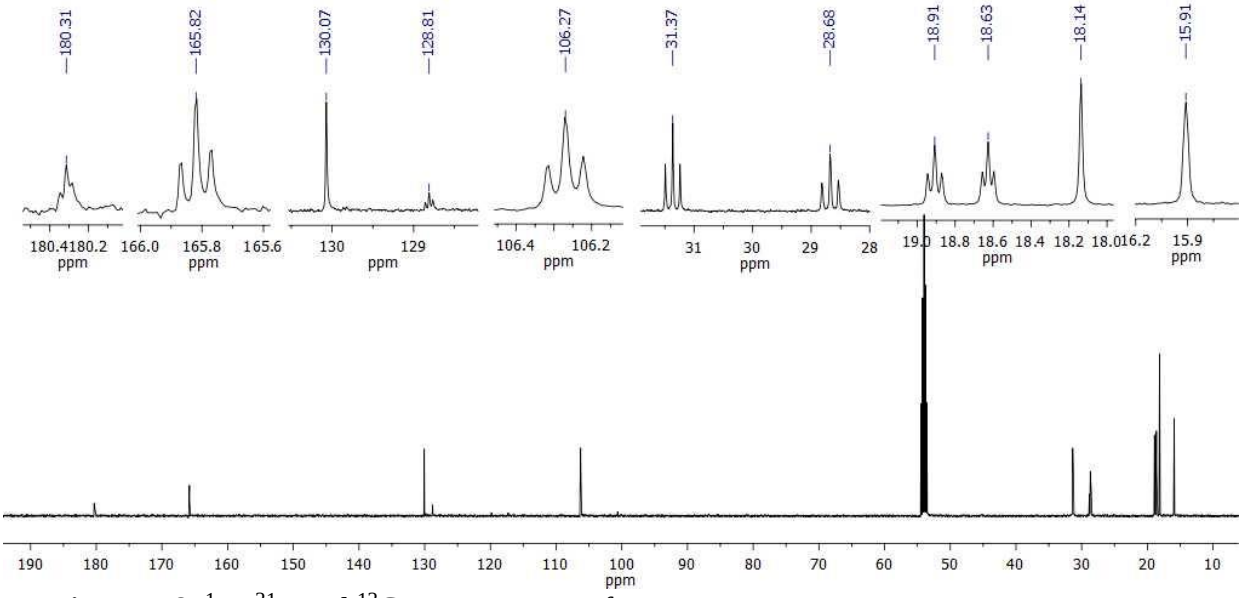

Figure 4.8. ^{1}H. ^{31}P and ^{13}C NMR spectra of **1c**

^{1}H NMR spectrum (CD_2Cl_2, 300 MHz) and $^{31}P\{^{1}H\}$ spectrum (CD_2Cl_2, 121 MHz) (inset) of [(^{iPr}POCOP)Ir(H)(CO)$_2$][OTf], **1e**

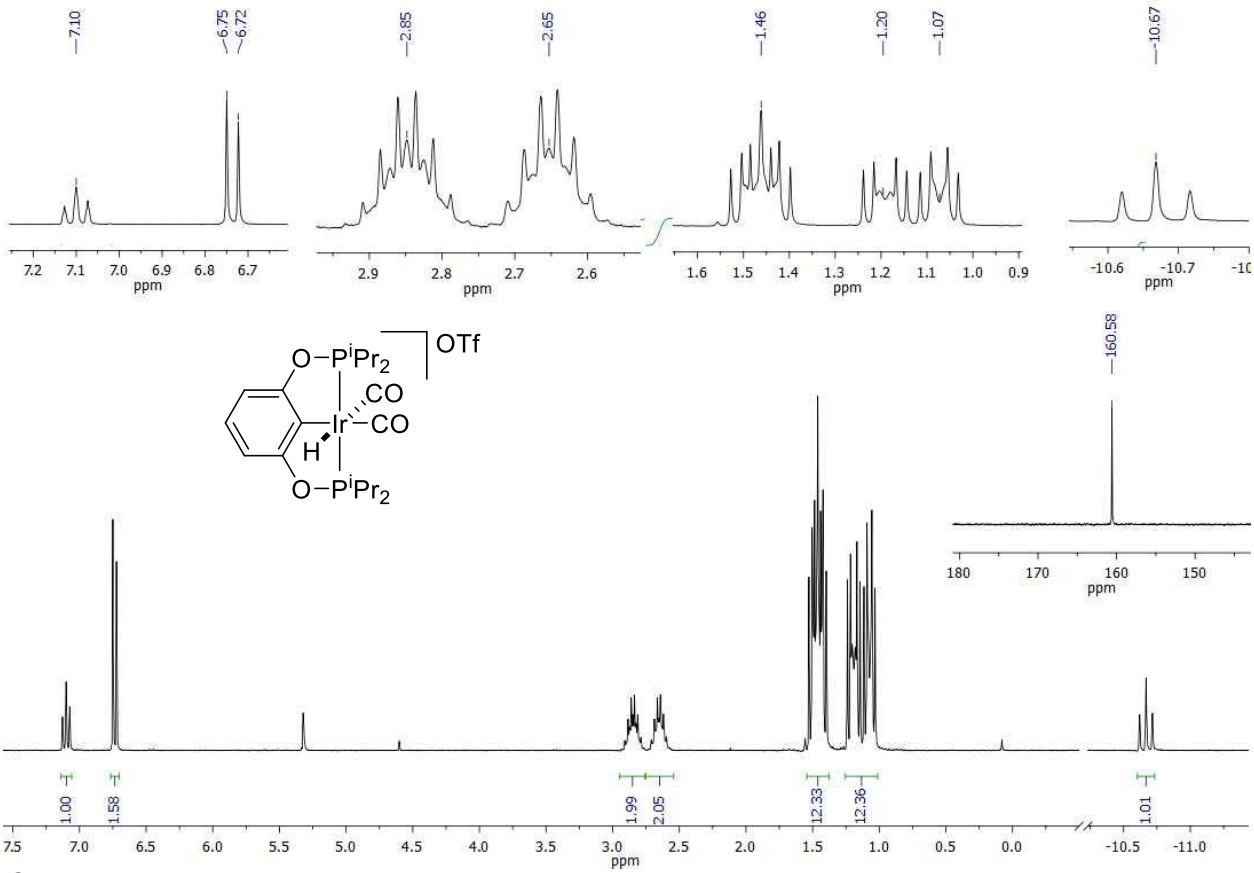

^{13}C NMR spectrum (CD_2Cl_2, 126 MHz), **1e**

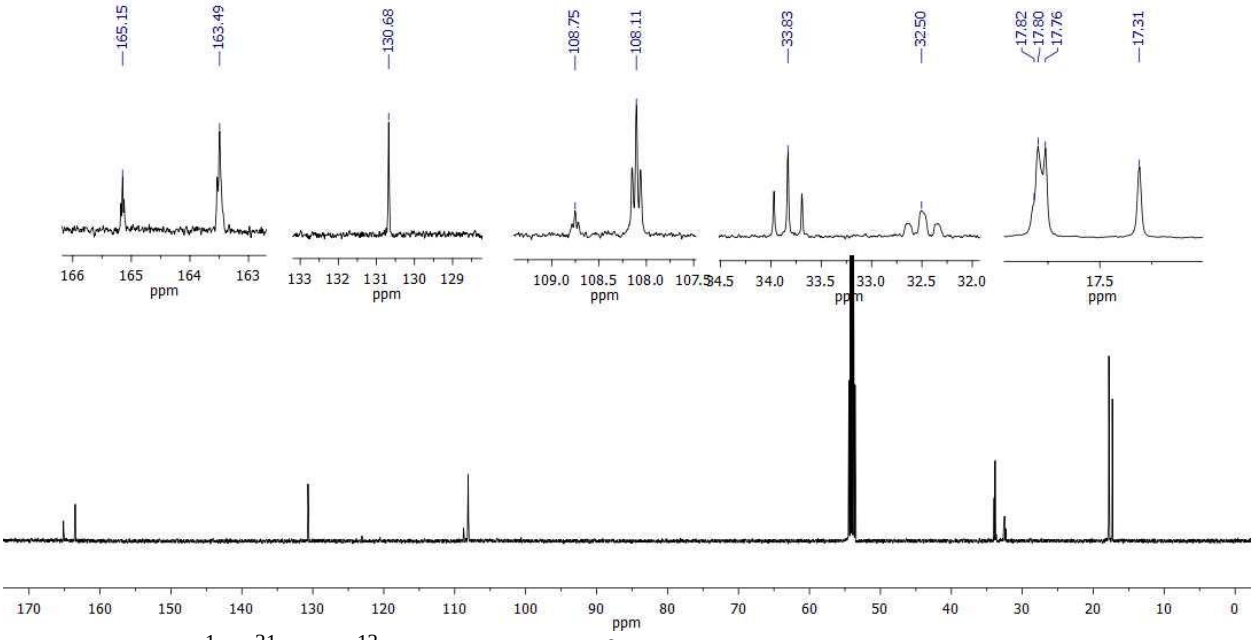

Figure 4.9. ^{1}H. ^{31}P and ^{13}C NMR spectra of **1e**

^{1}H NMR spectrum (CD_2Cl_2, 500 MHz) and $^{31}P\{^{1}H\}$ spectrum (CD_2Cl_2, 121 MHz) (inset) of [(^{iPr}PCPIr(H)(CO)$_2$][OTf], **3e**

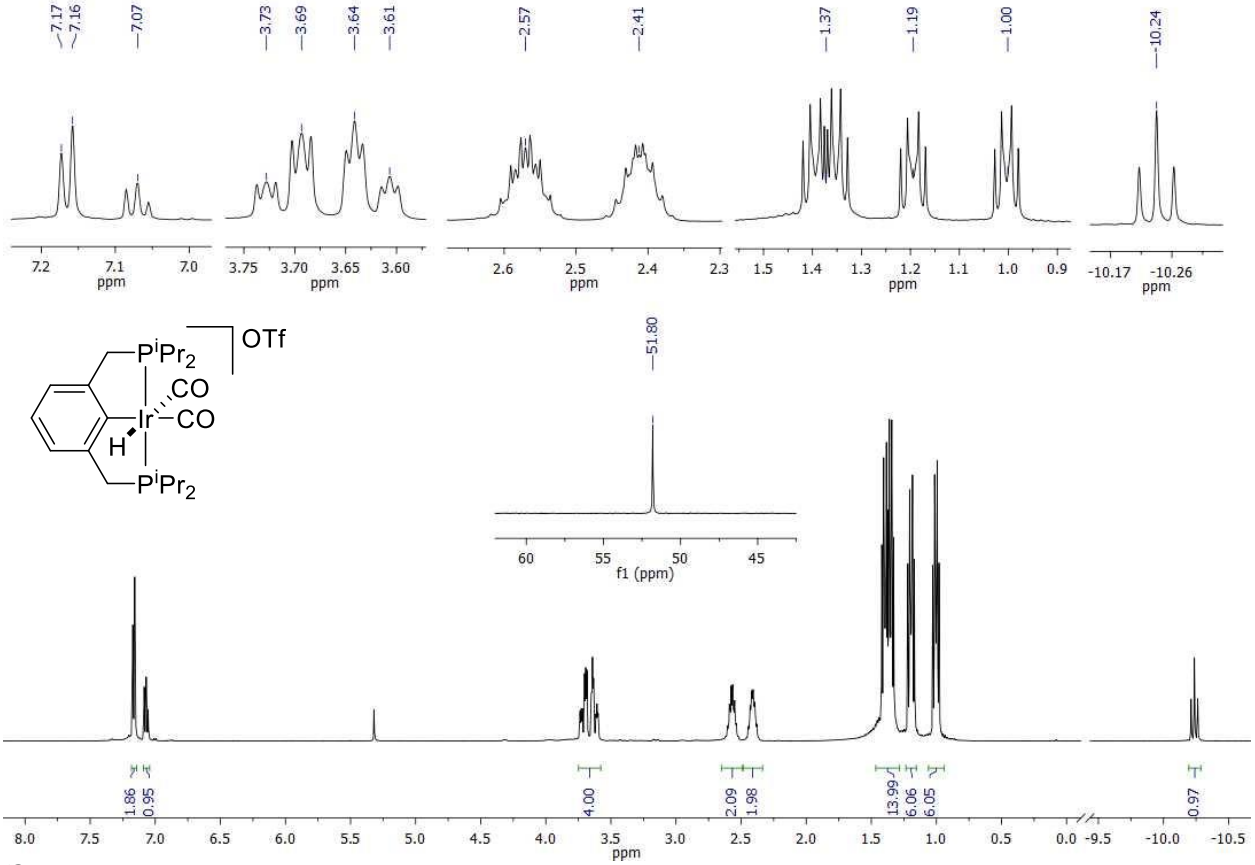

^{13}C NMR spectrum (CD_2Cl_2, 126 MHz), **3e**

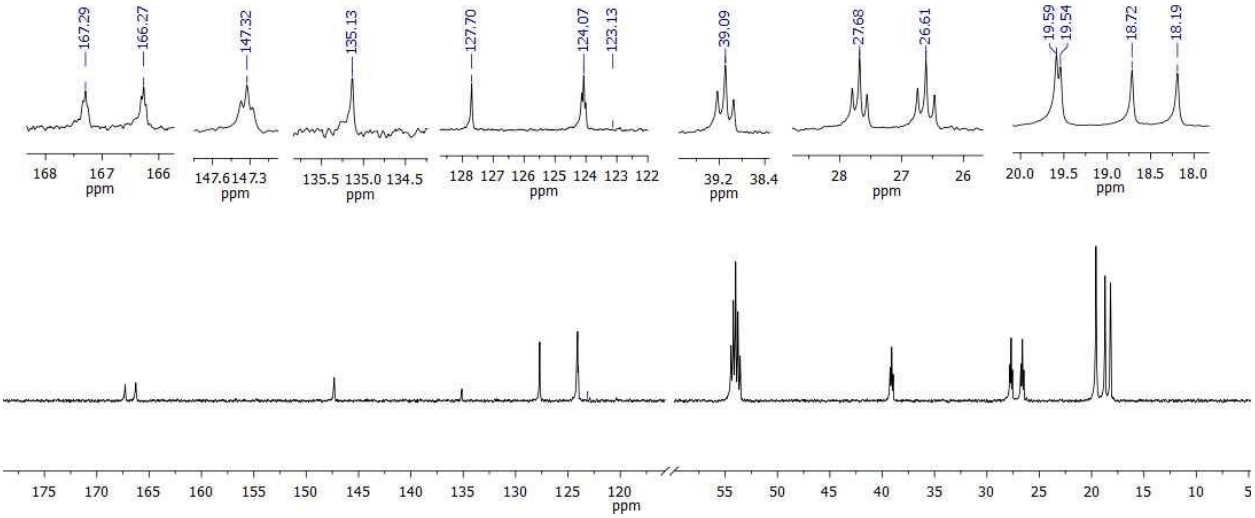

Figure 4.10.^{1}H. ^{31}P and ^{13}C NMR spectra of **3e**

^{1}H NMR spectrum (CD_2Cl_2, 300 MHz) and $^{31}P\{^{1}H\}$ spectrum (CD_2Cl_2, 121 MHz) (inset) of [(^{tBu}PCP)Ir(H)(CO)$_2$][OTf], **4e**

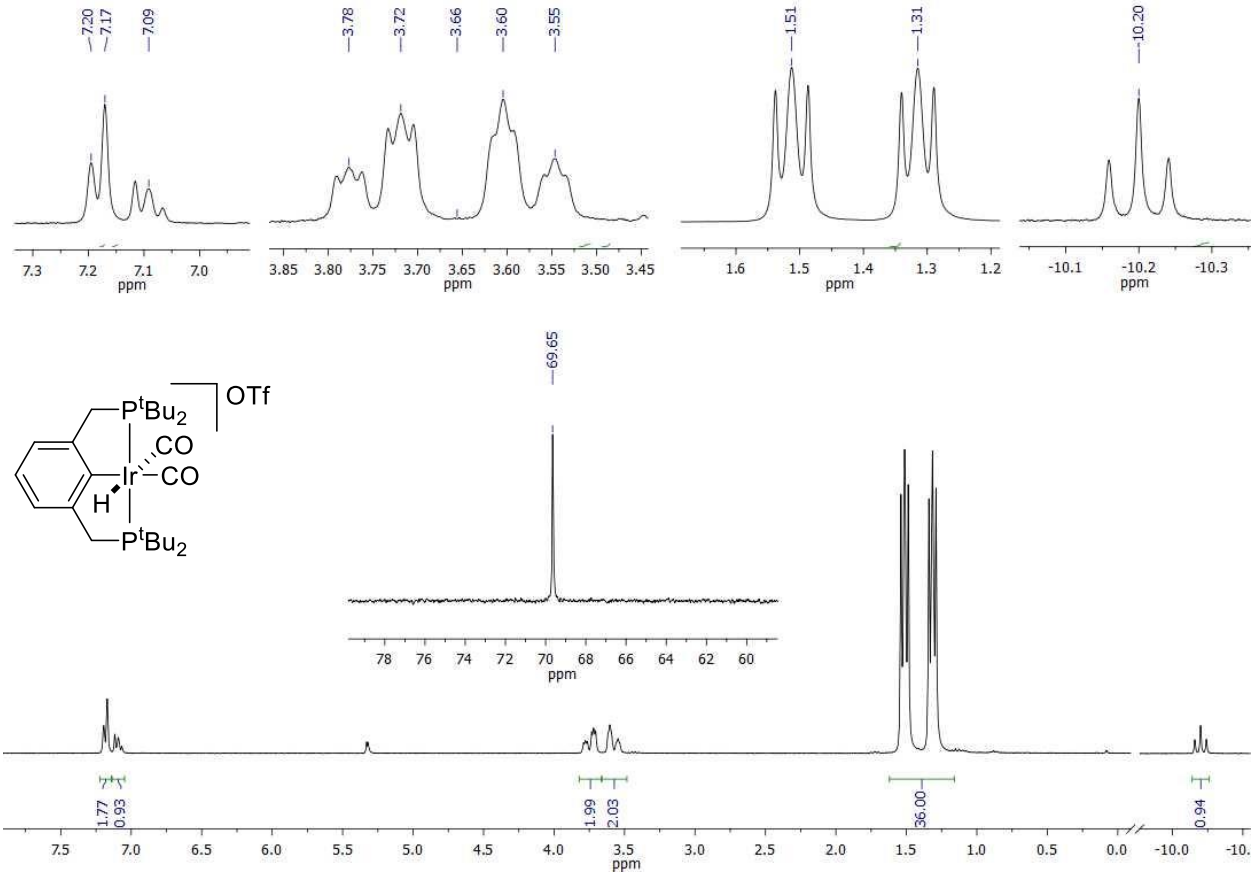

^{13}C NMR spectrum (CD_2Cl_2, 126 MHz), **4e**

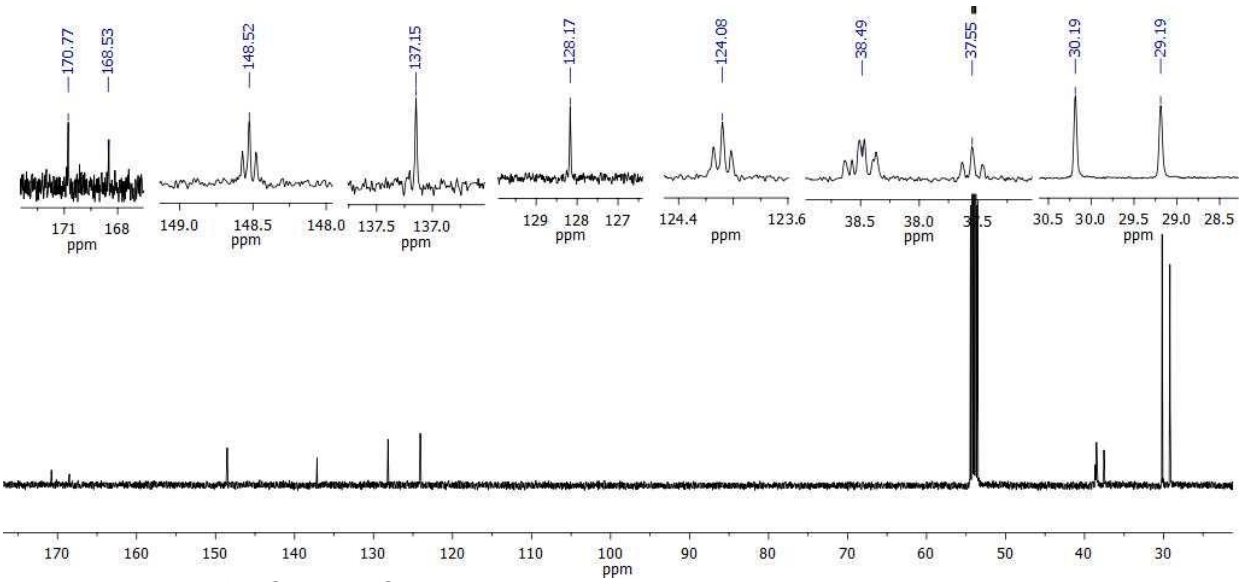

Figure 4.11. ^{1}H. ^{31}P and ^{13}C NMR spectra of **4e**

^{1}H NMR spectrum (CD_2Cl_2, 300 MHz) and $^{31}P\{^{1}H\}$ spectrum (CD_2Cl_2, 121 MHz) (inset) of [(^{iPr}PCP)Ir(H)(CO)$_2$][BF_4], **3f**

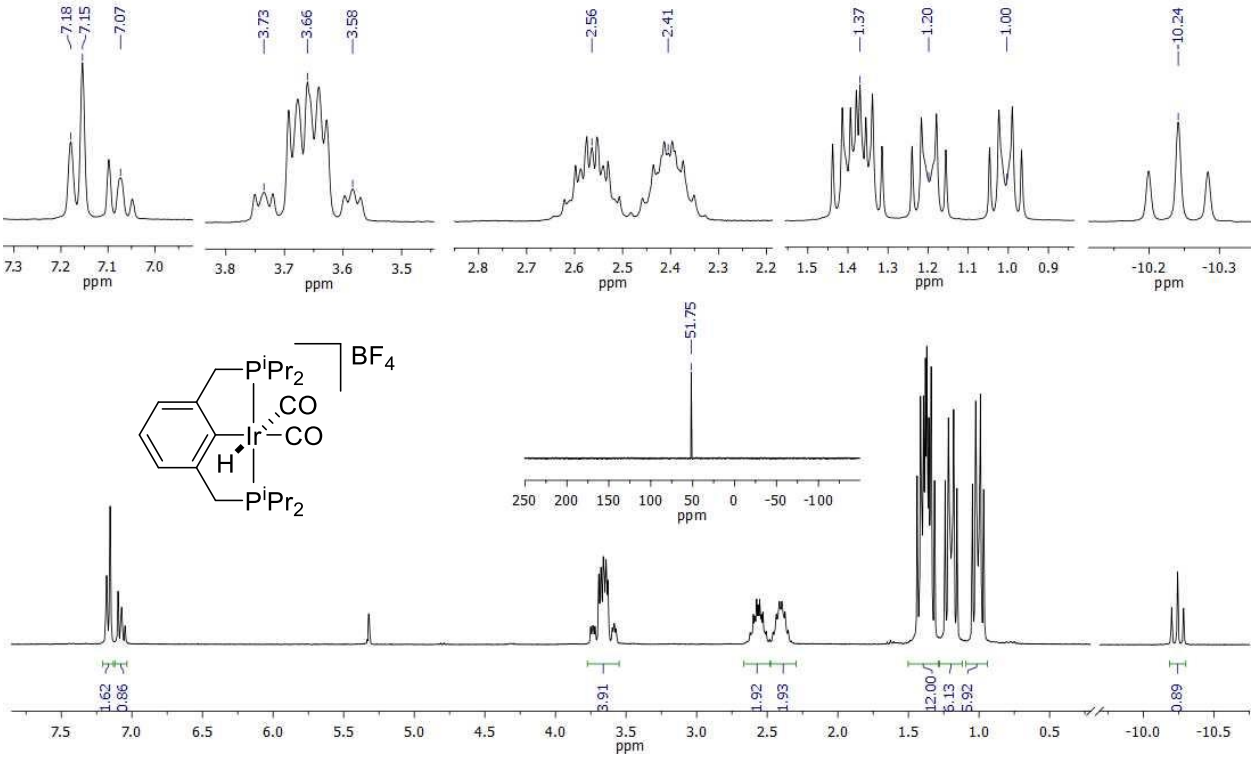

^{13}C NMR spectrum (CD_2Cl_2, 176 MHz), **3f**

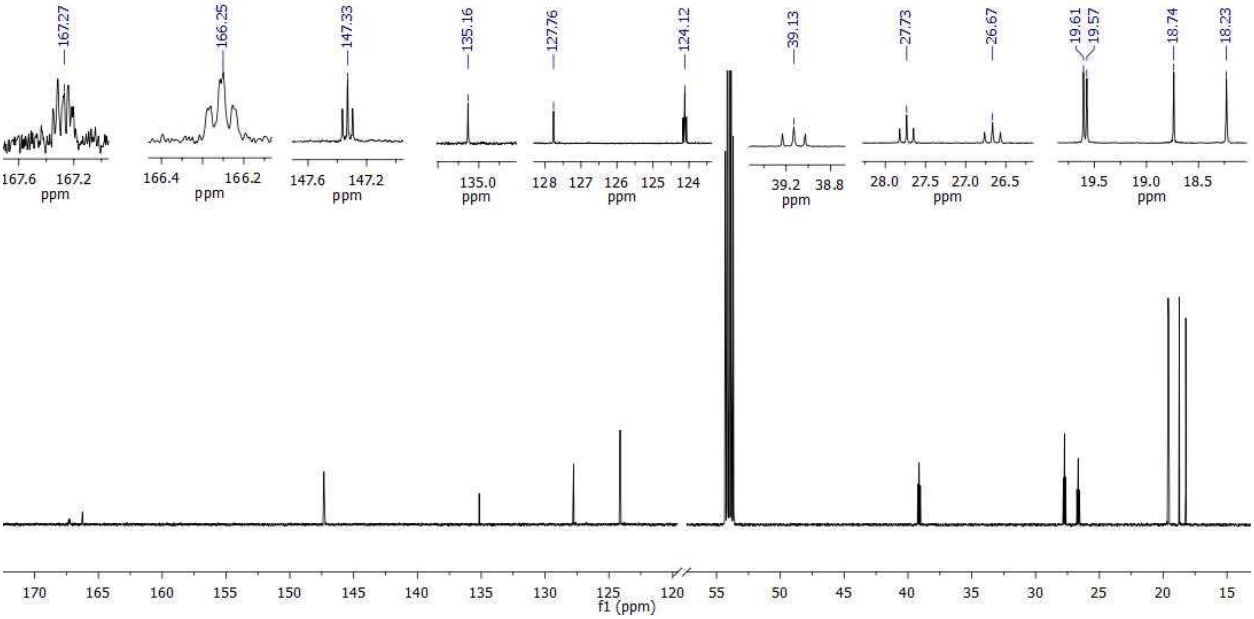

Figure 4.12. ^{1}H. ^{31}P and ^{13}C NMR spectra of **3f**

^{1}H NMR spectrum (CD_2Cl_2, 300 MHz) and $^{31}P\{^{1}H\}$ spectrum (CD_2Cl_2, 121 MHz) (inset) of [(^{tBu}PCPIr(H)(CO)$_2$][BF_4], **4f**

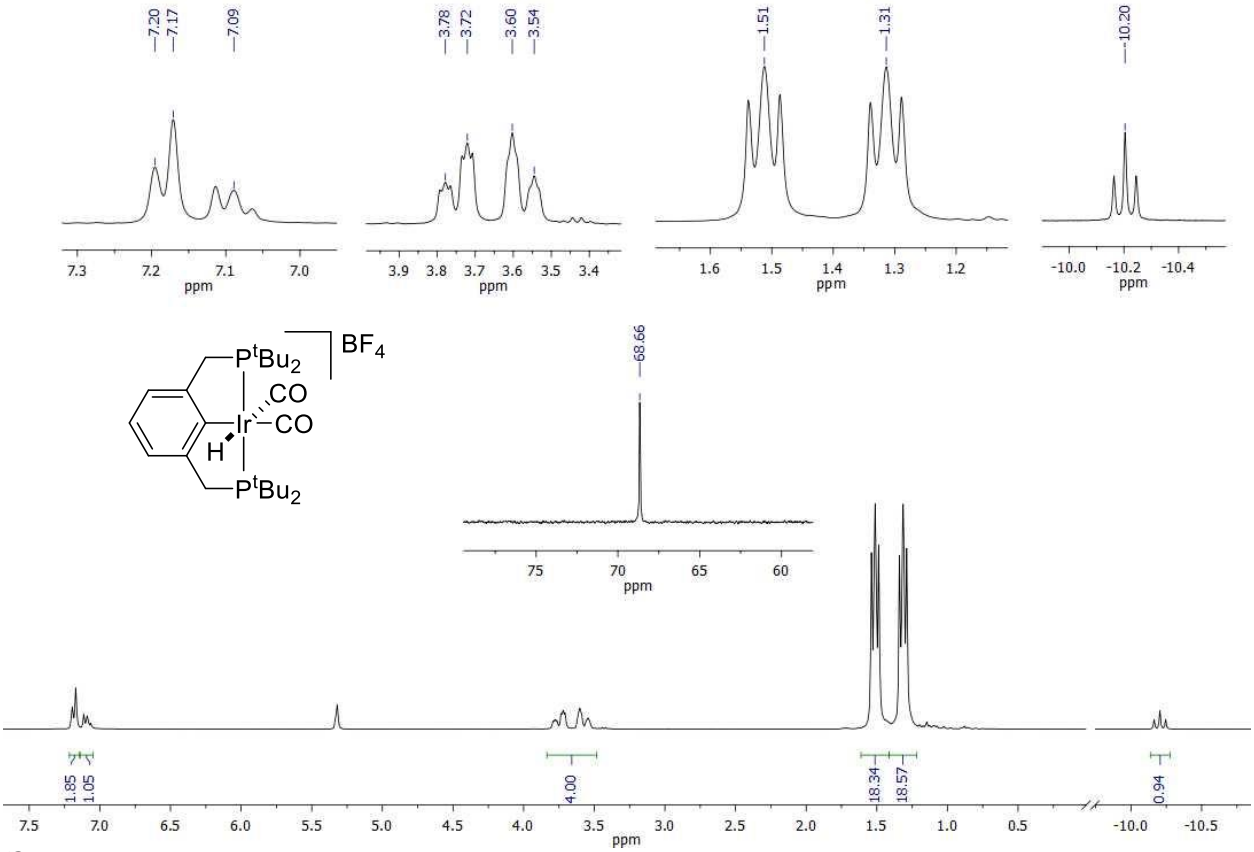

^{13}C NMR spectrum (CD_2Cl_2, 126 MHz), **4f**

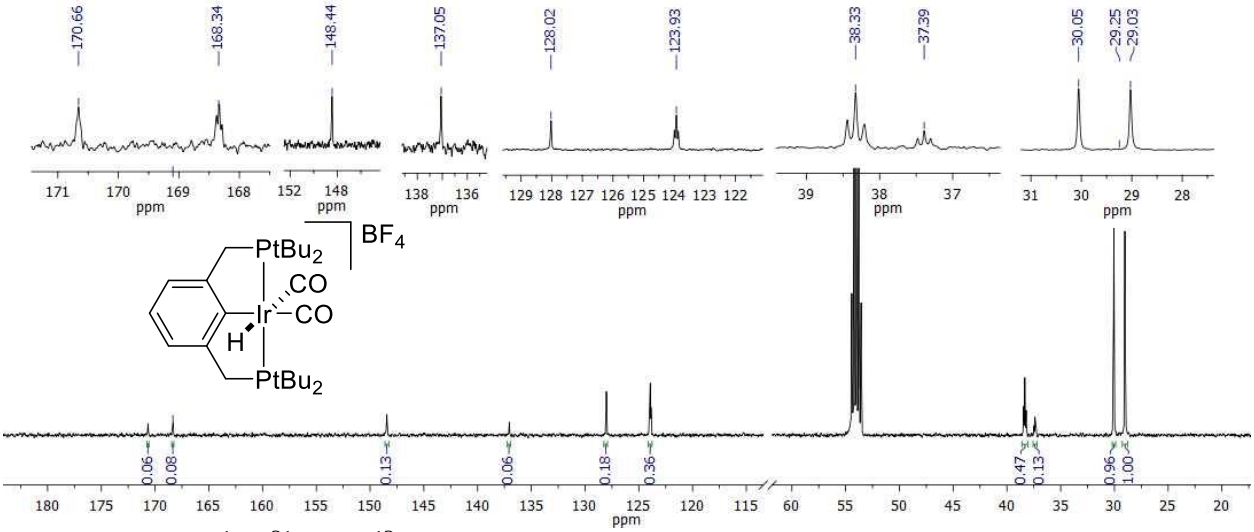

Figure 4.13. ^{1}H. ^{31}P and ^{13}C NMR spectra of **4f**

4.8 Supplemental Information for X-ray crystallography

Table 4.6. X-ray crystallographic parameters:

	^{iPr}POCOPIr(H)(CO)(OTf)	^{tBu}PCPIr(H)(CO)(OTf)	^{iPr}POCOPIr(H)(CO)$_2$[OTf]	^{tBu}PCPIr(H)(CO)$_2$[OTf]
Empirical formula	$C_{20}H_{32}F_3IrO_6P_2S$	$C_{26}H_{44}F_3IrO_4P_2S\bullet CH_2Cl_2$	$C_{21}H_{32}F_3IrO_7P_2S$	$C_{27}H_{44}F_3IrO_5P_2S\bullet CH_2Cl_2$
Formula weight	711.66	848.74	739.67	876.75
Temperature (K)	100(2)	100(2)	100(2)	100(2)
Wavelength (Å)	0.71073	0.71073	0.71073	0.71073
Crystal system	Orthorhombic	Monoclinic	Orthorhombic	Orthorhombic
Space group	P 2_1 2_1 2_1	P 2_1/n	P b c a	P b c a
Unit cell axes (Å)	a = 10.5174(7)	a = 16.5246(5)	a = 14.6048(15)	a = 15.492(5)
	b = 10.8905(8)	b = 12.6284(4)	b = 17.4510(18)	b = 24.393(5)
	c = 22.9325(16)	c = 17.5400(5)	c = 21.058(2)	c = 18.535(5
Unit cell angles (°)	α = 90	α = 90	α = 90	α = 90
	β = 90	β = 116.5530(10)	β = 90	β = 90
	γ = 90	γ = 90	γ = 90	γ = 90
Volume (Å^3)	2626.7(3)	3274.16(17)	5367.1(9)	7004(3)
Z	4	4	8	8
Density (calculated) (mg/m^3)	1.800	1.722	1.831	1.663
Absorption coefficient (mm^{-1})	5.338	4.451	5.231	4.166
F(000)	1400	1696	2912	3504
Crystal size (mm^3)	0.30 x 0.10 x 0.05	0.230 x 0.200 x 0.170	0.40 x 0.35 x 0.35	0.26 x 0.05 x 0.05
Theta range for data collection	1.78 to 28.66°	1.408 to 28.375°	1.93 to 26.02°	1.38 to 25.35°
Reflections collected	117186	15829	353041	129012
Independent reflections	6681	8154	5260	6335
R_{int}	0.0322	0.0244	0.0424	0.0892
Completeness to theta (%)	100.0	99.9	99.7	96.1
Max. and min. transmission	0.7762 and 0.2973			0.8188 and 0.4105
Data/Restraints/ parameters	6681 / 0 / 310	8154 / 0 / 376	5260 / 1 / 327	6335 / 321 / 578
Goodness-of-fit on F^2	1.066	1.051	1.067	1.203
Final R indices [I>2sigma(I)]	R1 = 0.0096, wR2 = 0.0227	R1 = 0.0195, wR2 = 0.0411	R1 = 0.0157, wR2 = 0.0371	R1 = 0.0689, wR2 = 0.1401
R indices (all data)	R1 = 0.0098, wR2 = 0.0228	R1 = 0.0235, wR2 = 0.0422	R1 = 0.0167, wR2 = 0.0377	R1 = 0.0787, wR2 = 0.1446

Table 4.6 continued

	^{iPr}PCPIr(H)(CO)$_2$[OTf]	^{iPr}PCPIr(H)(H$_2$O)(CO)[BF$_4$]	^{tBu}POCOPIr(H)(Cl)(CO)
Empirical formula	$C_{23}H_{36}F_3IrO_5P_2S$	$C_{21}H_{38}B_1F_4IrO_2P_2$	$C_{23}H_{40}ClIrO_3P_2$
Formula weight	735.72	663.6	654.14
Temperature (K)	100(2)	100(2)	100
Wavelength (Å)	0.71073	0.71073	0.71073
Crystal system	Orthorhombic	Triclinic	Orthorhombic
Space group	$Pmc2_1$	P-1	Pbca
Unit cell axes (Å)	a = 8.9556(7)	8.7574(10)	a = 12.2958(3)
	b = 14.9968(11)	11.6894(12)	b = 14.9618(4)
	c = 21.0354(17)	13.7367(15)	c = 28.3971(8)
Unit cell angles (°)	α = 90	α = 97.491(6)	α = 90
	β = 90	β = 104.330(6)	β = 90
	γ = 90	γ = 103.303(6)	γ = 90
Volume (Å^3)	2825.2(4)	1299.5(2)	5224.1(2)
Z	4	2	8
Density (calculated) (mg/m^3)	1.730	1.696	1.663
Absorption coefficient (mm^{-1})	4.963	5.304	5.357
F(000)	1456	656	2608.0
Crystal size (mm^3)	0.57 x 0.14 x 0.14	0.14 x 0.08 x 0.08	0.05 × 0.05 × 0.02
Theta range for data collection	1.936 to 28.302°	1.561 to 26.521°	2.868 to 61.084°
Reflections collected	26729	28698	57079
Independent reflections	7167	10308	7989
R_{int}	0.0252	0.0565	0.0845
Completeness to theta (%)	99.9	100.0	
Max. and min. transmission	0.5752 and 0.7457	0.5752 and 0.7457	
Data/Restraints/ parameters	7167/ 1 / 350	10308/ 4 / 294	7989/0/287
Goodness-of-fit on F^2	1.035	1.016	1.011
Final R indicies [I>2sigma(I)]	R1 = 0.0155, wR2 = 0.0340	R1 = 0.0447, wR2 = 01050	R_1 = 0.0361, wR_2 = 0.0622
R indices (all data)	R1 = 0.0164, wR2 = 0.0344	R1 = 0.0535, wR2 = 0.112	R_1 = 0.0673, wR_2 = 0.0721
Largest diff. peak and hole (e. Å^{-3})	0.440 and -0.370	2.843 and -2.305	1.45/-1.72

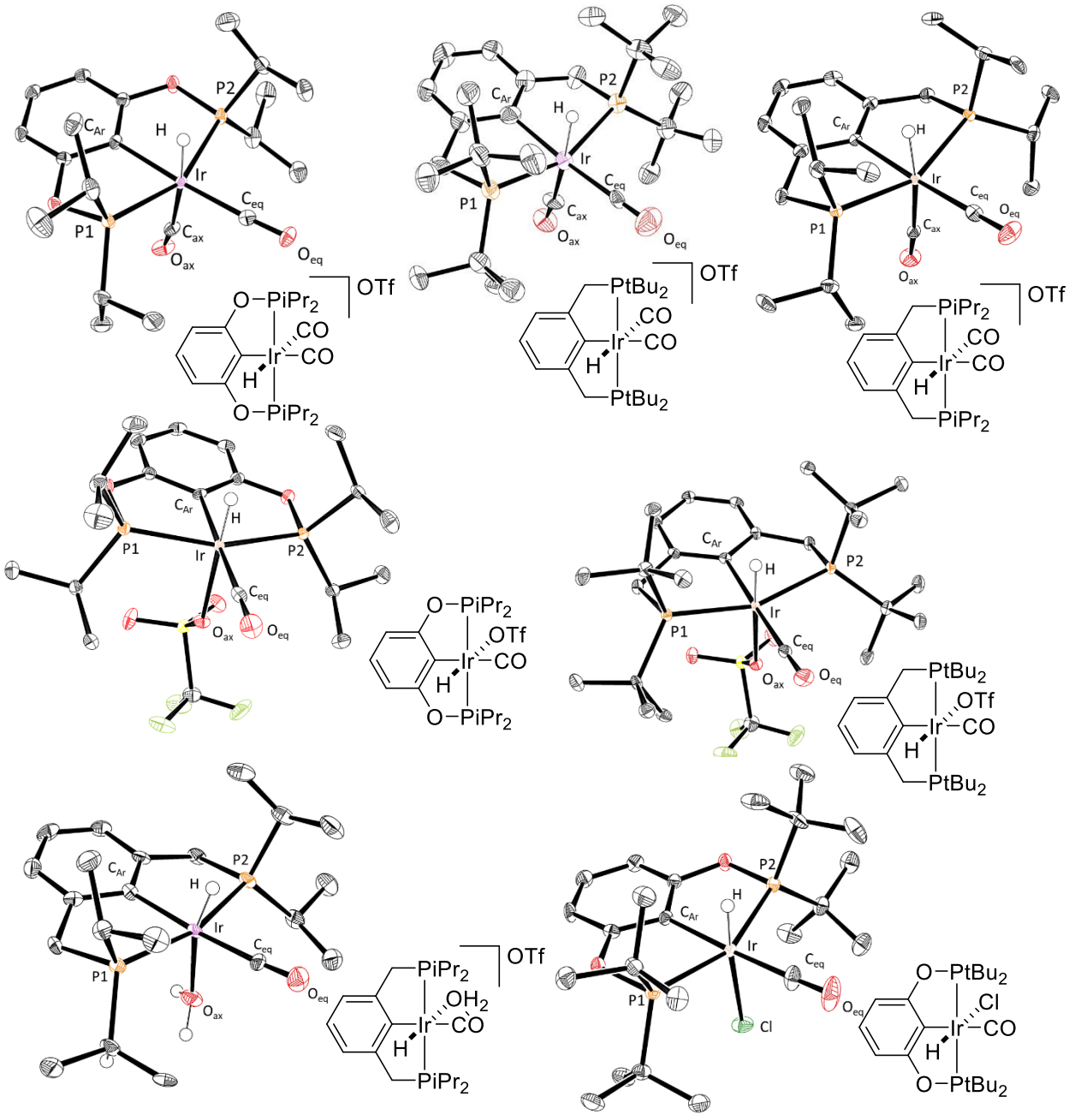

Figure 4.14. ORTEPs[48] of complexes crystallized

Details: ORTEP[48] structures of crystallized compounds drawn at 50% probability (hydrogen atoms have been omitted for clarity). [(^{iPr}POCOP)Ir(H)(CO)$_2$][OTf] crystallized with one molecule in the unit cell with one triflate counterion located in the outer sphere. [(^{iPr}PCPIr)(H)(CO)$_2$][OTf] crystallized as two molecules in the unit cell with a triflate counterion outer sphere. [(^{tBu}PCP)Ir(H)(CO)$_2$][OTf] crystallized as two molecules in the unit cell, one doubly disordered, with triflate counterion and one solvent molecule [CH_2Cl_2]. (^{iPr}POCOP)Ir(H)(CO)(OTf) crystallized as one molecule in the unit cell, triflate anion is bound to the Ir center trans- to the hydride. (^{tBu}PCP)Ir(H)(CO)(OTf) crystallized as one molecule in the unit cell and one solvent molecule [CH_2Cl_2], triflate anion is bound to the Ir center trans- to the hydride. [(^{iPr}PCP)Ir(H)(H_2O)(CO)][HBF_4] crystallized as one molecule in the unit cell, with water bound to Ir trans- to hydride, and BF_4 anion outer sphere. (^{tBu}POCOP)(H)(Cl)(CO) crystallized as a single molecule in the unit cell.

4.9 References

(1) Huff, C. A.; Sanford, M. S. Cascade Catalysis for the Homogeneous Hydrogenation of CO_2 to Methanol. *J. Am. Chem. Soc.* **2011**, *133* (45), 18122–18125.

(2) Rezayee, N. M.; Huff, C. A.; Sanford, M. S. Tandem Amine and Ruthenium-Catalyzed Hydrogenation of CO_2 to Methanol. *J. Am. Chem. Soc.* **2015**, *137* (3), 1028–1031.

(3) Kothandaraman, J.; Goeppert, A.; Czaun, M.; Olah, G. A.; Prakash, G. K. S. Conversion of CO_2 from Air into Methanol Using a Polyamine and a Homogeneous Ruthenium Catalyst. *J. Am. Chem. Soc.* **2016**, *138*, 2–5.

(4) Dang, T. T.; Boeck, F.; Hintermann, L. Hidden Brønsted Acid Catalysis: Pathways of Accidental or Deliberate Generation of Triflic Acid from Metal Triflates. *J. Org. Chem.* **2011**, *76* (22), 9353–9361.

(5) vom Stein, T.; Meuresch, M.; Limper, D.; Schmitz, M.; Hölscher, M.; Coetzee, J.; Cole-Hamilton, D. J.; Klankermayer, J.; Leitner, W. Highly Versatile Catalytic Hydrogenation of Carboxylic and Carbonic Acid Derivatives Using a Ru-Triphos Complex: Molecular Control over Selectivity and Substrate Scope. *J. Am. Chem. Soc.* **2014**, *136* (38), 13217–13225.

(6) Brewster, T. P.; Rezayee, N. M.; Culakova, Z.; Sanford, M. S.; Goldberg, K. I. Base-Free Iridium-Catalyzed Hydrogenation of Esters and Lactones. *ACS Catal.* **2016**, *6* (5), 3113–3117.

(7) Korstanje, T. J.; Ivar van der Vlugt, J.; Elsevier, C. J.; de Bruin, B. Hydrogenation of Carboxylic Acids with a Homogeneous Cobalt Catalyst. *Science* **2015**, *350* (6258), 298–302.

(8) Dub, P. A.; Ikariya, T. Catalytic Reductive Transformations of Carboxylic and Carbonic Acid Derivatives Using Molecular Hydrogen. *ACS Catal.* **2012**, *2* (8), 1718–1741.

(9) Choi, J.; MacArthur, A. H. R.; Brookhart, M.; Goldman, A. S. Dehydrogenation and Related Reactions Catalyzed by Iridium Pincer Complexes. *Chem. Rev.* **2011**, *111* (3), 1761–1779.

(10) Huang, Z.; Brookhart, M.; Goldman, A. S.; Kundu, S.; Ray, A.; Scott, S. L.; Vicente, B. C. Highly Active and Recyclable Heterogeneous Iridium Pincer Catalysts for Transfer Dehydrogenation of Alkanes. *Adv. Synth. Catal.* **2009**, *351* (1–2), 188–206.

(11) Punji, B.; Emge, T. J.; Goldman, A. S. A Highly Stable Adamantyl-Substituted Pincer-Ligated Iridium Catalyst for Alkane Dehydrogenation. *Organometallics* **2010**, *29* (12), 2702–2709.

(12) Mucha, N. T.; Waterman, R. Iridium Pincer Catalysts for Silane Dehydrocoupling: Ligand Effects on Selectivity and Activity. *Organometallics* **2015**, *34* (15), 3865–3872.

(13) Kosanovich, A. J.; Press, L. P.; Ozerov, O. V. Boryl Transfer Reactivity of a POCOP-Supported Ir-Diboryl: Reduction of CO_2 to CO and Borylation of Other Small Molecules. *J. Organomet. Chem.* **2017**, *845*, 19–24.

(14) Goldberg, J. M.; Wong, G. W.; Brastow, K. E.; Kaminsky, W.; Goldberg, K. I.; Heinekey, D. M. The Importance of Steric Factors in Iridium Pincer Complexes. *Organometallics* **2015**, *34* (4), 753–762.

(15) Goldberg, J. M.; Cherry, S. D. T.; Guard, L. M.; Kaminsky, W.; Goldberg, K. I.; Heinekey, D. M. Hydrogen Addition to (Pincer)Ir^{I}(CO) Complexes: The Importance of Steric and Electronic Factors. *Organometallics* **2016**, *35* (20), 3546–3556.

(16) Goldberg, J. M.; Goldberg, K. I.; Heinekey, D. M.; Burgess, S. A.; Lao, D. B.; Linehan, J. C. Detection of an Iridium-Dihydrogen Complex: A Proposed Intermediate in Ionic Hydrogenation. *J. Am. Chem. Soc.* **2017**, *139* (36), 12638–12646.

(17) Rybtchinski, B.; Ben-David, Y.; Milstein, D. Unexpected Isomerization of a *Cis* - into a *Trans* - Dihydride Complex. A Neutral Late Transition Metal Complex as a Hydride Donor. *Organometallics* **1997**, *16* (17), 3786–3793.

(18) Lekich, T. T.; Gary, J. B.; Bellows, S. M.; Cundari, T. R.; Guard, L. M.; Heinekey, D. M. H_2 Addition to (^{Me4}PCP)Ir(CO): Studies of the Isomerization Mechanism. *Dalton Trans.* **2018**, *47* (45), 16119–16125.

(19) Heinekey, D. M.; Oldham, W. J. Coordination Chemistry of Dihydrogen. *Chem. Rev.* **1993**, *93* (3), 913–926.

(20) Crabtree, R. H. Dihydrogen Complexation. *Chem. Rev.* **2016**, *116* (15), 8750–8769.

(21) Crabtree, R. H. Dihydrogen Complexes: Some Structural and Chemical Studies. *Acc. Chem. Res.* **1990**, *23* (4), 95–101.

(22) Morris, R. H. Brønsted-Lowry Acid Strength of Metal Hydride and Dihydrogen Complexes. *Chem. Rev.* **2016**, *116* (15), 8588–8654.

(23) Pons, V.; Heinekey, D. M. An Elongated Dihydrogen Complex of Iridium. *J. Am. Chem. Soc.* **2003**, *125* (28), 8428–8429.

(24) Lao, D. B.; Owens, A. C. E.; Heinekey, D. M.; Goldberg, K. I. Partial Deoxygenation of Glycerol Catalyzed by Iridium Pincer Complexes. *ACS Catal.* **2013**, *3* (10), 2391–2396.

(25) Ahmed Foskey, T. J.; Heinekey, D. M.; Goldberg, K. I. Partial Deoxygenation of 1,2-Propanediol Catalyzed by Iridium Pincer Complexes. *ACS Catal.* **2012**, *2* (6), 1285–1289.

(26) Findlater, M.; Bernskoetter, W. H.; Brookhart, M. Proton-Catalyzed Hydrogenation of a d^8 Ir(I) Complex Yields a Trans Ir(III) Dihydride. *J. Am. Chem. Soc.* **2010**, *132* (13), 4534–4535.

(27) Crabtree, R. H. *The Organometallic Chemistry of the Transition Metals*, 6th ed.; John Wiley & Sons, Inc.: Hoboken, NJ, USA, 2014.

(28) Morales-Morales, D.; Redón, R.; Wang, Z.; Lee, D. W.; Yung, C.; Magnuson, K.; Jensen, C. M. Selective Dehydrogenation of Alcohols and Diols Catalyzed by a Dihydrido Iridium PCP Pincer Complex. *Can. J. Chem.* **2001**, *79*, 823–829.

(29) Polukeev, A. V.; Petrovskii, P. V.; Peregudov, A. S.; Ezernitskaya, M. G.; Koridze, A. A. Dehydrogenation of Alcohols by Bis(Phosphinite) Benzene Based and Bis(Phosphine) Ruthenocene Based Iridium Pincer Complexes. *Organometallics* **2013**, *32* (4), 1000–1015.

(30) Yuan, M. L.; Xie, J. H.; Zhu, S. F.; Zhou, Q. L. Deoxygenative Hydrogenation of Amides Catalyzed by a Well-Defined Iridium Pincer Complex. *ACS Catal.* **2016**, *6* (6), 3665–3669.

(31) Kundu, S.; Choliy, Y.; Zhuo, G.; Ahuja, R.; Emge, T. J.; Warmuth, R.; Brookhart, M.; Krogh-Jespersen, K.; Goldman, A. S. Rational Design and Synthesis of Highly Active Pincer-Iridium Catalysts for Alkane Dehydrogenation. *Organometallics* **2009**, *28* (18), 5432–5444.

(32) Liu, F.; Goldman, A. S. Efficient Thermochemical Alkane Dehydrogenation and Isomerization Catalyzed by an Iridium Pincer Complex. *Chem. Commun.* **1999**, No. 7, 655–656.

(33) Zhu, K.; Achord, P. D.; Zhang, X.; Krogh-Jespersen, K.; Goldman, A. S. Highly Effective Pincer-Ligated Iridium Catalysts for Alkane Dehydrogenation. DFT Calculations of Relevant Thermodynamic, Kinetic, and Spectroscopic Properties. *J. Am. Chem. Soc.* **2004**, *126* (40), 13044–13053.

(34) Goldman, A. S.; Krogh-Jespersen, K. Why Do Cationic Carbon Monoxide Complexes Have High C-O Stretching Force Constants and Short C-O Bonds? Electrostatic Effects, Not σ-Bonding. *J. Am. Chem. Soc.* **1996**, *118* (48), 12159–12166.

(35) Göttker-Schnetmann, I.; White, P. S.; Brookhart, M. Synthesis and Properties of Iridium Bis(Phosphinite) Pincer Complexes (*p*-XPCP)IrH_2, (*p*-XPCP)Ir(CO), (*p*-XPCP)Ir(H)(Aryl), and {(*p*-XPCP)Ir}H_2{μ-N_2} and Their Relevance in Alkane Transfer De. *Organometallics* **2004**, *23* (8), 1766–1776.

(36) Krogh-Jespersen, K.; Czerw, M.; Zhu, K.; Singh, B.; Kanzelberger, M.; Darji, N.; Achord, P. D.; Renkema, K. B.; Goldman, A. S. Combined Computational and Experimental Study of Substituent Effects on the Thermodynamics of H_2, CO, Arene, and Alkane Addition to Iridium. *J. Am. Chem. Soc.* **2002**, No. 9, 10797–10809.

(37) Geilen, F. M. A.; Engendahl, B.; Harwardt, A.; Marquardt, W.; Klankermayer, J.; Leitner, W. Selective and Flexible Transformation of Biomass-Derived Platform Chemicals by a Multifunctional Catalytic System. *Angew. Chem. Int. Ed.* **2010**, *49* (32), 5510–5514.

(38) Geilen, F. M. a; Engendahl, B.; H, M.; Leitner, W. Selective Homogeneous Hydrogenation of Biogenic Carboxylic Acids with [Ru(TriPhos)H]$^+$: A Mechanistic Study. *J. Am. Chem. Soc.* **2011**, No. 133, 14349–14358.

(39) Wesselbaum, S.; Moha, V.; Meuresch, M.; Brosinski, S.; Thenert, K. M.; Kothe, J.; vom Stein, T.; Englert, U.; Hölscher, M.; Klankermayer, J.; et al. Hydrogenation of Carbon Dioxide to Methanol Using a Homogeneous Ruthenium–Triphos Catalyst: From Mechanistic Investigations to Multiphase Catalysis. *Chem. Sci.* **2015**, *6* (1), 693–704.

(40) Kütt, A.; Rodima, T.; Saame, J.; Raamat, E.; Mäemets, V.; Kaljurand, I.; Koppel, I. A.; Garlyauskayte, R. Y.; Yagupolskii, Y. L.; Yagupolskii, L. M.; et al. Equilibrium Acidities of Superacids. *J. Org. Chem.* **2011**, *76* (2), 391–395.

(41) Zhao, W.; Sun, J. Triflimide ($HNTf_2$) in Organic Synthesis. *Chem. Rev.* **2018**, *118* (20), 10349–10392.

(42) Antoniotti, S.; Dalla, V.; Duñach, E. Metal Triflimidates: Better than Metal Triflates as Catalysts in Organic Synthesis-the Effect of a Highly Delocalized Counteranion. *Angew. Chem. Int. Ed.* **2010**, *49* (43), 7860–7888.

(43) Brotherton, R. J.; Weber, C. J.; Guibert, C. R.; Little, J. L. Boron Compounds. In *Ullmann's Encyclopedia of Industrial Chemistry*; Wiley-VCH Verlag GmbH & Co. KGaA: Weinheim, Germany, 2000; Vol. 92, pp 1–853.

(44) Yuan, M. L.; Xie, J. H.; Zhou, Q. L. Boron Lewis Acid Promoted Ruthenium-Catalyzed Hydrogenation of Amides: An Efficient Approach to Secondary Amines. *ChemCatChem* **2016**, *8* (19), 3036–3040.

(45) Guard, L. M.; Hebden, T. J.; Linn, D. E.; Heinekey, D. M. Pincer-Supported Carbonyl Complexes of Cobalt(I). *Organometallics* **2017**, *36* (16), 3104–3109.

(46) Srimani, D.; Mukherjee, A.; Goldberg, A. F. G.; Leitus, G.; Diskin-Posner, Y.; Shimon, L. J. W.; Ben David, Y.; Milstein, D. Cobalt-Catalyzed Hydrogenation of Esters to Alcohols: Unexpected Reactivity Trend Indicates Ester Enolate Intermediacy. *Angew. Chem. Int. Ed.* **2015**, *54* (42), 12357–12360.

(47) Moulton, C. J.; Shaw, B. L. Transition Metal–Carbon Bonds. Part XLII. Complexes of Nickel, Palladium, Platinum, Rhodium and Iridium with the Tridentate Ligand 2,6-Bis[(di-t-butylphosphino)methyl]phenyl. *J. C. S., Dalton.* **1976**, No. 11, 1020–1024.

(48) Farrugia, L. J. ORTEP-3 for Windows - A Version of ORTEP-III with a Graphical User Interface (GUI). *J. Appl. Crystallogr.* **1997**.

Chapter Five. Further applications of (pincer)Ir(CO) pre-catalysts

5.1 Introduction

5.1.1 Motivations: Catalyst incompatibility in tandem cascades

This chapter describes our efforts to extend the chemistry of (pincer)Ir(CO) pre-catalysts to additional transformations. Our primary focus was implementing these complexes in cascades for conversion of CO_2 to methanol (MeOH) via ester intermediates, building on work discussed in Chapter 4. Seminal work by Sanford demonstrated the conversion of CO_2 to MeOH via a methyl formate (MF) ester intermediate using a combination of three catalysts in a single vessel: a CO_2 hydrogenation cat. A, transesterification cat. B and ester hydrogenation cat. C (Scheme 5.1).[1] In the initial report, only 21 TON MeOH were achieved. Due to the incompatibility of cat. C with cat. B, cat. C was physically separated from cat. A and cat. B in an open vessel inside the reactor. MF produced by cat. A / cat. B was transported through the reactor atmosphere by diffusion to the solution containing cat. C. Hydrogenation activity was further limited by the interaction of basic sites on cat. C with CO_2.[1]

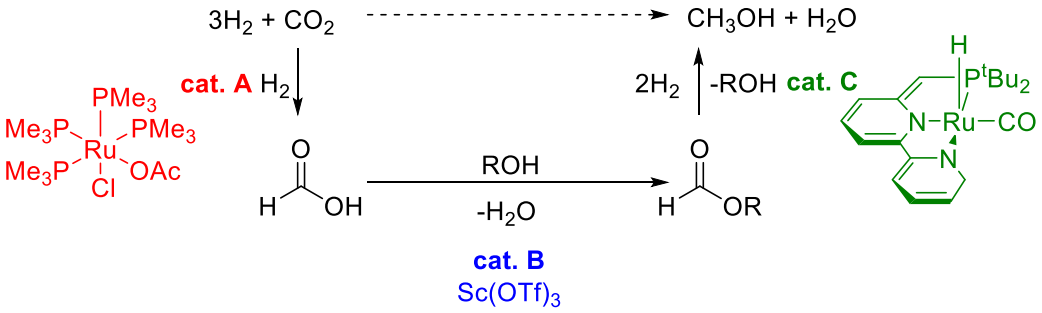

Scheme 5.1. Schematic for cascade hydrogenation of CO_2 to MeOH via an ester intermediate. Adapted from Sanford[1]

5.1.2 Selection of cat. A and cat. C for next-generation cascades

We sought to improve the Sanford system by using (pincer)Ir(CO) complexes identified as active ethyl formate (EF) hydrogenation pre-catalysts as cat. C. As these pre-catalysts do not have a basic site on the ligand to interact with CO_2, and many combinations are acid tolerant or acid accelerated, we hoped to avoid co-compatibility problems present in the initial Sanford cascade. In Chapter Four, we demonstrated that CO coordination to the Ir(III) center of (pincer)Ir(CO) based pre-catalysts in the presence of acids to form of complexes of the type [(pincer)Ir$(CO)_2$(H)](X) dramatically reduces EF hydrogenation activity.

Due to the CO inhibition of ester hydrogenation and facile PPh_3 coordination to **1c**, we were concerned about similar inhibition by coordination of trimethylphosphine (PMe_3), which is liberated from the Ru$(PMe_3)_4$(Cl)(OAc) cat. A[2] used in the initial report by Sanford. We found that sterically bulkier triphenylphosphine (PPh_3) coordinates readily to [(^{iPr}POCOP)Ir(H)(CO)][OTf] complex **1c**, as evidenced by a change in the hydride signal from a virtual triplet at δ -25.19 to a doublet of virtual triplets, -12.64 ppm, $^2J_{PH}$ = 13.26, $^2J_{PH}$ = 130 Hz), with additional splitting arising from PPh_3 bound at the metal center (see section 5.8.2, **Figure 5.2**). This is corroborated by observation of consistent signals in the ^{31}P NMR spectrum, a doublet at 151.0 ppm, and a triplet at -22.79 ppm, ($^2J_{PP}$ = 17.15 Hz) in a 2:1 ratio, corresponding to the POCOP phosphine arms and PPh_3, respectively. These changes in NMR shifts and splitting are analogous reported observations of trialkylphosphine coordination to complexes based on (^{Me}PCP)Ir(CO)[3], as well as (^{iPr}POCOP)Ir and (^{tBu}POCOP)Ir.[4]

We hoped to circumvent phosphine coordination to the Ir and associated deactivation by replacing the four PMe_3 ligands on Ru$(PMe_3)_4$(Cl)(OAc) by a tetradentate chelating phosphine ligand, preventing phosphine ligand dissociation from the ruthenium center, and thus improve the

co-compatibility between cat. A and cat. C. A ruthenium complex with a tetradentate phosphine ligand, (tetraphos)Ru(H)$_2$, (tetraphos = tris[2-(diphenylphosphino)ethyl]phosphine was chosen to be the CO_2 hydrogenation catalyst, cat. A. The iron[5] and cobalt[6] based variants have been reported by Beller and coworkers as efficient catalysts for hydrogenation of CO_2 to alkyl formates in the presence of base. The ruthenium-based complex was shown within our group to be a suitable cat. A alternative for hydrogenation of CO_2 to formate in the presence of acid and alcohol.[7] Scheme 5.2 illustrates this combination of pre-catalysts studied for hydrogenation of CO_2 to MeOH in this chapter.

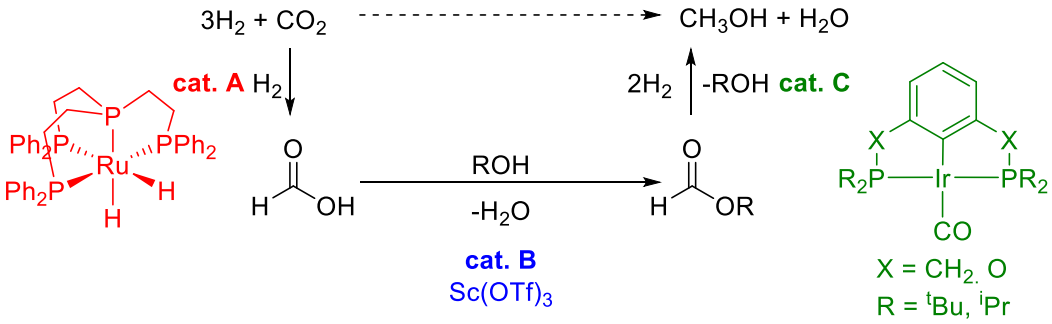

Scheme 5.2. CO_2 to MeOH cascade investigated in this work

To this end, we first investigated the CO_2 tolerance of EF hydrogenation by (pincer)Ir(CO) pre-catalysts. We then assessed selected cat. B / cat. C combinations in the full cascade. In addition, we sought to apply the (pincer)Ir pre-catalysts to related transformations reported with known ester hydrogenation catalysts; our attempts to catalyze the dehydrogenative coupling of alcohols to esters (the reverse reaction of ester hydrogenation), as well as efforts towards using formic acid (FA) as an alternative hydrogen source to H_2 are described.

5.2 CO_2 tolerance for EF hydrogenation by (pincer)Ir(CO) pre-catalysts

We assessed the CO_2 tolerance of (pincer)Ir(CO) pre-catalysts to evaluate their potential as ester hydrogenation catalysts in cascades for CO_2 hydrogenation to MeOH. Because the pincer ligands on these complexes do not have an available basic site, we hypothesized that they would

not be susceptible to deactivation by reactions with CO_2. To evaluate CO_2 tolerance of the catalysts, EF hydrogenation experiments were carried out in the presence of CO_2. Using EF as substrate in 1,4-dioxane solvent and with pre-catalysts (^{iPr}POCOP)Ir(H)(CO)(OTf) (**1c**) or (^{tBu}PCP)Ir(CO) (**4a**), reactors were charged with 10 bar CO_2 prior to the addition of 50 bar H_2, resulting in a total pressure of 60 bar. The results of these experiments are shown in Table 5.1.

Table 5.1. EF hydrogenation by **1c** and **4a** in the presence of CO_2

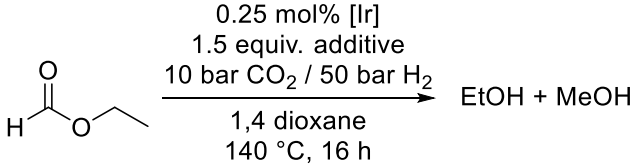

Entry	Pre-catalyst	TON MeOH equiv. (st. dev.)	TON EtOH equiv.	Total ethyl equiv.
1	**1c**	91 (9)	123	213
2	**4a**	52 (27)	71.3	231
3*	**1c**	149 (16)	193	353
4*	**4a**	163 (10)	187	360

Conditions: 0.25 mol% [Ir], 4 mmol EF, 2 mL 1,4-dioxane, 10 bar CO_2 and 50 bar H_2, 140 °C, 16 hours. MeOH equiv = MeOH + MF, EtOH equiv = ethanol + 2x diethyl ether – MF, Total ethyl equiv. = EtOH equiv. + EF equiv. Entries based on the average of two or three trials. *50 bar H_2, no CO_2, results from Chapter Four.

We observed 91 TON to MeOH products (TON MeOH = MeOH + MF) with **1c** pre-catalyst and 52 TON MeOH over 16 hours when using **4a** (compared to 149 and 163 TON without CO_2 present (entries 3 and 4). Fewer C_1 equivalents arising from the formate portion of the substrate (C_1 = MeOH + 2 MF + EF) were recovered in the experiment with an added CO_2 atmosphere, than in analogous experiments without CO_2 atmosphere. However, the production of MeOH indicates that these pre-catalysts are active under these conditions and thus have some tolerance to CO_2. We also noted incomplete mass balance of "ethyl equivalents" (C_2 fragments arising from the ethoxy portion of EF) for reactions with added CO_2. Just over 200 C_2 "ethyl equivalents" were retained in both experiments in the presence of CO_2, out of 400 total equivalents introduced (calculated by comparison to internal standard). Losses of this magnitude were not observed in reactions

pressurized with only H_2. This loss of material was reproduced over numerous independent trials, but we were unable to determine the origin of the decrease. We speculate that the two-part pressurization may be contributing to physical loss of substrate from the reactors. If CO_2 pressurization is in fact causing a physical loss of material from the reactor, this problem may be overcome in future studies by improved engineering of the reactor setup. Observed EF hydrogenation activity in the presence of CO_2 suggests that **1c** and **4a** are reasonable candidates for use in CO_2 to MeOH catalytic cascades with acid co-catalysts. We thus moved forward with implementing (pincer)Ir(CO) catalysts in a cascade for hydrogenating CO_2 to MeOH.

5.3 Application of (pincer)Ir pre-catalysts to cascade catalysis: cat. C

Ir(I) pre-catalysts (^{iPr}POCOP)Ir(CO) (**1a**), (^{iPr}PCP)Ir(CO) (**3a**), and (^{tBu}PCP)Ir(CO) **4a** were evaluated as cat. C options, as described in Table 2. We had found that **1a** and **3a** require activation by addition of acid to display high activity for EF hydrogenation, while **4a** does not, and may be inhibited by triflic acid (HOTf). No additional acid was added to the reactors, as we hoped that trace HOTf generated under reaction conditions from scandium triflate ($Sc(OTf)_3$) might be sufficient to activate **1a** and **3a** pre-catalysts. The combination (tetraphos)$Ru(H)_2$/$Sc(OTf)_3$ / **1a** resulted only in the formation of EF (143 TON based on [Ru]), but no MeOH production, meaning that **1a** is not catalyzing the hydrogenation of EF (Table 5.2, entry 1). Using **3a** as cat. C, 19 TON of MeOH were produced, while 121 TON of EF were generated (entry 2), indicating limited ester hydrogenation catalyzed by **3a.** Based on the results from Chapter 4, we expected both **1a** and **3a** to be more active in the presence of HOTf; these results suggest that there is not sufficient acid present under the conditions studied to adequately activate **1a** or **3a**. In contrast, using **4a** cat. C resulted in generation of 88 TON MeOH and 56 TON EF, and the TON MeOH observed suggests insufficient acid generated to significantly inhibit **4a**.

Table 5.2. Cascade conversion of CO_2 to MeOH

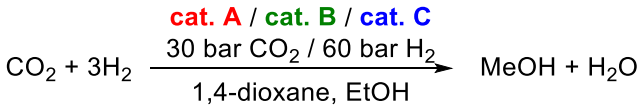

Entry	cat. C	Time (h)	cat. A (μmol)	cat. B (μmol)	cat. C (μmol)	MeOH/[Ir] (TON)	EF/[Ru] (TON)
1	**1a**	16	4.1	16.7	5.0	**0**	143
2	**3a**	16	4.1	16.7	5.0	**19**	121
3	**4a**	16	4.1	16.7	4.9	**88**	56
4*	**4a**	16	4.1	16.7	4.9	**178**	0
5*	**4a**	65	4.1	16.3	5.2	**390**	0

Conditions: Cat. A = (tetraphos)Rr$(H)_2$, cat. B = $Sc(OTf)_3$, 2 mL 1,4-dioxane, 0.5 mL EtOH, 30 bar CO_2/60 bar H_2, 140 °C. *5.0 Ultra high purity H_2. All entries from one trial.

These differences in activity may be due in part to the difference in initial solvent composition in cascade reactions (1,4-dioxane/EtOH) versus the hydrogenation conditions (only 1,4-dioxane). We speculate that some protonation of alcohol solvent by HOTf may reduce the availability of (pincer)Ir(H)$(CO)^+$ species formed by protonation of (pincer)Ir(CO) by HOTf, and also result in more (pincer)Ir(CO) or (pincer)Ir$(H)_2$(CO). Based the low activity of (^{iPr}pincer)Ir(CO) and (^{iPr}pincer)Ir$(H)_2$(CO) pre-catalysts studied in Chapter Four, we would expect this to reduce EF hydrogenation by **1a** and **3a**. Since **4a** was active for EF hydrogenation in the absence of added acid, the protonation of solvent instead of iridium would be expected to result in an active EF hydrogenation catalyst. It would be interesting to follow up these observations with an investigation of the effect of excess alcohol on EF hydrogenation.

We also assessed the effect of H_2 gas purity. The use of 5.0 Ultra high purity H_2 (99.999 % H_2) improved the overall activity when using **4a** (178 vs 88 TON MeOH after 16 hours, entries 4 and 5), and complete consumption of EF. With a longer reaction time of 65 hours, 390 TON of MeOH were generated, and there was no measurable EF observed. We did not further investigate the cause of this difference, but note that sensitivity of ester hydrogenation catalysis to hydrogen grade has been observed previously.[8,9]

Overall, these results represent a significant improvement for CO_2 to MeOH cascade catalysis from the original system published by Sanford (390 TON vs 21).[1] Additionally, with acid-tolerant ester hydrogenation catalysts, it is no longer necessary to use separate vessels for cat. A/cat. B vs cat. C. We are optimistic that future optimization, including the investigation of alternatives for cat. B will further increase the overall efficiency of the cascade.

5.4 Investigation of alternative acids for use as cat. B

Having confirmed the activity of the cascade combination (tetraphos)$Ru(H)_2$/$Sc(OTf)_3$/**4a**, we next attempted improve to cascade activity by optimizing cat. B. We focused on acid additives that facilitated high activity for EF hydrogenation. The most active catalyst combinations observed in studies in Chapter 4 were **3a** and/or **1a** with $HNTf_2$, $(C_6F_5)_3B$, and HBF_4**.**Et_2O.

Table 5.3: Investigation of cat. B alternatives in CO_2 to MeOH cascade

Entry*	cat. B	cat. C	cat. A (μmol)	cat. B (μmol)	cat. C (μmol)	MeOH/[Ir] (TON)	EF/[Ru] (TON)
1	$HNTf_2$	**4a**	4.1	19.2	5.0	**0**	68
2	$HNTf_2$	**3a**	4.1	16.3	4.9	**0**	43
3	HBF_4**.**Et_2O	**3a**	5.9	18.4	5.0	**0**	26
4	$(C_6F_5)_3B$	**4a**	4.1	25.0	5.0	**0**	0
5	$(C_6F_5)_3B$	**3a**	4.1	25.0	5.0	**0**	0

Conditions: Cat A. = (tetraphos)$Rr(H)_2$,, 2 mL 1,4-dioxane, 0.5 mL EtOH, 30 bar CO_2/60 bar H_2, 140 °C, 16 h. *5.0 Ultra high purity H_2. All entries represent one trial.

Table 5.3 presents the results of initial screening of these acid additives. We observed that $(C_6F_5)_3B$ was not an effective cat. B, resulting in no production of EF, and therefore no MeOH (Entries 4 and 5). $HNTf_2$ resulted in the formation of a small amount of EF but did not facilitate hydrogenation of EF to MeOH with either **4a** or **3a** (entries 1 and 2). Additionally, HBF_4**.**Et_2O cat. B only resulted in 23 TON EF observed and no MeOH. These results were surprising, as the **3a** with HBF_4**.**Et_2O and $HNTf_2$ were very active for EF hydrogenation alone. Overall, these acids were less effective at promoting EF formation than $Sc(OTf)_3$. It is possible that the Sc^{3+} Lewis

acid offers benefits over protic acids and $(C_6F_5)_3B$. It would be interesting to compare the activity of $Sc(NTf_2)_3$ with $Sc(OTf)_3$, the triflumidate anion seems more compatible with EF hydrogenation by (pincer)Ir(CO) catalysts.

5.5 Attempted alcohol dehydrogenative coupling of ethanol

Alcohol dehydrogenative coupling (ADH), is the microscopic reverse of the ester hydrogenation reaction. Many pre-catalysts active for ester hydrogenation, including Milstein's catalyst,[10] also facilitate ADH reactions.[11–13] We were curious whether (pincer)Ir(CO) catalysts are also competent for this transformation. Based on NIST thermochemistry data, dehydrogenative coupling of ethanol (EtOH) to ethyl acetate is favorable by ΔG = -3.6 kcal/mol at 100 °C, and is unfavorable by ΔG = 11.5 kcal/mol at 25 °C.[14] Removal of H_2 over the course of the reaction is expected to help drive the dehydrogenative coupling.

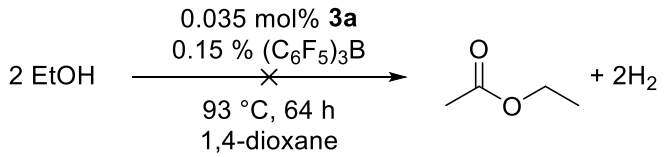

Figure 5.1. Reaction scheme for alcohol dehydrogenative coupling reactions

The combination of **3a** and $(C_6F_5)_3B$ was chosen, as it was extremely active for EF hydrogenation but does not include a protic acid that would catalyze dehydration of EtOH to diethyl ether (Figure 2). Disappointingly, over the course of 65 hours at reflux (93 °C), formation of trace amounts of diethyl ether and no production of ethyl acetate was observed.

5.6 Transfer hydrogenation using FA as the hydrogen source

Formic acid (FA) is an attractive alternative to molecular hydrogen, due to the relative ease of transport and storage and avoidance of high H_2 pressures.[15,16] Additionally, it may be produced from renewable biomass starting materials, whereas most hydrogen used industrially today is

produced from hydrocarbons, including natural gas or coal.[17,18] The use of FA as in homogeneous transfer hydrogenations of ester substrates has previously reported.[19,20] We hypothesized that the acid-tolerant (pincer)Ir(CO) complexes may be able to use H_2 from FA to hydrogenate carbonyl substrates by transfer hydrogenation.

We first investigated the transfer hydrogenation of acetone, as ketones are more easily hydrogenated then esters.[21] A NMR tube was charged with 5 equiv. acetone and 10 equiv. FA to **1c** in 1,4-dioxane (Figure 2). After mixing for 16 hours, ^{1}H NMR spectroscopy did not show any changes in acetone and FA quantities. However, a small amount of **1b** was observed. The tube was then heated at 100 °C for four hours, and resonances corresponding to isopropanol, the hydrogenation product of acetone appeared, as did a resonance for H_2. Additionally, the ^{31}P NMR signal corresponding to **1b** increased in relative intensity to other Ir species observed in solution. After 18 hours of additional heating at 100 °C, FA was consumed and the isopropanol signal increased, as the acetone was consumed concurrently. No additional changes occurred with further heating. Notably, dicarbonyl complex **1e** was not detected at any time point, suggesting that no CO is produced; FA decomposition to CO and H_2O is not occurring under these conditions.

We repeated the experiment with EF and did not observe conversion to MeOH and EtOH, even after extended heating at 100 °C. FA was consumed after 20 hours of heating at 100 °C, and H_2 was observed in the ^{1}H NMR spectrum. We attempted the transfer hydrogenation of EF with increased substrate and FA concentration. Due to the expected pressure increase from FA decomposition, these reactions were carried out in high-pressure reactors. No EF hydrogenation was observed in a reaction with 4:1 FA:EF and 0.25 mol% **1c** stirred at 100 °C for 16 hours. However, about 75% of the FA was consumed, and CO_2 was observed in the ^{13}C NMR spectrum of the reaction solution. In an effort to reduce FA decomposition, an identical experiment was

pressurized with 4 bar H_2. The added H_2 pressure did not appreciably slow FA decomposition. In all cases, pressure increased in the high-pressure reactor at comparable rates (Figure 5.3, section 5.8.3). Use of **1a** instead of **1c** produced an identical result. These experiments show that the decomposition of FA to H_2 and CO_2 is faster than transfer hydrogenation of EF by **1c**.

The observation that FA decomposes to H_2 and CO_2 in the presence of **1c** also has implications for EF hydrogenation catalysis. The acid-catalyzed reaction of EF and water can generate FA and EtOH. Subsequent FA decomposition may be a contributing factor to the loss of C_1 equivalents in EF hydrogenation by (pincer)Ir(CO) catalysts. Furthermore, the absence of any observation of **1e** suggests that FA decomposition to CO and H_2O is not the source of CO, and thus is not contributing to the generation catalytically inactive [(pincer)Ir(H)$(CO)_2$][X] complexes. We note that the decomposition of FA by (pincer)Ir(CO) may also be occurring under cascade conditions, potentially working against CO_2 hydrogenation by cat. A. This suggests that ensuring rapid conversion of FA to EF by transesterification will be important to maintaining and/or increasing the CO_2 to MeOH cascade.

5.7 Conclusions

The (pincer)Ir(CO) are a promising alternative to previously studied ester hydrogenation catalysts for application. While these catalysts were not found to be efficient for ADH and transfer hydrogenation using FA as a hydrogen source, they did show activity in CO_2 hydrogenation cascade systems. When **4a** was implemented in a cascade system with $ScOTf_3$ and (tetraphos)Ru$(H)_2$ catalysts, we observed 390 TON of MeOH produced from the hydrogenation of CO_2 after 65 hours, without additional optimization. This represents a significant increase from the 21 TON in the initial system developed by Sanford,[1] and to our knowledge is the second example of three-component cascade conversion of CO_2 to MeOH under acidic conditions. Our results are

comparable to the best results observed by Leitner and co-workers using a (triphos)Ru-based catalyst and $HNTf_2$, 442 TON after 24 hours at the same temperature and pressures (140 °C, 30 bar CO_2/60 bar H_2).[22] We hope to further improve upon these results by optimizing cascade parameters such as catalyst concentrations, solvent and temperature. Our understanding of EF hydrogenation with these pre-catalysts will guide future improvements, and high-throughput screening is likely to be a useful tool for conducting these optimizations.

5.8 Experimental

5.8.1 General Considerations

Experiments and manipulations were performed using Schlenk technique under N_2 atmosphere or a nitrogen-filled glovebox, unless otherwise specified. All solvents and liquid reagents were degassed with N_2 prior to use. 1,4-dioxane and formic acid were stored over 4Å molecular sieves, and EtOH was stored over 3Å molecular sieves. $HNTf_2$ was purified by sublimation. All other reagents were used as received. NMR spectra were obtained on a Bruker AV-500, DRX-500 or AV300 NMR instrument. High-pressure experiments were conducted using a Parr Series 5000 Multi Reactor system, equipped with stirring and pressure monitoring. Reactor temperature was monitored by thermacouples embedded in the aluminum heating block and regulated by SpecView software. (tetraphos)$Ru(H)_2$, (tetraphos = tris[2-(diphenylphosphino)ethyl]phosphine was synthesized according to literature procedures.[23] (pincer)Ir(CO) complexes were synthesized as described in Chapter 4.

*5.8.2 Reaction of **1c** with PPh_3*

A J-Young NMR tube was charged with 3.62 mg (0.013 mmol) PPh_3, and transferred to a N_2 atmosphere glovebox, where 7.2 mg (0.010 mmol) **1c** was added. The tube was sealed, removed

from the box, and approximately 0.4 mL CD_2Cl_2 was added to the tube via vacuum transfer to give a pale peach solution. The contents of the tube were analyzed by ^1H and ^{31}P NMR spectroscopy.

5.8.3 NMR spectra of [(^{iPr}POCOP)Ir(H)(CO)(PPh$_3$)][OTf]

^1H NMR spectrum (CD_2Cl_2, 300 MHz) of [(^{iPr}POCOP)Ir(H)(CO)(PPh$_3$)][OTf]

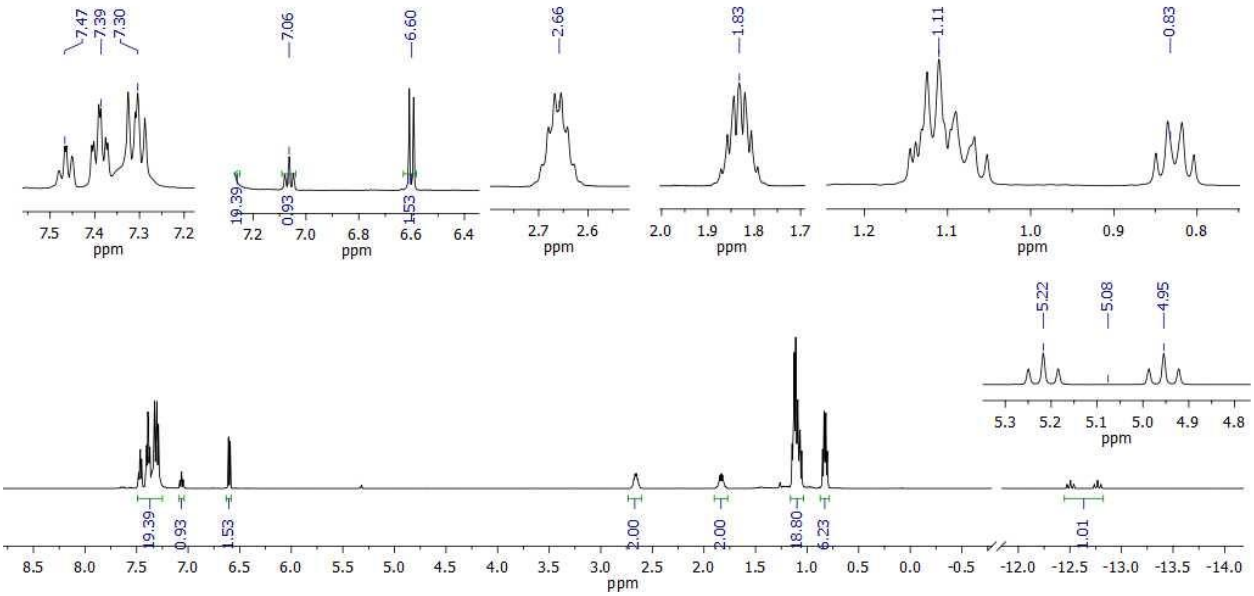

$^{31}P\{^1H\}$ NMR spectrum (CD_2Cl_2, 202.3 MHz) of [(^{iPr}POCOP)Ir(H)(CO)(PPh$_3$)][OTf]

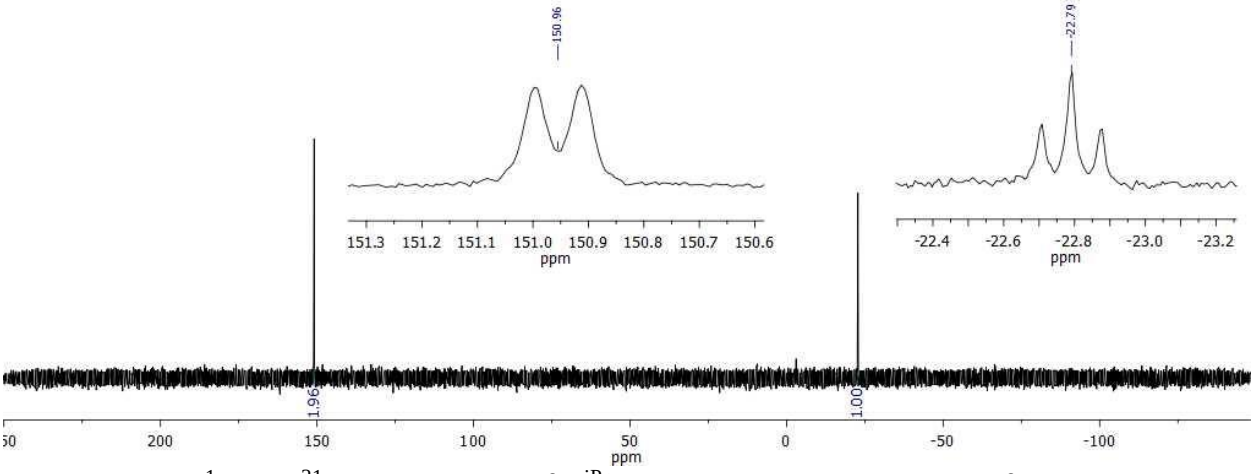

Figure 5.2. ^1H and ^{31}P NMR spectra of [(^{iPr}POCOP)Ir(H)(CO)(PPh$_3$)][OTf]

5.8.4 Cascade hydrogenation of CO_2 to MeOH

Sample procedure for high pressure reactor experiment for cascade reaction

In a N_2 atmosphere glovebox, 3.2 mg (0.0041 mmol) (tetraphos)$Ru(H)_2$, 8.2 mg (0.017 mmol) $Sc(OTf)_3$ and 3.0 mg (0.0049 mmol) **4a** were weighed into a PTFE Parr reactor liner. 1,4-dioxane (2 mL) and EtOH (0.5 mL) were added via syringe. The reactor was equipped with a stir bar, closed, removed from the glove box, and pressurized. The reactor was heated to 140 °C and stirred at 300 rpm. After 16 hours, the reactor was removed from the heat, allowed to cool for twenty minutes in air and then cooled on ice. The reactor was vented, opened and the contents were analyzed.

Sample procedure for pressurization with CO_2 and H_2

Reactors were attached to the manifold, and the manifold was purged with CO_2. Reactors were pressurized with 10 bar CO_2 and vented three times to exchange the atmosphere, then pressurized to 30 bar CO_2 and closed. The manifold was purged with H_2, and then pressurized to 90 bar. The reactors were opened to H_2 for ~3 seconds, then sealed, and the manifold was vented. This results in 30 bar CO_2 and 60 bar H_2 in the reactor.

Analysis of high-pressure reactor experiments

The vented Parr reactor was opened, and 50.0 μL mesitylene were added to the reactor via syringe. The contents of the reactor were agitated to ensure good mixing. For ^{13}C experiments, 4.5-5 mg $Cr(acac)_3$ were massed into a NMR tube. A 500 μL aliquot of solution was placed into the tube. Quantitative ^{13}C NMR spectra were collected using an inverse-gated pulse sequence. Alkyl carbon signals of substrate and product were integrated versus the mesitylene methyl signal.

5.8.5 Transfer hydrogenation experiments

Transfer hydrogenation of Acetone, EF

A J-Young NMR tube was charged with 7.1 mg (0.01 mmol) **1c**, 0.4 mL 1,4-dioxane and C_6D_6 capillary. 3.7 μL (0.049 mmol) of acetone (N_2 sparged) and 3.7 μL (0.098 mmol) FA were added via a volumetric glass capillary to give a pale yellow solution. The tube was allowed to mix overnight on an apparatus that rotated the tube slowly. The tube was heated at 100 °C. Reaction was monitored by ^{1}H NMR spectroscopy.

EF substrate: Experiment conducted as above, with 10 μL (0.12 mmol) EF, 9.4 μL (0.25 mmol) FA.

Transfer hydrogenation in high-pressure reactors:

Following the general high-pressure reactor procedure above, a PTFE-lined reactor was charged with 7.1 mg **1c**, 323 μL (4.0 mmol) EF, and 600 μL (16 mmol) FA in 1 mL 1,4 dioxane. The reactor was pressurized to 4 bar H_2, and heated for 16 hours at 100°C. Reactors were worked up and contents were analyzed as described above. The pressures measured in the reactors over the course of the reaction are shown in Figure 5.3 below.

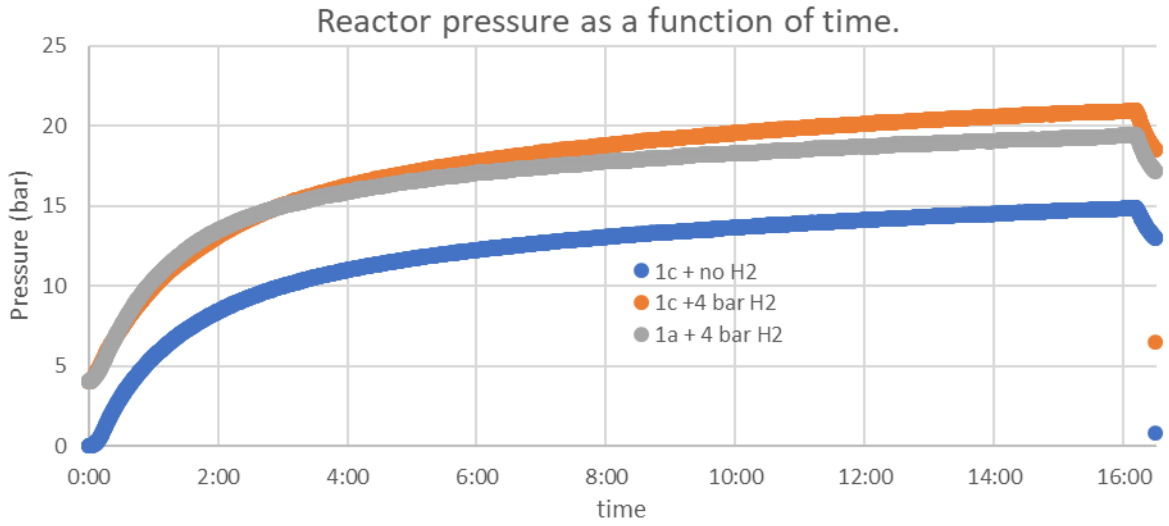

Figure 5.3. Pressure traces for transfer hydrogenation reactions with (orange, grey) and without (blue) added H_2 atmosphere. Time in hours.

5.8.6 Alcohol dehydrogenative coupling

Into a 25 mL Schlenk flask was weighed 12.8 mg (0.025 mmol) $(C_6F_5)_3B$ and 4.0 mg (0.060 mmol) **3a**. 2.0 mL 1,4-dioxane and 1.0 mL EtOH were added via syringe. The Schlenk flask was equipped with a reflux condenser and vent bubbler. The flask was heated at reflux in an oil bath. A NMR sample consisting of a 500 µl aliquot was removed by syringe, 5 µL mesitylene internal standard, and C_6D_6 capillary was analyzed by ^{1}H NMR spectroscopy with 1,4-dioxane signal suppression. Ethyl acetate was not observed.

5.9 References

(1) Huff, C. A.; Sanford, M. S. Cascade Catalysis for the Homogeneous Hydrogenation of CO_2 to Methanol. *J. Am. Chem. Soc.* **2011**, *133* (45), 18122–18125.

(2) Munshi, P.; Main, A. D.; Linehan, J. C.; Tai, C. C.; Jessop, P. G. Hydrogenation of Carbon Dioxide Catalyzed by Ruthenium Trimethylphosphine Complexes: The Accelerating Effect of Certain Alcohols and Amines. *J. Am. Chem. Soc.* **2002**, *124* (27), 7963–7971.

(3) Lekich, T. T.; Gary, J. B.; Bellows, S. M.; Cundari, T. R.; Guard, L. M.; Heinekey, D. M. H_2 Addition to (^{Me4}PCP)Ir(CO): Studies of the Isomerization Mechanism. *Dalton Trans.* **2018**, *47* (45), 16119–16125.

(4) Anderson, T. S.; Briand, G. G.; Brüning, R.; Decken, A.; Margeson, M. J.; Pickard, H. M.; Trevors, E. E. Synthesis, Characterization and Reactivity of (Dithiolato)Indium Complexes. *Polyhedron* **2017**, *135*, 101–108.

(5) Federsel, C.; Boddien, A.; Jackstell, R.; Jennerjahn, R.; Dyson, P. J.; Scopelliti, R.; Laurenczy, G.; Beller, M. A Well-Defined Iron Catalyst for the Reduction of Bicarbonates and Carbon Dioxide to Formates, Alkyl Formates, and Formamides. *Angew. Chem. Int. Ed.* **2010**, *49* (50), 9777–9780.

(6) Federsel, C.; Ziebart, C.; Jackstell, R.; Baumann, W.; Beller, M. Catalytic Hydrogenation of Carbon Dioxide and Bicarbonates with a Well-Defined Cobalt Dihydrogen Complex. *Chem. Eur. J.* **2012**, *18* (1), 72–75.

(7) Dr. Amy Chu, Private Communication.

(8) Rezayee, N. M.; Samblanet, D. C.; Sanford, M. S. Iron-Catalyzed Hydrogenation of Amides to Alcohols and Amines. *ACS Catal.* **2016**, *6* (10), 6377–6383.

(9) Rezayee, N. M.; Huff, C. A.; Sanford, M. S. Tandem Amine and Ruthenium-Catalyzed Hydrogenation of CO_2 to Methanol. *J. Am. Chem. Soc.* **2015**, *137* (3), 1028–1031.

(10) Zhang, J.; Leitus, G.; Ben-David, Y.; Milstein, D. Facile Conversion of Alcohols into Esters and Dihydrogen Catalyzed by New Ruthenium Complexes. *J. Am. Chem. Soc.* **2005**, *127* (31), 10840–10841.

(11) Gusev, D. G. Dehydrogenative Coupling of Ethanol and Ester Hydrogenation Catalyzed by Pincer-Type YNP Complexes. *ACS Catal.* **2016**, *6* (10), 6967–6981.

(12) Spasyuk, D.; Vicent, C.; Gusev, D. G. Chemoselective Hydrogenation of Carbonyl Compounds and Acceptorless Dehydrogenative Coupling of Alcohols. *J. Am. Chem. Soc.* **2015**, *137* (11), 3743–3746.

(13) Spasyuk, D.; Gusev, D. G. Acceptorless Dehydrogenative Coupling of Ethanol and Hydrogenation of Esters and Imines. *Organometallics* **2012**, *31* (15), 5239–5242.

(14) Chase, J. M. NIST-JANAF Themochemical Tables, Fourth Edition. In *NIST Chemistry WebBook*; National Institute of Standards and Technology,: Gaithersburg MD, 2018; p https://doi.org/10.18434/T4D303.

(15) Corma Canos, A.; Iborra, S.; Velty, A. Chemical Routes for the Transformation of Biomass into Chemicals. *Chem. Rev.* **2007**, *107* (6), 2411–2502.

(16) Wang, W.; Niu, M.; Hou, Y.; Wu, W.; Liu, Z.; Liu, Q.; Ren, S.; Marsh, K. N. Catalytic Conversion of Biomass-Derived Carbohydrates to Formic Acid Using Molecular Oxygen. *Green Chem.* **2014**, *16* (5), 2614–2618.

(17) Häussinger, P.; Lohmüller, R.; Watson, A. M. Hydrogen, 2. Production. In *Ullmann's Encyclopedia of Industrial Chemistry*; Wiley-VCH Verlag GmbH & Co. KGaA: Weinheim, Germany, 2011; Vol. 224.

(18) Häussinger, P.; Lohmüller, R.; Watson, A. M. Hydrogen, 3. Purification. In *Ullmann's Encyclopedia of Industrial Chemistry*; Wiley-VCH Verlag GmbH & Co. KGaA: Weinheim, Germany, 2011; Vol. 224.

(19) Wang, S.; Dorcet, V.; Roisnel, T.; Bruneau, C.; Fischmeister, C. Ruthenium and Iridium Dipyridylamine Catalysts for the Efficient Synthesis of γ-Valerolactone by Transfer Hydrogenation of Levulinic Acid. *Organometallics* **2017**, *36* (3), 708–713.

(20) Fábos, V.; Mika, L. T.; Horváth, I. T. Selective Conversion of Levulinic and Formic Acids to γ-valerolactone with the Shvo Catalyst. *Organometallics* **2014**, *33* (1), 181–187.

(21) Dub, P. A.; Ikariya, T. Catalytic Reductive Transformations of Carboxylic and Carbonic Acid Derivatives Using Molecular Hydrogen. *ACS Catal.* **2012**, *2* (8), 1718–1741.

(22) Wesselbaum, S.; Moha, V.; Meuresch, M.; Brosinski, S.; Thenert, K. M.; Kothe, J.; vom Stein, T.; Englert, U.; Hölscher, M.; Klankermayer, J.; et al. Hydrogenation of Carbon Dioxide to Methanol Using a Homogeneous Ruthenium–Triphos Catalyst: From Mechanistic Investigations to Multiphase Catalysis. *Chem. Sci.* **2015**, *6* (1), 693–704.

(23) Bianchini, C.; Perez, P. J.; Peruzzini, M.; Zanobini, F.; Vacca, A. Classical and Nonclassical Polyhydride Ruthenium(II) Complexes Stabilized by the Tetraphosphine $P(CH_2CH_2PPh_2)_3$. *Inorg. Chem.* **1991**, *30* (2), 279–287.

BIBLIOGRAPHY

Acosta-Ramirez, A.; Bertoli, M.; Gusev, D. G.; Schlaf, M. Homogeneous Catalytic Hydrogenation of Long-Chain Esters by an Osmium Pincer Complex and Its Potential Application in the Direct Conversion of Triglycerides into Fatty Alcohols. *Green Chem.* **2012**, *14* (4), 1178–1188.

Adkins, H.; Wojcik, B.; Adkins, H. Hydrogenation of Amides to Amines. *J. Am. Chem. Soc.* **1934**, *56* (1), 247.

Ahmed Foskey, T. J.; Heinekey, D. M.; Goldberg, K. I. Partial Deoxygenation of 1,2-Propanediol Catalyzed by Iridium Pincer Complexes. *ACS Catal.* **2012**, *2* (6), 1285–1289.

Alberico, E.; Lennox, A. J. J.; Vogt, L. K.; Jiao, H.; Baumann, W.; Drexler, H.-J.; Nielsen, M.; Spannenberg, A.; Checinski, M. P.; Junge, H.; et al. Unravelling the Mechanism of Basic Aqueous Methanol Dehydrogenation Catalyzed by Ru–PNP Pincer Complexes. *J. Am. Chem. Soc.* **2016**, *138* (45), 14890–14904.

Almeida, M. L. S.; Beller, M.; Wang, G. Z.; Bäckvall, J. E. Ruthenium(II)-Catalyzed Oppenauer-Type Oxidation of Secondary Alcohols. *Chem. Eur. J.* **1996**, *2* (12), 1533–1536.

Anderson, T. S.; Briand, G. G.; Brüning, R.; Decken, A.; Margeson, M. J.; Pickard, H. M.; Trevors, E. E. Synthesis, Characterization and Reactivity of (Dithiolato)Indium Complexes. *Polyhedron* **2017**, *135*, 101–108.

Anten, J. O. P.; Surburg, H. Flavors and Fragrances, 2. Aliphatic Compounds. In *Ullmann's Encyclopedia of Industrial Chemistry*; Wiley-VCH Verlag GmbG & Co. KGaA: Weinheim, 2015; pp 1–55.

Antoniotti, S.; Dalla, V.; Duñach, E. Metal Triflimidates: Better than Metal Triflates as Catalysts in Organic Synthesis-the Effect of a Highly Delocalized Counteranion. *Angew. Chem. Int. Ed.* **2010**, *49* (43), 7860–7888.

Artús Suàrez, L.; Culakova, Z.; Balcells, D.; Bernskoetter, W. H.; Eisenstein, O.; Goldberg, K. I.; Hazari, N.; Tilset, M.; Nova, A. The Key Role of the Hemiaminal Intermediate in the Iron-Catalyzed Deaminative Hydrogenation of Amides. *ACS Catal.* **2018**, 8751–8762.

Balaraman, E.; Gnanaprakasam, B.; Shimon, L. J. W.; Milstein, D. Direct Hydrogenation of Amides to Alcohols and Amines under Mild Conditions. *J. Am. Chem. Soc.* **2010**, *132* (47), 16756–16758.

Balaraman, E.; Gunanathan, C.; Zhang, J.; Shimon, L. J. W.; Milstein, D. Efficient Hydrogenation of Organic Carbonates, Carbamates and Formates Indicates Alternative Routes to Methanol Based on CO_2 and CO. *Nature Chem.* **2011**, *3* (8), 609–614.

Beamson, G.; Papworth, A. J.; Philipps, C.; Smith, A. M.; Whyman, R. Selective Hydrogenation of Amides Using Rh/Mo Catalysts. *J. Catal.* **2010**, *269* (1), 93–102.

Bertoli, M.; Choualeb, A.; Lough, A. J.; Moore, B.; Spasyuk, D.; Gusev, D. G. Osmium and Ruthenium Catalysts for Dehydrogenation of Alcohols. *Organometallics* **2011**, *30* (13), 3479–3482.

Bianchini, C.; Perez, P. J.; Peruzzini, M.; Zanobini, F.; Vacca, A. Classical and Nonclassical Polyhydride Ruthenium(II) Complexes Stabilized by the Tetraphosphine $P(CH_2CH_2PPh_2)_3$. *Inorg. Chem.* **1991**, *30* (2), 279–287.

Bielinski, E. A.; Lagaditis, P. O.; Zhang, Y.; Mercado, B. Q.; Würtele, C.; Bernskoetter, W. H.; Hazari, N.; Schneider, S. Lewis Acid-Assisted Formic Acid Dehydrogenation Using a Pincer-Supported Iron Catalyst. *J. Am. Chem. Soc.* **2014**, *136* (29), 10234–10237.

Blum, Y.; Shvo, Y. Catalytic Reactive Ruthenium Intermediates in the Homogeneous Oxidation of Alcohols to Esters. *Isr. J. Chem.* **1984**, *24*, 144–148.

Bornschein, C.; Werkmeister, S.; Wendt, B.; Jiao, H.; Alberico, E.; Baumann, W.; Junge, H.; Junge, K.; Beller, M. Mild and Selective Hydrogenation of Aromatic and Aliphatic (Di)Nitriles with a Well-Defined Iron Pincer Complex. *Nat. Commun.* **2014**, *5* (1), 1–11.

Bouveault, L. .; Blanc, G. Préparation Des Alcools Primaires Au Moyen Des Acides Correspondants. *C. R. Hebd. Seances Acad. Sci.* **1903**, 1676–1678.

Brewster, T. P.; Miller, A. J. M.; Heinekey, D. M.; Goldberg, K. I. Hydrogenation of Carboxylic Acids Catalyzed by Half-Sandwich Complexes of Iridium and Rhodium. *J. Am. Chem. Soc.* **2013**, *135* (43), 16022–16025.

Brewster, T. P.; Rezayee, N. M.; Culakova, Z.; Sanford, M. S.; Goldberg, K. I. Base-Free Iridium-Catalyzed Hydrogenation of Esters and Lactones. *ACS Catal.* **2016**, *6* (5), 3113–3117.

Brotherton, R. J.; Weber, C. J.; Guibert, C. R.; Little, J. L. Boron Compounds. In *Ullmann's Encyclopedia of Industrial Chemistry*; Wiley-VCH Verlag GmbH & Co. KGaA: Weinheim, Germany, 2000; Vol. 92, pp 1–853.

Bryndza, H. E.; Fong, L. K.; Paciello, R. A.; Tam, W.; Bercaw, J. E. Relative Metal-Hydrogen, -Oxygen, -Nitrogen, and -Carbon Bond Strengths for Organoruthenium and Organoplatinum Compounds; Equilibrium Studies of $Cp^*(PMe_3)_2RuX$ and (DPPE)MePtX Systems. *J. Am. Chem. Soc.* **1987**, *109* (5), 1444–1456.

Cantillo, D. Mechanistic Insights on the Ruthenium-Catalyzed Hydrogenation of Amides - C-N vs. C-O Cleavage. *Eur. J. Inorg. Chem.* **2011**, 3008–3013.

Casey, C. P.; Beetner, S. E.; Johnson, J. B. Spectroscopic Determination of Hydrogenation Rates and Intermediates during Carbonyl Hydrogenation Catalyzed by Shvo's Hydroxycyclopentadienyl Diruthenium Hydride Agrees with Kinetic Modeling Based on Independently Measured Rates of Elementary Reactions. *J. Am. Chem. Soc.* **2008**, *130* (7), 2285–2295.

Casey, C. P.; Singer, S. W.; Powell, D. R.; Hayashi, R. K.; Kavana, M. Hydrogen Transfer to Carbonyls and Imines from a Hydroxycyclopentadienyl Ruthenium Hydride: Evidence for Concerted Hydride and Proton Transfer. *J. Am. Chem. Soc.* **2001**, *123* (6), 1090–1100.

Casey, C. P.; Vos, T. E.; Singer, S. W.; Guzei, I. A. Protonated Aminocyclopentadienyl Ruthenium Hydride Reduction of Benzaldehyde and the Conversion of the Resulting Ruthenium Triflate to a Ruthenium Hydride with H_2 and Base. *Organometallics* **2002**, *21* (23), 5038–5046.

Chakraborty, S.; Dai, H.; Bhattacharya, P.; Fairweather, N. T.; Gibson, M. S.; Krause, J. A.; Guan, H. Iron-Based Catalysts for the Hydrogenation of Esters to Alcohols. *J. Am. Chem. Soc.* **2014**, *136* (22), 7869–7872.

Chakraborty, S.; Lagaditis, P. O.; Förster, M.; Bielinski, E. A.; Hazari, N.; Holthausen, M. C.; Jones, W. D.; Schneider, S. Well-Defined Iron Catalysts for the Acceptorless Reversible Dehydrogenation-Hydrogenation of Alcohols and Ketones. *ACS Catal.* **2014**, *4* (11), 3994–4003.

Chase, J. M. NIST-JANAF Themochemical Tables, Fourth Edition. In *NIST Chemistry WebBook*; National Institute of Standards and Technology,: Gaithersburg MD, 2018; p https://doi.org/10.18434/T4D303.

Che, M. Nobel Prize in Chemistry 1912 to Sabatier: Organic Chemistry or Catalysis? *Catal. Today* **2013**, *218–219*, 162–171.

Chen, T.; Li, H.; Qu, S.; Zheng, B.; He, L.; Lai, Z.; Wang, Z. X.; Huang, K. W. Hydrogenation of Esters Catalyzed by Ruthenium PN^3-Pincer Complexes Containing an Aminophosphine Arm. *Organometallics* **2014**, *33* (15), 4152–4155.

Cheng, T. Y.; Brunschwig, B. S.; Bullock, R. M. Hydride Transfer Reactions of Transition Metal Hydrides: Kinetic Hydricity of Metal Carbonyl Hydrides. *J. Am. Chem. Soc.* **1998**, *120* (50), 13121–13137.

Choi, J.; MacArthur, A. H. R.; Brookhart, M.; Goldman, A. S. Dehydrogenation and Related Reactions Catalyzed by Iridium Pincer Complexes. *Chem. Rev.* **2011**, *111* (3), 1761–1779.

Chu, P.-S.; True, N. S. Pressure-Dependent Gas-Phase NMR Studies of Tetrahydropyran Ring Inversion. *J. Phys. Chem.* **1985**, 2625–2630.

Clarke, M. L. Recent Developments in the Homogeneous Hydrogenation of Carboxylic Acid Esters. *Catal. Sci. Technol.* **2012**, *2* (12), 2418.

Comas-Vives, A.; Ujaque, G.; Lledós, A. Hydrogen Transfer to Ketones Catalyzed by Shvo's Ruthenium Hydride Complex: A Mechanistic Insight. *Organometallics* **2007**, *26* (17), 4135–4144.

Conley, B. L.; Pennington-Boggio, M. K.; Boz, E.; Williams, T. J. Discovery, Applications, and Catalytic Mechanisms of Shvo' s Catalyst. *Chem. Rev.* **2010**, *110* (4), 2294–2312.

Constable, D. J. C.; Dunn, P. J.; Hayler, J. D.; Humphrey, G. R.; Leazer, Jr., J. L.; Linderman, R. J.; Lorenz, K.; Manley, J.; Pearlman, B. A.; Wells, A.; et al. Key Green Chemistry Research Areas—a Perspective from Pharmaceutical Manufacturers. *Green Chem.* **2007**, *9* (5), 411–420.

Corma Canos, A.; Iborra, S.; Velty, A. Chemical Routes for the Transformation of Biomass into Chemicals. *Chem. Rev.* **2007**, *107* (6), 2411–2502.

Crabtree, R. H. Dihydrogen Complexation. *Chem. Rev.* **2016**, *116* (15), 8750–8769.

Crabtree, R. H. Dihydrogen Complexes: Some Structural and Chemical Studies. *Acc. Chem. Res.* **1990**, *23* (4), 95–101.

Crabtree, R. H. *The Organometallic Chemistry of the Transition Metals*, 6th ed.; John Wiley & Sons, Inc.: Hoboken, NJ, USA, 2014.

Csjernyik, G.; Éll, A. H.; Fadini, L.; Pugin, B.; Bäckvall, J.-E. Efficient Ruthenium-Catalyzed Aerobic Oxidation of Alcohols Using a Biomimetic Coupled Catalytic System. *J. Org. Chem.* **2002**, *67* (5), 1657–1662.

Dang, T. T.; Boeck, F.; Hintermann, L. Hidden Brønsted Acid Catalysis: Pathways of Accidental or Deliberate Generation of Triflic Acid from Metal Triflates. *J. Org. Chem.* **2011**, *76* (22), 9353–9361.

Dodds, D. L.; Cole-Hamilton, D. J. Catalytic Reduction of Amides Avoiding $LiAlH_4$ Or B_2H_6. In *Sustainable Catalysis*; Peter J. Dunn, K. K. (Mimi) Hii, Michael J. Krische, and M. T. W., Ed.; John Wiley & Sons, Inc.: Hoboken, New Jersey, 2013; pp 1–36.

Dub, P. A.; Gordon, J. C. Metal-Ligand Bifunctional Catalysis: The "Accepted" Mechanism, the Issue of Concertedness, and the Function of the Ligand in Catalytic Cycles Involving Hydrogen Atoms. *ACS Catal.* **2017**, *7* (10), 6635–6655.

Dub, P. A.; Gordon, J. C. The Mechanism of Enantioselective Ketone Reduction with Noyori and Noyori-Ikariya Bifunctional Catalysts. *Dalton Trans.* **2016**, *45* (16), 6756–6781.

Dub, P. A.; Henson, N. J.; Martin, R. L.; Gordon, J. C. Unravelling the Mechanism of the Asymmetric Hydrogenation of Acetophenone by [RuX_2(Diphosphine)(1,2-Diamine)] Catalysts. *J. Am. Chem. Soc.* **2014**, *136* (9), 3505–3521.

Dub, P. A.; Ikariya, T. Catalytic Reductive Transformations of Carboxylic and Carbonic Acid Derivatives Using Molecular Hydrogen. *ACS Catal.* **2012**, *2* (8), 1718–1741.

Eisenstein, O.; Crabtree, R. H. Outer Sphere Hydrogenation Catalysis. *New J. Chem.* **2013**, *37* (1), 21–27.

Elangovan, S.; Garbe, M.; Jiao, H.; Spannenberg, A.; Junge, K.; Beller, M. Hydrogenation of Esters to Alcohols Catalyzed by Defined Manganese Pincer Complexes. *Angew. Chem. Int. Ed.* **2016**, *55* (49), 15364–15368.

Espinosa-Jalapa, N. A.; Nerush, A.; Shimon, L. J. W.; Leitus, G.; Avram, L.; Ben-David, Y.; Milstein, D. Manganese-Catalyzed Hydrogenation of Esters to Alcohols. *Chem. Eur. J.* **2017**, *23* (25), 5934–5938.

Fábos, V.; Mika, L. T.; Horváth, I. T. Selective Conversion of Levulinic and Formic Acids to γ-Valerolactone with the Shvo Catalyst. *Organometallics* **2014**, *33* (1), 181–187.

Farrugia, L. J. ORTEP-3 for Windows - A Version of ORTEP-III with a Graphical User Interface (GUI). *J. Appl. Crystallogr.* **1997**.

Federsel, C.; Boddien, A.; Jackstell, R.; Jennerjahn, R.; Dyson, P. J.; Scopelliti, R.; Laurenczy, G.; Beller, M. A Well-Defined Iron Catalyst for the Reduction of Bicarbonates and Carbon Dioxide to Formates, Alkyl Formates, and Formamides. *Angew. Chem. Int. Ed.* **2010**, *49* (50), 9777–9780.

Federsel, C.; Ziebart, C.; Jackstell, R.; Baumann, W.; Beller, M. Catalytic Hydrogenation of Carbon Dioxide and Bicarbonates with a Well-Defined Cobalt Dihydrogen Complex. *Chem. Eur. J.* **2012**, *18* (1), 72–75.

Filonenko, G. A.; Aguila, M. J. B.; Schulpen, E. N.; Van Putten, R.; Wiecko, J.; Müller, C.; Lefort, L.; Hensen, E. J. M.; Pidko, E. A. Bis-N-Heterocyclic Carbene Aminopincer Ligands Enable High Activity in Ru-Catalyzed Ester Hydrogenation. *J. Am. Chem. Soc.* **2015**, *137* (24), 7620–7623.

Findlater, M.; Bernskoetter, W. H.; Brookhart, M. Proton-Catalyzed Hydrogenation of a d^8 Ir(I) Complex Yields a Trans Ir(III) Dihydride. *J. Am. Chem. Soc.* **2010**, *132* (13), 4534–4535.

Frisch, M. J.; Trucks, G. W.; Schlegel, H. B.; Scuseria, G. E.; Robb, M. A.; Cheeseman, J. R.; Scalmani, G.; Barone, V.; Mennucci, B.; Petersson, G. A.; et al. Gaussian09. *Gaussian 09*. 2009.

Geilen, F. M. A.; Engendahl, B.; Harwardt, A.; Marquardt, W.; Klankermayer, J.; Leitner, W. Selective and Flexible Transformation of Biomass-Derived Platform Chemicals by a Multifunctional Catalytic System. *Angew. Chem. Int. Ed.* **2010**, *49* (32), 5510–5514.

Geilen, F. M. a; Engendahl, B.; Hölscher, M.; Klankermayer, J.; Leitner, W. Selective Homogeneous Hydrogenation of Biogenic Carboxylic Acids with [Ru(TriPhos)H]+: A Mechanistic Study. *J. Am. Chem. Soc.* **2011**, *133* (36), 14349–14358.

Goldberg, J. M.; Cherry, S. D. T.; Guard, L. M.; Kaminsky, W.; Goldberg, K. I.; Heinekey, D. M. Hydrogen Addition to (Pincer)Ir^{I}(CO) Complexes: The Importance of Steric and Electronic Factors. *Organometallics* **2016**, *35* (20), 3546–3556.

Goldberg, J. M.; Goldberg, K. I.; Heinekey, D. M.; Burgess, S. A.; Lao, D. B.; Linehan, J. C. Detection of an Iridium-Dihydrogen Complex: A Proposed Intermediate in Ionic Hydrogenation. *J. Am. Chem. Soc.* **2017**, *139* (36), 12638–12646.

Goldberg, J. M.; Wong, G. W.; Brastow, K. E.; Kaminsky, W.; Goldberg, K. I.; Heinekey, D. M. The Importance of Steric Factors in Iridium Pincer Complexes. *Organometallics* **2015**, *34* (4), 753–762.

Goldman, A. S.; Krogh-Jespersen, K. Why Do Cationic Carbon Monoxide Complexes Have High C-O Stretching Force Constants and Short C-O Bonds? Electrostatic Effects, Not σ-Bonding. *J. Am. Chem. Soc.* **1996**, *118* (48), 12159–12166.

Göttker-Schnetmann, I.; White, P. S.; Brookhart, M. Synthesis and Properties of Iridium Bis(Phosphinite) Pincer Complexes (*p*-XPCP)IrH_2, (*p*-XPCP)Ir(CO), (*p*-XPCP)Ir(H)(Aryl), and {(*p*-XPCP)Ir}H_2{μ-N_2} and Their Relevance in Alkane Transfer De. *Organometallics* **2004**, *23* (8), 1766–1776.

Greener Solvent Alternatives. Sigma-Aldrich Co, LLC.: St. Louis, MO 2015, pp 1–4.

Grey, R. A.; Pez, G. P.; Wallo, A. Anionic Metal Hydride Catalysts. 2. Application to the Hydrogenation of Ketones, Aldehydes, Carboxylic Acid Esters and Nitriles. *J. Am. Chem. Soc.* **1981**, *103* (25), 7536–7542.

Grey, R. A.; Pez, G. P.; Wallo, A.; Corsi, J. Homogeneous Catalytic Hydrogenation of Carboxylic Acid Esters to Alcohols. *J. Chem. Soc. Chem. Commun.* **1980**, 783–784.

Guard, L. M.; Hebden, T. J.; Linn, D. E.; Heinekey, D. M. Pincer-Supported Carbonyl Complexes of Cobalt(I). *Organometallics* **2017**, *36* (16), 3104–3109.

Gusev, D. G. Dehydrogenative Coupling of Ethanol and Ester Hydrogenation Catalyzed by Pincer-Type YNP Complexes. *ACS Catal.* **2016**, *6* (10), 6967–6981.

Gusev, D. G.; Spasyuk, D. M. Revised Mechanisms for Aldehyde Disproportionation and the Related Reactions of the Shvo Catalyst. *ACS Catal.* **2018**, *8* (8), 6851–6861.

Haack, K. J.; Hashiguchi, S.; Fujii, A.; Ikariya, T.; Noyori, R. The Catalyst Precursor, Catalyst, and Intermediate in the Ru^{II}-Promoted Asymmetric Hydrogen Transfer between Alcohols and Ketones. *Angew. Chem. Int. Ed.* **1997**, *36* (3), 285–288.

Han, Z.; Rong, L.; Wu, J.; Zhang, L.; Wang, Z.; Ding, K. Catalytic Hydrogenation of Cyclic Carbonates: A Practical Approach from CO_2 and Epoxides to Methanol and Diols. *Angew. Chem. Int. Ed.* **2012**, *51* (52), 13041–13045.

Hasanayn, F.; Harb, H. A Metathesis Model for the Dehydrogenative Coupling of Amines with Alcohols and Esters into Carboxamides by Milstein's [Ru(PNN)(CO)(H)] Catalysts. *Inorg. Chem.* **2014**, *53* (16), 8334–8349.

Hasanayn, F.; Morris, R. H. Symmetry Aspects of H2 Splitting by Five-Coordinate D6 Ruthenium Amides, and Calculations on Acetophenone Hydrogenation, Ruthenium Alkoxide Formation, and Subsequent Hydrogenolysis in a Model Trans-Ru(H)2(Diamine)(Diphosphine) System. *Inorg. Chem.* **2012**, *51* (20), 10808–10818.

Häussinger, P.; Lohmüller, R.; Watson, A. M. Hydrogen, 2. Production. In *Ullmann's Encyclopedia of Industrial Chemistry*; Wiley-VCH Verlag GmbH & Co. KGaA: Weinheim, Germany, 2011; Vol. 224.

Häussinger, P.; Lohmüller, R.; Watson, A. M. Hydrogen, 3. Purification. In *Ullmann's Encyclopedia of Industrial Chemistry*; Wiley-VCH Verlag GmbH & Co. KGaA: Weinheim, Germany, 2011; Vol. 224.

Heinekey, D. M.; Oldham, W. J. Coordination Chemistry of Dihydrogen. *Chem. Rev.* **1993**, *93* (3), 913–926.

Hirosawa, C.; Wakasa, N.; Fuchikami, T. Hydrogenation of Amides by the Use of Bimetallic Catalysts Consisting of Group 8 to 10, and Group 6 or 7 Metals. *Tetrahedron Lett.* **1996**, *37* (37), 6749–6752.

Hopmann, K. H. How Accurate Is DFT for Iridium-Mediated Chemistry? *Organometallics* **2016**, *35* (22), 3795–3807.

Huang, Z.; Brookhart, M.; Goldman, A. S.; Kundu, S.; Ray, A.; Scott, S. L.; Vicente, B. C. Highly Active and Recyclable Heterogeneous Iridium Pincer Catalysts for Transfer Dehydrogenation of Alkanes. *Adv. Synth. Catal.* **2009**, *351* (1–2), 188–206.

Huber, G. W.; Iborra, S.; Corma, A. Synthesis of Transportation Fuels from Biomass: Chemistry, Catalysts, and Engineering. *Chem. Rev.* **2006**, *106* (9), 4044–4098.

Huff, C. A.; Kampf, J. W.; Sanford, M. S. Role of a Noninnocent Pincer Ligand in the Activation of CO_2 at (PNN)Ru(H)(CO). *Organometallics* **2012**, *31* (13), 4643–4645.

Huff, C. A.; Sanford, M. S. Cascade Catalysis for the Homogeneous Hydrogenation of CO_2 to Methanol. *J. Am. Chem. Soc.* **2011**, *133* (45), 18122–18125.

Iron, M. A.; Ben-Ari, E.; Cohen, R.; Milstein, D. Metal–ligand Cooperation in the *Trans* Addition of Dihydrogen to a Pincer Ir(I) Complex: A DFT Study. *Dalton Trans.* **2009**, 9433–9439.

Jadhav, S. G.; Vaidya, P. D.; Bhanage, B. M.; Joshi, J. B. Catalytic Carbon Dioxide Hydrogenation to Methanol: A Review of Recent Studies. *Chem. Eng. Res. Des.* **2014**, *92* (11), 2557–2567.

Jayarathne, U.; Zhang, Y.; Hazari, N.; Bernskoetter, W. H. Selective Iron-Catalyzed Deaminative Hydrogenation of Amides. *Organometallics* **2017**, *36* (2), 409–416.

Jeong, Y.; Kim, D. Y.; Choi, Y.; Ryu, J. S. Intramolecular Hydroalkoxylation in Brønsted Acidic Ionic Liquids and Its Application to the Synthesis of (±)-Centrolobine. *Org. Biomol. Chem.* **2011**, *9* (2), 374–378.

Jiao, H.; Junge, K.; Alberico, E.; Beller, M. A Comparative Computationally Study about the Defined M(II) Pincer Hydrogenation Catalysts (M = Fe, Ru, Os). *J. Comput. Chem.* **2016**, *37*, 168–176.

Johnson, J. B.; Bäckvall, J. E. Mechanism of Ruthenium-Catalyzed Hydrogen Transfer Reactions. Concerted Transfer of OH and CH Hydrogens from an Alcohol to a (Cyclopentadienone)Ruthenium Complex. *J. Org. Chem.* **2003**, *68* (20), 7681–7684.

Junge, K.; Wendt, B.; Jiao, H.; Beller, M. Iridium-Catalyzed Hydrogenation of Carboxylic Acid Esters. *ChemCatChem* **2014**, *6* (10), 2810–2814.

Karvembu, R.; Prabhakaran, R.; Natarajan, K. Shvo's Diruthenium Complex: A Robust Catalyst. *Coord. Chem. Rev.* **2005**, *249*, 911–918.

Khusnutdinova, J. R.; Milstein, D. Metal-Ligand Cooperation. *Angew. Chem. Int. Ed.* **2015**, *54* (42), 12236–12273.

Kitamura, M.; Nakatsuka, H. Mechanistic Insight into NOYORI Asymmetric Hydrogenations. *Chem. Commun.* **2011**, *47* (3), 842–846.

Korstanje, T. J.; Ivar van der Vlugt, J.; Elsevier, C. J.; de Bruin, B. Hydrogenation of Carboxylic Acids with a Homogeneous Cobalt Catalyst. *Science* **2015**, *350* (6258), 298–302.

Kosanovich, A. J.; Press, L. P.; Ozerov, O. V. Boryl Transfer Reactivity of a POCOP-Supported Ir-Diboryl: Reduction of CO_2 to CO and Borylation of Other Small Molecules. *J. Organomet. Chem.* **2017**, *845*, 19–24.

Kothandaraman, J.; Goeppert, A.; Czaun, M.; Olah, G. A.; Prakash, G. K. S. Conversion of CO_2 from Air into Methanol Using a Polyamine and a Homogeneous Ruthenium Catalyst. *J. Am. Chem. Soc.* **2016**, *138* (3), 778–781.

Krogh-Jespersen, K.; Czerw, M.; Summa, N.; Renkema, K. B.; Achord, P. D.; Goldman, A. S. On the Mechanism of (PCP)Ir-Catalyzed Acceptorless Dehydrogenation of Alkanes: A Combined Computational and Experimental Study. *J. Am. Chem. Soc.* **2002**, *124* (38), 11404–11416.

Krogh-Jespersen, K.; Czerw, M.; Zhu, K.; Singh, B.; Kanzelberger, M.; Darji, N.; Achord, P. D.; Renkema, K. B.; Goldman, A. S. Combined Computational and Experimental Study of Substituent Effects on the Thermodynamics of H_2, CO, Arene, and Alkane Addition to Iridium. *J. Am. Chem. Soc.* **2002**, No. 9, 10797–10809.

Kubas, G. J.; Ryan, R. R.; Swanson, B. I.; Vergamini, P. J.; Wasserman, H. J. Characterization of the First Examples of Isolable Molecular Hydrogen Complexes, $M(CO)_3(PR_3)_2(H_2)$ (M = Mo, W; R = Cy, *i*-Pr). Evidence for a Side-on Bonded H_2 Ligand. *J. Am. Chem. Soc.* **1984**, *106* (2), 451–452.

Kundu, S.; Choliy, Y.; Zhuo, G.; Ahuja, R.; Emge, T. J.; Warmuth, R.; Brookhart, M.; Krogh-Jespersen, K.; Goldman, A. S. Rational Design and Synthesis of Highly Active Pincer-Iridium Catalysts for Alkane Dehydrogenation. *Organometallics* **2009**, *28* (18), 5432–5444.

Kuriyama, W.; Matsumoto, T.; Ogata, O.; Ino, Y.; Aoki, K.; Tanaka, S.; Ishida, K.; Kobayashi, T.; Sayo, N.; Saito, T. Catalytic Hydrogenation of Esters. Development of an Efficient Catalyst and Processes for Synthesising (R)-1,2-Propanediol and 2-(l-Menthoxy)Ethanol. *Org. Process Res. Dev.* **2012**, *16*, 166–171.

Kütt, A.; Rodima, T.; Saame, J.; Raamat, E.; Mäemets, V.; Kaljurand, I.; Koppel, I. A.; Garlyauskayte, R. Y.; Yagupolskii, Y. L.; Yagupolskii, L. M.; et al. Equilibrium Acidities of Superacids. *J. Org. Chem.* **2011**, *76* (2), 391–395.

Lao, D. B.; Owens, A. C. E.; Heinekey, D. M.; Goldberg, K. I. Partial Deoxygenation of Glycerol Catalyzed by Iridium Pincer Complexes. *ACS Catal.* **2013**, *3* (10), 2391–2396.

Latifi, E.; Marchese, A. D.; Hulls, M. C. W.; Soldatov, D. V.; Schlaf, M. $[Ru(Triphos)(CH_3CN)_3](OTf)_2$ as a Homogeneous Catalyst for the Hydrogenation of Biomass Derived 2,5-Hexanedione and 2,5-Dimethyl-Furan in Aqueous Acidic Medium. *Green Chem.* **2017**, *19*, 4666–4679.

Laxmi, Y. R. S.; Bäckvall, J.-E. Mechanistic Studies on Ruthenium-Catalyzed Hydrogen Transfer Reactions. *Chem. Commun.* **2000**, 611–612.

Lecomte, P.; Jérôme, C. Recent Developments in Ring-Opening Polymerization of Lactones. *Adv. Polym. Sci.* **2012**, *245*, 173–218.

Lei, M.; Pan, Y.; Ma, X. The Nature of Hydrogen Production from Aqueous-Phase Methanol Dehydrogenation with Ruthenium Pincer Complexes under Mild Conditions. *Eur. J. Inorg. Chem.* **2015**, 794–803.

Lekich, T. T.; Gary, J. B.; Bellows, S. M.; Cundari, T. R.; Guard, L. M.; Heinekey, D. M. H_2 Addition to (^{Me4}PCP)Ir(CO): Studies of the Isomerization Mechanism. *Dalton Trans.* **2018**, *47* (45), 16119–16125.

Li, H.; Wang, X.; Huang, F.; Lu, G.; Jiang, J.; Wang, Z. X. Computational Study on the Catalytic Role of Pincer Ruthenium(II)-PNN Complex in Directly Synthesizing Amide from Alcohol and Amine: The Origin of Selectivity of Amide over Ester and Imine. *Organometallics* **2011**, *30* (19), 5233–5247.

Li, Y.-N.; Ma, R.; He, L.-N.; Diao, Z.-F. Homogeneous Hydrogenation of Carbon Dioxide to Methanol. *Catal. Sci. Technol.* **2014**, *4* (6), 1498–1512.

Liu, F.; Goldman, A. S. Efficient Thermochemical Alkane Dehydrogenation and Isomerization Catalyzed by an Iridium Pincer Complex. *Chem. Commun.* **1999**, 655–656.

Magano, J.; Dunetz, J. R. Large-Scale Carbonyl Reductions in the Pharmaceutical Industry. *Org. Process Res. Dev.* **2012**, *16* (6), 1156–1184.

Matlack, A. S. Green Chemistry, Applications. In *Kirk-Othmer Encyclopedia of Chemical Technology*; American Cancer Society, 1990; pp 1–33.

Matsumura, K.; Arai, N.; Hori, K.; Saito, T.; Sayo, N.; Ohkuma, T. Chiral Ruthenabicyclic Complexes: Precatalysts for Rapid, Enantioselective, and Wide-Scope Hydrogenation of Ketones. *J. Am. Chem. Soc.* **2011**, *133* (28), 10696–10699.

McAlees, A. J.; McCrindle, R. Catalytic Hydrogenations of Cyclic Imides and Ayhydrides. *J. Chem. Soc. C* **1969**, No. 19, 2425.

Menashe, N.; Salant, E.; Shvo, Y. Efficient Catalytic Reduction of Ketones with Formic Acid and Ruthenium Complexes. *J. Organomet. Chem.* **1996**, *514* (1–2), 97–102.

Menashe, N.; Shvo, Y. Catalytic Disproportionation of Aldehydes with Ruthenium Complexes. *Organometallics* **1991**, *10* (11), 3885–3891.

Meuresch, M.; Westhues, S.; Leitner, W.; Klankermayer, J. Tailor-Made Ruthenium-Triphos Catalysts for the Selective Homogeneous Hydrogenation of Lactams. *Angew. Chem. Int. Ed.* **2016**, *55* (4), 1392–1395.

Miller, A. J. M.; Heinekey, D. M.; Mayer, J. M.; Goldberg, K. I. Catalytic Disproportionation of Formic Acid to Generate Methanol. *Angew. Chem. Int. Ed.* **2013**, *52* (14), 3981–3984.

Mills, M. R.; Barnes, C. L.; Bernskoetter, W. H. Influences of Bifunctional PNP-Pincer Ligands on Low Valent Cobalt Complexes Relevant to CO_2 Hydrogenation. *Inorg. Chem.* **2018**, *57* (3), 1590–1597.

Morales-Morales, D.; Redón, R.; Wang, Z.; Lee, D. W.; Yung, C.; Magnuson, K.; Jensen, C. M. Selective Dehydrogenation of Alcohols and Diols Catalyzed by a Dihydrido Iridium PCP Pincer Complex. *Can. J. Chem.* **2001**, *79*, 823–829.

Morris, R. H. Brønsted-Lowry Acid Strength of Metal Hydride and Dihydrogen Complexes. *Chem. Rev.* **2016**, *116* (15), 8588–8654.

Morris, R. H. Exploiting Metal-Ligand Bifunctional Reactions in the Design of Iron Asymmetric Hydrogenation Catalysts. *Acc. Chem. Res.* **2015**, *48* (5), 1494–1502.

Moulton, C. J.; Shaw, B. L. Transition Metal–carbon Bonds. Part XLII. Complexes of Nickel, Palladium, Platinum, Rhodium and Iridium with the Tridentate Ligand 2,6-Bis[(Di-t-Butylphosphino)Methyl]Phenyl. *J. C.S.Dalton.* **1976**, No. 11, 1020–1024.

Mucha, N. T.; Waterman, R. Iridium Pincer Catalysts for Silane Dehydrocoupling: Ligand Effects on Selectivity and Activity. *Organometallics* **2015**, *34* (15), 3865–3872.

Munshi, P.; Main, A. D.; Linehan, J. C.; Tai, C. C.; Jessop, P. G. Hydrogenation of Carbon Dioxide Catalyzed by Ruthenium Trimethylphosphine Complexes: The Accelerating Effect of Certain Alcohols and Amines. *J. Am. Chem. Soc.* **2002**, *124* (27), 7963–7971.

N. M. A. Paul Sabatier-biographical https://www.nobelprize.org/nobel_prizes/chemistry/laureates/1912/sabatier-bio.html (accessed Jun 25, 2017).

Nguyen, D. H.; Trivelli, X.; Capet, F.; Swesi, Y.; Favre-Réguillon, A.; Vanoye, L.; Dumeignil, F.; Gauvin, R. M. Deeper Mechanistic Insight into Ru Pincer-Mediated Acceptorless Dehydrogenative Coupling of Alcohols: Exchanges, Intermediates, and Deactivation Species. *ACS Catal.* **2018**, *8* (5), 4719–4734.

Nielsen, M.; Junge, H.; Kammer, A.; Beller, M. Towards a Green Process for Bulk-Scale Synthesis of Ethyl Acetate: Efficient Acceptorless Dehydrogenation of Ethanol. *Angew. Chem. Int. Ed.* **2012**, *51* (23), 5711–5713.

Noyori, R. Asymmetric Catalysis: Science and Opportunities (Nobel Lecture). *Angew. Chem. Int. Ed.* **2002**, *41* (12), 2008–2022.

Noyori, R.; Ohkuma, T. Asymmetric Catalysis by Architectural and Functional Molecular Engineering: Practical Chemo- and Stereoselective Hydrogenation of Ketones. *Angew. Chem. Int. Ed.* **2001**, *40* (1), 40–73.

Ogata, O.; Nakayama, Y.; Nara, H.; Fujiwhara, M.; Kayaki, Y. Atmospheric Hydrogenation of Esters Catalyzed by PNP-Ruthenium Complexes with an N-Heterocyclic Carbene Ligand. *Org. Lett.* **2016**, *18* (15), 3894–3897.

Ohkuma, T.; Ooka, H.; Hashiguchi, S.; Ikariya, T.; Noyori, R. Practical Enantioselective Hydrogenation of Aromatic Ketones. *J. Am. Chem. Soc.* **1995**, *117* (9), 2675–2676.

Olah, G. A.; Fung, A. P.; Malhotra, R. Synthetic Methods and Reactions; 99. Preparation of Cyclic Ethers over Superacidic Perfluorinated Resinsulfonic Acid (Nafion-H) Catalyst. *Synthesis* **1981**, *6*, 474–476.

Olah, G. A.; Goeppert, A.; Prakash, G. K. S. *Beyond Oil and Gas: The Methanol Economy*, 2nd ed.; Wiley-VCH Verlag GmbH & Co. KGaA: Weinheim, Germany, 2009.

Oldenhuis, N. J.; Dong, V. M.; Guan, Z. Catalytic Acceptorless Dehydrogenations: Ru-Macho Catalyzed Construction of Amides and Imines. *Tetrahedron* **2014**, *70* (27–28), 4213–4218.

Papa, V.; Cabrero-Antonino, J. R.; Alberico, E.; Spanneberg, A.; Junge, K.; Junge, H.; Beller, M. Efficient and Selective Hydrogenation of Amides to Alcohols and Amines Using a Well-Defined Manganese–PNN Pincer Complex. *Chem. Sci.* **2017**, *8* (5), 3576–3585.

Pavlova, A.; Meijer, E. J. Understanding the Role of Water in Aqueous Ruthenium-Catalyzed Transfer Hydrogenation of Ketones. *ChemPhysChem* **2012**, *13* (15), 3492–3496.

Per Ahlberg. Advanced Information on the Nobel Prize in Chemistry 2001: Catalytic Asymmetric Synthesis. 2001, pp 1–12.

Polukeev, A. V.; Petrovskii, P. V.; Peregudov, A. S.; Ezernitskaya, M. G.; Koridze, A. A. Dehydrogenation of Alcohols by Bis(Phosphinite) Benzene Based and Bis(Phosphine) Ruthenocene Based Iridium Pincer Complexes. *Organometallics* **2013**, *32* (4), 1000–1015.

Pons, V.; Heinekey, D. M. An Elongated Dihydrogen Complex of Iridium. *J. Am. Chem. Soc.* **2003**, *125* (28), 8428–8429.

Pritchard, J.; Filonenko, G. A.; Van Putten, R.; Hensen, E. J. M.; Pidko, E. A. Heterogeneous and Homogeneous Catalysis for the Hydrogenation of Carboxylic Acid Derivatives: History, Advances and Future Directions. *Chem. Soc. Rev.* **2015**, *44* (11), 3808–3833.

Punji, B.; Emge, T. J.; Goldman, A. S. A Highly Stable Adamantyl-Substituted Pincer-Ligated Iridium Catalyst for Alkane Dehydrogenation. *Organometallics* **2010**, *29* (12), 2702–2709.

Qu, S.; Dai, H.; Dang, Y.; Song, C.; Wang, Z. X.; Guan, H. Computational Mechanistic Study of Fe-Catalyzed Hydrogenation of Esters to Alcohols: Improving Catalysis by Accelerating Precatalyst Activation with a Lewis Base. *ACS Catal.* **2014**, *4* (12), 4377–4388.

Rezayee, N. M.; Huff, C. A.; Sanford, M. S. Tandem Amine and Ruthenium-Catalyzed Hydrogenation of CO_2 to Methanol. *J. Am. Chem. Soc.* **2015**, *137* (3), 1028–1031.

Rezayee, N. M.; Samblanet, D. C.; Sanford, M. S. Iron-Catalyzed Hydrogenation of Amides to Alcohols and Amines. *ACS Catal.* **2016**, *6* (10), 6377–6383.

Riehl, J. F.; Jean, Y.; Eisenstein, O.; Pélissier, M. Theoretical Study of the Structures of Electron-Deficient d^6 ML_5 Complexes. Importance of a π-Donating Ligand. *Organometallics* **1992**, *11* (2), 729–737.

Riehl, J. F.; Pélissier, M.; Eisenstein, O. Influence of a Cis Hydride on a Coordinated H_2 Ligand. Ab Initio Calculations. *Inorg. Chem.* **1992**, *31* (16), 3344–3345.

Riemenschneider, W.; Bolt, H. M. Esters, Organic. *Ullmann's Encycl. Ind. Chem.* **2005**, 8676–8694.

Rybtchinski, B.; Ben-David, Y.; Milstein, D. Unexpected Isomerization of a *Cis* - into a *Trans* - Dihydride Complex. A Neutral Late Transition Metal Complex as a Hydride Donor. *Organometallics* **1997**, *16* (17), 3786–3793.

Sabatier, P.; Senderens, J. B. Transformation Des Aldéhydes et Des Cétones En Alcools Par Hydrogénation Catalytique. *C. R. Hebd. Seances Acad. Sci.* **1903**, *137*, 301–303.

Sarazin, Y.; Carpentier, J. F. Discrete Cationic Complexes for Ring-Opening Polymerization Catalysis of Cyclic Esters and Epoxides. *Chem. Rev.* **2015**, *115* (9), 3564–3614.

Saudan, L. A. Hydrogenation of Esters. In *Sustainable Catalysis*; Dunn, P. J., Hii, K. K. (Mimi), Kirsche, Michael, J., Williams, M. T., Eds.; John Wiley & Sons, Inc.: Hoboken, New Jersey, 2013; pp 37–61.

Schneck, F.; Assmann, M.; Balmer, M.; Harms, K.; Langer, R. Selective Hydrogenation of Amides to Amines and Alcohols Catalyzed by Improved Iron Pincer Complexes. *Organometallics* **2016**, *35* (11), 1931–1943.

Smith, A. M.; Whyman, R. Review of Methods for the Catalytic Hydrogenation of Carboxamides. *Chem. Rev.* **2014**, *114* (10), 5477–5510.

Smith, N. E.; Bernskoetter, W. H.; Hazari, N.; Mercado, B. Q. Synthesis and Catalytic Activity of PNP-Supported Iron Complexes with Ancillary Isonitrile Ligands. *Organometallics* **2017**, *36* (20), 3995–4004.

Spasyuk, D.; Gusev, D. G. Acceptorless Dehydrogenative Coupling of Ethanol and Hydrogenation of Esters and Imines. *Organometallics* **2012**, *31* (15), 5239–5242.

Spasyuk, D.; Smith, S.; Gusev, D. G. From Esters to Alcohols and Back with Ruthenium and Osmium Catalysts. *Angew. Chem. Int. Ed.* **2012**, *51* (11), 2772–2775.

Spasyuk, D.; Smith, S.; Gusev, D. G. Replacing Phosphorus with Sulfur for the Efficient Hydrogenation of Esters. *Angew. Chem. Int. Ed.* **2013**, *52* (9), 2538–2542.

Spasyuk, D.; Vicent, C.; Gusev, D. G. Chemoselective Hydrogenation of Carbonyl Compounds and Acceptorless Dehydrogenative Coupling of Alcohols. *J. Am. Chem. Soc.* **2015**, *137* (11), 3743–3746.

Spectral Database for Organic Compounds (SDBS); proton NMR spectrum; SDBS No.: 10291; RN 592-90-5 http://riodb01.ibase.aist.go.jp/sdbs/ (accessed Jul 1, 2014).

Spentzos, A. Z.; Barnes, C. L.; Bernskoetter, W. H. Effective Pincer Cobalt Precatalysts for Lewis Acid Assisted CO_2 Hydrogenation. *Inorg. Chem.* **2016**, *55* (16), 8225–8233.

Srimani, D.; Mukherjee, A.; Goldberg, A. F. G.; Leitus, G.; Diskin-Posner, Y.; Shimon, L. J. W.; Ben David, Y.; Milstein, D. Cobalt-Catalyzed Hydrogenation of Esters to Alcohols: Unexpected Reactivity Trend Indicates Ester Enolate Intermediacy. *Angew. Chem. Int. Ed.* **2015**, *54* (42), 12357–12360.

Teunissen, H. T.; Elsevier, C. J. Homogeneous Ruthenium Catalyzed Hydrogenation of Esters to Alcohols. *Chem. Commun.* **1998**, *3* (13), 1367–1368.

Teunissen, H. T.; Elsevier, C. J. Ruthenium Catalysed Hydrogenation of Dimethyl Oxalate to Ethylene Glycol. *Chem. Commun.* **1997**, 667–668.

van Putten, R.; Uslamin, E. A.; Garbe, M.; Liu, C.; Gonzalez-de-Castro, A.; Lutz, M.; Junge, K.; Hensen, E. J. M.; Beller, M.; Lefort, L.; et al. Non-Pincer-Type Manganese Complexes as Efficient Catalysts for the Hydrogenation of Esters. *Angew. Chem. Int. Ed.* **2017**, *56* (26), 7531–7534.

vom Stein, T.; Meuresch, M.; Limper, D.; Schmitz, M.; Hölscher, M.; Coetzee, J.; Cole-Hamilton, D. J.; Klankermayer, J.; Leitner, W. Highly Versatile Catalytic Hydrogenation of Carboxylic and Carbonic Acid Derivatives Using a Ru-Triphos Complex: Molecular Control over Selectivity and Substrate Scope. *J. Am. Chem. Soc.* **2014**, *136* (38), 13217–13225.

Wang, S.; Dorcet, V.; Roisnel, T.; Bruneau, C.; Fischmeister, C. Ruthenium and Iridium Dipyridylamine Catalysts for the Efficient Synthesis of γ-Valerolactone by Transfer Hydrogenation of Levulinic Acid. *Organometallics* **2017**, *36* (3), 708–713.

Wang, W.; Niu, M.; Hou, Y.; Wu, W.; Liu, Z.; Liu, Q.; Ren, S.; Marsh, K. N. Catalytic Conversion of Biomass-Derived Carbohydrates to Formic Acid Using Molecular Oxygen. *Green Chem.* **2014**, *16* (5), 2614–2618.

Werkmeister, S.; Junge, K.; Beller, M. Catalytic Hydrogenation of Carboxylic Acid Esters, Amides, and Nitriles with Homogeneous Catalysts. *Org. Process Res. Dev.* **2014**, *18*, 289–302.

Werkmeister, S.; Junge, K.; Wendt, B.; Alberico, E.; Jiao, H.; Baumann, W.; Junge, H.; Gallou, F.; Beller, M. Hydrogenation of Esters to Alcohols with a Well-Defined Iron Complex. *Angew. Chem. Int. Ed.* **2014**, *53* (33), 8722–8726.

Werle, P.; Moraweitz, M.; Lundmark, S.; Sörensen Kent; Karvinen, E.; Juha, L. Alcohols, Polyhydric. In *Ullmann's Encyclopedia of Industrial Chemistry*; 2008; Vol. 8, pp 255–271.

Werpy, T.; Petersen, G.; Aden, A.; Bozell, J.; Holladay, J.; White, J.; Manheim, A. Top Value Added Chemicals from Biomass Volume I - Results of Screening for Potential Candidates from Sugars and Synthesis Gas. US Department of Energy 2004, pp 1–76.

Wesselbaum, S.; Moha, V.; Meuresch, M.; Brosinski, S.; Thenert, K. M.; Kothe, J.; vom Stein, T.; Englert, U.; Hölscher, M.; Klankermayer, J.; et al. Hydrogenation of Carbon Dioxide to Methanol Using a Homogeneous Ruthenium–Triphos Catalyst: From Mechanistic Investigations to Multiphase Catalysis. *Chem. Sci.* **2015**, *6* (1), 693–704.

Widegren, M. B.; Harkness, G. J.; Slawin, A. M. Z.; Cordes, D. B.; Clarke, M. L. A Highly Active Manganese Catalyst for Enantioselective Ketone and Ester Hydrogenation. *Angew. Chem. Int. Ed.* **2017**, *56* (32), 5825–5828.

Wylie, W. N. O.; Morris, R. H. Ester Hydrogenation Catalyzed by a Ruthenium(II) Complex Bearing an N-Heterocyclic Carbene Tethered with an "NH_2" Group and a DFT Study of the Proposed Bifunctional Mechanism. *ACS Catal.* **2013**, *3* (1), 32–40.

Yang, X. A Self-Promotion Mechanism for Efficient Dehydrogenation of Ethanol Catalyzed by Pincer Ruthenium and Iron Complexes: Aliphatic versus Aromatic Ligands. *ACS Catal.* **2013**, *3* (12), 2684–2688.

Yang, X. Mechanistic Insights into Ruthenium-Catalyzed Production of H_2 and CO_2 from Methanol and Water: A DFT Study. *ACS Catal.* **2014**, *4* (4), 1129–1133.

Yuan, M. L.; Xie, J. H.; Zhou, Q. L. Boron Lewis Acid Promoted Ruthenium-Catalyzed Hydrogenation of Amides: An Efficient Approach to Secondary Amines. *ChemCatChem* **2016**, *8* (19), 3036–3040.

Yuan, M.-L.; Xie, J.-H.; Zhu, S.-F.; Zhou, Q.-L. Deoxygenative Hydrogenation of Amides Catalyzed by a Well-Defined Iridium Pincer Complex. *ACS Catal.* **2016**, *6*, 3665–3669.

Yuwen, J.; Chakraborty, S.; Brennessel, W. W.; Jones, W. D. Additive-Free Cobalt-Catalyzed Hydrogenation of Esters to Alcohols. *ACS Catal.* **2017**, *7* (5), 3735–3740.

Zell, T.; Ben-David, Y.; Milstein, D. Unprecedented Iron-Catalyzed Ester Hydrogenation. Mild, Selective, and Efficient Hydrogenation of Trifluoroacetic Esters to Alcohols Catalyzed by an Iron Pincer Complex. *Angew. Chem. Int. Ed.* **2014**, *53* (18), 4685–4689.

Zhang, J.; Leitus, G.; Ben-David, Y.; Milstein, D. Efficient Homogeneous Catalytic Hydrogenation of Esters to Alcohols. *Angew. Chem. Int. Ed.* **2006**, *45* (7), 1113–1115.

Zhang, J.; Leitus, G.; Ben-David, Y.; Milstein, D. Facile Conversion of Alcohols into Esters and Dihydrogen Catalyzed by New Ruthenium Complexes. *J. Am. Chem. Soc.* **2005**, *127* (31), 10840–10841.

Zhang, L.; Han, Z.; Zhao, X.; Wang, Z.; Ding, K. Highly Efficient Ruthenium-Catalyzed N-Formylation of Amines with H_2 and CO_2. *Angew. Chem. Int. Ed.* **2015**, *54* (21), 6186–6189.

Zhang, L.; Raffa, G.; Nguyen, D. H.; Swesi, Y.; Corbel-Demailly, L.; Capet, F.; Trivelli, X.; Desset, S.; Paul, S.; Paul, J. F.; et al. Acceptorless Dehydrogenative Coupling of Alcohols Catalysed by Ruthenium PNP Complexes: Influence of Catalyst Structure and of Hydrogen Mass Transfer. *J. Catal.* **2016**, *340*, 331–343.

Zhang, Q.; Bell, R.; Truong, T. N. Ab Initio and Density Functional Theory Studies of Proton Transfer Reactions in Multiple Hydrogen Bond Systems. *J. Phys. Chem.* **1995**, *99* (2), 592–599.

Zhang, Y.; MacIntosh, A. D.; Wong, J. L.; Bielinski, E. A.; Williard, P. G.; Mercado, B. Q.; Hazari, N.; Bernskoetter, W. H. Iron Catalyzed CO_2 Hydrogenation to Formate Enhanced by Lewis Acid Co-Catalysts. *Chem. Sci.* **2015**, *6* (7), 4291–4299.

Zhao, W.; Sun, J. Triflimide ($HNTf_2$) in Organic Synthesis. *Chem. Rev.* **2018**, *118* (20), 10349–10392.

Zhu, K.; Achord, P. D.; Zhang, X.; Krogh-Jespersen, K.; Goldman, A. S. Highly Effective Pincer-Ligated Iridium Catalysts for Alkane Dehydrogenation. DFT Calculations of Relevant Thermodynamic, Kinetic, and Spectroscopic Properties. *J. Am. Chem. Soc.* **2004**, *126* (40), 13044–13053.

VITA

Zuzana Culakova was born in 1989 in Bratislava, Slovakia. She grew up in Rochester NY, where she graduated from Brighton High School in 2007. She then attended Yale University in New Haven, CT, where she graduated with a Bachelor of Science in chemistry in 2011. During her time there, she conducted a senior research project under the supervision of Professor Nilay Hazari, studying CO_2 activation by metal-hydride bonds. Zuzana spent two years working, including a one year term as a Chesapeake Conservation Corps volunteer at Echo Hill Outdoor School in Maryland, prior to attending graduate school at the University of Washington in Seattle, WA. While at UW, Zuzana worked with Professor Karen I. Goldberg on developing new catalysts for the homogeneous hydrogenation of carbonyl-containing substrates, particularly esters. She also spent 6 months at the Université de Montpellier 2, in Monpellier, France, studying computational chemistry methods under the guidance of Professor Odile Eisenstein. Zuzana obtained the degree of Doctor of Philosophy in chemistry in 2018.